α-Amanitin-based Small Format-Drug Conjugates for Prostate Cancer Therapy: Enabling Anti-Tumor Activity by Tuning Pharmacokinetic Properties

Dissertation

zur Erlangung des akademischen Grades
Doctor rerum naturalium (Dr. rer. nat.)

vorgelegt von
Francesca Gallo

Organische und Bioorganische Chemie
Fakultät für Chemie
Universität Bielefeld

Mai 2020

The work described herein was carried out between October 2015 and October 2018 at Heidelberg Pharma Research GmbH, Dept. of Chemistry under the supervision of Prof. Dr. Andreas Pahl and Dr. Christoph Müller.

1. **Referee:**

   Prof. Dr. Andreas Pahl
   Heidelberg Pharma Research GmbH
   Pharmacology and Toxicology, Institute of Experimental and Clinical Pharmacology and Toxicology
   Erlangen-Nürnberg University

2. **Referee:**

   Prof. Dr. Norbert Sewald
   Organic and Bioorganic Chemistry, Institute of Biochemistry
   Bielefeld University

Printed on permanent paper °° ISO 9706

Statement

I, Francesca Gallo, confirm that I have written all this dissertation by myself. No parts of the text have been copied from third parties or other academic works without due attribution, and sources used in the present work have been duly referenced and attributed. All the tools and sources I have used in this work are indicated and cited.

Heidelberg, May 2020 _____

Signature

Statement of Contribution

The study described herein was a joint work with the PhD candidate Barbara Korsak, Heidelberg Pharma Research GmbH, Dept. of Biochemistry.

Chapters III-IV

F.G. designed, synthesised and characterized the compounds; B.K. conceived and carried out the *in vitro* studies and analysed the data; F.G. contributed to the data interpretation.

Chapter V

B.K. conceived and planned the *in vivo* studies and analysed the data; F.G. contributed to the data interpretation.

Chapters VI-VIII

F.G. designed, synthesised and characterized the compounds; B.K. conceived and carried out the *in vitro* studies; acquired and analysed the data; F.G. contributed to the data interpretation.

Chapter IX

F.G. conceived the idea; designed, synthesised and characterized the compounds; B.K. conceived and carried out the *in vitro* experiments; conceived and planned the *in vivo* studies; analysed the data; F.G. contributed to the data interpretation.

Publications and patents related to this work

Gallo, F.; Korsak, B.; Müller, C.; Hechler, T.; Pahl, A.; Kulke, M.; Werner, S.; Lutz, C. PSMA-targeting amanitin conjugates. WO/2019/057964, March 28, 2019.

To my parents and my sister

for their endless love, support and encouragement

"…one must distrust the almost-the-same […], the practically identical, the approximate, the or-even, all surrogates, and all patchwork. The difference can be small, but they can lead to radically different consequences, like a railroad's switch points; the chemist's trade consists in good part in being aware of these differences, knowing them close up, and foreseeing their effects. And not only the chemist's trade."

(Primo Levi, The Periodic Table)

Acknowledgements

Before we get into the thick of science, I would like to spend a few words for all those people who guided, supported and helped me along the way to this professional and personal achievement.

Firstly, I would like to thank my mentors Prof. Dr. Andreas Pahl and Dr. Christoph Müller for their support and invaluable guidance. The critical feedbacks, suggestions and encouragements I got from Prof. Dr. Pahl throughout this work served me to move forward on this project and grow as young scientist. I am especially grateful to Dr. Müller for his readiness to help me and for inspiring me the qualities of a good scientist and chemist. Both, Prof. Dr. Pahl and Dr. Müller, read drafts of this dissertation and made invaluable comments and suggestions.

I am also thankful to Dr. Torsten Hechler and Dr. Michael Kulke. Although they did not directly supervise my work, their knowledge and expertise in biochemistry and pharmacology enabled me to get a deeper insight into the different issues covered by this reserch work and to broaden my knowledge.

The path to this work has been not always straightforward and easy. I owe, therefore, a debt of gratitude to my collague and friend Barbara Korsak for her unwavering support along the way at work as well as in life and for her essential contribution to this project.

My gratitude is also extended to Prof. Dr. Harald Kolmar and his research group, which hosted me during my secondment at Darmstadt University. Prof. Dr. Kolmar always conveyed to me a spirit of enthusiasm and excitement in regard to research, and encouraged me to believe that results of our labor might be interesting, which has been for me a strong driving force to complete this work.

The support from all the Heidelberg Pharma team was essential to fully develop this project as well. Mrs Nicole Straube deserves a special thank for her kind, sincere and constant support in the daily life and for helping me to settle down in Heidelberg.

I am also thankful to Prof. Dr. Norbert Sewald. His idea of the Magicbullet network gave us young people the opportunity to take the first steps in the research in an international, multicultural framework. I benefitted from the expertise of all the scientists the network was made of. Their thoughtful comments and expression of concern regarding the project encouraged me to move forward on it.

The Magicbullet project turned out to be a wonderful three-year journey with amazing people. I shared unforgettable moments with them that I will surely miss.

I am sincerely grateful to my father Carmine and my mother Maria for their encouragement to believe in myself and pursue my goals, to be independent and not to give up when facing the

difficulties, for being constantly present in my life even though far away apart and for their unwavering support. I am extremely grateful to my sister Rossella as well. She has been always patiently next to me helping and guiding me with her motherly advices. Their example shaped the person I am and I owe to them all my achievements so far.
(Sono sinceramente grata a mio padre Carmine e a mia madre Maria per il loro incoraggiamento a credere in me stessa e a perseguire i miei obiettivi, ad essere indipendente e a non arrendermi davanti alle difficoltá, per essere costantemente presenti nella mia vita anche se lontani e per il loro incrollabile supporto. Sono estremamente grata anche a mia sorella Rossella. Mi è sempre stata pazientemente vicina aiutandomi e guidandomi con i suoi consigli materni. Il loro esempio ha plasmato la persona che sono e a loro devo i traguardi che ho raggiunto finora nella mia vita.)

Lastly, I would like to express my sincere gratitude to my friends Michele, Alberto, Salvatore, Corinna. They have been part of this journey. I shared with them the most significant moments of it: the good, the funny and the hard ones. Always next to me, always ready to help and support me, I never felt alone and I could see first hand what friendship truly is.

Grazie!
Thank you!
Danke!

Table of contents

Abbreviations and acronyms

ac= acetamide

ACN= acetonitrile

AcOH= acetic acid

ACUPA= 2-[3-(5-amino-1-carboxypentyl)ureido]pentanedioic acid

ADA= anti-drug antibody

ADC= Antibody Drug Conjugate

ADCC= antibody-dependent cell-mediated cytotoxicity

ALCL= anaplastic large-cell lymphoma

ALL= acute lymphoblastic leukemia

AML= acute myeloid leukemia

AR= androgen receptor

ATP= adenosinetriphosphate

bac= bromoacetamide

BCR-ABL= breakpoint cluster region-Abelson

BMPS= 3-(maleimido)propanoic acid *N*-hydroxysuccinimide ester

Bn= benzyl

Boc= *tert*-butyloxycarbonyl

CDC= complement-dependent cytotoxicity

CDR= complementary-determining region

CML= chronic myeloid leukemia

cpAb= chemically programmed antibody

CuAAC= Copper-catalyzed azide-alkyne cycloaddition

CURL= compartment for uncoupling of receptor and ligand

DAD= diode array detector

DAR= drug-to-antibody ratio

DBCO-SU= dibenzocyclooctine *N*-hydroxysuccinimide ester

DBCO= dibenzocyclooctine

DC= drug conjugate

DCC= dicyclohexylcarbodiimide

DCM= dichloromethane

DCU= dicyclohexylurea

DHFR= dihydrofolate reductase

DIPEA= *N*, *N*- diisopropylethylamine

DMF= dimethylformamide

DMSO= dimethylsulfoxide

DNA= deoxyribonucleic acid

DPR= drug-to-protein ratio

DSC= disuccinimidyl carbonate

DTNP= 2,2´-dithiobis(5-nitropyridine)

DTT= dithiothreithol

DUPA= 2-[3-(1,3-dicarboxylpropyl)-ureido]pentanedioic acid

EC_{50}= half maximal effective concentration

ECMS= *N*-maleimidocaproyloxysuccinimide ester

EEDQ= 2-ethoxy-1-ethoxycarbonyl-1,2-dihydroquinoline

EG= ethylene glycol

EtOAc= ethyl acetate

Fab= antigen binding fragment

Fc= fragment crystallizable

FcRn= neonatal Fc receptor

Fmoc= fluorenylmethyloxycarbonyl

GLP-1= glucagon-like peptide-1

GRPr= gastrin releasing peptide receptor

GSH= glutathione

HBED-CC= *N*, *N´*-bis[2-hydroxy-5-(carboxyethyl)benzyl]ethylenediamine-*N*,*N´*-diacetic acid

HBTU= 3-[bis(dimethylamino)methyliumyl]-3*H*-benzotriazol-1-oxide hexafluorophosphate

HOBt= N-hydroxybenzotriazole

HOSu= hydroxysuccinimide

HRP= horseradish peroxidase

i.v.= intravenous

IgG= immunoglobulin G

KFDC= knottin-Fc-drug conjugateLiBr= lithium bromide

LiHMDS= lithium bis(trimethylsilyl) amide

LNCaP= lymph node carcinoma of the prostate

LPR= linker-to-protein ratio

ma= maleimidoacetyl

mAb= monoclonal antibody

mCRPC= metastatic castration-resistant prostate cancer

MED= minimum effective dose

MeOH= methanol

MG= minigastrin

MM= multiple myeloma

MMAE= monomethyl auristatin E

MMAF= monomethyl auristatin F

MoA= mode of action

mp= maleimidopropyl

MTA= microtubule-targeting agent

MTBE= methyl *tert*-butyl ether

MTD= maximum tolerated dose

Mtt= 4-methyltrytil

MW= microwave

NaH= sodium hydride

Npys= 2-(5-nitropyridylsulfenyl)

OATP1B3= organic anion transporter polypeptide 1B3

p.i.= post-injection

PABA= *p*-aminobenzyl alcohol

PBS= phosphate-buffered solution

PC3= prostate cancer 3

PCa= prostate cancer

PD= pharmacodynamics

PDB= pyrrolobenzodiazepine

PEI= polyethylenimine

PIN= prostatic intrepithelial neoplasia

PK= pharmacokinetics

PKM= pharmacokinetics-modifying linker

PMPA (2-PMPA)= 2-(phosphomethyl)pentane-1,5-dioic acid

PRRT= peptide-receptor radionuclide therapy

PSMA= Prostate-Specific Membrane Antigen

q1w= once per week

RNA= ribonucleic acid

RNAP= RNA polymerase

RP-HPLC= reversed phase-high perfomance liquid chromatography

rt= room temperature

s.c.= subcutaneously

S= selectivity factor

SCID= severe combined immunodeficiency

SDS-PAGE= Sodium Dodecyl Sulphate - PolyAcrylamide Gel Electrophoresis

SEC-FPLC= size exclusion-fast protein liquid chromatography

SEC= size exclusion chromatography

SEM= trimethylsilylethoxymethyl

SEMCl= 2-(trimethylsilyl)ethoxymethyl chloride

SMDC= Small Molecule Drug Conjugate

SPPS= solid phase peptide synthesis

SrtA= sortase A

T.I.= targeting index

$t_{1/2}$= half-life

t1w= twice per week

T2DM= type-2 diabetes mellytus

TBAF= tetrabutylammonium fluoride

TBDMSCl= *tert*-butyldimethylsilyl chloride

TBS= *tert*-butyldimethylsilyl

TBTU= 2-(1H-benzotriazole-1-yl)-1,1,3,3-tetramethylaminium tetrafluoroborate

^{t}Bu= *tert*-butyl

TEA= triethylamine

TEV= Tobacco Etch Virus

TFA= trifluoroacetic acid

TFE= 2,2,2- trifluoethanol

THF= tetrahydrofuran

TIS= triisopropylsilane

TopI= topoisomerase I

TopII= topoisomerase II

Tris= tris (hydroxymethyl) aminomethane

Trt= triphenylmethyl

VEGF-A= vascular endothelial growth factor A

xs= excess

Amino acid	One letter code	Three letters code
Alanine	A	Ala
Arginine	R	Arg
Aspartic acid	D	Asp
Cysteine	C	Cys
Glutamic acid	E	Glu
Glutamine	Q	Gln
Glycine	G	Gly
Histidine	H	His
Isoleucine	I	Ile
Leucine	L	Leu
Lysine	K	Lys
Methionine	M	Met
Methionine	M	Met
Phenylalanine	F	Phe
Proline	P	Pro
Serine	S	Ser
Threonine	T	Thr
Tryptophne	W	Trp
Tyrosine	Y	Tyr
Valine	V	Val

Abstract

Antibody-Drug Conjugates (ADCs) based on antibodies as tumor-homing vehicles of cytotoxic drugs, represent a breakthrough in cancer treatment with seven approved products. High specific recognition of tumor-associated antigens provided by antibodies allows the preferential localization of the cytotoxic drug at the tumor site, reducing the systemic toxicity of conventional chemotherapy. While majority of the most advanced ADCs is directed against hematological cancers, treatment of solid tumors with ADCs remains still challenging. The unique physiology of a solid tumor and the large size of ADCs impair the penetration and the even distribution of these therapeutics in the tumor tissue. As format alternative to ADCs, Small Molecule-Drug Conjugates (SMDCs) which utilize small organic ligands as tumor-homing vehicles are recently gaining growing attention due to their potential better tumor-penetrating properties.

The first part of the present study (Chapters 3-5) describes the design and preclinical characterization of a small library of SMDCs. The products herein described were designed to target prostate cancer cells by means of a small glutamate-urea-based ligand known as DUPA. DUPA binds with high affinity to Prostate Specific Membrane Antigen (PSMA), a validated target of virtually all prostate cancers. α-Amanitin, a natural toxin isolated from the green death cap mushroom *Amanita phalloides*, which acts as potent RNA polymerase II inhibitor of eukaryotic cells, was investigated as innovative SMDC drug payload. Variation of the linker and conjugation chemistry between the targeting moiety and the drug payload led to the first-generation of PSMA-targeting α-amanitin-based SMDCs.

The most promising candidates selected from the initial screening of the *in vitro* activity were further characterized *in vivo* in murine models. The limited antitumor activity associated to their poor pharmacokinetic properties fuelled research into a variety of strategies to optimize the pharmacokinetic properties and increase the therapeutic efficacy of the PSMA-targeting α-amanitin-based SMDCs, which are described in the second part of this study (Chapters 6-9). The attempts led ultimately to the generation of a Small Molecule-Fc-Drug Conjugate (Fc-SMDC) by grafting a PSMA-targeting α-amanitin-based SMDC onto an IgG_1-Fc fragment. Combination within a single platform of a small organic ligand with well-known targeting and internalization properties, a drug payload with unique mode of action and favourable physiochemical properties, and an Fc portion providing extended circulatory half-life led to an ADC-like therapeutic with outstanding antitumor activity, but yet much smaller than a conventional ADC.

Chapter 1
Introduction

1.1 Cancer

Cancer is the second leading cause of mortality worlwide and number of deaths will likely rise to 13 milions per year till 2030, due to the growth and aging of the population.[1] According to the most recent estimates from the International Agency for Research on Cancer –IARC- (2018), lung cancer is the most common cancer for incidence and mortality worldwide. Following lung cancer, prostate cancer is the most commonly diagnosed among men, while breast cancer is the most common malignancy diagnosed among women and the leading cause of cancer death.[2]

Cancer is a set of related diseases of deregulated cellular behaviour driven by genetic mutations.[3] Malignant cells are enabled to escape the mechanisms controlling the normal cellular homeostatsis by acquisition of oncogenic attributes and loss of tumor suppressive functions. Cancer cells are then able to unlimitedly proliferate, evade cell death signals, rewire their energy metabolism, spread to distant sites -a process known as metastasis-, and evade immune control, features collectively known as "hallmarks" of cancer. [4, 5]

1.2 The war on cancer: chemotherapy

The era of chemotherapy can be traced back to the 1940s when it was observed that soldiers accidentally exposed to mustard gas in World War II had depleted bone marrow and reduced lymph nodes.[6] In 1943 this observation led to the application of a closely related mustard gas derivative, the nitrogen mustard, in the treatment of lymphoma. Shortly after, the Farber´s discovery that folic acid stimulates proliferation of acute lymphoblastic leukemia (ALL) cells prompted the development of the folic acid analogue methotrexate (**1**, **Figure 1**), an inhibitor of dihydrofolate reductase (DHFR), which was the first drug to cure a solid tumor in humans in 1950s.[7]

It took almost a decade to identify the mode of action of these chemotherapeutics, which are effective at killing cancer cells by interfering with DNA integrity and/or replication.[8]

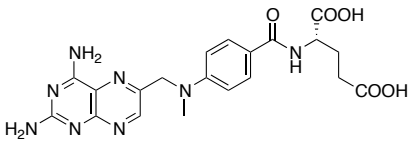

Methotrexate (antimetabolites) (**1**)
Dihydrofolate reductase inhibition

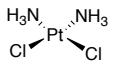

Cisplatin (platinum complexes) (**2**)
DNA-alkylation

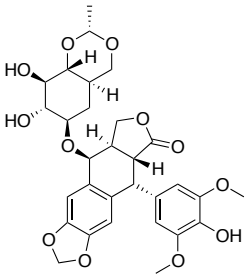

Etoposide (podophyllotoxins) (**3**)
DNA-topoisomerase II inhibition

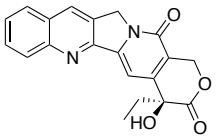

Camptothecin (triterpenoids) (**4a**)
DNA-topoisomerase I inhibition

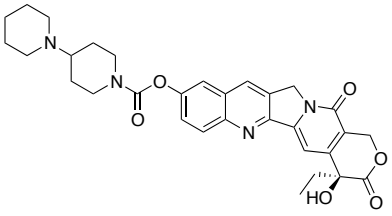

Irinotecan (triterpenoids) (**4b**)
DNA-topoisomerase I inhibition

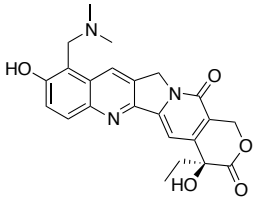

Topotecan (triterpenoids) (**4c**)
DNA-topoisomerase I inhibition

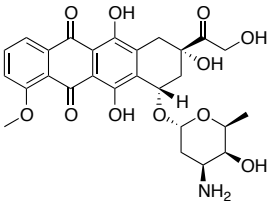

Doxorubicin (anthracyclines) (**5a**)
DNA-intercalation (multitarget)[a]

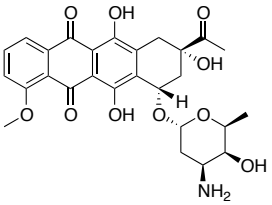

Daunorubicin or **daunomycin** (anthracyclines) (**5b**)
DNA-intercalation (multitarget)[a]

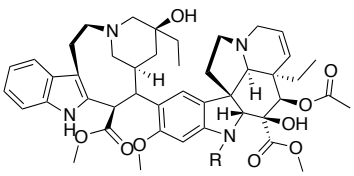

Vincristine (R= CHO) (Vinca alkaloids) (**6a**)
Vinblastine (R= CH_3) (**6b**)
Microtubule polymerization inhibition

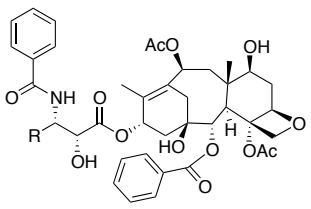

Paclitaxel (R= Ph) (**7a**)
Docetaxel (R= O^{t}Bu) (**7b**)
Microtubule polymerization inhibition

Figure 1. Molecular structure and mode of action of the most common chemotherapeutics. [a] multitarget: other mode of action are known.

In majority of cases, the early cancer therapeutics were discovered by serendipity and moved into clinical use before there was a clear indication of their mechanism of action.

The accidental discovery of cytotoxicity of cisplatin (cis-diamminedichloroplatinum(II); **2**) in the 1960s[9] boosted the development of platinum-based analogs, like carboplatin and oxaliplatin, which act by forming DNA crosslinks, resulting in the inhibiton of DNA, RNA and protein synthesis.[10]

A different way to interfere with the functions of DNA is targeting the DNA-topoisomerase complexes. Topoisomerases I and II (TopI and TopII) are enzymes responsible for the DNA unwinding by cleaving and rejoining the single- or the double-stranded DNA, respectively. Etoposide (**3**), a semisynthetic derivative of podophyllotoxin isolated from the American Mayapple, was demonstrated to stabilize the TopoII-DNA cleavage complex. Campothecin (**4a**), isolated from the chinese ornamental tree *Campotheca acuminata* in the mid 1950s, and its analogues, irinotecan (**4b**) and topotecan (**4c**), target the TopoI-DNA covalent complex. The poisoning interaction of these compounds with DNA-topoisomerase complexes prevents the DNA religation process leading to permanent damages.[11]

Among the most effective anticancer drugs, the anthracycline antibiotics, doxorubicin (**5a**) and daunorubicin (**5b**), isolated early in the 1960s from *Streptomyces peucetius*[12] have the widest spectrum of activity in human cancers.[13] Although their major mode of action is as TopII poison, a large body of evidence suggests alternative mechanisms as DNA intercalating-, alkylating- and cross linking-agents as well as inhibitors of the helicase activity.[11]

Over 50 years ago the isolation of *Vinca alkaloids* from perwinkle leaves paved the way to the application in cancer treatment of a novel class of chemotherapeutics, the microtubule-targeting agents (MTAs). Microtubules, a dynamic assembly of tubulin heterodimers are an important target in anticancer therapy due to their crucial role in mitosis and cell division.[14]

As reported by Jordan *et al.*, the vinca alkaloids, e.g. vincristine (**6a**) and vinblastine (**6b**), act by destroying mitotic spindles and depolymerizing microtubules at high concentration.[15] Other MTAs, the taxanes, paclitaxel (**7a**) and its semisynthetic analogue docetaxel (**7b**), exert the same cytotoxic effect by stabilizing microtubules and increasing microtubule polymerization.[16]

1.3 Why chemotherapy can fail?

These early anticancer drugs still constitute the majority of chemotherapeutics applied today in the clinical management of cancer and they can successfully cure some cancers. However, they are not effective for all types of cancers and their use is associated to severe side effects.

Most common acute toxicities arise from lack of target specificity. Anticancer drugs affect cancer cells as well as normal rapidly dividing cells, e.g. bone marrow, gut mucosa and hair

follicles cells.[17] Generally, some agents may also compromise the function of post-mitotic tissues, such as heart muscle and peripheral nerves,[18, 19] and cause severe injury to organs with a rich blood supply and an active role in drug metabolism, like kidneys and liver.[20, 21]
Therefore, the therapeutic index (**Figure 2**) **-** defined as the ratio between the highest exposure to the drug which does not result in any unacceptable toxicity to the highest exposure that produces the desired efficacy **-** associated to such chemotherapeutics is rather low.[22, 23]

Although chemotherapy has led to improvements in patient´s survival and quality of life, most of patients develop progressive disease after initial responding to treatments.
Intrinsic or acquired tumor resistance to anticancer drugs is actually a primary limiting factor of the effectiveness of anticancer treatments, accounting for more than 90% of treatment failures in patients with metastatic diseases.[24] The extensive genetic heterogeneity and the high rate of mutations of tumor cells may result in the selection and overgrowth of drug-resistant variants and subsequent acquisition of drug resistance.
The phenomenon of acquired tumor resistance to anticancer compounds is generally a combination of different mechanisms. Some of these mechanisms, such as loss of cell surface receptor or transporter, alteration of the specifc target, or specific metabolism of a drug, result in resistance to only a number of related drugs. However, most often tumor cells express mechanisms that confer resistance to several structurally and functionally unrelated drugs, leading to multidrug resistance (MDR). MDR phenotype is mostly associated with modulation of expression or activity of the drug efflux pump P-glycoprotein and the multidrug resistance-associated protein 1 (MRP1). These proteins drive the outwardly transport of substrates against a concentration gradient, thereby reducing the intracellular drug concentration. MDR is also associated to the increased drug detoxification, capacity to repair DNA lesions or inhibition of cell apoptosis.[7], [25, 26]

A significant milestone in cancer therapy was achieved with the introduction of drugs combination. Cancer drugs with different mode of action and minimally overlapping toxicity profiles can be usually combined at full doses to overcome tumor heterogeneity and its implication in drug resistance.[27]
Despite these strategies can certainly improve the outcomes of traditional chemotherapies, systemic toxicity to the host and the narrow therapeutic index remain the major drawbacks of cytotoxic agents.

In order to improve the therapeutic index, either the potency of the cytotoxic agents can be increased to lower the minimum effective dose (MED) or the tumor selectivity can be improved to increase the maximum tolerated dose (MTD) (**Figure 2**).[28]

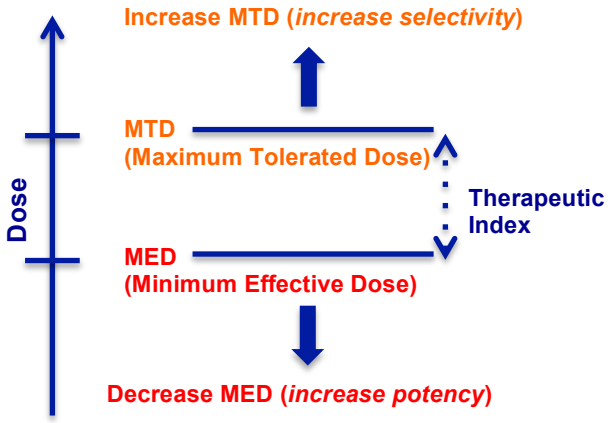

Figure 2. Strategy to optimize the therapeutic index. The therapeutic index can be optimized either by increasing the potency of the cytotoxic drug to lower the minimum effective dose (MED) or by increasing the tumor selectivity to increase the maximum tolerated dose (MTD). Adapted with permission from Chari, R. V. J. *et al*. *Angew*. *Chem*. *Int*. *Ed*. **2014**, *53*, 3796-3827, Wiley-VCH.

An intensive programme for collecting and screening plant and marine sources led to the discovery of several agents with higher potency than known compounds.

One of the first compounds to be discovered was maytansine (**8**, **Figure 3**), an ansa macrolide isolated in 1972 from the East African shrub *Maytenus ovatus*.[29-30]

It was found to be a potent mitotic inhibitor showing *in vitro* potency in the low picomolar range.[31] However, its clinical development was discontinued after phase II trial due to its poor efficacy and severe side effects. Indeed, the MTD reported in humans (2 mg/m^2) was much lower than that of other anticancer drugs.[32]

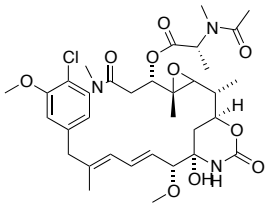

Maytansine (maytansinoids) (**8**)
Tubulin polymerization inhibition

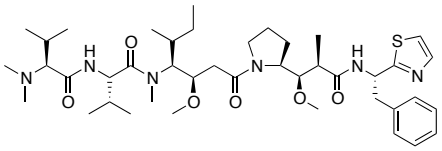

Dolastatin-10 (dolastatins) (**9a**)
Tubulin polymerization inhibition

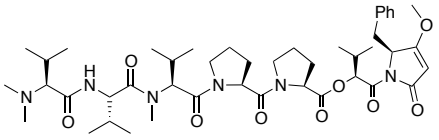

Dolastatin-15 (dolastatins) (**9b**)
Tubulin polymerization inhibition

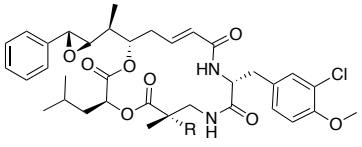

Cryptophicin 1 (R= H; crytophicins) (**10a**)
Cryptophicin 52 (R= CH_3; crytophicins) (**10b**)
Tubulin polymerization inhibition

Figure 3. Molecular structure and mode of action of the most potent tubulin-binding agents.

Other MTAs, the small linear peptides dolastatin-10 (**9a**) and dolastatin-15 (**9b**), were isolated

from the sea hare *Dolabella auricularia*. Like maytansine, dolastatins inhibit the tubulin polymerization inducing *in vitro* cell death at picomolar concentrations. Despite their *in vitro* potency, both compounds failed in human clinical trials to demonstrate high antitumor activity and therapeutic benefits. [33-36]

Similarly, the clinical evaluation of a synthetic analogue of cryptophicin 1 (**10a**), the cryptophicin 52 (**10b**), one of the most potent tubulin-destabilizing agent (100-1000-fold more potent than paclitaxel and vinblastine)[37] isolated from the cyanobacteria *Nostoc* sp., was discontinued due to the very low achievable doses (MTD 1.5 mg/m^2)[38] and insufficient therapeutic activity in humans.

Taken together, these observations show that the mere increase of potency of cytotoxic drugs does not necessarily increase the therapeutic window of chemotherapy.

1.4 Targeted cancer therapy

The alternative approach to improve the therapeutic window is to increase the tumor selectivity of the therapeutic agents.

An in-depth understanding of the tumor biology and pharmacology at molecular level fuelled efforts to develop agents able to interfere selectively with molecular targets and processes deemed important for the survival and proliferation of tumor cells.

Some of these targets are genetically altered in cancer cells and are essential to sustain the neoplastic phenotype, phenomenon known as oncogene addiction.[39] The pioneering example of molecule successfully targeting an addictive oncoprotein is Imatinib mesylate (Gleevec®, Novartis), approved by FDA in 2001 for the treatment of chronic myeloid leukemia (CML). Imatinib is a small molecule inhibitor of the BCR-ABL (Breakpoint Cluster Region-Abelson) tyrosine kinase, a mutant fusion protein present in almost all CML patients and that promotes cancer cells growth through the aberrant phosphorylation of the target protein.[40, 41] Thus far (January 2020), 46 protein kinase inhibitors have received FDA approval for different tumor indications.[42]

1.4.1 Monoclonal antibodies

Other molecular markers of cancer cells with a role in tumor growth or progression can be targeted with high affinity and specificity by monoclonal antibodies (mAbs).

In 1975, introduction of the hybridoma technology by Köhler and Milstein[43] enabled the production in mice of a single purified antibody to the antigen of interest in large amount. This

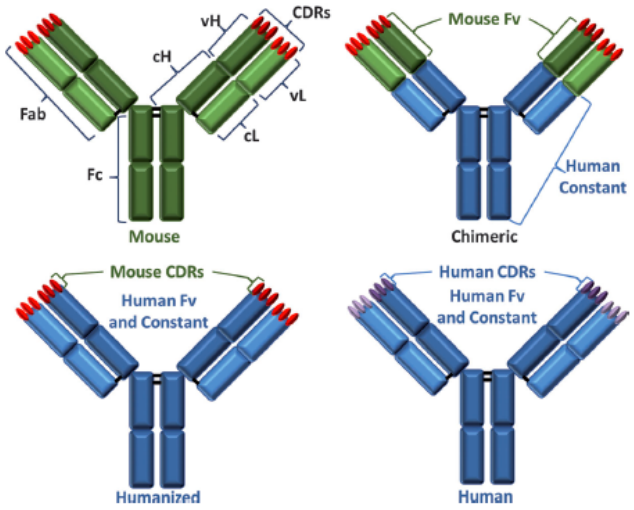

Figure 4. Schematic representation of murine, chimeric, humanized, and human antibody. The murine sequences are shown in green and the human in blue. In a chimeric antibody, the mouse heavy and light chain V region sequences are joined onto human heavy and light chain C regions. In a humanized antibody the mouse CDRs (red) are grafted onto human V-region FRs and expressed with human C regions. Reprinted with permission from Chari, R. V. J. *et al*. *Angew*. *Chem*. *Int*. *Ed*. **2014**, *53*, 3796-3827, Wiley-VCH.

discovery started the era of antibodies in therapy. However, the initial overall clinical outcomes were poor due to the high immunogenicity of the murine mAbs in humans.

A significant goal was achieved with humanization of murine antibodies by grafting the complementary-determining regions (CDRs) of the desired murine antibody onto a recombinant human immunoglobulin backbone (**Figure 4**).[44] Nowadays, advanced strategies, such as the phage display technology and transgenic mice partially reconstituted with human immunoglobulin genes, allow to generate fully human antibodies (**Figure 4**) with significantly longer half-life ($t_{1/2}$ three weeks) than their murine counterparts ($t_{1/2}$ two-three days).[28]

Therapeutic antibodies elicit their anti-tumor effects by targeting receptors overexpressed or expressed in mutated form on the tumor cells compared to normal tissues. An example of such antibodies is trastuzumab (Herceptin®, Roche), which targets the HER2/neu protein overexpressed in some breast cancers. Alternatively, other therapeutic antibodies target tumor-stroma interactions, such as the mAb bevacizumab (Avastin®, Genentech/Roche) that neutralizes the vascular endothelial growth factor A (VEGF-A), blocking angiogenesis and leading to the tumor starvation.[45,46] In addition, antibodies can also mediate activation of the immune system of the recepient through their Fc (fragment crystallizable) portion, inducing antibody-dependent cell-mediated cytotoxicity (ADCC) or complement-dependent cytotoxicity (CDC).

As of November 2019, over 30 antibodies have been approved by FDA for treatment of solid or hematologic malignancies, and 40 novel antibodies were in late-stage clinical evaluation for cancer indications.[47a-b] However, while antibodies for hematologic malignancies are used as single agents, antibodies approved for solid tumors may result poorly effective and are typically used in combination with chemotherapy.

1.5 Tumor-Targeted Drug Conjugates

The advent of the targeted drug delivery technology has led to a paradigm shift in cancer chemotherapy. Attaching a cytotoxic payload to a targeting moiety which recognizes cancer cell-specific receptors provides a mechanism to selectively deliver a cytotoxic drug to cancer cells. The general structure of this class of smart drugs is depicted in **Figure 5** and consist of a targeting moiety covalently linked to a cytotoxic agent via a synthetic linker.

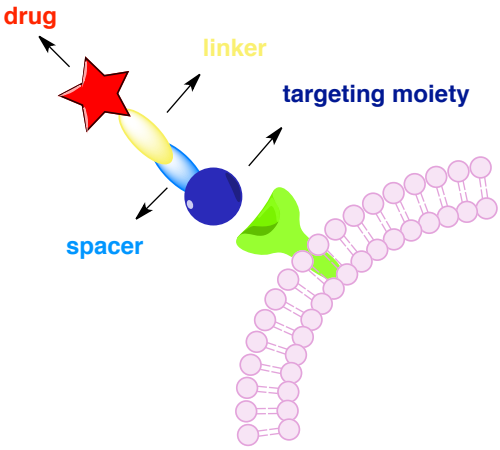

Figure 5. General structure of a targeted drug conjugate. The carrier (or targeting moiety, blue) is tethered to a drug cargo (red) via a synthetic linker (yellow). A spacer (cyan) can be included to enhance the hydrophilicity or to reduce the steric hindrance and ensure the binding to the target receptor (green).

Antibody-drug conjugates (ADCs) make-up the largest portion of this growing class of therapeutics. First generation ADCs relied on cytotoxic payloads with a well-established mode of action, such as methotrexate, doxorubicin or vinca alkaloids. These early ADCs failed in the clinics to demonstrate antitumor efficacy due to the low drug potency, linker instability, and lack of selective antigen expression. In addition, high immmunogenic response was observed, as initially murine mAbs were used.[48, 49]

Although currently over 65 ADCs for cancer indications have entered early or late stage clinical trials,[50] to date only seven have received approval by FDA (**Figure 6**).

The first ADC to be approved by FDA in 2000 was gemtuzumab ozogamicin (Mylotarg®, Wyeth then Pfizer; **11a**), an anti-CD33 mAb conjugated to calicheamicin via an acid-labile hydrazone linker. It was approved for the treatment of acute myeloid leukemia (AML). However, a follow-up study revealed no overall survival improvements and a higher fatal toxicity rate over conventional chemotherapy, leading Pfizer to voluntarily withdraw it from market in 2010.[51] Gemtuzumab ozogamicin was reapproved by FDA in 2017 for the treatment of CD33-positive AML patients at different dosing regimen.

First approval of gentuzumab ozogamicin was followed by the approval of:

- brentuximab vedotin (Adcetris®, Seattle Genetics; **12a**), an anti-CD30 mAb conjugated to monomethylauristatine E (MMAE) via an enzymatic cleavable linker. It was approved in 2011 for the treatment of Hodgkin´s lymphoma and anaplastic large-cell lymphoma (ALCL).
- trastuzumab emtansine (also known as ado-trastuzumab emtansine or T-DM1; Kadcyla®, Roche; **13a**), an anti-HER2 mAb coupled through a non-reducible thioether

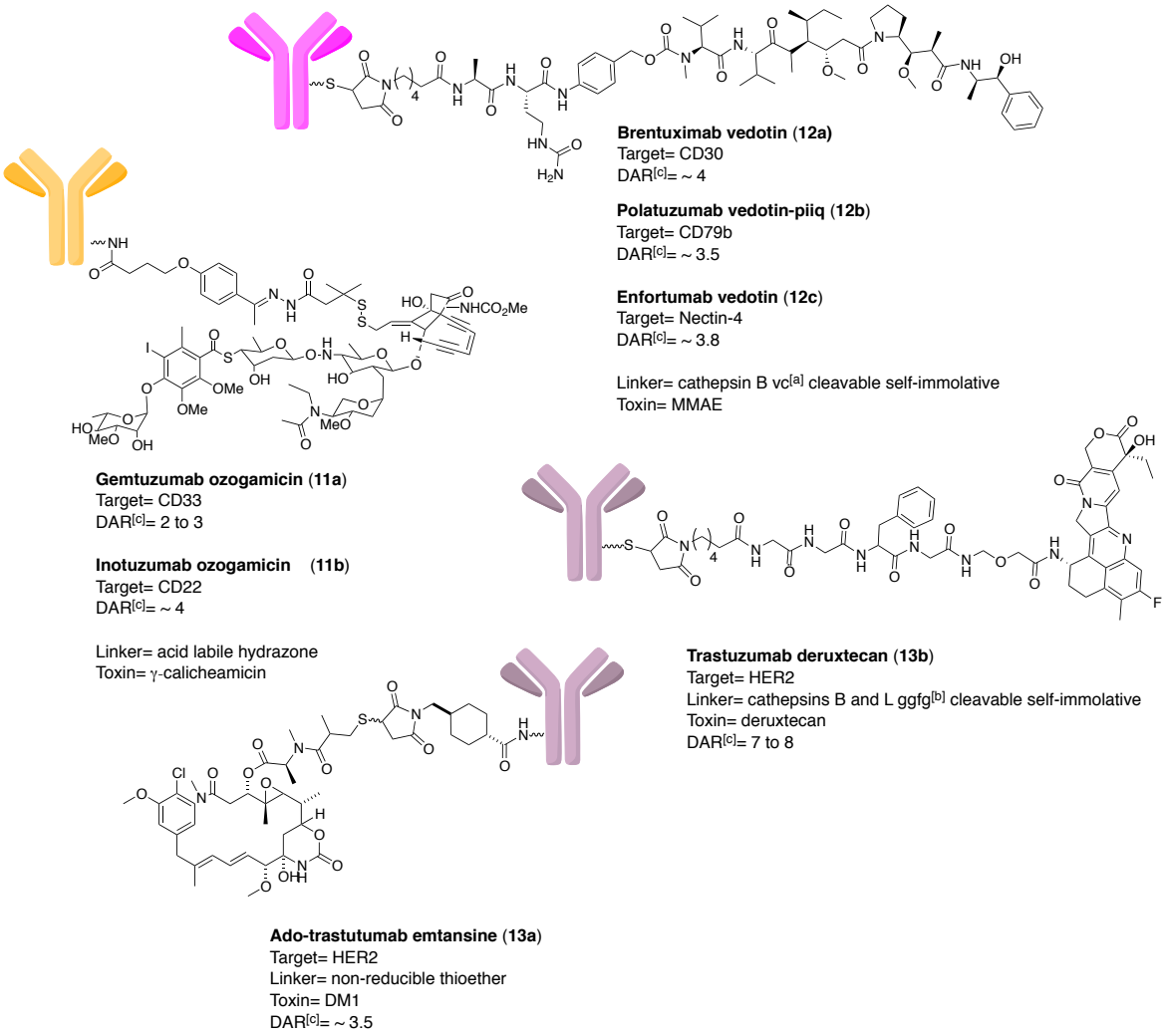

Figure 6. Schematic representation of the seven approved ADCs. Molecular structure, target, linker type, toxin and DAR are reported. [a] vc= valine-citrulline; [b] ggfg= glycinglycin-phenylalanine-glycine; [c]DAR= drug-to-antibody ratio.

linker to a maytansine derivative. T-DM1 has received approval in 2013 for the treatment of HER2-positive metastatic breast cancer.

- inotuzumab ozogamicin (Besponsa®, Pfizer; **11b**), an anti-CD22 antibody tethered to calicheamicin via a hydrazone linker. In 2017 it was approved for the treatment of ALL.(50, 52, 53a)
- polatuzumab vedotin (Polivy™, Seattle Genetics; **12b**), an CD79b mAb coupled to MMAE via an enzymatic cleavable linker. It received approval by FDA in 2019 for treatment of adults with relapsed or refractory diffuse large B-cell lymphoma in combination with bendamustine and rituximab (Rituxan®; Genentech/Roche).(53b)
- enfortumab vedotin (Padcev™, Astellas Pharma/Seattle Genetics; **12c**) consists of a Nectin-4-directed antibody conjugated through an enzymatic cleavable linker to MMAE. In 2019 enfortumab vedotin was approved in the United States for the treatment of adult patients with locally advanced or metastatic urothelial cancer.(53b)

- trastuzumab deruxtecan (Enhertu, AstraZeneca/Daiichi Sankyo; **13b**), an anti-HER2 mAb connected to the TopI inhibitor deruxtecan via an enzymatic cleavable linker. Approved in 2019, it is indicated for the treatment of adults with unsectable or metastatic HER2-positive breast cancer.[53b]

Despite advances to improve ADCs' stability, safety and homogeneity, ADCs still suffer from some limitations regarding solid tumor penetration, immunogenicity and manufacturing issues.
In the last decades formats alternative to antibodies have been investigated for tumor targeting applications, ranging from small molecules to peptides, aptamers, novel protein scaffolds and antibody fragments (**Figure 7**).
Smaller ligand markedly differ, often advantageously, in their pharmacokinetic profile, antigenicity, and ability to penetrate solid tumors compared to their larger counterparts.[54]

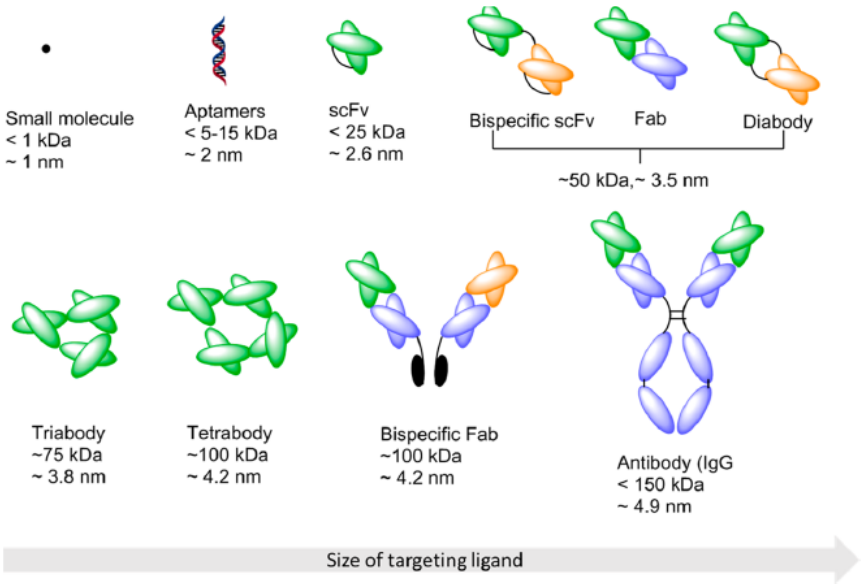

Figure 7. Commonly used targeting agents reported in order of size. Molecular weight and Stokes-Einstein radius are shown. Reprinted with permission from Srinivasarao, M. and Low, P. S. *Chem. Rev.* **2017**, *117*, 12133-12164. Copyright 2017, American Chemical Society.

1.6 Other formats *versus* mAbs. Are they a viable alternative?

1.6.1 Tumor uptake, penetration and retention

In order to reach the tumor site, a targeted agent has to flow through the blood to the tumor, to be transported through the capillary wall (extravasation), to diffuse within the tissue and to bind the target receptor at the cell surface.[55]

A solid tumor environment poses unique challenges regarding the use of mAbs-based therapies. Limited extravasation and translocation through tumor interstitium, heterogenous blood supply and high pressure within the tumor tissue may limit diffusion of ADCs to low perfused areas.[56] A further factor limiting the tumor uptake of an ADC is the "antigen barrier effect". The high binding affinity for the target antigen which characterize antibodies, and the target antigen expression near the blood vessels can lead to the rapid trapping and accumulation of the ADC in the perivascular area (**Figure 8**).[57] Rudnick *et al*. compared the tumor uptake and penetration of four different anti-HER2 antibodies with a range of affinities for the same antigen epitope. It was found that antibodies with moderate affinity provided the highest accumulation in the tumor, in comparison to the highest affinity antibody. The tumor penetration of the antibody with the lowest affinity (K_d= 270 nM) was approximately > 80 μm, while for the antibody with the highest affinity (K_d= 0.09 nM) was limited to an average distance from the nearest blood vessel of < 40 μm.[58]

The result is a very low level of total ADC typically reaching the solid tumor. Dosimetry studies with radiolabeled mAbs in cancer patients have demonstrated that the tumor uptake ranges from 0.003% to 0.1% of injected dose per gram (ID/g) of

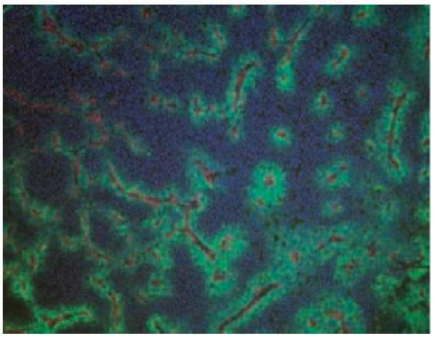

Figure 8. Trapping of Trastuzumab (13) in the proximity of blood vessels. Microscopic image of tumor tissue after Trastuzumab-FITC conjugate injection. Trastuzumab-FITC conjugate is stained in green, tumor blood vessels and nuclei are stained in red and blue, respectively. Adapted from *Cancer Res*., Copyright 2007, *67*(1), 254-261, Dennis M. S. *et al*. Imaging Tumors with an Albumin-Binding Fab, a Novel Tumor-Targeting Agent , with permission from AACR.

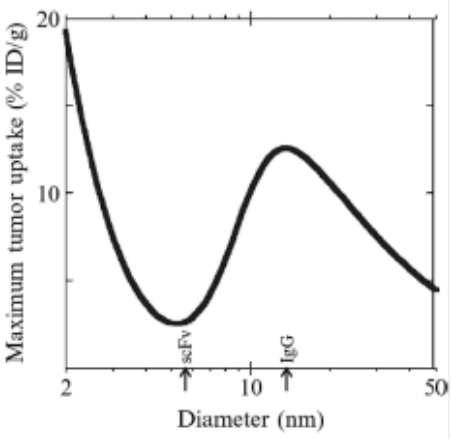

Figure 9. Predicted maximum tumor uptake against size of the targeting agent. Parameters used for the predicted maximum tumor uptake against targeting agent´s size were appropriate for HER2 binding molecules with K_d= 1 nM and labeled with ^{99}Tc. Readapted from *Methods Enzymol. 503*, Wittrup K. D. *et al*., Practical theoretic guidance for the design of tumor-targeting agent, 255-268, Copyright 2012, with permission from Elsevier.

tissue.[59]

However, the tumor uptake is the result of two opposite trends, i.e. extravasation and systemic clearance. According to the model developed by Wittrup *et al*., that predicts the tumor uptake dependance on molecular size, a local optimum is represented by agents with a size similar to IgG molecules (**Figure 9**).[60] Although it has been experimentally proved that extravasation rate drops with increasing molecular size, this effect is partially compensated for by the long systemic circulation of large molecular agents. ADCs have circulation times up to several days. For example, the FDA approved Adcetris ($M_r \approx 150\ 000$) has a half-life of 4-6 days before being cleared from circulation. This is a consequence of the reduced filtration rates through the kidney glomerular barrier, and the neonatal Fc receptor (FcRn) recycling process.[54] These factors contribute to the longer circulation times of the ADCs providing prolonged conjugate exposure to the target tissue and more absolute antibody delivered to the tumor site. However, the advantage in terms of tumor uptake provided to ADCs by longer circulation time can be negatively counterbalanced by the increased chances of premature drug release and consequent systemic drug distribution (**Figure 10**).[57]

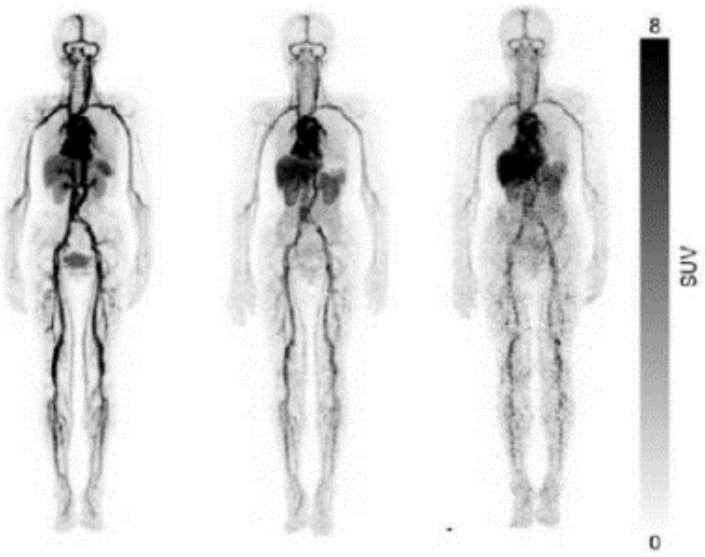

Figure 10. Microscopic distribution of ^{64}Cu-DOTA-Trastuzumab in breast cancer patients (1, 24 and 48 h) after intravenous administration. The majority of the injected antibodies do not reach its target *in vivo*, but virtually all molecules accumulate (at least transiently) in execretory organs. SUV: standardized uptake value. This research was originally published in *JNM*. Tamura, K. *et al*. *J. Nucl. Med*. 2013, 54(11), 1869-1875. © SNMMI.

Formats in the size range of antibody fragments, like scFv, Fabs and the like, reside in the so-called "death valley" (**Figure 9**). The molecular size range of these agents (e.g. Fab ~ 2.9 nm, 48 kDa) prevents them from rapidly extravasating into tumor, while inducing rapid renal clearance from circulation thus, preventing sufficient accumulation into tumor site.[60]

While agents with a hydrodynamic radius < 5 nm are predicted to penetrate tumor more rapidly because of faster diffusion and extravasation, they need high affinity (K_d ~ 10 nM or lower) to be retained in the tumor, as small unbound molecules can easily be cleared from tumor through intravasation. On the contrary, antibodies can achieve similar retention at lower affinity

(ranging from 10^{-8} to 10^{-6} M) because larger unbound molecules intravasate slowly and those ones with moderate affinity are able to bind repeatedly and remain in the tumor.[60]

1.6.2 Immunogenicity and safety profile

In biologic drug development an important aspect to consider is the risk of eliciting an immune response through the production of anti-drug antibodies (ADAs) with a potential impact on the pharmacokinetics, efficacy and safety drug profile.

Large-sized targeted drug conjugate, such as ADCs can often induce immune responses. ADAs may develop against the protein component itself, the linker and/or the linker-drug moiety.

Divergence of primary structure and glycosylation pattern from the human counterpart may account for the immune response to the therapeutic protein. The linker and/or the linker-drug moiety can act as haptens once conjugated to a mAb, determining immune responses. The formation and internalization of immune complexes by nontargeted tissues can result in significant toxicity.

Furthermore, the hydrophobicity of commonly used cytotoxic drugs can induce the formation of aggregation-prone regions increasing the risks of immunogenicity.[61]

When an immunogenic response takes place, increased blood clearance and reduced exposure are generally observed, thereby compromising the efficacy of the biotherapeutic.[62]

Small-molecule drug conjugates are usually non-immunogenic. [54]

Severe side effects need to be limited if concentrations required for efficacy need to be obtained in patients. In this perspective, formats smaller than mAbs can make the difference. Lack of the Fc domanin reduces cross-reactivity with Fc receptors-expressing normal cells and lower plasma exposure limits toxicity to non-targeted tissues. Overall, this can help to improve the therapeutic window which needs to be 10-fold higher for solid tumors than for haemotological indications to drive the penetration deep in the tumor.[60]

Taken together, these considerations suggest that a novel class of targeted therapeutics consisting of a small ligand with homing properties conjugated to a potent cytotoxic payload through a linker, known as Small Molecule Drug Conjugates (SMDCs), may overcome some of the limitations associated to ADCs. Indeed, SMDCs are expected to extravasate more rapidly reaching the targeted site, to be non-immunogenic and easier to manufacture.

1.7 Linker

At the basic level, linkers provide functional handles for tethering the targeting agent to the drug payload.

Additionally, fine tuning of the linker chemistry allows to optimize the pharmacokinetic and

pharmacodynamic properties of the targeted conjugate. Critical aspects of the linker chemistry are related to the physical properties of the linker itself and to the mechanism of drug release.

1.7.1 Hydrophilicity

Modulation of the linker hydrophilicity is generally necessary to compensate for the hydrophobicity of the most commonly used cytotoxic drugs. Enhancing the overall hydrophilicity can increase the effector solubility and reduce the nonspecific adsorption of low molecular weight drug conjugates to nontargeted tissues. Examples of such linkers are PEGs (polyethylene glycol) of different lengths, short peptide sequences or peptidoglycans, which allow to modulate the conjugate hydrophilicity without compromising the plasma stability and/or raising immunogenic responses. [63]

1.7.2 Linker cleavability

Non-cleavable linkers require degradation of the drug conjugate within lysosomes after internalization to release the active drug. Therefore, when a drug conjugate with a non-cleavable linker is designed, differences in potency between the drug itself and the conjugate metabolites must be taken into consideration.
The main advantage of incorporating an alkyl or a polymeric non-cleavable linker into a drug conjugate is the higher stability in plasma in comparison to many cleavable linkers.[64]
Non-cleavable hydrophilic linkers are generally preferred to overcome multi-drug resistance issues. In this case, the linker anchored to the drug payload will confer resistance to the efflux pumping and will improve the overall efficacy as long as it does not negatively impact the drug potency.

When the drug payload must be released inside the cell in order to interact with its molecular target, incorporation of a cleavable linker is the elected strategy. For a targeted conjugate to be selective and potent, the linker employed should possess the following two key properties: 1) high stability in circulation to avoid off-target payload release, and 2) allow efficient payload release inside the target cell.

Reducible cleavable linkers

Disulfide linkers (**Figure 11a**) rely on the difference in reduction potential between intracellular compartments and plasma. Reduced glutathione inside the tumor cells is significantly higher than in normal cells. Tumor cells also present enzymes from the disulfide isomerase family, which can contribute to cleave disulfide bonds in the cellular compartments.

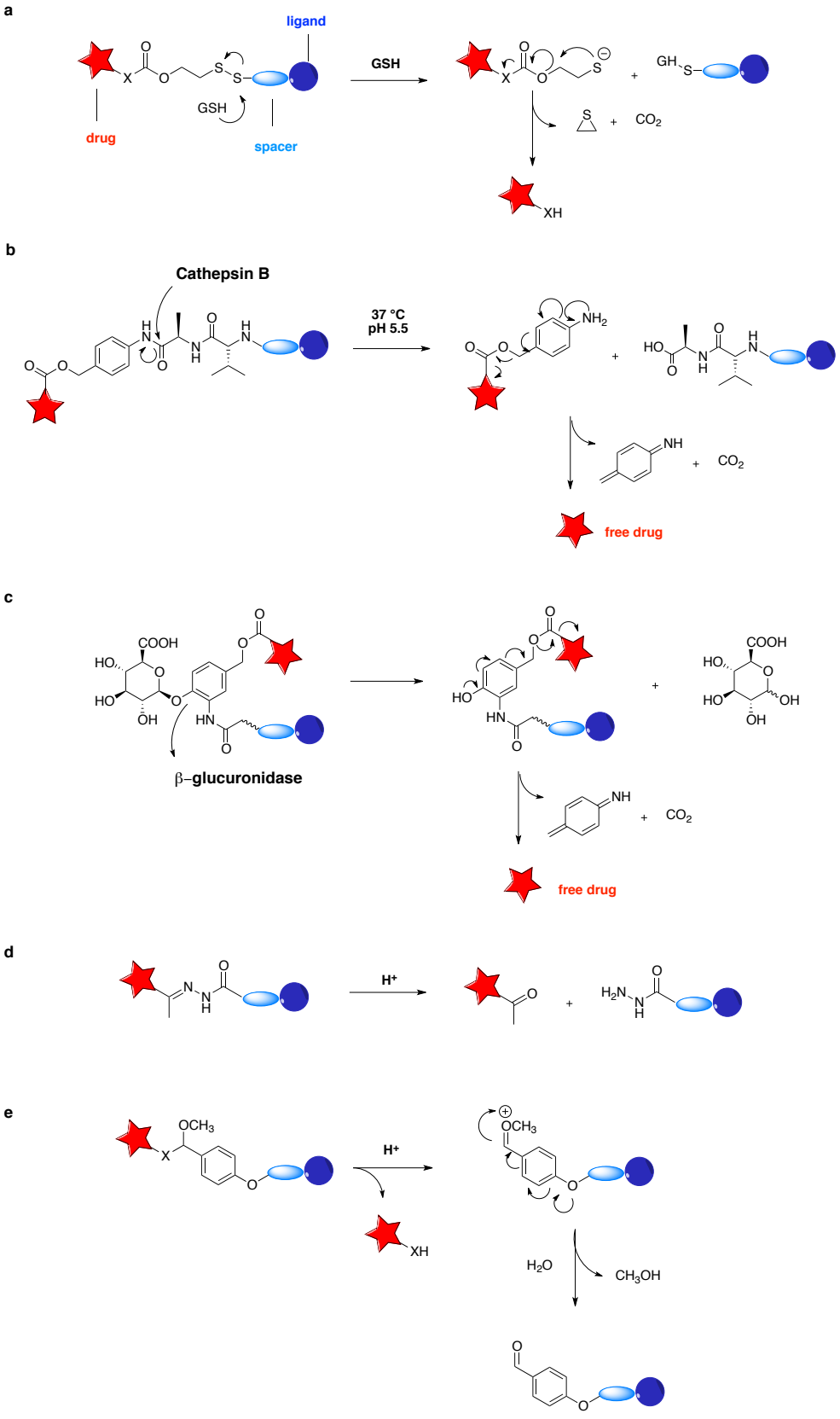

Figure 11. Common strategies for the intracellular drug release. a) The reduction of a disulfide bond by excess of intracellular reduced glutathione (GSH) triggers the release of the unmodified drug. **b, c)** The lysosomal enzymes cathepsin B or β-glucuronidase can initiate the drug release by cleaving a pepide linker (in this case valine-alanine) or a sugar linker, respectively. **d, e)** The high intracellular concentration of protons within some endosomal compartments (for instance, lysosomes) can induce the drug release by cleaving the high-pH-sensitive bridge (for example, hydrazones **d** or acetals **e**).

For this reason, disulfide bonds are expected to be more stable in circulation and interstitial fluids than inside the target cell.[65]

Enzymatic cleavable linkers

Unlike chemically sensitive linkers, enzymes cleavable linkers are designed to be hydrolized by enzymes recognizing specific peptide sequences or carbohydrate patterns, which are abudant in the lysosomal compartments. The pool of enzymes in the intracellular compartments is usually different from those in the blood circulation and some of these enzymes are even upregulated or activated inside tumor cells, like cathepsins or β-glucoronidase. These differences can be exploited for the selective drug release inside the target cells (**Figure 11b** and **c**).[65]

Acid-sensitive linkers

Acid-sensitive linkers, like hydrazone or acetals (**Figure 11d** and **e)**, are designed to be stable at the neutral pH of the blood circulation and undergo hydrolysis at the increased acidic conditions of the cellular compartments. However, in clinical studies this linker type has been associated to the non-specific release of the free drug.[65]

The instability of the hydrazone linker and the premature drug release have been supposed to been the primary cause behind the poor efficacy of Mylotarg and its narrow therapeutic window.

1.8 Cytotoxic payloads

One of the main reason for the clinical failure of the early ADCs was the low potency of the cytotoxic payload. Taking into account that only 1-2% of the administered ADC dose will ultimately reach the intracellular target, the intracellular concentration of the cytotoxic drug is rather low.

Hence, highly potent cytotoxic drugs with an IC_{50} in the picomolar range have been generally the choice in second generation ADCs and SMDCs design.[66]

The toxic payload should be small in size to reduce the risk of immunogenicity, and allow derivatization with the linker without loss of potency.[54]

In the selection of the optimal drug payload a second biological aspect to consider is the drug susceptibility to drug efflux mechanisms in order to avoid occurence of total drug resistance in those tumors that upregulate drug efflux transporters.

Acceptable aqueous solubility and stability as conjugate in aqueous formulations are important chemical requirements for a toxic payload in order to prevent any aggregation or precipitation

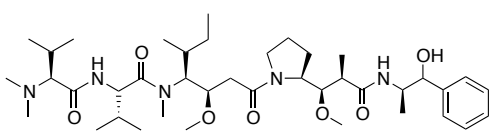

MMAE (dolastatins) (**14**)
Tubulin polymerization inhibition

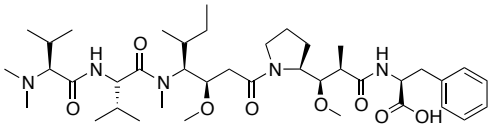

MMAF (dolastatins) (**15**)
Tubulin polymerization inhibition

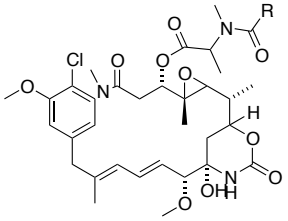

DM1 (R= CH_2CH_2SH) (maytansinoids) (**16**)
DM4 (R= $CH_2CH_2CH(CH_3)_2SH$) (**17**)
Microtubule polymerization inhibition

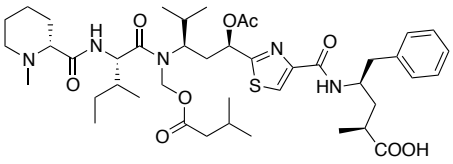

Tubulysin D (tubulysin) (**18**)
Microtubule polymerization inhibition

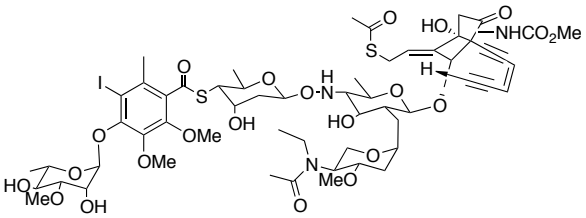

Calicheamicin (calicheamucin) (**19**)
DNA cleavage

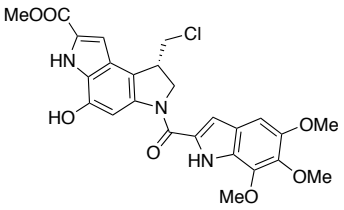

Duocarmycin SA (duocarmycins) (**20**)
DNA cleavage

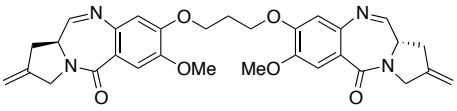

SGJ-316 (pyrrolobenzodiazepines) (**21**)
DNA-alkylation

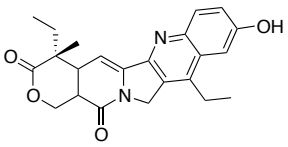

SN-38 (campothecins) (**22**)
DNA-TopI inhibition

Figure 12. Structure and mode of action of some of the most cytotoxic compounds currently used as payload in ADCs and SMDCs.

issues.[67] Interestingly, two-thirds of the ADCs and most of the SMDCs currently undergoing clinical trials are based on the wide class of antimitotic agents which are usually too toxic to be used as drugs in the unconjugated form: auristatins (monomethyl auristatin E (MMAE) **14** and MMAF **15**, **Figure 12**), which are synthetic derivatives of dolastatin-10 (**9a**, **Figure 3**); maytansinoids, i. e. DM1 (**16**, and DM4, **17**, **Figure 12**), derived from maytansine (**8**, **Figure 3**);[68] and tubulysins (**18**, **Figure 12**), peptides isolated from myxobacteria, which induce cell apoptosis by inhibiting microtubule polymerization. However, antimitotic agents are still far from ideal drug payloads, since they often fail to completely eradicate solid tumors and may lead to onset of resistance and toxicity issues.[69]

A second class of clinically validated drug payloads are the calicheamicin (Mylotarg®, **19**), and duocarmycin derivatives (**20**), that binds the minor groove of DNA causing DNA damaging and thus, inducing cells death at concentration in the picomolar range (**Figure 12**).

Novel more potent cytotoxic compounds currently under investigations are:

- *pyrrolobenzodiazepine* (PDB) dimers (**21**, **Figure 12**), naturally occuring antitumor antibiotics that bind the minor groove DNA inducing lethal lesions. PDB dimers have been reported not to show cross-resistance with conventional chemotherapeutics;
- *campothecin analogues*, like the irinotecan active metabolite SN-38 (**22**, **Figure 12**), a DNA-TopI inhibitor three orders of magnitude more potent than the parent drug.[70]
- *α-amanitin*.

1.8.1 α-Amanitin

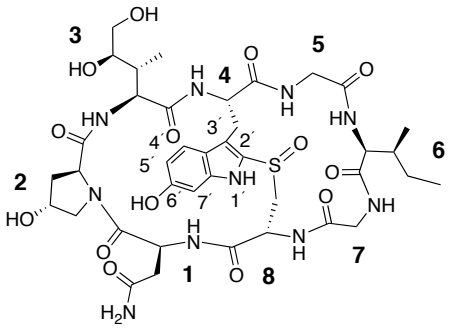

Figure 13. Structure of α-amanitin. α-Amanitin, a bicyclic octapeptide, is the main component and the most investigated of the structurally-related amatoxins.

α-Amanitin (**Figure 13**) belongs to a group of nine structurally-related compounds, known as amatoxins. They were isolated for the first time in 1941 by Wieland and Hallermeyer from the death cap mushroom *Amanita phalloides* (**Figure 14**).[71]

Amatoxins are the most dangerous natural toxins responsible for approximately 95% of mushroom poisonings worldwide. Ingestion of *Amanita phalloides* mushroom is life-threatening causing hepatic failure and kidney damages.[72]

Amatoxins are produced by ribosomal synthesis followed by post translational modifications, such as cyclization and hydroxylation of some amino acids.[73] The common structural motif is a bicyclic octapeptide backbone cross-linked between the Trp^4 and Cys^8 residues through a sulfoxide moiety.

Among all amatoxins, α-amanitin is the main component and the most investigated one. The molecular targets of α-amanitin are the RNA polymerase II and III (RNAP II and III), with the RNAP II being the most sensitive. The enzyme catalyzes the transcription of DNA into precursors of mRNA in the eukaryotic cells.[74] Calf tymus polymerase II has been shown to bind α–amanitin very tightly with a K_d of 3.1 x 10^{-9} M and a complex-dissociation half-life of 100 h at 0 °C. [75]

Figure 14. Death Cap mushroom *Amanita phalloides*. *Amanita phalloides* is the Amanita species with the highest toxin content by weight.

As revealed by the crystal structure of the yeast RNAP II in complex with α-amanitin solved by Bushnell *et al*., the

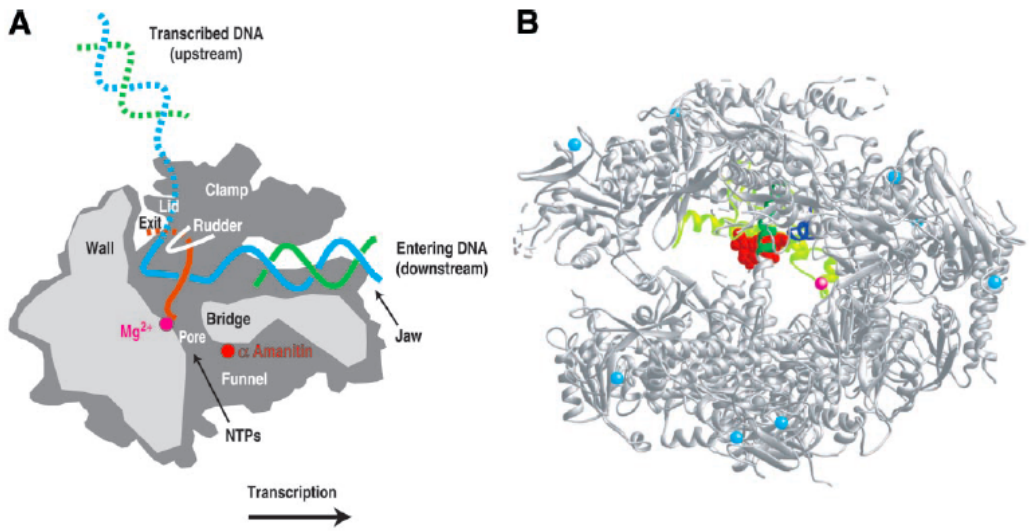

Figure 15. α-Amanitin bound to RNAP II. A) Cutaway view of RNAP II-transcribing complex showing α-amanitin location (red dot) in relation to the nucleic acids and enzyme functional elements. **B)** Ribbon representation of the RNAP II structure (top view): zinc atoms (blue), active site magnesium (magenta), region of Rbp1 around α-amanitin (funnel in light green and bridge helix in dark green), region of Rbp2 around α-amanitin (dark blue) and α-amanitin (red). Reprinted from Bushnell, D. A.; Cramer, P. and Kornberg, R. D. *PNAS* 2002, *99*(3), 1218-1222. Copyright 2002, National Academy of Sciences.

binding site of α-amanitin is located beneath the bridge helix across the cleft between the two largest RNAP II subunits, Rbp1 and Rbp2 (**Figure 15**). Several hydrogen bonds are involved in the interaction, including key H-bonds to the hydroxyproline **2** and 4,5- dihydroxyisoleucine **3** side chains.[76]

Interaction of α-amanitin with the bridge helix reduces its flexibility and constrains the movement required for the translocation of the polymerase along the DNA backbone. This slows down the translocating rate from several thousands to a few nucleotides per minute, leading to the cell death.[77] Nguyen *et al*. have suggested that binding to RNAP II triggers degradation of the catalytic subunit Rpb1, resulting in the irreversible inhibition of RNAP II. However, the Rbp1 degradation mechanism has still to be identified.[78]
α-Amanitin binds to the RNAP II with a stoichiometry of 1:1. It has been estimated that the copy number per cell of RNAP II is approximately corresponding to a concentration of 10^{-8} M. Therefore, the α-amanitin concentration in the cytoplasm required to slow down transcription is rather low (approx. 10^{-8} M).[79]

Liver injury is usually the major lesion which occurs in men upon α-amanitin intoxication. Infact, α-amanitin is rapidly eliminated from the blood and distributed to the liver and the kidneys, where it may accumulate. In the liver, accumulation of α-amanitin causes apoptosis and necrosis of the hepatocytes. The organic anion transporting polypeptide 1B3 (OATP1B3), exclusively expressed on the sinusoidal membrane of human hepatocytes, has been identified as the main human uptake transporter for amatoxins (**Figure 16**).[80, 81]

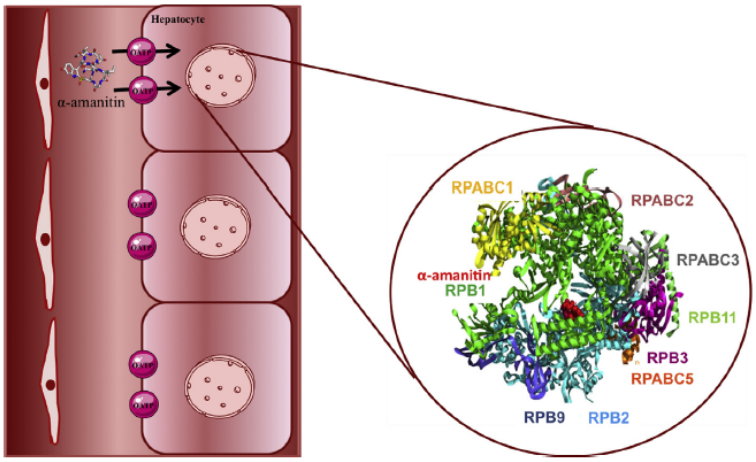

Figure 16. Simplified model of α-amanitin uptake in the human hepatocytes. Uptake of α-amanitin in the human hepatocytes is mediated by the organic anion transporting polypeptide (OATP1B3) expressed on the sinusoidal membrane of human hepatocytes. Once in the hepatocytes, α–amanitin inhibits the RNAP II activity leading to nucleoli fragmentation. Reprinted from *Food Chem. Toxicol. 86*, Garcia, J. *et al*. *Amanita Phalloides* poisoning: Mechanisms of toxicity and treatment, 41-55, Copyright 2015, with permission from Elsevier.

Nephrotoxicity has been also reported. Studies in mice have demonstrated that the appearance of kidney toxicity is dose-dependent and largely affects the proximal convoluted tubules.
Therefore, it has been postulated that nephrotoxicity is probably due to the filtration of α-amanitin by glomeruli and subsequent reabsorption of the toxin from preurin in the cells of proximal convoluted tubules, where it accumulates. First lesions appear within 15-30 min and rapidly evolve towards extensive necrosis 72 hours after administration.[82]

The unique mode of action (MoA) of α-amanitin is particularly promising for application to cancer therapy.
Most cancer-related deaths are due to secondary cancers occuring in post-therapy patients. Cancer persistance and resurgence are supposed to be related to the presence of a large fractions of quiescent tumor cells, which are out of the cell cycle and not-dividing, but fully able to return to the cell cycle. Quiescent tumor cells do not respond to treatment with conventional anticancer drugs. However, since they mantain active a basal transcriptional machinery to mantain transcripts and proteins necessary for cell survival,[83] α-amanitin addresses the ability to target both actively proliferating and quiescent tumor cells.
Applicability of α-amanitin in cancer therapy is further supported by a phenomenon called "collateral vulnerability". A study published in 2015 by Liu and co-workers[84] showed that hemizygous deletion (deletion of one of the two gene copies) of TP53, a well-known tumor-suppressor gene, is common in human cancers and often encompasses neighboring genes essential for the cell survival. The study revealed that *POLR2A* gene, which encodes the largest subunit of RNAPII is often co-deleted with TP53 in human colorectal cancers. Hemizygous deletion of *POLR2A* is tightly associated with decreased abudance of RNAP II rendering cancer cells more vulnerable to α-amanitin inhibition.

1.8.1.1 α-Amanitin based ADCs

Despite the strong potential of α-amanitin in cancer therapy, its high liver toxicity (estimated oral LD_{50} in humans 0.1 mg/kg body weight)[85] hampered its clinical application as free toxin. However, the toxicity issue can be overcome by conjugation to monoclonal antibodies.
The great advantage of using α-amanitin as ADC payload is its water-soluble structure, which facilitates conjugation reactions and reduces tendency of the resulting immunoconjugates to aggregate, even at high DAR. The hydrophilic nature of α-amanitin preserves the activity in MDR-expressing cells, being a poor substrates for the MDR transporters. Accumulation in non-targeted tissues of α-amanitin or any derivative thereof released from dying tumor cells after ADC breakdown is unlikely, as mammals excrete amatoxins very fast in the urine (half-life in mice approx. only 30 minutes).[73]

A chimeric anti-epithelial cell adhesion molecule (EpCAM) antibody (chHEA125) conjugated to α-amanitin (chiHEA125-Ama, **23**; **Figure 17**) via glutarate linkage and dicyclohexylcarbodiimide cross-linking chemistry showed *in vitro* activity in picomolar range against a variety of adenocarcinoma cell lines. Complete tumor regression was observed in 90% of mice bearing pancreatic xenografts at doses corresponding to 100 µg/kg of α-amanitin.[73]

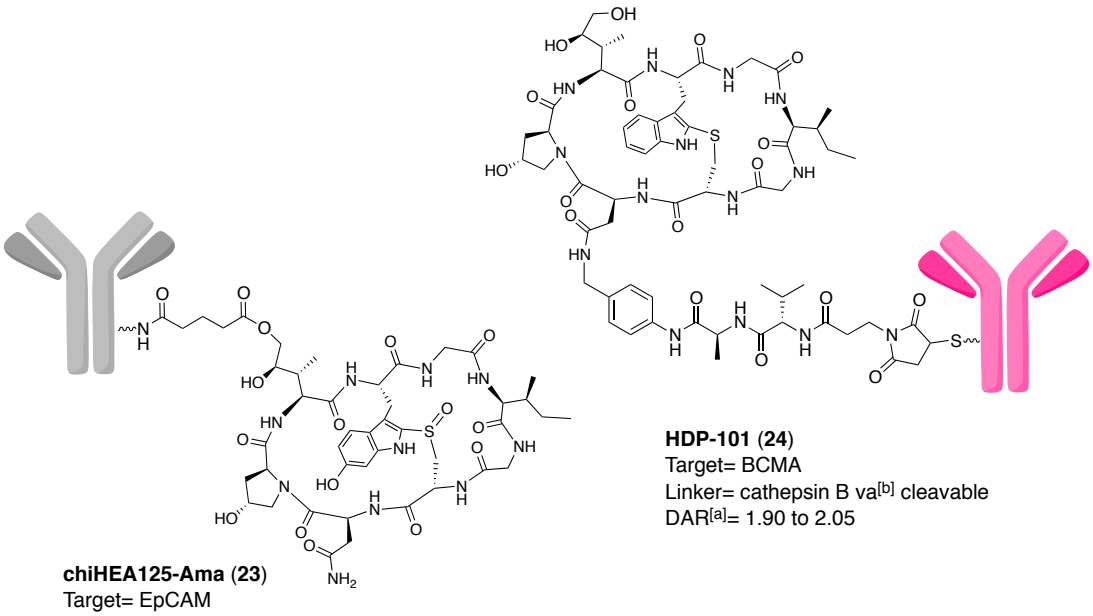

Figure 17. Structure, target, linker type, and DAR of selected α-amanitin-based ADCs. [a] DAR= drug to antibody ratio; [b] va= valine-alanine.

Heidelberg Pharma Research GmbH is currently investigating an α-amanitin-based ADC toward the anti-B-cell maturation antigen (BCMA). A synthetic derivative of α-amanitin is conjugated to the cysteine residues present within the anti-BCMA antibody thiomab via a

valine-alanine (va) cathepsin B cleavable linker (HDP-101, **24**; **Figure 17**). Initial preclinical studies revealed promising data. The conjugate showed strong *in vitro* potency and led to complete tumor remission in mouse models for multiple myeloma (MM) even at very low doses (0.1 mg/kg). Tolerability studies in non-human primates identified a favourable therapeutic window. A first-in-human trial with HDP-101 is expected to start in the second half of 2020.[86]

1.8.1.2 α-Amanitin based SMDCs

To date, the α-amanitin-based SMDCs described in literature target almost exclusively the cell-surface receptor $\alpha_v\beta_3$ integrin widely expressed on the tumor vasculature of several human cancers.

Bodero *et al*. conjugated α-amanitin to a cyclo[DKP-isoDGR] integrin ligand via a va cleavable linker (**25**, **Figure 18**). The conjugate failed to demonstrate selective *in vitro* cytotoxicity against $\alpha_v\beta_3$- expressing cells. Only a slight increase in the cytoxic activity in comparison to the unconjugated toxin could be detected. However, the authors argued that this might be due to the unspecific conjugate uptake mediated by integrins other than the target.[87]

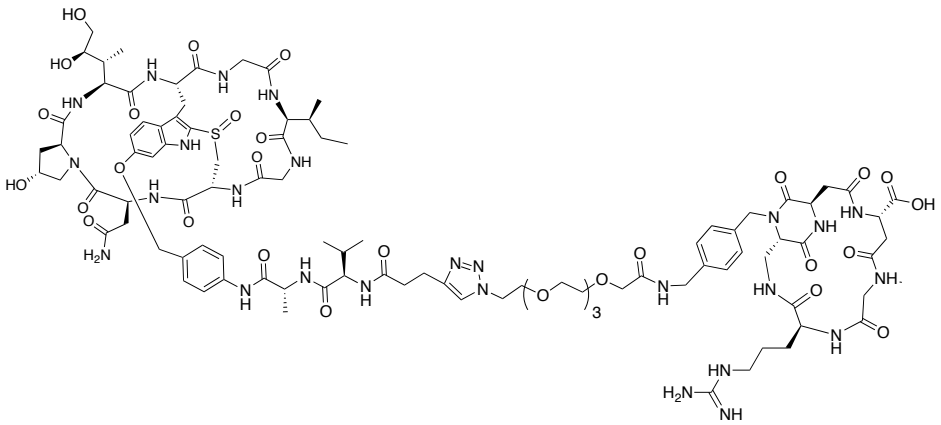

cyclo[DKP-isoDGR]-PEG-4-Val-Ala-α–amanitin (25)
Target= $\alpha_v\beta_3$ integrin
Linker= cathepsin B va[a] cleavable self-immolative

Figure 18. Structure of an α-amanitin-based SMDC targeting the integrin $\alpha_v\beta_3$. α-Amanitin is conjugated to a synthetic integrin ligand, the cyclo[DKP-isoDGR] via a cathepsin B clevable linker. [a]va= valine-alanine.

In another example, Perrin and co-workers coupled via copper-catalyzed azide-alkyne cycloaddition (CuAAC) the cycloRGD integrin ligand cRGDfK to synthetic analogues of α-amanitin. The resulted conjugates, bearing either a stable or a reducible linker, were only partially more effective at cell killing than α-amanitin. As postulated by the authors, increased cytotoxicity of the conjugates was likely due to proximity of the toxin to the cell surface and subsequent entry through a fluid-phase endocytic pathway not related to the integrin expression.[88]

1.9 Target antigen

The design of a successful targeted drug conjugate is based on a thoughful combination of three main components: the targeting agent, the linker, and the drug payload. A fourth equally important factor is the careful selection of the target antigen.

It is widely accepted that the target antigen should be highly expressed on tumor cells with ideally limited or no expression on normal tissues. A threefold overexpression on cancer cells is generally considered sufficient to reduce risks of on-target off-site toxicity. For example, T-DM1 (**13**, **Figure 6**) targets HER2 antigen, whose expression level on HER2-positive cancer cells is two magnitude orders larger than on other tissues.[68]

Despite the experimental evidence suggests that there is no correlation between the antigen expression level and the efficacy, studies on lymphoma and prostate cancer have shown that a minimum threshold value of antigen expression is required. *In vitro* cytotoxicity studies of an anti-PSMA auristatin conjugate (PSMA ADC, Progenics/Seattle Genetics) proved that 10^4 receptors per cell serve as threshold level for selective cytotoxic activity.[89]

Homogenous antigen expression, although preferred, is not a strict requirement. Non-homogenous expression can be addressed by the so-called "bystander effect", which exploits the ability of certain payloads or payload metabolites to diffuse out of the cell, after being

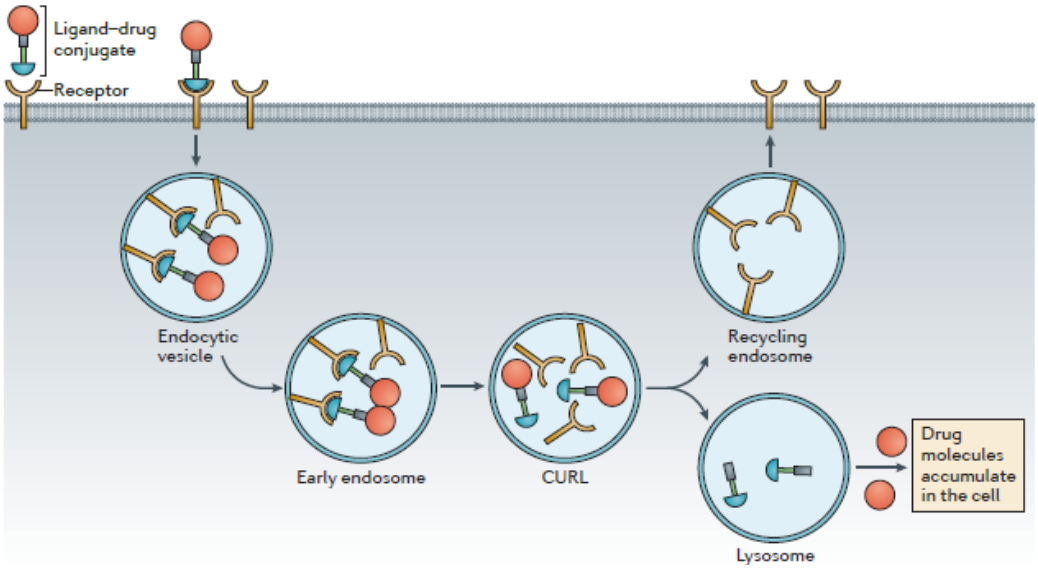

Figure 19. A targeted drug-conjugate entry into the cell. Upon endocytosis, drug-conjugates are trafficked through different cellular compartments, depending on the receptor exploited for the conjugate internalization. The most common compartmemts the conjugate is trafficked through include: early endosomes; compartments for uncoupling of receptor and ligands (CURLs), where the receptor may dissociate from the conjugate; recycling endosomes, which can deliver the internalized receptors back to the cell surface; lysosomes, where the receptor and the conjugate can be degraded. Reprinted by permission from Springer Nature Customer Service Centre GmbH: Nature Publishing Group, *Nat. Rev. Drug. Disc.*, Principles in the design of ligand-targeted cancer therapeutics and imaging agents, Srinivasarao, M. *et al.*, 2015.

released, and induce cell death to the antigen-negative neighboring cells.[90] It is worth to note that the most advanced ADCs in clinics and most of the approved ones are for hematological indications, which are usually characterized by highly homogenous antigen expression and frequently low antigen density.[91] In addition to these features, the target antigen should be accessible to the circulating agent on the cell surface (in the case of solid tumors) and well internalized by receptor-mediated endocytosis.

Following receptor-mediated endocytosis, the receptor-bound targeted agent will be trafficked to an intracellular compartment, such as an endosome, a compartment for uncoupling of receptor and ligand (CURL) or a lysosome. Upon dissociation within a CURL, receptor and drug may sort into separate compartments, allowing the receptor to be degraded or recycled back to the cell surface for another round of endocytosis (**Figure 19**). As the possibility for a drug-conjugate to be internalized depends on the availability of empty receptors on the cell surface, rate of receptors replenishment and internalization efficiency are other important parameters to take into account and they are largely determined by the type of receptor and cell. These parameters are actually crucial in defining the dosing frequency, as any drug administered more often than the receptors recycling rate will rise the risk of off-target toxicity due to rejection of drug by saturated targeted tissue.[54]

However, several studies have reported that even some non-internalizing antigen targeted ADCs can as well display significant efficacy, at least at preclinical level, by exploiting the above-mentioned bystander effect.[92]

Even though traditionally attention has been focused on antigens expressed on tumor cell surface, there is a growing interest in targeting antigens expressed in the tumor neovasculature, sub-endothelial extracellular matrix and in the tumor stroma.[93, 94]

Besides the variety of receptors exploited in the field of ADCs, the number of receptors targeted by SMDCs is quite limited. The most targeted are: the folate receptor, the somatostatin receptor, the bombesin receptor, the carbonic anhydrase IX (CAIX) and the prostate-specific membrane antigen (PSMA).[57, 63]

1.10 Prostate cancer (PCa): an unmet clinical need

Prostate Cancer (PCa) is the second leading cause of men cancer-related mortality with 1,276,106 new cases and 358,989 deaths occurred worldwide in 2018.[95]

Molecular hallmarks of PCa include aberrant signaling of androgen-receptor (AR), which is established as the primary oncogenic driver of growth and progression of PCa.
Clinically localized disease are usually treated with surgery or radiation. However, after these primary interventations, a subset of patients have a high risk of recurrence or development of locally advanced or metatstatic disease.
The mainstay therapy for patients who ultimately developed advanced, metastatic disease is based on targeting the AR cascade via androgen deprivation, antiandrogens and neoadjuvant chemotherapy. However, after rapid initial responses, patients within 6 to 12 months stop responding to androgen ablation therapy and progress to metastatic castration-resistant prostate cancer (mCRPC) correlated to a median survival of 9 to 12 months. The main treatment modality in mCRPC is represented by the taxane-based chemotherapeutics, Taxotere™ (docetaxel) and Jevtana™ (cabazitaxel).[96] Although prolonging the overall patients' survival, systemic toxicity due to lack of target specificity may narrow the therapeutic window and lead to severe side effects which affect the patients' quality of life.

Against this background, there is a growing effort in developing therapies targeting tumor-associated antigens for the treatment of mCRPC. Amongst cell-surface molecules, PSMA is the only clinically validated biomarker of PCa and it is currently the most investigated target antigen for the development of antigen-targeted therapies.

1.10.1 Prostate-Specific Membrane Antigen (PSMA)

Structure

Prostate-Specific Membrane Antigen (PSMA), also known as glutamate carboxypeptidase II (GCPII), *N*-acetyl-α-linked acidic dipeptidase I (NAALAdase I), or folate hydrolase 1 (FOLH1), is a 750-aminoacid type II transmembrane glycoprotein. As a class II membrane protein, the structure consists of a short cytoplasmic amino terminus (1-19aa), a membrane-spanning segment (20-44aa) and a large extracellular domain (45-750aa). The crystal structure of the extracellular domain reveals a highly symmetric glycosylated homodimer which folds in three distinct domains: the protease domain, the apical domain and the C-terminal domain (**Figure 20**). In a large cavity at the interface of the domains is located the active site. It features two zinc ions bridged by a catalytic water molecule which is involved in the hydrolysis of the peptide bonds.
Co-crystal structures of GCPII in complex with the inhibitor GPI-18431 or the substrate N-acetylaspartylglutamate (NAAG) (**Figure 21**) revealed details of the binding site which consists of two pockets designated as S1 and S1'.[97] The S1' (pharmacophore) pocket is fine-tuned for the recognition of the C-terminal L-configurated glutamate moieties. Because of its importance

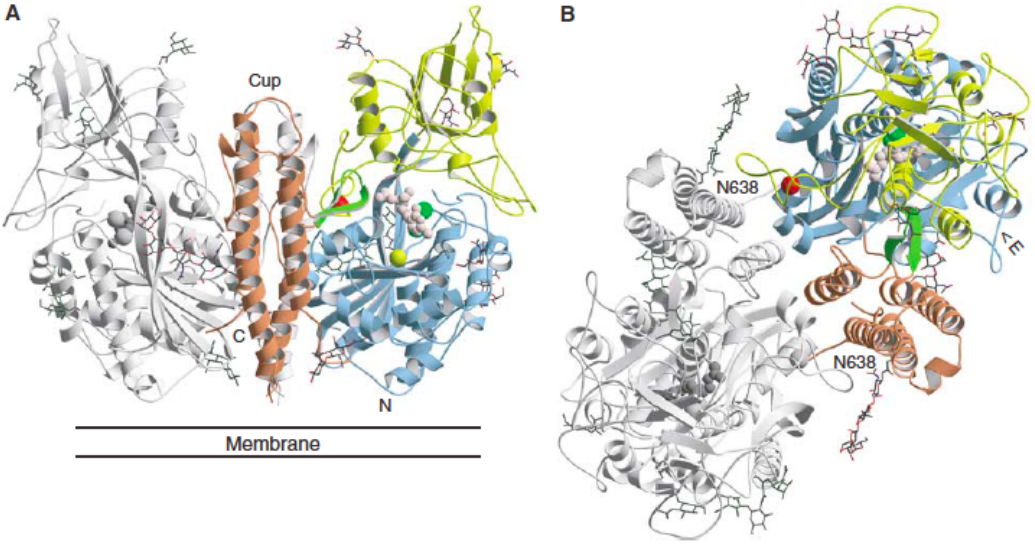

Figure 20. Three-dimensional structure (A and B) and surface representation of the ~20Å deep funnel leading to the catalytic site (C) of PSMA. A, B) One subunit is shown in grey, while the other is colored according to organization in domains. Dinuclear zinc cluster in the active site is indicated by dark green spheres, the Ca^{2+} ion by a red sphere near the monomer-monomer interface, and the Cl^{-} ion by a yellow sphere. The glutarate sensor is shown in light green. **C)** Yellow, Zn^{2+} ions. Inhibitor GPI-18431 in stick model. Readapted with permission from Mesters, J. R. *et al*. *EMBO J*. 2006, *25*(6), 1375-1384, Copyright 2006, John Wiley & Sons.

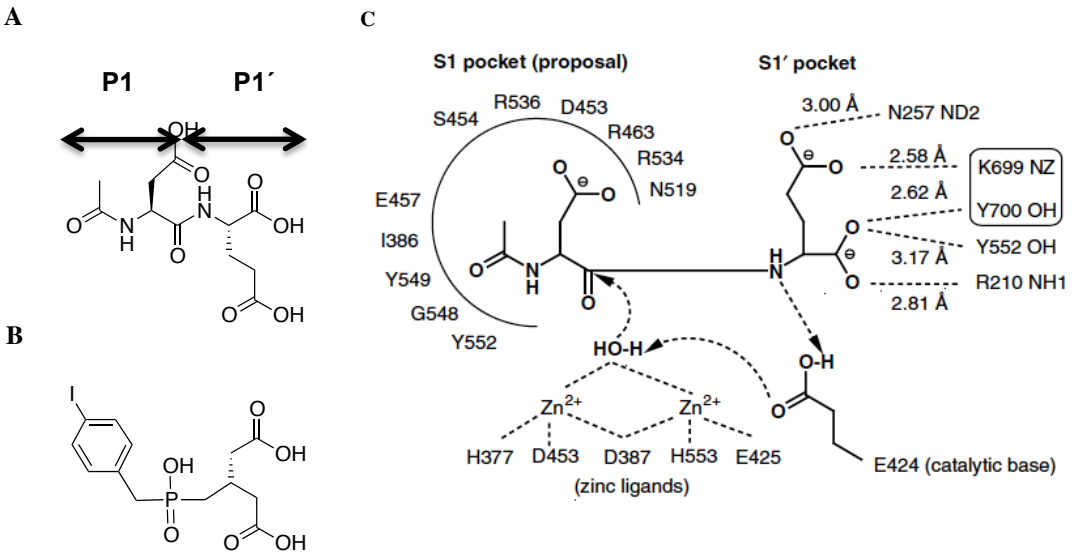

Figure 21. Structure for A) *N*-acetyl-L-aspartyl-L-glutamate (NAAG) B) (S)-2-(4-iodobenzyl-phosphonomethyl)-pentanedioic acid (GPI-18431) and scheme of the catalytic site, indicating the NAAG substrate as bound to the enzyme (C). Readapted with permission from Mesters, J. R. *et al*. *EMBO J*. 2006, *25*(6), 1375-1384, Copyright 2006, John Wiley & Sons.

in probing the S1' pocket for the presence or absence of the glutarate moiety, the loop carrying the side chains of Lys699 and Tyr700 is known as the "glutarate sensor". [97]

The main feature of the S1 pocket is the "arginine patch" composed of the arginine residues 463, 534, and 536 and implicated in the preferential recognition of negatively charged P1 residues of the ligand, as shown by the crystal structure in complex with the NAAG substrate (**Figure 20C**).[97] While the Arg534 is kept in a fixed position by interacting with the S1-bound chloride ion, both Arg536 and Arg 463 retain a certain flexibility which is likely responsible of less strict substrate specificity requirements within the S1 pocket.[98]

A ~20 Å deep narrowing funnel lined with hydrophobic residues that consitute the "S1 accessory hydrophobic pockets" runs from the surface to the active site.

In 2010 Zhang *et al*. reported on the serendipitous discovery of an additional arene-binding site at the entrance of this tunnel. The PSMA arene-binding site is formed from the indole group of Trp541, the guanidinium group of Arg511, and at the bottom of the cleft by Arg463 side chain. It was proved that this additional site can contribute through stacking interactions to enhance inhibitors' binding affinity.[99]

Expression and function

In physiological conditions, PSMA is expressed on prostate epithelial cells and some extra-prostatic tissues including kidneys (proximal tubules), nervous system glia (astrocytes), and small bowel (jejunal brush border). [100, 101]

In the nervous system glia, where PSMA has been recognized to be identical to GCPII, it catalyzes the hydrolysis of NAAG, one of the most abundant neurotrasmitters in the central nervous system (CNS), in *N*-acetylaspartate and glutamate, the major excitatory neurotransmitter in the CNS.

At the jejunal brush border, PSMA functions as FOLH1, allowing the release of the γ–linked glutamates from dietary poly-glutamated folates to be absorbed

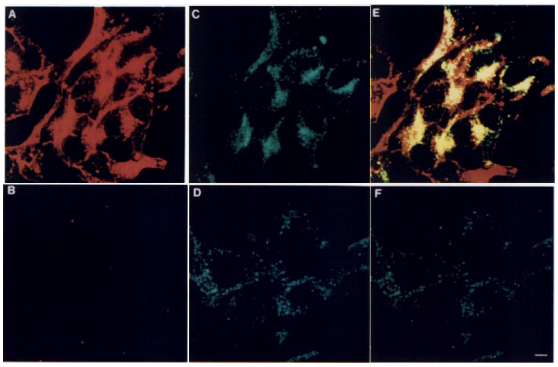

Figure 22. Confocal microscopy analysis of the anti-PSMA$_{extr}$ J591 antibody internalization. PSMA-positive LNCaP cells were incubated with mAb J591 and FITC-conjugated transferrin (**A**, **C** and **E**) or the anti-PSMA$_{intr}$ 7EC11.C5 and transferrin (an endosomal marker) conjugated to the fluorescent dye FITC (**B**, **D** and **F**) for 2 h and processed for IF. FITC-conjugated transferrin uptake is shown (**C** and **D**). Images A and C were merged to obtain image in E showing colocalization of J591 and FITC-conjugated transferrin in yellow. Images B and D were merged in F, in which only transferrin is seen because 7EC11.C5 neither binds nor internalized. Reprinted from *Cancer Res*. Copyright 1998, *58*, 4055-4060, Liu, H. *et al*., Constitutive and Antibody-induced Internalization of Prostate-specific Membrane Antigen, with permission from AACR.

and transported to the rest of the body.[102] The precise function of PSMA on prostatic epithelium and proximal renal tubules remains mainly unknown, but studies suggest that it is related to the folate reuptake in the kidneys and secretion of monoglutamated folates into the seminal fluid. [103] Unlike other prostate biomarkers, like prostate specific antigen (PSA), PSMA is a membrane bound protein, not shed in the circulation.[96]

PSMA undergoes constitutive internalization reflecting recycling of a structural protein through a plasma membrane location. The internalization rate is up to threefold enhanced in a dose-dependent manner by binding of a PSMA specific antibody (**Figure 22**), which may suggest a role for PSMA as transporter of a naturally-occuring ligand which is yet unknown.[104] The endocytic pathways of PSMA-antibody complex was recently identified by Liu *et al*.[105] as clathrin-mediated endocytosis, macropinocytosis, and clathrin-, calveolae-independent endocytosis.

1.10.1.2 PSMA: a validated target for PCa

Extensive PSMA expression has been described in the primary disease and the most common sites of metastases, namely bone and lymph nodes. Studies on human tissue specimens demonstrated that PSMA is 100- to 1000-fold overexpressed in nearly all PCas compared to normal tissues.[106]

PCa tissues show high level of PSMA enzymatic activity. *In vitro* studies suggest a correlation between the folate hydrolase activity of PSMA and the increased folate uptake by high-rate proliferating cells. Rapidly dividing-cells require an abudant supply of reduced folate for DNA synthesis, methylation (formation of methionine for polyamine synthesis), and cell division. Increased expression of PSMA may allow PCa cells to uptake folate for replication by deglutamating the poly-γ-glutamated folate released by the surrounding dead and dying cells,[107] thereby contribuiting to the development and progression of PCa.

Recently, Kaittanis *et al*.[108] have also demonstrated the role of PSMA in the activation of the tumor-supporting signaling cascade by PI3K via the metabotropic glutamate receptor (mGluRI), which co-localizes on the plasma membrane of PCa cells with PSMA. It has been suggested that PSMA contributes through its carboxypeptidase activity to the activation of mGluRI by releasing glutamate from glutamated substrates and vitamin B9.

PSMA expression has been also shown to correlate with disease severity. A study involving tissue specimens from 184 patients by Bostwick and co-workers showed an increase in PSMA staining from benign prostatic epithelium (69.5% cells positive) to high-grade prostatic

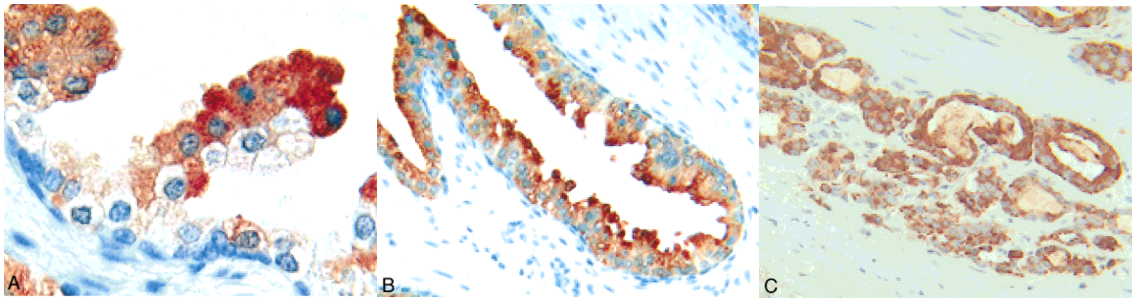

Figure 23. Immunoreactivity of PSMA in epithelial cell cytoplasm. A) Benign epithelium with heterogeneity in staining of the secretory cell layer; **B)** high-grade prostatic intraepithelial neoplasia with intense staining of virtually all secretory cells; **C)** adenocarcinoma, Gleason score 7, with intense staining in virtually every cell. Reprinted with permission from Bostwick M. D., D. G. *et al*. *Cancer* 1998, *82*(11), 2256-2261, Copyright 2000, John Wiley and Sons.

intraepithelial neoplasia (PIN; 77.9% of cells positive) to prostate adenocarcinoma (80.2% of cells positive) (**Figure 23**).[100]

In adenocarcinoma PSMA expression has shown to be associated with pathological stage and tumor grade with a strong expression in poorly-differentiated and metastatic tissues.

A variation in the pattern and cellular localization of PSMA has been also observed between normal prostate epithelium and primary and metastatic tumors. In contrast to a diffuse cytoplasmic PSMA positivity observed in healthy and benign tissues, a more prominent luminal positivity has been observed in poorly-differentiated primary tumors and metastatic tissues.[109]

As mentioned, in the context of targeted therapeutic approches for a successful therapy outcome strongly preferred is the homogenous expression of the membrane target, as any variations may limit access of the therapeutic agent to the target cells. In case of PSMA, it has been demonstrated that within 99.6% of PCa patients resulted positive to PSMA, 93.6% expressed PSMA in highly homogenous manner.[110]

An interesting finding is that PSMA is up-regulated under androgen-deprivation conditions. Initiation of androgen deprivation therapy induces early but temporary PSMA upregulation, downregulation upon prolonged treatment and, finally, overexpression in androgen-resistant

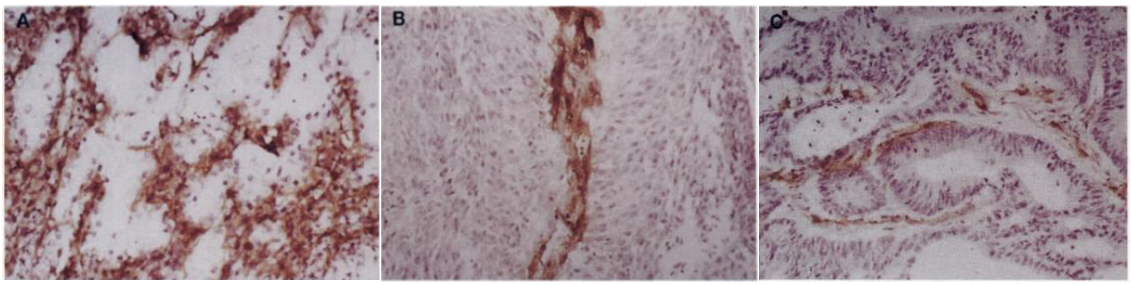

Figure 24. Examples of three different solid tumor types showing expression of PSMA by neovascular endothelium. Immunohistochemical reactivity of anti-PSMA J591 antibody to neovasculature of renal, (**A**); urothelial (**B**) and colon (**C**). Adapted from *Clin. Cancer Res*., Copyright ©1997, *57*, 3629-3634, Liu, H. *et al*., Monoclonal antibodies to the extracellular domain of Prostate-Specific Membrane Antigen also react with tumor vascular endothelium, with permission from AACR.

tumors. Upregulation of PSMA was first described in 1996 after culturing the androgen-sensitive human prostate adenocarcinoma LNCaP cells in androgen depleted media.[109]
Evans *et al*. reported an inverse relationship between AR and PSMA expression and that it can be assessed both *in vitro* and *in vivo* by PET (positron emission tomography) imaging.[111]

The relationship between androgen suppression and PSMA expresssion creates a state of "conditionally enhanced vulnerability", that means an enhanced tumor cell vulnerability to PSMA-targeted therapeutic agents increasing the overall quantity of agent delivered to tumor cells. Preclinical studies in castrate-resistant animal models showed a synergistic and enhanced anti-tumor response when castration therapy was combined with a PSMA-targeted ADC. This approach also improves the therapeutic window as normal tissues expressing low levels of PSMA are AR-negative. Therefore, this finding further supports the application of PSMA-targeted therapy in PCa treatment.[112]
PSMA is also discussed as target in anti-angiogenetic therapy, since it is ovrexpressed even on the neovasculature of several non-prostatic solid tumors, such as kidney, bladder, breast, lung, colon, and melanoma (**Figure 24**).

In PCa, PSMA expression is limited to malignant epithelial cells and PSMA is generally not expressed on neovasculature, with the exception of a few PCas. On the contrary, in case of non-prostatic tumors, PSMA expression, even within the same section, is limited to the luminal site of the new blood vessel endothelial cells, facilitating access for targeted agents.[96, 113]
PSMA expression on tumor vasculature suggests a role of PSMA in neoangiogenesis. Studies in PSMA-null animals have showed that modulation of β_1 integrin activation mediated by PSMA actually enhances endothelial invasiveness.[114] However, the exact role of PSMA in tumor angiogenesis has not yet completely understood.

1.11 PSMA-targeting technologies for PCa

1.11.1 PSMA-targeted ADCs

The involvement of PSMA in cancer and its well-established properties has raised the interest in the development of PSMA-targeted therapeutics.

The extensive exploration of tubulin inhibitors as ADC payloads for PCa has been supported by the fact that microtubule inhibitors (docetaxel and cabazitaxel) represent a cornerstone in PCa treatment.
Two PSMA-targeting ADCs exploiting tubulin inhibitors have been evaluated in clinical trials as treatment for patients with mCRPC.

MLN2704 (Seattle Genetics) is a deimmunized form of the $PSMA_{extr}$-targeting murine antibody J591 coupled to DM1 (ImmunoGen; **26, Figure 25**) through a methylated disulfide bond.
Poor response and severe neurotoxicity were reported in phase I/II clinical trial. The narrow .therapeutic window was identified as consequence of the rapid drug deconjugation occured in circulation, leading ultimately to suboptimal drug delivery to the targeted site.(115)

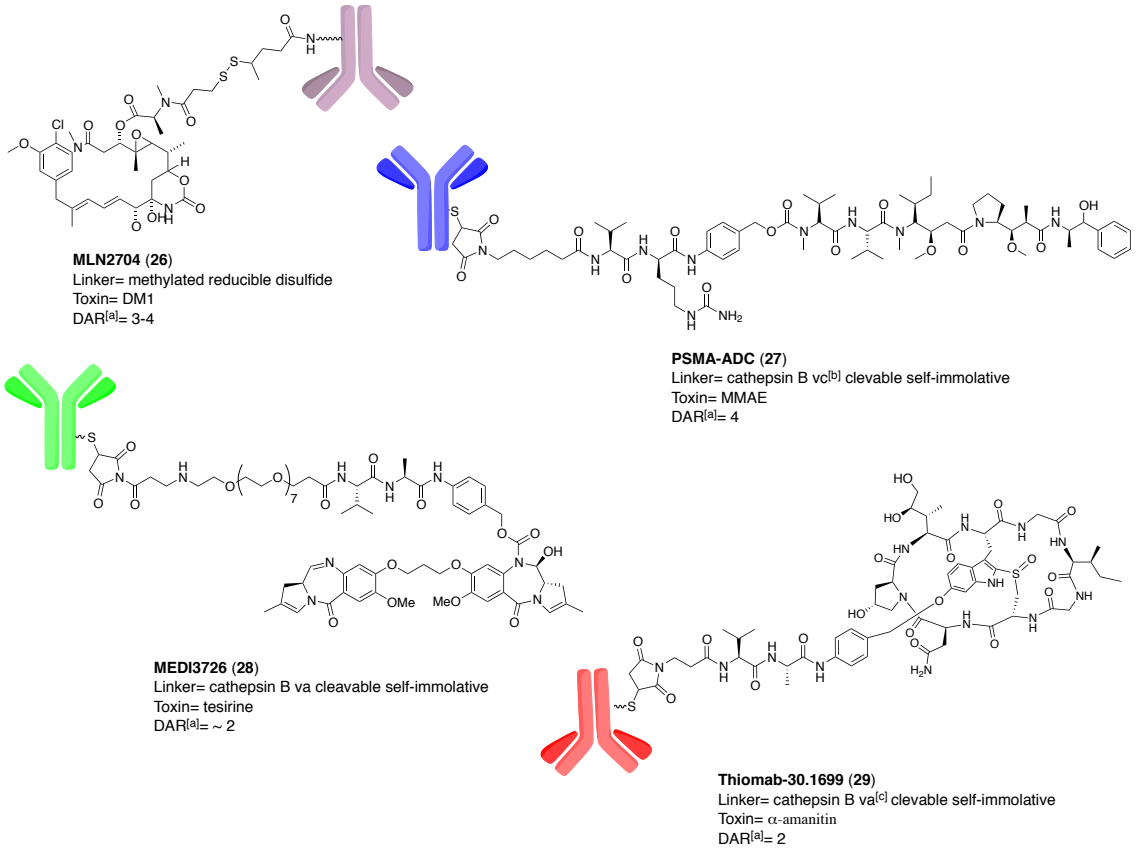

Figure 25. Structure, linker type, payload and DAR of the most advanced PSMA-targeted ADCs. [a]DAR= drug-to-antibody ratio; [b] vc= valine-citrulline; [c] va= valine-alanine.

PSMA ADC (Progenics Pharmaceuticals; **27**, **Figure 25**) is a fully human IgG1 mAb conjugated by thiol-maleimide chemsitry to vc-MMAE (valine-citrulline MMAE; Seattle Genetics). In phase II clinical trial it showed anti-tumor activity (PSA and/or circulating tumor cells response). However, radiographic response rates were low in evaluable patients and treatment–related toxicities were common.(116)

At present, while further clinical development of these tubulin inhibitor-based ADCs as stand-alone agents has been discontinued, other PSMA-targeting ADCs based on novel toxins are under evaluation.

Recently, the humanized J591 antibody conjugated to the pyrrolobenzodiazepine dimer tesirine MEDI3726 (ADCT-401; MedImmune; **28, Figure 25**) via a valine-alanine self-immolative

linker has entered the phase I/Ib clinical trial as treatment for patients with mCRPC, based on the promising precinical data. Studies in LNCaP and castration-resistant CWR22Rv1 PCa xenografts and in LuCaP patient-derived xenografts (PDX) models showed potent antitumor activity with the induction of durable tumor regression.[117]

Thiomab-30.1699 (Heidelberg Pharma Research GmbH; **29, Figure 25**) is an anti-PSMA thiomab antibody coupled to α-amanitin through a valine-alanine cathepsin B cleavable self-immolative linker via thiol-maleimide conjugation chemistry. *In vivo* studies in LNCaP xenograft models have shown potent anti-tumor activity with complete tumor remission achieved in the majority of animals after single or multiple doses. Safety profiling in non-human primates demonstrated a good therapeutic index and tolerability without overt toxicity.[118]

1.11.2 PSMA-targeted SMDCs

1.11.2.1 PSMA small molecule inhibitors

Although the naturally-occuring ligand of PSMA has not yet been identified, as mentioned, it has been well established that PSMA is identical to GPCII in the CNS. The majority of the PSMA ligands currently available have been actually designed to inhibit GPCII, as high level of glutamate resulting from its activity can cause neuronal damages and neurological disorders.

Nearly all GPCII inhibitors are originally derived from its natural substrate NAAG (**Figure 26**). A first class of inhibitors encompasses derivatives or mimetics of glutamic acid which occupies the S1' pocket and is connected through a linker L to a zinc-binding group (ZBG), such as phospho(i)nate or thiol. The history of NAALADase inhibitors dates back to 1996 with the discovery by Jackson *et al*. of the potent inhibitor 2-phosphonomethylpentanedioic acid (2-PMPA; **Figure 27**), which showed robust neuroprotective activity by inhibiting GPCII. It served later as template for the development of other related potent inhibitors.[119]

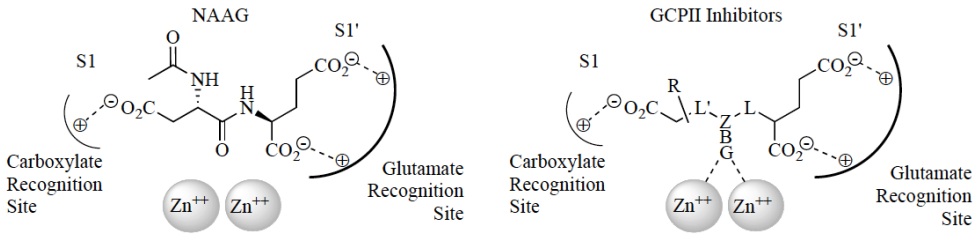

Figure 26. NAAG-based design of NAALADase inhibitors. Republished with permission of Eureka Science (FZC), from Structure-Activity Relantionship of Glutamate Carboxypeptidase II (GCPII) Inhibitors, Tsukamoto, T. *et al*. *Curr*. *Med*. *Chem*. 2012, *19*(9); permission conveyed through Copyright Clearance Center, Inc.

Other inhibitors designed as NAAG-like dipeptide analogues in which the peptide bonding

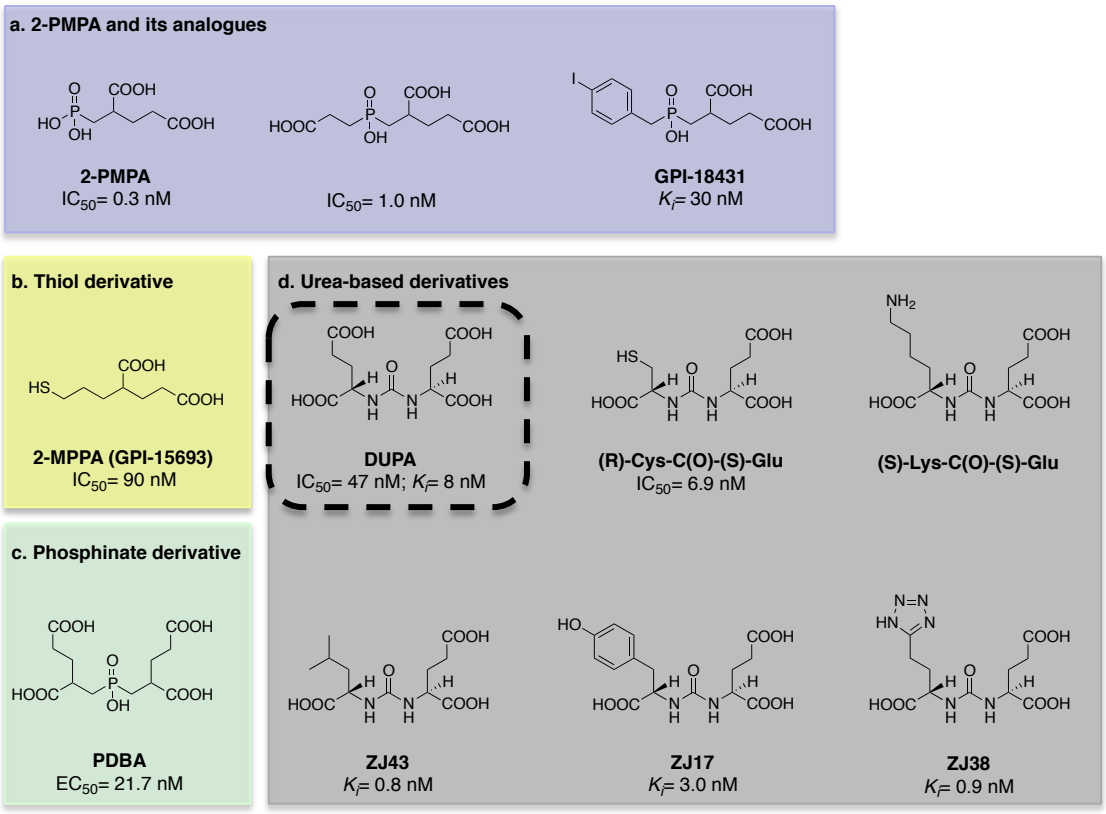

Figure 27. Selected small-molecule GCPII/PSMA inhibitors.

group was replaced by a zinc-binding group resistant to hydrolysis are shown in **Figure 26**.

The most common ZBGs are phosphinates and ureas, with the latter being the most advanced into clinical trials for diagnostic and therapeutic applications.[98]

The urea-based inhibitors were designed on the basis of the phosphinate inhibitor 4,4´-phosphinicobis-(butane-1,3-dicarboxylic acid) (PDBA; **Figure 27**).

Replacement of the central phosphinate moiety with the urea linkage led to the discovery in the early 2000s of the 2-[3-(1,3-dicarboxylpropyl)-ureido]pentanedioic acid, also known as DUPA (**Figure 27**).[120]

Extensive SAR studies revealed that amino acids on both sides of the urea linkage are required to be L- configurated to preserve potent GPCII inhibition activity.

1.11.2.2 Urea-based PSMA inhibitors: DUPA and its analogues

As human GPCII and PSMA are encoded by the same gene, this class of GPCII inhibitors have found wide application in the diagnosis and therapy of PCa as PSMA-targeting ligands, with DUPA and its mimic ACUPA (2-(3-((S)-5-amino-1-carboxypentyl)ureido)pentanedioic acid) being the most investigated.

From docking studies, carrying out by using a high resolution crystal structure of the protein, an extendend overlay of the interactions with the enzyme's active site between the inhibitor GPI-18431 and the DUPA ligand was revealed (**Figure 28**). However, the γ'-carboxylic group was

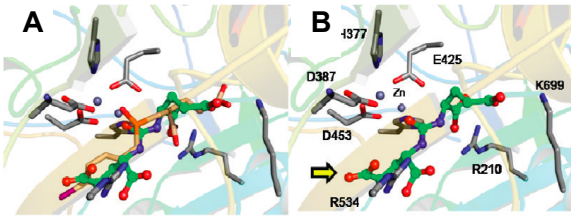

Figure 28. Superimposition of docked DUPA (green) with GPI-18431 (brown) (A) and docking interactions of DUPA (green) in the active site of GPCII. (B). DUPA was found to share the greatest number of docking interactions with GPI-18431 (**A**). The urea oxygen of DUPA coordinates with the zinc atoms in the active site. The α- and α´-carboxylic acids interact with the residues Arg210 and Arg534 of GPCII. The γ-carboxylic acid forms a salt bridge with Lys699 of the enzyme (**B**). Yellow arrow indicates γ´-carboxylic acid of DUPA. Reprinted with permission from Kularatne, S. A. *et al*. *Mol*. *Pharm*. 2009, *6*(3), 790-800, Copyright 2009, American Chemical Society.

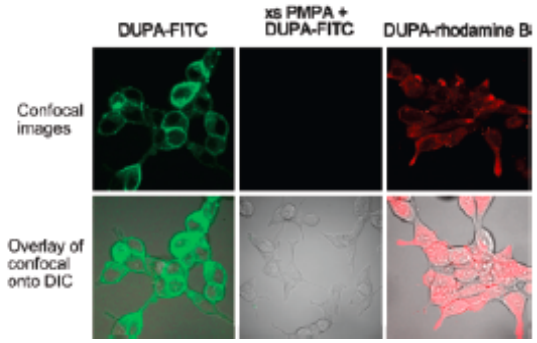

Figure 29. Binding and internalization of fluorescent DUPA-FITC (in presence and absence of 2-PMPA) and DUPA-rhodamine B to LNCaP cells by confocal microscopy. DIC= differential interface constrast images. Reprinted with permission from Kularatne, S. A. *et al*. *Mol*. *Pharm*. 2009, *6*(3), 780-789, Copyright 2009, American Chemical Society.

predicted not be involved in any binding interactions, as shown by the yellow arrow in **Figure 28**, thus, providing an accessible site for conjugation to imaging and therapeutic agents.[122]

The tumor-targeting and internalization properties of such low molecular weight PSMA ligands have been extensively validated.

DUPA ligand conjugated to two different pH-sensitive fluorescent dyes, FITC and rhodamine B, was demonstrated by optical methods to bind PSMA-expressing LNCaP cells in a manner that could be completely inhibited by an excess of the 2-PMPA competitor, suggesting PSMA-specificity.

The apparent different intracellular distribution for the two different DUPA fluorescent conjugates revealed by confocal miscroscopy images (**Figure 29**) is due to the different dye sensitivity at intracellular pH, suggesting that DUPA conjugates are internalized and trafficked through endosomes where only the acid pH-sensitive FITC fluorescence is quenched.[123]

Nuclear medicine applications have provided evidence of the tumor-targeting properties of DUPA and its analogues also in humans.

^{99m}Tc-MIP-1404 (Progenics Pharmaceuticals Inc.; **Figure 30A**) for SPECT/CT (single photon emission computed tomography/computed tomography) entered into clinics in 2010. It has been one of the first small molecule imaging probes to demonstrate specific PSMA targeting in PCa patients with rapid localization in bone and lymph node lesions (**Figure 30B**).[124]

This agent is currently undergoing phase III clinical trial to evaluate its sensitivity and specificity to detect PCa in comparison to histopathology (NCT02615067).

Remarkable modulation of binding affinity and tumor uptake was observed upon modifications of the linker chemistry.

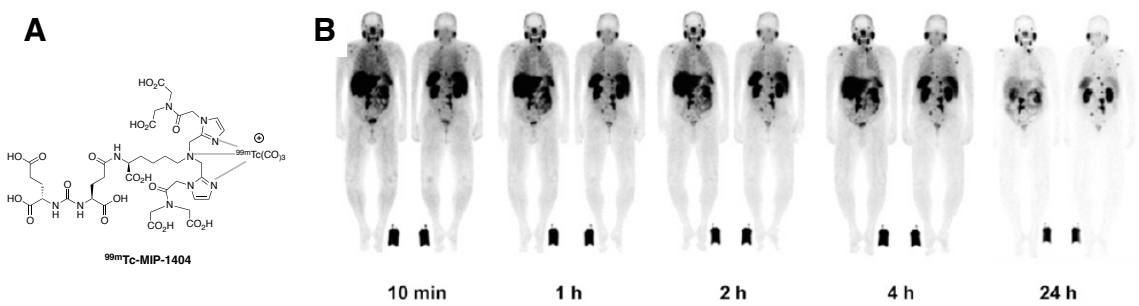

Figure 30. Structure of ^{99m}Tc -MIP-1404 (A) and whole-body planar image of ^{99m}Tc-MIP-1404 at different time points after intravenous injection showing biodistribution in patients with metastatic PCa (B). Suspected metastatic lesions in the bone, lymph nodes, and prostate bed were observed within 10 min after injection with a better constrast observed at 2 and 4 h after injection. The uptake in the metastatic lesions and salivary glands were seen even at 24 h after injection. This research was originally published in *JNM*. Vallabhajosula, S. *et al*., ^{99m}Tc-labeled Small Molecule Inhibitors of Prostate-Specific Membrane Antigen: Pharmacokinetics and Biodistribution Studies in Healthy Subjects and Patients with Metastatic Prostate Cancer *J. Nucl. Med*. 2014, *55*(11), 1791-1798. © SNMMI.

It has been demonstrated that relatively short linker and hydrophobic distal functionalities able to engage the nonpolar residues within the entrance of the PSMA tunnel can lead to more efficient binding and internalization.

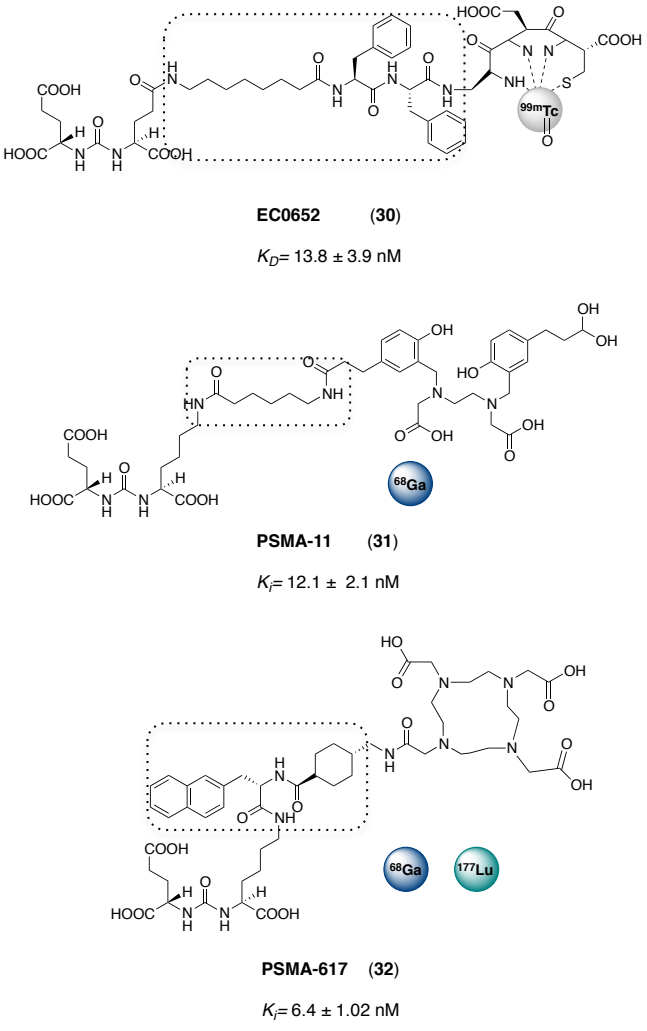

Figure 31. Selected PSMA-targeting radiolabeled agents for imaging (30, 31) or theranostic (32) applications showing structural rearrangement of the linker moiety for enhanced binding affinity. Dashed box contains the linker moiety.

In 2009 Kularatne *et al*. conjugated DUPA to a Dap-Asp-Cys chelating moiety through spacers of different lenghts and hydrophobicity. Docking studies revealed that coupling the DUPA motif to an 8-aminooctanoic acid to avoid steric interference with narrow regions at the base of the tunnel, followed by two phenylalanine residues to contact the hydrophobic pockets close to the mouth of the tunnel, generated an agent with high affinity and specificity.

The resulting ^{99m}Tc-labeled radiotracer (**30**, **Figure 31**) was evaluated in biodistribution studies in nu/nu LNCaP xenograft mice, showing high tumor uptake and prolonged tumor retention (12.4%

ID g^{-1} at 4 h post injection) with little accumulation in other tissues except the kidneys.[123]
The DUPA-^{99m}Tc agent (**30**) was later transferred to clinical evaluation, demonstrating in phase 0 study, sponsored by Endocyte (EC0652), high specificity for PCa and it is currently under evaluation in phase 1b study as investigational companion imaging agent (NTC02202447).
Benesova *et al*. described the design and evaluation of a compound termed PSMA-617 (**32**, **Figure 31**), a HBED-CC-coupled PSMA radioligand, developed as the DOTA-theranostic counterpart of PSMA-11 (**31**, **Figure 31**). The chelator DOTA was conjugated through a naphthylic spacer designed to mimic the proven biological interactions of HBED-CC with the PSMA's tunnel-like region. The presence of the naphthylic spacer resulted in a more potent and efficiently internalized inhibitor. Infact, ^{68}Ga-PSMA-617 was superior to ^{68}Ga-PSMA-11 for binding affinity (K_i= 6.4 ± 1.02 nM for ^{68}Ga-PSMA-617 and 12.1 ± 2.1 nM for ^{68}Ga-PSMA-11) as well as for efficacy of internalization into cancer cells (17.67 ± 4.34% IA/10^6 LNCaP cells). In biodistribution studies in LNCaP tumor-bearing mice major differences were observed in kidney accumulation (25.3% ID/g for PSMA-11 and 1.36% ID/g for PSMA-617) and tumor uptake and retention (2.89% ID/g for PSMA-11 and 4.50% ID/g for PSMA-617 at 24 h post injection).[125]
PSMA-617 labeled with the particles emitter ^{177}Lu is currently being evaluating in phase II trial as therapeutic option in mCRPC patients who have progressed after standard treatments, showing high response rates (NCT03511664).[126]

Collectively, these studies demonstrate the importance of including a spacer between the PSMA-targeting ligand and the cargo.

1.11.2.3 PSMA-targeted SMDCs

The ability of small molecule PSMA inhibitors to deliver cargos to PCa cells has prompted the development of PSMA-targeting SMDCs for PCa treatment.

To this end, Low and co-workers conjugated DUPA to indenoisoquinoline Top1, a potent inhibitor of topoisomerase 1 (MGM GI_{50}= 87 nM in the NCI´s panel of 60 human cancer cell lines), through the same peptide spacer as in EC0652 (**30**), and a disulfide self-immolative linker. The DUPA-indenoisoquinoline conjugate (**33**, **Figure 32**) exhibited a selective cytotoxic activity against PSMA-positive 22RV1 cells and complete cessation of tumor growth with no toxicity.[127]

A structure-related conjugate was obtained by linking the DUPA motif to a tubulysin B hydrazide derivative (TubH; EC0347), a derivative of tubulysin B, via a similar peptide spacer and a disulfide bond. In order to mitigate the overall hydrophobicity of the resulted conjugate

(**34, Figure 32**), the peptide spacer was partially modified with hydrophilic groups without loss of potency. The DUPA-TubH conjugate (**34**) was reported to have cell-killing specificity *in vitro* and to induce prominent tumor regression in LNCaP xenograft models over the treatment period, without signs of significant toxicity. [122]

An analog compound is EC1169 (Endocyte; **35, Figure 32**), a conjugate of ACUPA ligand to TubH through a spacer including an aromatic moiety as first building block and a disulfide self-immolative linker. The resulting targeting moiety was proved to be 17-fold more potent than 2-PMPA in inhibition of PSMA, showing that at least one aromatic moiety is a requisite for higher affinity.

Among several other related compounds, it was selected as the best clinical candidate, due to the favourable outcomes reported in *in vivo* studies, where it was shown to be more effective than docetaxel (the most active chemotherapeutic agent approved for PCa) at curing animals bearing LNCaP tumors without overt toxicity.[128a]

As of January 2020, phase Ib study of EC1169 in taxane-exposed mCRPC patients is active but not-recruiting (NCT02202447). Little has been published about clinical data, although phase 1b data showing that 6.5 mg/m^2 is well tolerated.[128b]

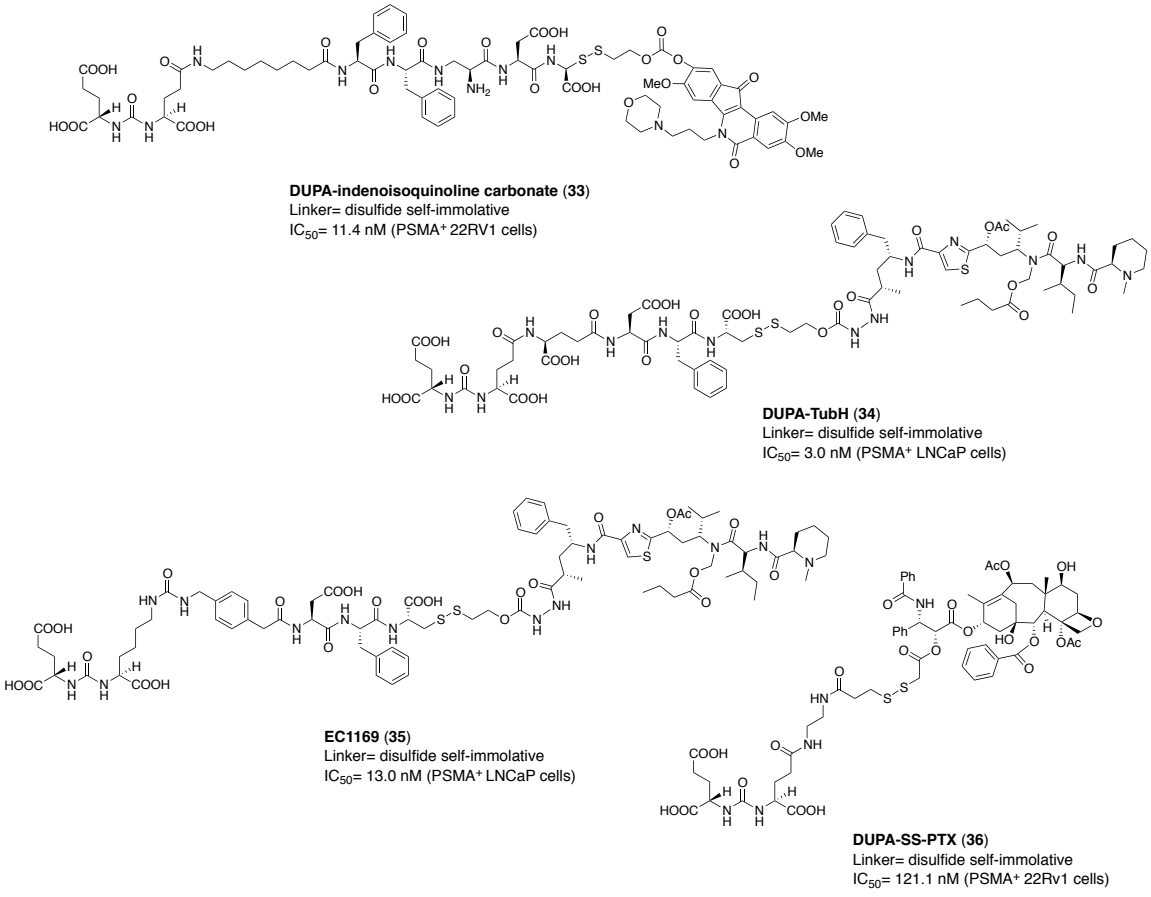

Figure 32. Structure, linker type and *in vitro* potency of some of the PSMA-targeting DUPA-based SMDCs described in literature.

However, this compound does no longer appear in the Endocyte´s pipeline which is currently focused on targeted radioligand therapy.

Another work describing a DUPA-SS-paclitaxel conjugate (**36**, **Figure 32**) highlights the importance of introducing an optimized spacer between the PSMA binding motif and the bulky drug cargo for efficient targeting and internalization of the conjugate. The direct conjugation of DUPA to paclitaxel through a disulfide reducible linker led to loss of drug potency *in vitro*. The anti-tumor response observed *in vivo* for the conjugate and the unconjugated drug were comparable. This observation suggests that the anti-tumor response reported for the conjugate can be attributed to the release of the toxin from conjugate in the tumor environment and to the consequent passive uptake.[129]

Chapter 2

Objectives

Despite the recent advances in the treatment of advanced PCa, there still remain an unmet clinical need that could be addressed with the recent ADC technology.

However, as discussed in section 1.11.1, the majority of the PSMA-targeted ADCs in clinical trials have not progressed much further beyond phase I. Indeed, treating solid cancers with large macromolecules remains challenging and risky due to the unique tumor physiology and the specific ADC pharmacokinetic properties.

Small formats, like peptides or small organic ligands, hold the promise to achieve better tumor penetration and reduce drug exposure to non-targeted tissues thus, providing potentially a wider therapeutic window than antibodies.

The properties of targeted drug-conjugate using PSMA-targeting small molecules as homing ligands have been widely demonstrated, with the PSMA-targeting tubulysin B hydrazide conjugate EC1169 (**35**, **Figure 32**) entered also the phase I clinical trial.

Although highly potent microtubule inhibitors (auristatins, maytansinoids and tubulysins) still represent the most commonly applied ADC and SMDC payloads, they may not be suitable payloads for all kind of malignancies. Different mechanisms of resistance expressed by some forms of cancer can alter the cancer cells sensitivity to the treatment, reducing its effectiveness. Clinically proven payloads for ADCs and SMDCs, like MMAE and DM1 (**14** and **16**, respectively, **Figure 12**) are well known substrates for the MDR transporters. Likewise, a recent work has demonstrated that, in contrast to the parent drug, tubulysin B hydrazide (EC0347) is an excellent substrate for the P-glycoprotein efflux transporter,[130] which is widely expressed by PCa cells.[131]

As mentioned, a growing trend is nowadays shifting towards other potent agents with different modes of action, including PDB dimers and α-amanitin.

In the preclinical setting, α-amanitin-based ADCs have proved outstanding activity in therapy-resistant cancers and in slowly-growing tumors, as often observed for prostate cancers. In a proof-of-concept study, an anti-PSMA-α-amanitin ADC showed proliferation-independent toxicity when tested on both proliferating and growth-arrested LNCaP cells.[132]

These observations, along with the positive outcomes reported recently for the PSMA-targeted Thiomab-30.1699 (**29**, **Figure 26**) lead to consider α-amanitin an optimal drug payload for the treatment of PCa.

Supported by these findings, the aim of this project was to validate the targeted delivery of α-amanitin to PCa cells by means of PSMA-targeting small ligands.

As hydrophilic and membrane impermeable payload, α-amanitin relies on the receptor-mediated internalization of the construct to exert its effect on the intracellular RNAP II target.

DUPA is one of the highest affinity PSMA ligands known to enhance, upon binding, the receptor internalization, to be endocytosed through clathrin-coated pits and released into cytosol, while PSMA recycles back to the surface for another round of endocytosis.[123, 127]

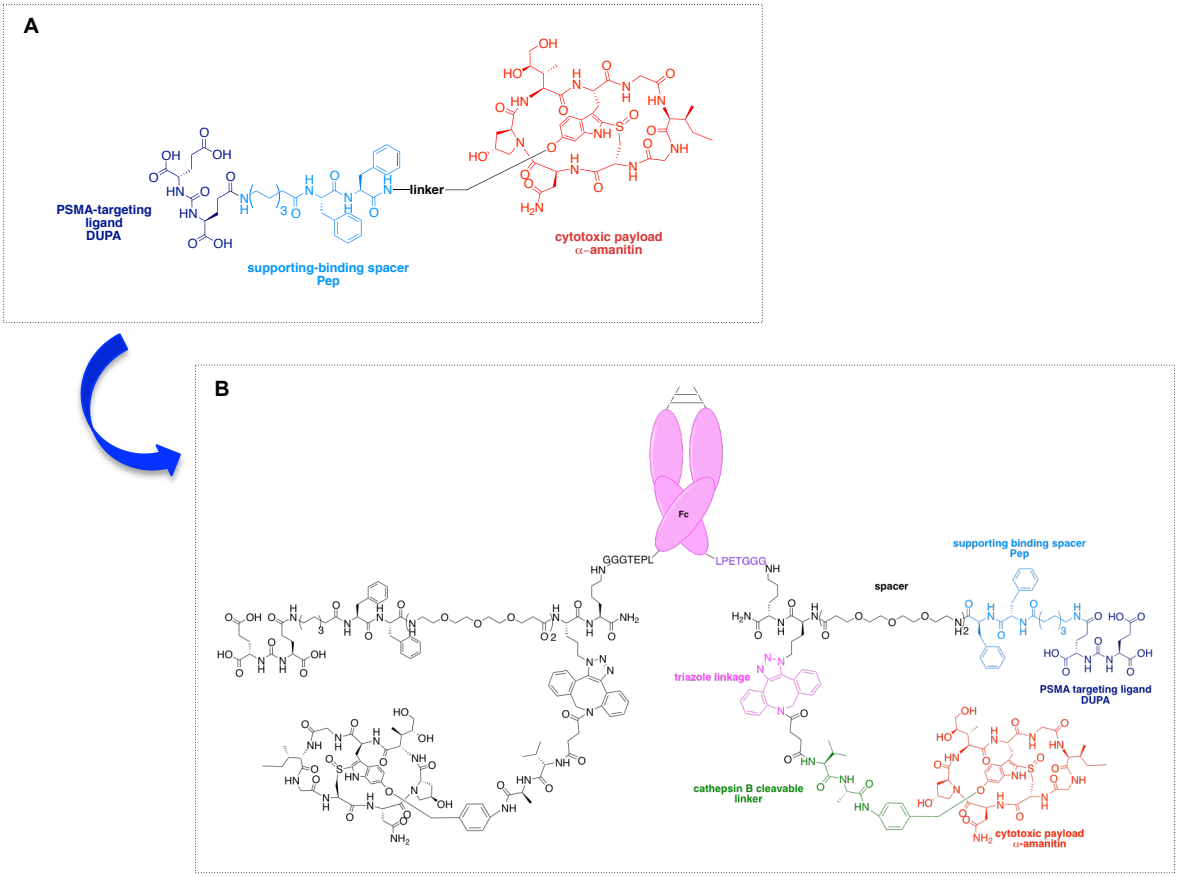

Figure 33. General overview of the project. A) General structure of the PSMA-targeted DUPA-Pep-α-amanitin SMDCs. DUPA-Pep-α-amanitin SMDCs are constituted of the PSMA-targeting ligand DUPA (blue), the supporting-binding spacer 8-Aoc-Phe-Phe (Pep; cyan), a variable linker (black), and the cytotoxic payload α-amanitin (red). **B)** PSMA-targeted DUPA-Pep-α-amanitin grafted onto a human IgG_1-Fc fragment (Fc-SMDC). Linker is shown in green; conjugation chemistry is shown in magenta.

The properties of DUPA to promote the payload delivery and accumulation at tumor site with a moderate to good specificity, prompted its investigation in the present study as homing ligand to deliver α-amanitin to PCa cells.

Because previous studies with DUPA-targeted radioimaging agents have demonstrated that optimal binding occured with a spacer containing two phenylalanine residues at the appropriate distance (8-Aoc-Phe-Phe),[123] this peptidic spacer, that herein will be named as Pep, was incorporated in the design of DUPA-Pep-α-amanitin SMDCs.

In an effort to assess the optimal approach for this treatment modality, DUPA-Pep-α-amanitin SMDCs with a range of linkers and different conjugation strategies (**Figure 33)** were designed and investigated for their anti-tumor activity *in vitro*.

The anti-tumor activity, pharmacokinetics (PK) and biodistribution profiling in animal models was also assessed for the most promising candidates.

Based on the preclinical data, different strategies to optimize the *in vivo* properties of the DUPA-Pep-α-amanitin SMDCs were pursued. In the end, the study was expanded to investigate whether grafting the DUPA-Pep-α-amanitin moiety onto an IgG_1-Fc (immunoglobulin G-fragment crystallizable) scaffold could enhance the PK profile and lead to a successful candidate therapeutics (**Figure 33**).

Chapter 3
The thiosuccinimide-linked SMDCs

It is widely accepted that designing a successful targeted drug-conjugate requires the accurate selection of the linker system which bridges the targeting moiety with the drug payload. Selection of the appropriate linker strategy is highly dependent on different factors, including the targeting ligand, the cytotoxic payload, and the target indication.
Linkers should primarily be stable in plasma over the period of time the targeting agent is in circulation and ensure the payload release once the conjugate is internalized.

Lysosomally dipeptide cleavable linkers are among the most promising linker systems for the ADCs undergoing clinical trials, with the valine-citrulline (Val-Cit) dipeptide linker exploited in 20% of ADCs [133] including the PSMA-targeted ADC **27** (PSMA-ADC; **Figure 26**).[116]
The Val-Cit dipeptide linker is a substrate for the highly active enzyme cathepsin B, a papain-like cysteine protease located in the lysosome. This enzyme is upregulated in a variety of tumors, included the prostate cancer, and particularly in the invasive and metastatic phenotypes.[134] The scarce presence of the enzyme in the extracellular environment is expected to confer stability and selectivity to the cathepsin B cleavable linkers.[134] Another important consideration which makes such cleavable linkers attractive for the ADC and SMDC technology is that cathepsin B is structurally and functionally fully conserved across the species facilitating the preclinical evaluation in animal models.[135]
To allow the enzyme to have access to the active site and cleave the dipeptide linker, a *p*-aminobenzyl alcohol (PABA) moiety is generally introduced between the linker and the drug. Following the cleavage, the self-immolative elimination of the PABA moiety will ensure the release of the unmodified drug payload.[136]
It is also known that cathepsin B is sensitive to other dipeptide substrates, i.e. valine-alanine (Val-Ala), valine-lysine (Val-Lys) and valine-arginine (Val-Arg), with the Val-Ala motif revealed promising in preclinical applications with the ADCs **28** (MEDI3726) and **29** (Thiomab-30.1699) (**Figure 26**) and in clinical studies with the ADC vadastuximab talirine (Seatte Genetics).[117, 118, 137]
Some examples of SMDCs featuring Val-Cit[138] or Val-Ala[87, 139] cleavable linkers are also described in literature.
As mentioned in section 1.11.2.2, DUPA-based drug-conjugates hold the property to be internalized and trafficked through the lysosomes [123, 127] highly rich in the active protease cathepsin

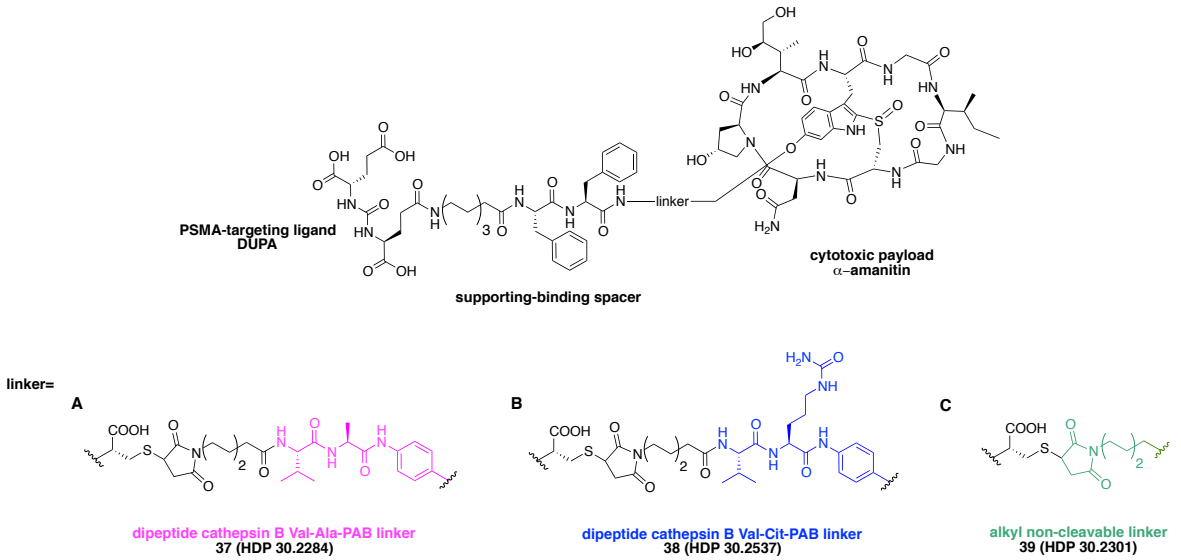

Figure 34. Structure of the DUPA-Pep-α-amanitin SMDCs obtained as thiosuccinimide adducts. Thiosuccinimide adducts featuring a **A)** cathepsin B-sensitive self-immolative linker va-PABA (**37**, **HDP 30.2284**); **B)** cathepsin B-sensitive self-immolative linker vc-PABA (**38**, **HDP 30.2537**); or **C**) maleimidocaproyl (mc) non-cleavable linker (**39**, **HDP 30.2301**).

B. This property supports the investigation of cathepsin B-cleavable linkers as toxin release-trigger system.

In the present study, design and synthesis of DUPA-Pep-α-amanitin SMDCs featuring cathepsin B sensitive linkers with two different dipeptide structures are described.

Because several studies[140] reported the superior stability in serum or in presence of other proteases of the Val-Cit (vc) and Val-Ala (va) dipeptide linkers over the linkers bearing protonable side chains (Val-Arg and Val-Lys), Val-Ala (**37**, **HDP 30.2284**; **Figure 34**) and Val-Cit motifs (**38**, **HDP 30.2537**; **Figure 34**) were selected as cleavage sites. The thiol-maleimide conjugation chemistry was employed as conjugation strategy due to its chemoselectivity and efficiency.

The linker synthesis efficiency, and the *in vitro* cytotoxic activity of the resulting SMDCs were evaluated aiming to identify the optimal dipeptide cathepsin B-sensitive linker for the DUPA-Pep-α-amanitin SMDCs. As comparison, an SMDC containing the non-cleavable maleimidocaproyl(mc)-α-amanitin drug linker was also investigated (**39**, **HDP 30.2301**; **Figure 34**).

3.1 Results

3.1.1 Chemistry. The PSMA-targeting sequence constituted by the binding motif DUPA followed by the supporting binding spacer 8-Aoc-Phe-Phe (Pep) was synthetized as common intermediate for the preparation of the DUPA-Pep-α-amanitin SMDCs **37**, **38** and **39**. The conjugation site was introduced at the *C*-terminus by adding a cysteine (Cys) residue to allow later on the conjugation by thiol-maleimide chemistry to the maleimide-containing α-amanitin derivatives.

Scheme 1. Synthesis of the DUPA precursor 42.

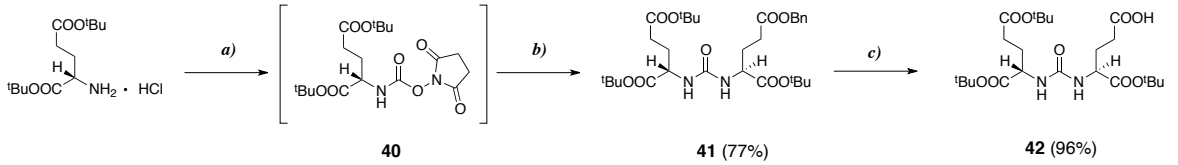

Reagents and conditions: ***a)*** DSC, TEA, DMF, 0°C, 1h; ***b)*** H-Glu(OBn)-O^{t}Bu•HCl, TEA, DMF, 0°C to rt, 24 h; ***c)*** H_2, Pd/C, EtOAc, rt, 24 h.

DUPA precursor (**42**) was synthetized according to the procedure reported by Kularatne *et al.*[123] with minor modifications in favour of easier-handling conditions, as shown in **Scheme 1**. The commercially available *tert*-butyl glutamic acid was first reacted with disuccinimidyl carbonate (DSC) to form the activated succidimidyl ester intermediate **40**. Following the addition of γ-benzoylated glutamic acid, the fully protected DUPA intermediate **41** was hydrogenated with activated palladium-carbon catalyst yielding the DUPA precursor **42** in high yield.

The DUPA-8-Aoc-Phe-Phe-Cys sequence **44** was assembled by automated microwave (MW)-assisted solid phase peptide synthesis (SPPS) by using standard Fmoc chemistry, as reported in **Scheme 2**. The resin-bound protected peptide was cleaved from the resin with a mildly acidic cleavage cocktail yielding the sequence **43**, which was subsequently fully deprotected under strong acidic conditions. Final product **44** was isolated by preparative chromatography in high yield.

Scheme 2. SPPS of the DUPA-8-Aoc-Phe-Phe-Cys (DUPA-Pep) sequence 44.

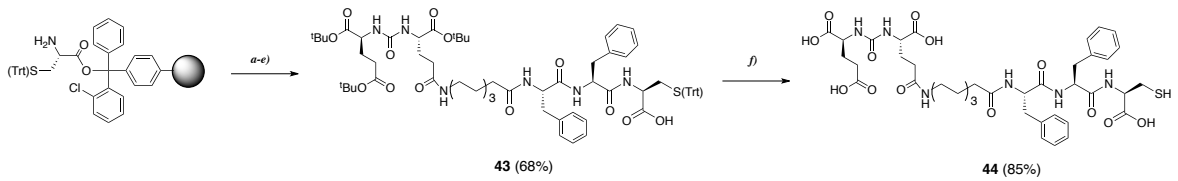

Reagents and conditions: ***a-c)*** i. Fmoc-AA-OH, HOBt, HBTU, DIPEA, DMF, 60 °C, 40 W, 10 min; ii. 20% piperidine/DMF, 60 °C, 40 W, 3 min; ***d)*** i. **42**, HOBt, HBTU, DIPEA, DMF, 60 °C, 40 W, 10 min; ii. 20% piperidine/DMF, 60 °C, 40 W, 3 min; ***e)*** TFE/AcOH/DCM (1:1:8, v:v.v), 23 °C, 1.5 h; ***f)*** TFA/TIS/H_2O (95:2.5:2.5, v:v:v), DTT.

As shown in **scheme 3**, the Michael-type addition between the thiol-containing DUPA-Pep-SH sequence **44** and the mc-vx-α-amanitin drug-linker (x= Ala or Cit; **48a-b**) was employed to generate the DUPA-Pep-mc-vx-α-amanitin SMDCs **37** (x= Ala; **HDP 30.2284**) and **38** (x= Cit; **HDP 30.2537**).

Scheme 3. Synthesis of the DUPA-Pep-vx-α-amanitin SMDCs 37 (x= Ala) and 38 (x= Cit).

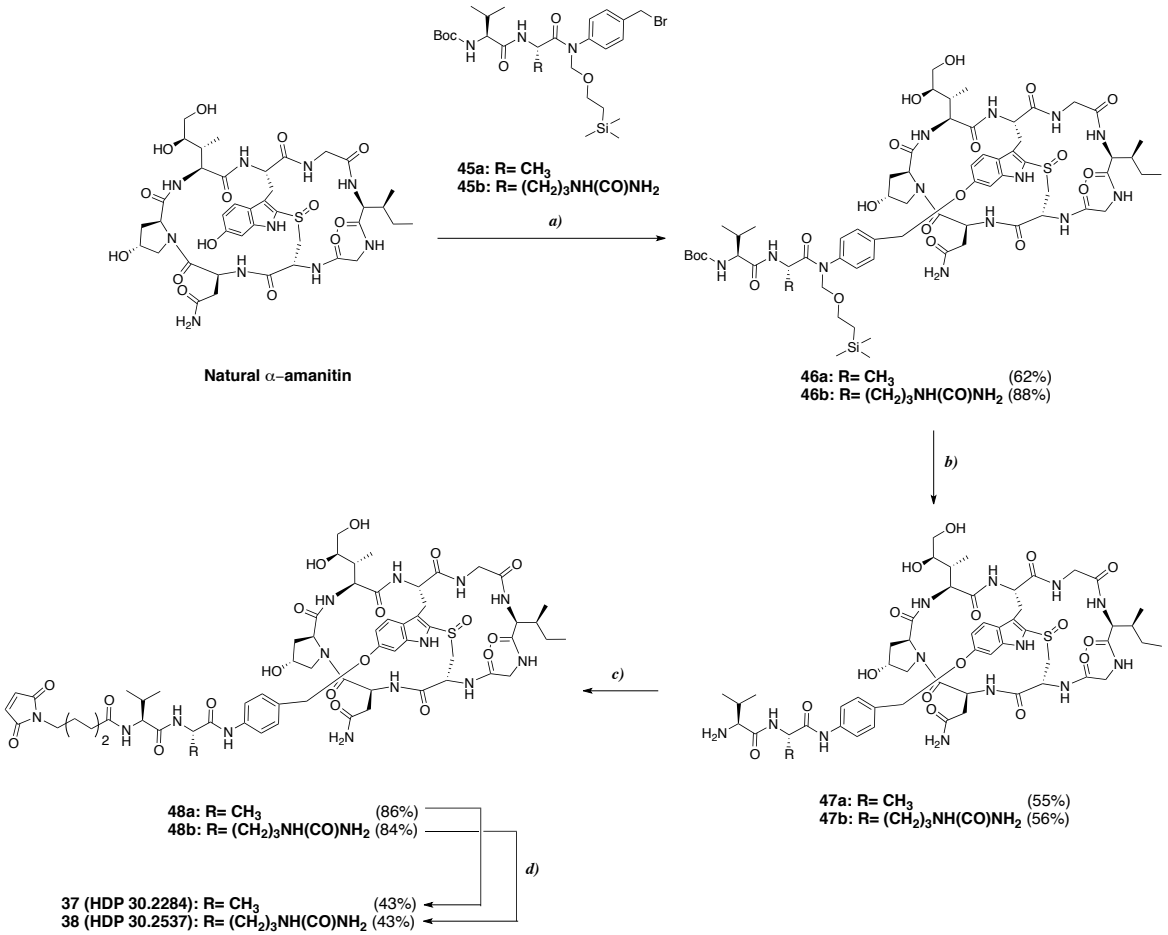

Reagents and conditions: ***a)*** **45a** or **45b**, Cs_2CO_3, DMA, rt, 4 h; ***b)*** i. TFA, rt, 2 min; ii. NH_3, pH 10; ***c)*** ECMS, DIPEA, DMF, rt, 2 h; ***d)*** **44**, DIPEA, DMSO, rt, 20 h.

The approach used to prepare the mc-vx-α-amanitin derivatives **48a** (x= Ala) and **48b** (x= Cit) is outlined in **Scheme 3**. The key step is the formation of an ether bond through alkylation of the phenolic hydroxy group in position 6´ (6`-OH) of the tryptophan residue of natural α-amanitin with the bromide linkers **45a-b**.[141] According to the literature,[79] conjugation at this site provides the highest stability in plasma. Subsequently, both *tert*-butyloxycarbonyl (Boc) and trimethylsilylethoxymethyl (SEM) protecting groups were removed by treating the intermediates **46a-b** with TFA followed by treatment with ammonia. The primary amine of intermedates **47a-b** was then reacted with *N*-maleimidocaproyl-oxysuccinimide ester (ECMS), providing the mc-vx-PABA-α-amanitin derivatives **48a-b**, which will be indicated onwards as mc-vx-α-amanitin.

Preparation of bromides **45a-b** (**Scheme 4**) was adapted from the literature.[142]

Scheme 4. Synthesis of the dipeptide *p*-benzylbromides 45a-b.

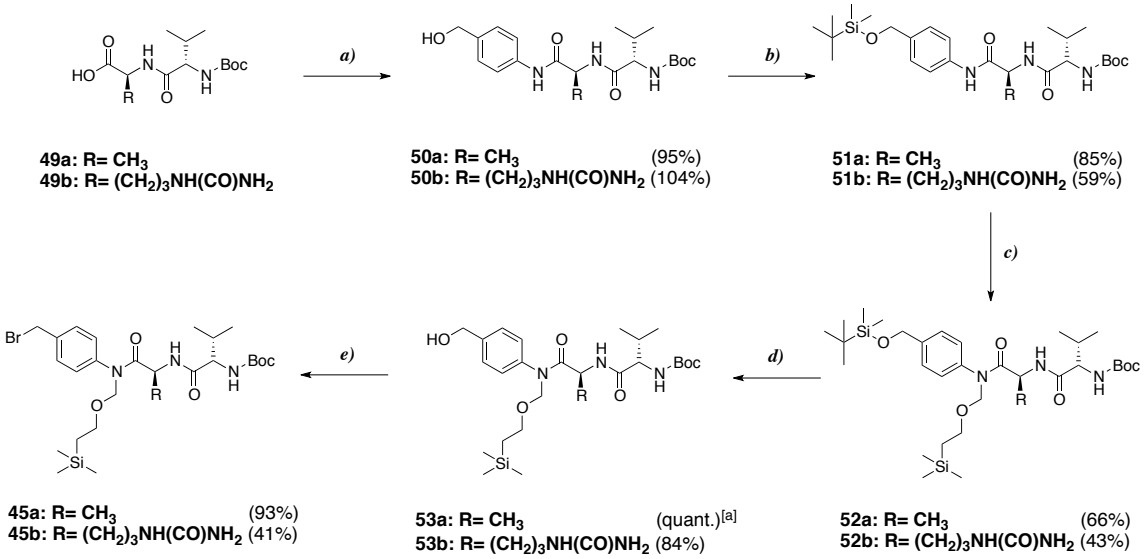

Reagents and conditions: ***a)*** EEDQ, PABA, THF, rt, 65 h; ***b)*** TBDMSCl, DIPEA, DMF, rt, 1 h; ***c)*** NaH, SEMCl, THF, rt, 1 h; ***d)*** TBAF, THF, rt, 20 min; ***e)*** i. $(CH_3SO_2)_2O$, DCM, 0 °C, 35 min; ii. LiBr, THF, 0 °C to rt, 3 h.

Synthesis of the dipeptide *p*-aminobenzylbromides **45a-b** (**Scheme 4**) started with the coupling of *p*-aminobenzylalcohol (PABA) to the corresponding Boc-protected dipeptide (**49a-b**) by using the 2-ethoxy-1-ethoxycarbonyl-1,2-dihydroquinoline (EEDQ) chemistry. The resulting alcohols **50a-b** were converted to the *tert*-butyldimethylsilyl (TBDMS) ethers **51a-b**. The anilide nitrogen of **51a-b** was then protected via alkylation with 2-(trimethylsilyl)ethoxymethyl chloride (SEMCl) and sodium hydride (NaH) to stabilize the final **45a-b** against base-promoted 1,6-elimination of bromide, affording the fully protected adducts **52a-b**. The TBS (*tert*-butyldimethylsilyl) protecting group was removed with tetrabutylammonium fluoride (TBAF) to achieve the benzyl alcohols **53a-b**, which were converted to the desired dipeptide *p*-benzylbromides **45a-b** upon treatment with methanesulfonic anhydride and lithium bromide (LiBr).

Preparation of the SMDC bearing the noncleavable linker DUPA-Pep-mc-α-amanitin **39** is illustrated in **Scheme 5**. Natural α-amanitin was alkylated at the designated conjugation site (6`-OH) with the protected 6-maleimido hexylbromide linker **54**. The heating-promoted *retro*-Diels Alder reaction allowed the removal of the 2,5-dimethylfuran protecting group. The resulting mc-α-amanitin derivative **56** was then converted to the conjugate DUPA-Pep-mc-α-amanitin (**39**, **HDP 30.2301**) by Michael-type addition of the thiol-containing DUPA-Pep-SH binding sequence **44**. Despite the Michael-type thiol-maleimide addition proceeds smoothly and rapidly, in this case reactions required several days to be completed**.**

Scheme 5. Synthesis of DUPA-Pep-mc-α-amanitin SMDC 39.

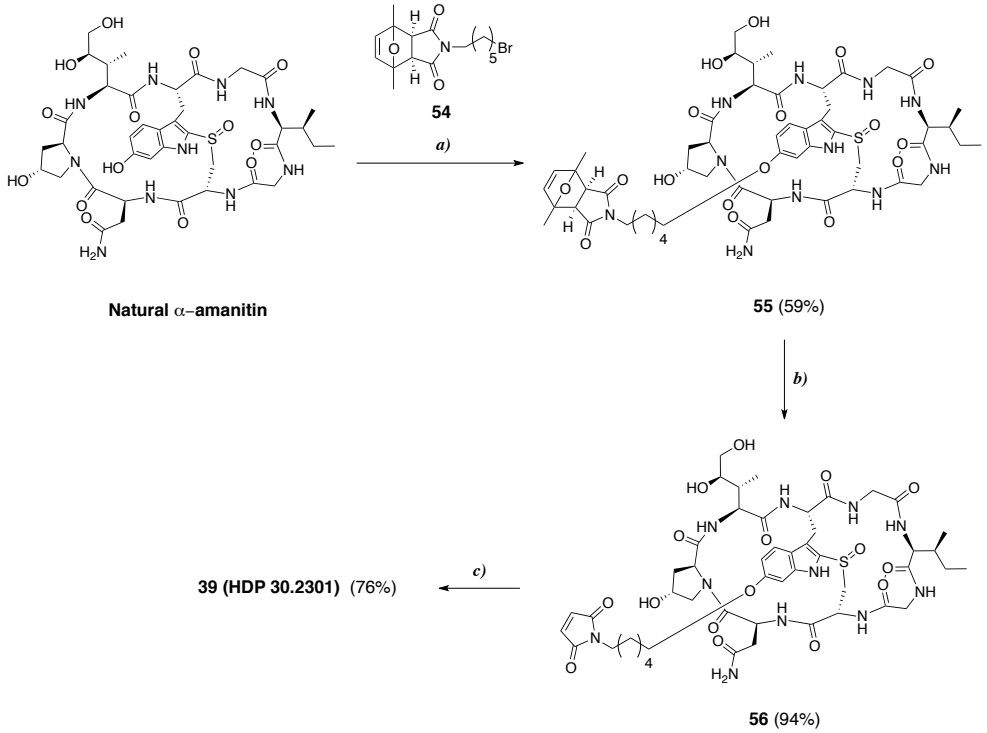

Reagents and conditions**:** ***a)*** **54**, $LiOH_{aq}$, DMSO, rt 3 h; ***b)*** DMSO, 100 °C, 1.5 h; ***c)*** **44**, TEA, DMF, rt, 72 h

The non-cleavable maleimido hexylbromide linker **54** was synthesized according to the procedure shown in **Scheme 6**. Commercially available maleimide was first protected with 2,5-dimethylfuran via a Diels-Alder reaction to furnish the *exo*-furan-maleimide adduct **58**, which is less labile to nucleophiles than the maleimide precursor. The resulting intermediate **58** was reacted with excess of 1,6-dibromohexane under basic conditions affording the target protected 6-maleimido hexylbromide **54**, which was isolated by flash chromatography in high yield.

Scheme 6. Synthesis of the 2,5-dimtehylfuran protected maleimidohexyl bromide 54.

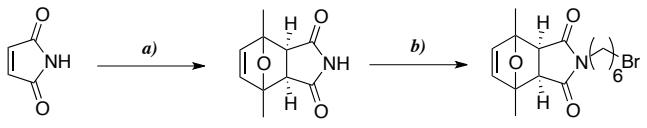

Reagents and conditions: ***a)*** 2,5-dimethylfuran, Et_2O, 90 °C, 12 h; ***b)*** K_2CO_3, DMF, 50 °C, 3 h.

All the target SMDCs were purified by preparative chromatography and lyophilized prior to their use in biological assays.

3.1.2 PSMA expression on prostate cancer cell lines. Flow cytometry was performed to confirm the expression level of PSMA on the cell surface. Immunofluorescent staining showed that LNCaP cells express high levels of PSMA on their surface while PC3 cells essentially lack of PSMA expression (**Figure 35**), as the non-stained histogram is completely overlapped to the anti-PSMA antibody stained histogram. These results are in good agreement with data reported in literature.[143]

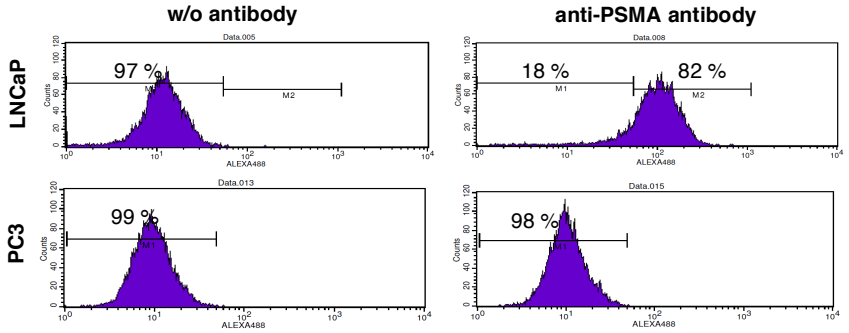

Figure 35. **PSMA expression analysis of LNCaP (top panel) and PC3 (lower panel) prostate cancer cell lines by flow cytometry**. LNCaP cells express high level of PSMA, while the PC3 cells are PSMA-negative. w/o= without

3.1.3 *In vitro* cytotoxic activity on human prostate cancer cell lines. Cytotoxicity of compounds **37**-**39** was assessed in comparison to α-amanitin, and in presence and absence of the PSMA inhibitor 2-PMPA (**Figure 36**). The PSMA-positive ($PSMA^+$) LNCaP and PSMA-negative ($PSMA^-$) PC3 cells were exposed for 96 h to increasing concentrations (10^{-9} to 10^{-5} M) of compound. Cell viability was quantified by the CellTiter-Glo® 2.0 luminescent assay. The dose-response curves and the calculated EC_{50} values are shown in **Figure 36**.

All the SMDCs tested showed high cytotoxicity on LNCaP cells, with EC_{50} values in the picomolar or low nanomolar range. The conjugates bearing the cathepsin B-sensitive linkers DUPA-Pep-mc-va-α-amanitin **(37**, **HDP 30.2284)** and DUPA-Pep-mc-vc-α-amanitin (**38**, **HDP 30.2537)** were slightly more potent (EC_{50} 0.86 and 2.10 nM, respectively) than the non-cleavable counterpart, the DUPA-Pep-mc-α-amanitin (**39**, **HDP 30.2301**; EC_{50} 6.10 nM). Indeed, there was ca. a 7-fold reduction in cell killing potency switching from the va-PABA cleavable linker (**37**) to the mc non-cleavable linker (**39**). The most potent conjugate **37** was approximately 555-fold more potent on $PSMA^+$ LNCaP cells than α-amanitin and ca. 1800-fold less toxic on $PSMA^-$ PC3 cells. The least potent conjugate (**39**) in this series was 90-fold more potent on LNCaP cells than α-amanitin and approximately 250-fold less toxic on PC3 cells.

Cytotoxicity of all tested DUPA-Pep-α-amanitin SMDCs was nearly quantitatively inhibited in presence of 100-fold molar excess of the PSMA inhibitor 2-PMPA, which is indicative of PSMA-mediated cellular uptake. This finding is further supported by the lack of significant toxicity on the $PSMA^-$ PC3 cells, on which the activity of the conjugates was essentially in the range of toxicity of the unconjugated toxin (EC_{50} ca. 10^{-7} M).

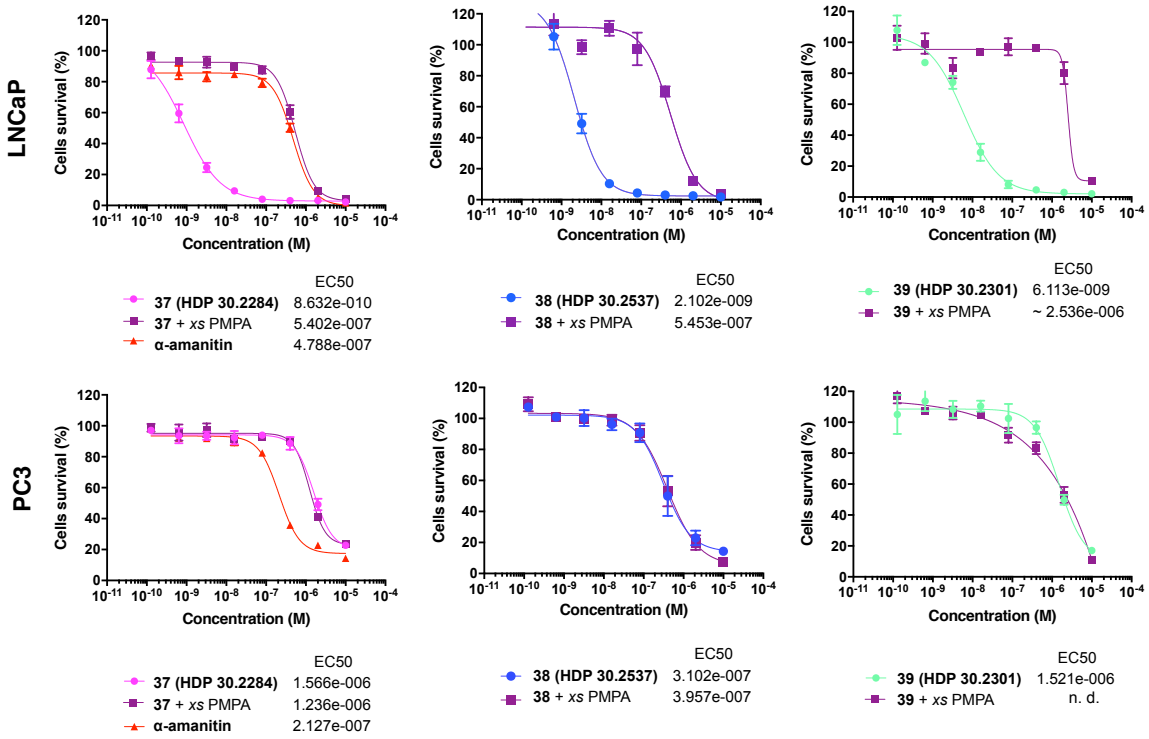

Figure 36. Dose-response curves for DUPA-Pep-mc-va-α-amanitin (37), DUPA-Pep-mc-vc-α-amanitin (38) and DUPA-Pep-mc-α-amanitin (39) SMDCs. Curves were generated by using ATP cell viability assay (CellTiter Glo® 2.0) after 96 h incubation with $PSMA^+$ LNCaP (top panel) and $PSMA^-$ PC3 (lower panel) cells. Compounds were tested in comparison to α-amanitin and in presence or absence of 100-fold molar excess (*xs*) of the PSMA inhibitor 2-PMPA (PMPA). Data points are average of triplicate wells compared to no treatment control.

3.1.4 *In vitro* plasma stability. Plasma stability of the mc-linked DUPA-Pep-mc-va-α-amanitin (**37**) and DUPA-Pep-mc-α-amanitin (**39**) SMDCs was determined by measuring the cytotoxic potential on $PSMA^+$ LNCaP cells through a CellTiter Glo® 2.0 assay. Prior to cytotoxicity assay each compound was incubated either in mouse plasma (MP) and human plasma (HP) at 37 °C for time points 0 to 72 h. This assay allows to determine the cytotoxicity of all active species present in plasma, included remaining conjugate and conjugate-related metabolites.

Dose-response curves and calculated EC_{50} values are shown in **Figure 37**.

Despite the difference in linker cleavability, SMDCs **37** and **39** displayed similar stability profile. After normalizing the potency following exposure to MP and HP at time point 0 h to the potency of the non-exposed conjugates, SMDCs **37** and **39** were found to be less potent by approximately 12- and 2-fold, respectively. Following the initial reduction of potency, conjugates were shown to be completely stable in MP during 6 h incubation, as the potency of conjugates measured from 0 and 6 h samples was intact. In contrast, incubated in HP at concentrations ≥ 10 nM for time points longer than 6 h, conjugates lost approximately 30% of their potency, as indicated by flattening of the curves. In the same concentration range conjugates retained ca. 80% of the potency after 72 h incubation in MP, suggesting higher stability of the mc-linked SMDCs in MP than in HP.

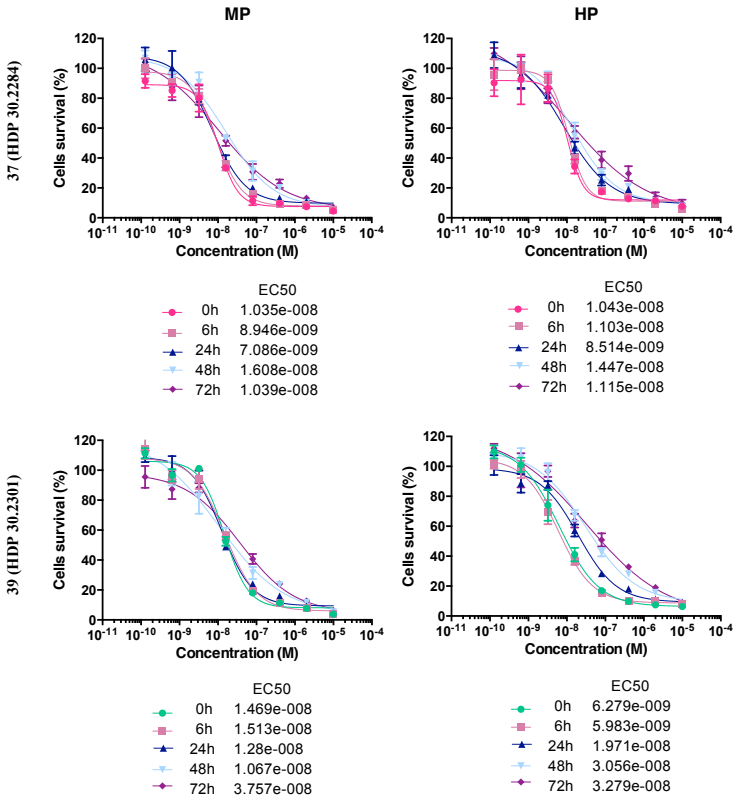

Figure 37. Plasma stability of DUPA-Pep-mc-va-α-amanitin (37) and DUPA-Pep-mc-α-amanitin (39) SMDCs. Cytotoxic potential at time points 0-72 h was assessed by CellTiter Glo® 2.0 assay upon 96 h incubation with $PSMA^+$ LNCaP cells. Prior to cytotoxicity assay, compounds were incubated in mouse plasma (MP; left panel) and human plasma (HP; right panel) for time points 0-72 h.

3.2 Discussion

To the best of our knowledge, this is the first report on the conjugation of α-amanitin to DUPA for the selective delivery of α-amanitin to PCa cells.

Similarly to ADCs, SMDCs are designed to bind to tumor-associated antigens and to release the drug payload inside the cells upon internalization. Controllable release of the payload can be achieved through the thoughtful design of the linker system.

The aim of this study was to investigate the effect of the linker cleavability on the *in vitro* activity and stability of the DUPA-Pep-α-amanitin SMDCs.

Synthesis was carried out via a modular approach with the initial synthesis and assembly of the targeting moiety, the construction of the distinct linker-α-amanitin payloads and the assembly of the entire DUPA-Pep-linker-α-amanitin constructs occurring as the final step of the synthetic process. The high synthetic flexibility of this modular approach allows for the future development of similar linker-α-amanitin derivatives bearing different conjugation handles.

Two different cathepsin B-sensitive linkers, the va-PABA and the vc-PABA, were examined.

Evaluation of the linker design demonstrated that the more hydrophobic Val-Ala motif was more amenable to workup and purification in comparison to the Val-Cit motif, and consequently higher yields were obtained.

The corresponding SMDCs, DUPA-Pep-mc-va-α-amanitin (**37**) and DUPA-Pep-mc-vc-α-amanitin (**38**), demonstrated both excellent *in vitro* potency and selectivity against the PSMA-positive LNCaP cells.

In contrast to the enzymatic-cleavable linkers, the non-cleavable linkers require degradation of the scaffold within the lysosome after internalization of the SMDC to release the active metabolite. Relying on this mechanism requires to take into account that the parent drug and the potential drug metabolite derived from lysosomal degradation might display a different potency. Therefore, not all payloads are suitable for derivatization with non-cleavable linkers. [64, 65]

Incorporation of non-cleavable linkers into α-amanitin-based ADCs does not have detrimental effects on the drug potency *in vitro*, suggesting that α-amanitin retains its activity, despite presumably still attached to part of the linker.[132]

In line with these observations, the DUPA-Pep-mc-α–amanitin (**39**) was *in vitro* approximately as potent as the conjugates **37** and **38** containing dipeptide linkers, supporting the applicability of this linker technology to our α-amanitin SMDCs.

Noteworthy, for all the compounds evaluated in this study an improved potency and toxicity of α-amanitin was reported on the PSMA-expressing cells.

		T.I.	***S***
25	cyclo[DKP-*iso*DGR]-EG_4-va-α–amanitin[87]	2.1 -	0.4[a] 4.4[b]
33	DUPA-SS-indenotecan[127]	0.18	-
34	DUPA-Pep-SS-TubH[122]	1.23	-
35	ACUPA-SS-TubH[128a]	0.28	-
36	DUPA-SS-PTX[129]	0.12	4.0
37	DUPA-Pep-mc-va-α-amanitin	555	1819
38	DUPA-Pep-mc-vc-α-amanitin	371	148
39	DUPA-Pep-mc-α-amanitin	78	249

Table 3. Targeting index (T.I.= $EC_{50(free\ toxin)}/EC_{50(SMDC)}$) and selectivity factor (*S* = $EC_{50(PSMA-)}/EC_{50(PSMA+)}$) of the DUPA-Pep-α -amantin SMDCs 37-39 compared to other DUPA-based SMDCs. For compound **25**, selectivity factor was calculated considering the EC_{50} on the $\alpha_v\beta_3$-negative [a]MDA-MB-46B and [b]A549 cells.

The targeting efficiency of a drug-conjugate can be quantified by calculation of the targeting index (*T.I.*) which takes into account the cytotoxicity on the receptor-positive cells of the free toxin

compared to that of the targeting SMDC, according to the following equation: *T.I.*= $EC_{50(free\ toxin)}/EC_{50(SMDC)}$.

The majority of the DUPA-based SMDCs described in literature so far feature hydrophobic payloads linked via unhindered disulfide linkers (section 1.11.2.3).

Such SMDCs display a cytotoxic potential in the activity range of unconjugated toxin, which results in a rather poor *T.I.* close to 1 or lower. These data suggest that cytotoxicity of such SMDCs is likely due to the passive uptake of the toxin following premature disulfide linker cleavage and drug release. Similarly, for the α-amanitin-based SMDCs targeting receptors other than PSMA, such as the integrin $\alpha_v\beta_3$, the *T.I.* is rather low. On the opposite, for the first array of DUPA-Pep-α-amanitin SMDCs here presented the *T.I.* was considerably higher with values in the range 78-555 (**Table 3**). A hydrophilic membrane-impermeable payload like α-amanitin requires active uptake and internalization in order to exert its cytotoxic effect. Our data show that conjugation of α-amanitin to DUPA increases its cytotoxicity on receptor-positive cells and thus, demonstrate that internalization of DUPA-Pep-α-amanitin SMDCs is indeed target-dependent. This hypothesis is further supported by the experimental data reported on the PSMA-negative cells. A greatly reduced toxicity of SMDCs **37**-**39** on the PSMA-negative cells was observed, leading to a high selectivity factor (*S*= $EC_{50(PSMA-)}/EC_{50(PSMA+)}$) ranging from 148 to 1819. The enhanced selectivity of the conjugates for the PSMA-expressing cells compared to the unconjugated α-amanitin suggests that the conjugates would have greater safety and selectivity than the unconjugated toxin.

For the majority of the DUPA-based SMDCs described in literature the selectivity factor could not be calculated, as no toxicity data on receptor-negative cells were available. However, it is interesting to compare the *S* values of the DUPA-Pep-α-amanitin SMDCs **37**-**39** and the SMDCs **25** and **36**. SMDC **36** is an example of DUPA-based conjugate featuring a hydrophobic payload with cell membrane-permeability properties attached via an unhindered disulfide linker (**Table 3**). The receptor-independent drug uptake following the premature cleavage in the extracellular environment of the disulfide linker might account for the comparable toxicity reported for the SMDC **36** on the receptor-positive and -negative cell lines. As result, the selectivity factor calculated for this conjugate is rather low, *S*= 4.0, which is 62- to 455-fold lower than for the α-amanitin-based DUPA conjugates **37**-**39**. This observation outlines the importance of designing the appropriate linker system in order to preserve the targeting properties of the homing ligand and reduce the toxicity on receptor-negative cells.

The α-amanitin-based SMDC **25** targeting the integrin $\alpha_v\beta_3$ bears the same drug-linker system as the DUPA-Pep-α-amanitin SMDCs **37**-**38**. However, the SMDC **25** displayed an approximately 413- to 4548-fold lower *S* value (*S*= 0.4 and 4.4 on MDA-MB-46B and A549 cells, respectively). than SMDC **37**.

Cytotoxicity of SMDC **25** was shown not to be correlated to the expression of the target receptor, the integrin $\alpha_v\beta_3$, on the tested cell lines which also express other integrin receptors ($\alpha_v\beta_5$ and $\alpha_5\beta_1$ for the U87 cells, $\alpha_v\beta_5$ and $\alpha_v\beta_6$ for the MDA-MB-46B cells).[87] The similar or even higher toxicity observed for the SMDC **25** on the receptor-negative cells compared to the receptor-positive cells might be related to lack of selectivity of the homing ligand for the target integrin $\alpha_v\beta_3$. On the opposite, the high selectivity of the small molecule DUPA for PSMA along with the cell-membrane-impermeable properties of α-amanitin led to the significant different toxicity observed for the SMDCs **37**-**38** on receptor-positive and -negative cells and to the high *S* values calculated (*S*=1819 and 148, respectively) for these SMDCs. Hence, selection of the target antigen and the appropriate ligand for that antigen are key requirements to be satisfied in order to achieve high selectivity.

Taking together, these data demonstrate that the accurate selection of the target antigen and the thoughtful combination of targeting ligand, linker system and toxic payload play a concerted role on the success of a drug conjugate.

As mentioned, an optimal linker for drug delivery is required to be highly stable in circulation, yet allowing efficient drug release at the target site to achieve maximal drug intratumoral accumulation. DUPA-Pep-mc-va-α-amanitin (**37**) and its non-cleavable analogue DUPA-Pep-mc-α-amanitin (**39**) were selected as model systems to elucidate the impact of linker on the stability in plasma and thus, the relationship of the linker stability to the conjugate activity.

Results from *in vitro* plasma stability studies suggest that loss of activity upon exposure to plasma is not primarily associated to the linker cleavability since activity of both conjugates was similarly affected.

According to the literature,[144] some degree of metabolic instability related to the L-configurated Phe-Phe structural motif can impair the performance of DUPA-targeted conjugates. Loss of targeting properties by conjugates **37** and **39** over prolonged exposure to plasma proteases could partly explain the reduction of potency observed for these conjugates.

Additionally, in the context of ADCs an extensive body of evidence suggests that the major factor accounting for the premature loss of DAR for the maleimde-based ADCs is the maleimide deconjugation through a *retro*-Michael mechanism. This mechanism, which equally affects cleavable- and non-cleavable linker-containing conjugates, is potentially due to the transfer of drug-linker payload to thiol-bearing species present in plasma.[145]

Binding to plasma proteins of the mc-linker-α-amanitin-moiety is expected to have a detrimental impact on the activity, as α-amanitin requires active cellular internalization to elicit its effect. Drug binding to human plasma proteins is typically higher than that to mouse plasma proteins[146] and would explain the higher reduction of activity observed for the conjugates upon incubation in human plasma rather than in mouse plasma.

However, elucidation of the exact mechanisms affecting the stability in plasma of DUPA-Pep-α-amanitin SMDCs requires further investigation.

Throughout this work, SMDCs **37** and **39** showed the most promising combination of facile chemistry manipulation and *in vitro* potency and, therefore, warrant further evaluation of their therapeutic potential *in vivo*.

Chapter 4

The disulfide-bridged SMDCs

In the last 40 years thiol-thiol conjugation, also known as disulfide chemistry, has been an extremely popular conjugation strategy, particularly due to its orthogonality.[147]

As mentioned, the linker should be stable in circulation and ensure the drug release inside the target cells. Therefore, the disulfide bond should possess high stability in circulation and low stability within the cell.

The basis for the use of disulfides in drug delivery is the different concentration of thiol-bearing species between the intra- and the extracellular environment. Upon internalization, disulfides are cleaved in the cytosol by reductants, such as (reduced) glutathione (GSH), which has an intracellular concentration of 1-10 mM.[148] Additionally, intracellular enzymes capable of reducing disulfide bonds, such as protein disulfide isomerases, may also contribute to the preferential disulfide cleavage inside the cell.[145] In the case of tumor cells, the particular state of hypoxia due to the irregular blood flow enhances the activity of reductive enzyme, leading to an even higher GSH concentration.[149]

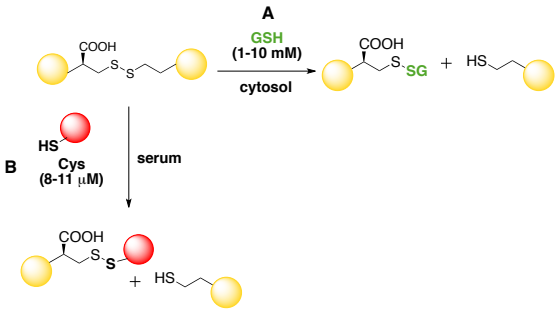

Figure 38. Possible thiol-exchange reactions which a disulfide bond undergoes to. A) In the cytosol a disulfide bond can exchange with the most abundant reductant, the glutathione (GSH). **B)** In circulation a disulfide bond can exchange with cysteine-bearing species.

In the extracellular environment, the concentration of GSH or cysteine is approximately 8-11 μM (**Figure 38**).[148]

However, lack of unique selectivity for reduction by $GSH_{intracell}$ *versus* $cysteine_{extracell}$ renders uncoupling the stability of the conjugate and the facility to release the payload inside the cell extremely challenging.

A general strategy to modulate the lability of the disulfide linker to thiol-exchange reactions is introducing some degree of steric hindrance around the disulfide bond through alkylation of the adjacent carbons. Introduction of alkyl groups around the disulfide linkage will enhance the stability in circulation, but will slow down the rate of drug release inside the cell.[150] Therefore, achieving the desired stability and rate of drug release is a matter of balance.

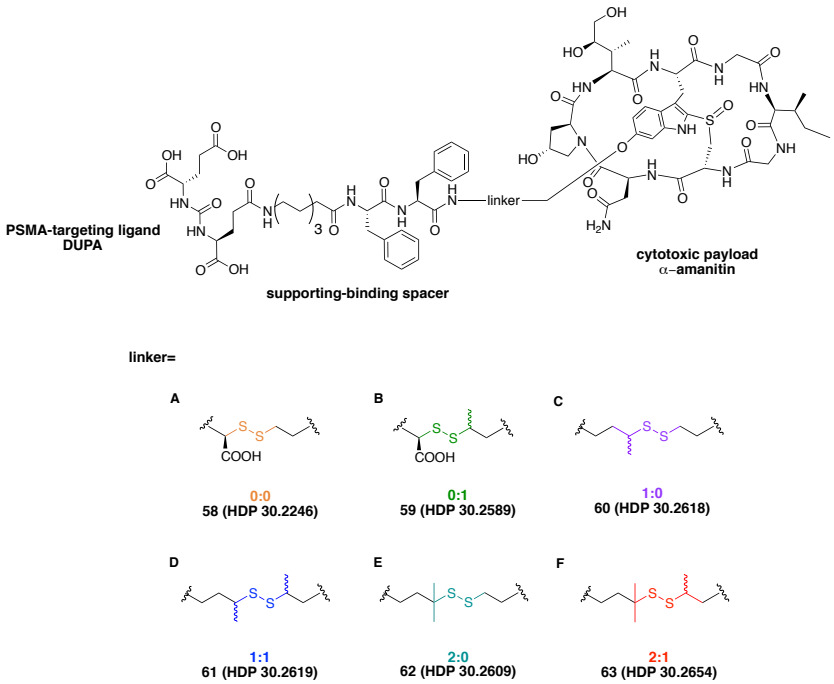

Figure 39. Structure of the DUPA-Pep-α-amanitin SMDCs bearing disulfide linkers with different degree of steric hindrance around the disulfide bond. Linker structure of: **A)** DUPA-Pep-SS-α-amanitin (**58**, 0:0); **B)** DUPA-Pep-SS(Me)-α-amanitin (**59**, 0:1); **C)** DUPA-Pep-(Me)SS-α-amanitin (**60**, 1:0); **D)** DUPA-Pep-(Me)SS(Me)-α-amanitin (**61**, 1:1); **E)** DUPA-Pep-$(Me)_2$SS-α-amanitin (**62**, 2:0); **F)** DUPA-Pep-$(Me)_2$SS(Me)-α-amanitin (**63**, 2:1).

Interestingly, most of the SMDCs that have entered the clinics, such as the SMDCs targeting the folate receptor [151] and the most promising PSMA-targeted SMDCs shown in **Figure 32** are based on unhindered self-immolative disulfide linkers,[122] [127-129] which through a 1,6-elimination reaction allow the release of the unmodified drug.

In an effort to investigate the disulfide bond as alternative strategy to release α-amanitin, a study was initiated with a panel of conjugates bearing disulfide linkers with different degree of steric hindrance to tune the linker lability to thiol-exchange reactions (**Figure 39**).

The study aimed to select the disulfide-bridged SMDC with the optimal *in vitro* activity and stability in plasma as candidate for *in vivo* studies.

In this study, the steric hindrance around the disulfide bond is indicated with the notation *x:y*, where *x* corresponds to the number of methyl groups on the carbon adjacent to the sulfur on the DUPA-Pep side of the disulfide bond, while *y* is equal to the number of methyl groups next to the sulfur on the α-amanitin side of the disulfide bond.

4.1 Results

4.1.1 Chemistry. The general design concept is based on the derivatization of natural α-amanitin with heterobifunctional phenol- and thiol-reactive crosslinkers as common intermediates for the preparation of the conjugates **58**-**63**. The monosubstitued linkers were used as mixture of stereoisomers, therefore, all the corresponding conjugates were obtained as mixture of diastereoisomers.

As outlined in **Scheme 7**, alkylation of the 6´-OH group of α-amanitin with the thiol-protected bromide crosslinkers **64**-**65** (both available in house), differing primarily in the addition of one methyl group next to the sulfur atom, yielded the thiol-protected α-amanitin derivatives **66**-**67**, respectively.

Scheme 7. Synthesis of the disulfide-activated α-amanitin derivatives 68-72 differing in the addition of methyl groups next to the sulfur atoms of the disulfide bond.

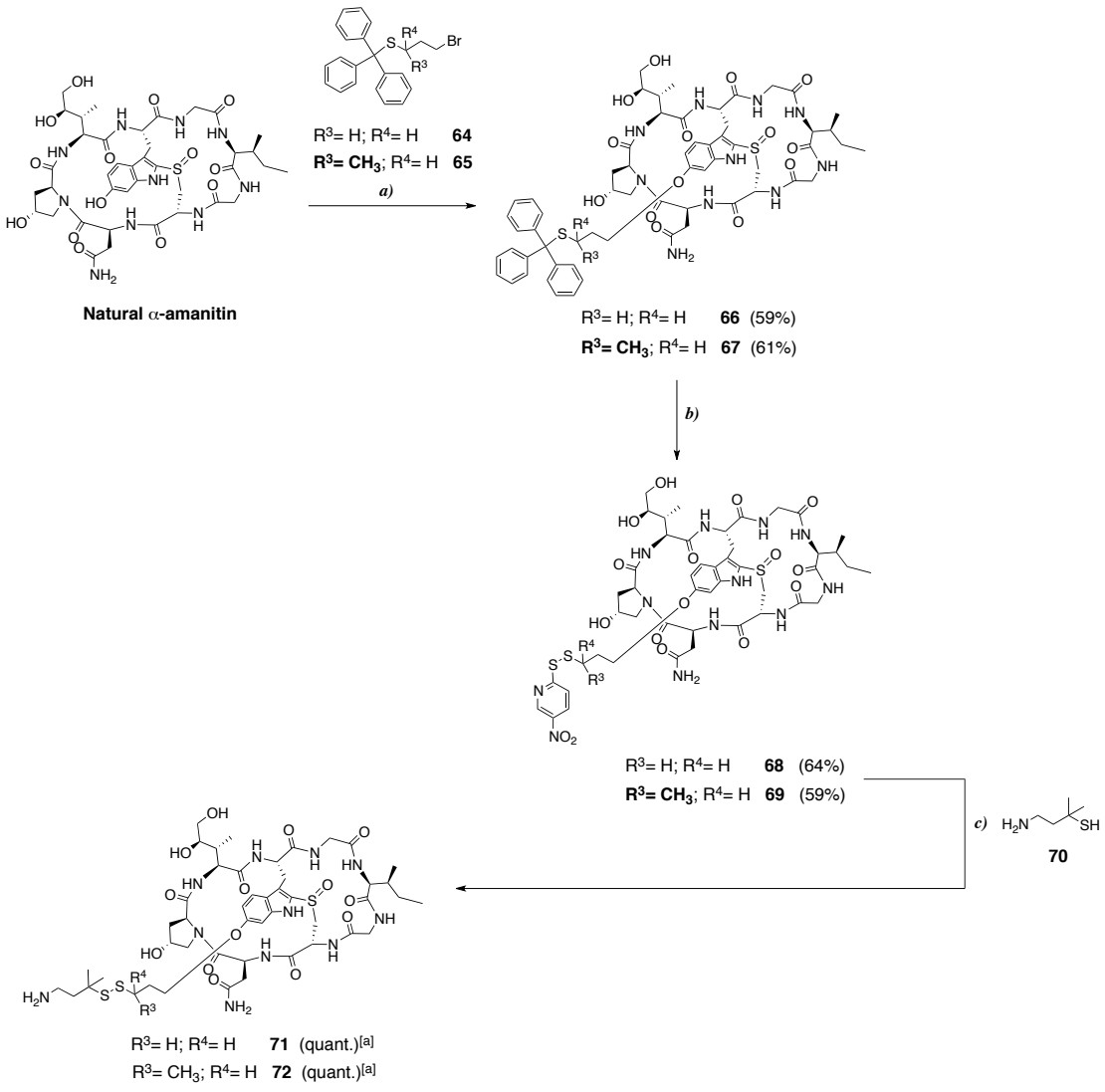

Reagents and conditions: ***a)*** **64** or **65**, NaOH 1M, DMSO, rt, 1.5 h; ***b)*** DTNP, TFA, rt, 4 min; ***c)*** **70**, rt, 1 h.

The trityl deprotection and disulfide activation was carried out as one-pot reaction by using the mild DTNP (2,2´-dithiobis(5-nitropyridine)) chemistry. The trityl-protected α-amanitin derivatives (**66**-**67**) were incubated with an acidic solution of DTNP. The thiol-protectant was removed and substituted by the 2-(5-nitropyridylsulfenyl) (Npys) group derived from the DTNP fragmentation, yielding the nitropyridyl disulfide derivatives **68**-**69**.

From the thiol exchange between the 2-(5-nitropyridyl)dithiol group of the α-amanitin derivative **68** with the heterobifunctional crosslinker **70**, the drug-dimethylated (2:0) disulfide linker **71** was obtained. Similarly, starting from the nitropyridyl methylated disulfide derivative **69**, reaction with the crosslinker **70** yielded the corresponding (2:1) disulfide drug-linker **72**.

Scheme 8. Synthesis of the unhindered DUPA-Pep-SS-α-amanitin (58) and the methylated disulfide-bridged DUPA-Pep-$(Me)_x$SS$(Me)_y$-α-amanitin (0:1, 59; 1:0, 60; 1:1, 61) SMDCs.

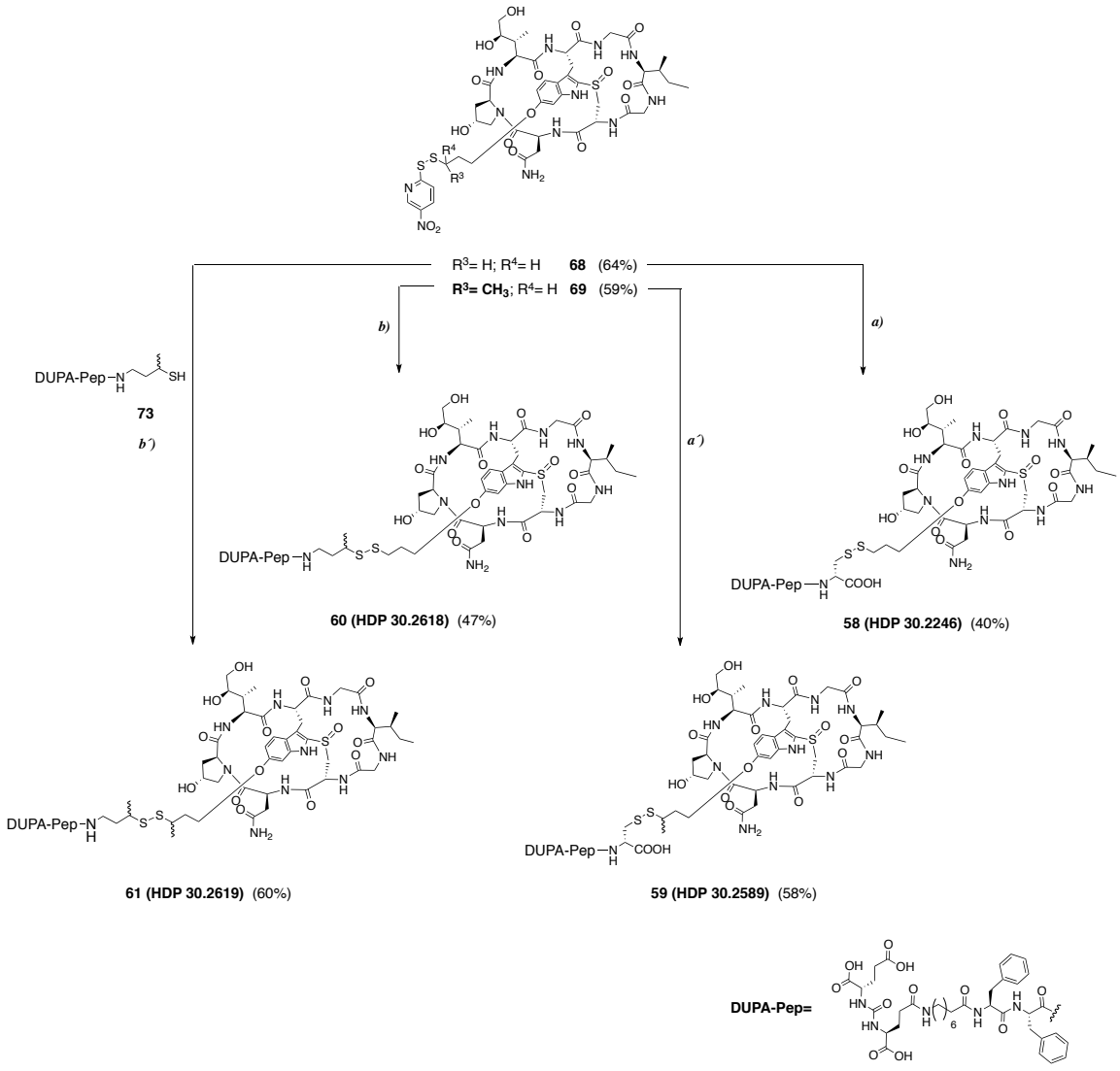

Reagents and conditions: ***a)*** **44**, DIPEA, DMSO, rt, approx. 3 h; ***b)*** **73**, DIPEA, MeOH, 30 min.

To assembly the unhindered (0:0; **58**, **HDP 30.2246**) and the monomethylated (0:1; **59**, **HDP 30.2589**) disulfide-bridged conjugates, the DUPA-Pep sequence **44** (**Scheme 2**) bearing a *C*-terminal cysteine residue was coupled to the nitropyridyl unhindered (**68**) or monomethylated (**69**) disulfide α-amanitin derivative, respectively, affording the desired conjugates in fair yields, as shown in **Scheme 8**.

The disulfide-bridged SMDCs, DUPA-Pep-Me-SS-α-amanitin (1:0; **60, HDP 30.2618**) and DUPA-Pep-Me-SS-Me-α-amanitin (1:1; **61, HDP 30.2619**), presenting a methyl group on the carbon adjacent to the disulfide bond on the DUPA-Pep side were assembled starting from the DUPA-Pep sequence bearing a methylated disulfide-reactive handle (**73**), which was synthesized as illustrated in **Scheme 9**. The fully protected DUPA-Pep sequence (**74**), assembled via SPPS according to the procedure already described in section 3.1.1, was activated at the *C*-terminus as *N*-hydroxysuccinimide(NHS)-ester by using the HOSu/DCC (hydroxysuccinimide/dicyclohexylcarbodiimide) chemistry. The NHS-ester activated intermediate **75** was coupled to the thiol-protected carboxylate-reactive linker presenting a methyl group next to the sulfur atom (**76**) affording, upon total deprotection, the pyridyl disulfide reactive DUPA-Pep sequence **73**.

This sequence was reacted with the nitropyridyl unhindered disulfide α-amanitin derivative (**68**) affording the SMDC **60** and with the monomethylated disulfide α-amanitin derivative (**69**) leading to the SMDC **61**, both isolated in moderate to good yields (**Scheme 8**).

Scheme 9. Synthesis of the DUPA-Pep sequence bearing the pyridyl disulfide reactive handle methylated on the carbon adjacent to the sulfur atom (73).

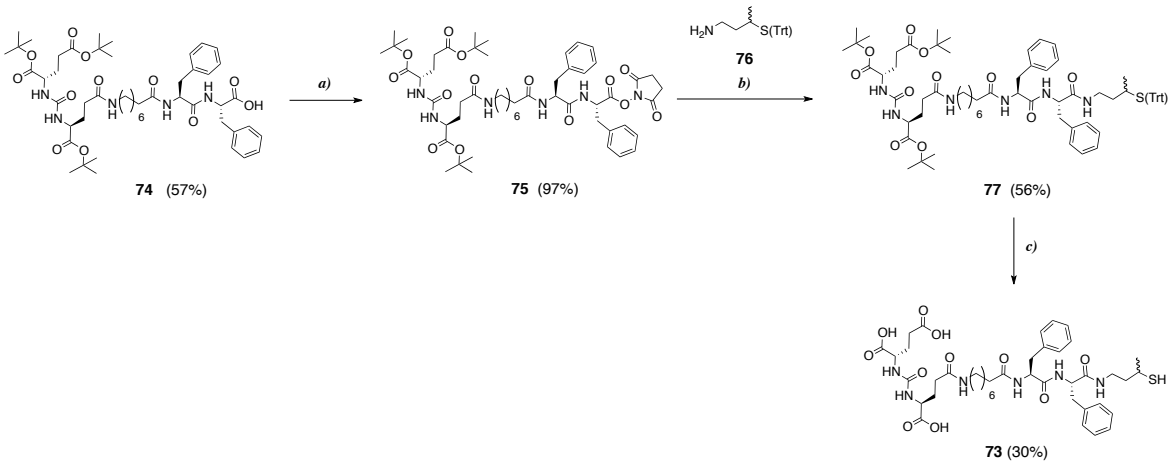

Reagents and conditions: ***a)*** HOSu, DCC, THF/H_2O, rt, 18 h; ***b)*** **76**, $NaHCO_3$, H_2O/THF, rt, 1 h; ***c)*** TFA/TIS/H_2O (95:2.5:2.5, v:v:v), rt, 1.5 h.

Scheme 10 outlines the synthetic strategy pursued to prepare the disulfide-bridged SMDCs with with disulfide bond format 2:0 and 2:1, the conjugates **62** (**HDP 30.2609**) and **63** (**HDP 30.2654**), respectively.

Scheme 10. Synthesis of the hindered disulfide-bridged DUPA-Pep-$(Me)_2$-SS-α-amanitin (2:0, 62) and DUPA-Pep-$(Me)_2$-SS-(Me)-α-amanitin (2:1, 63) SMDCs.

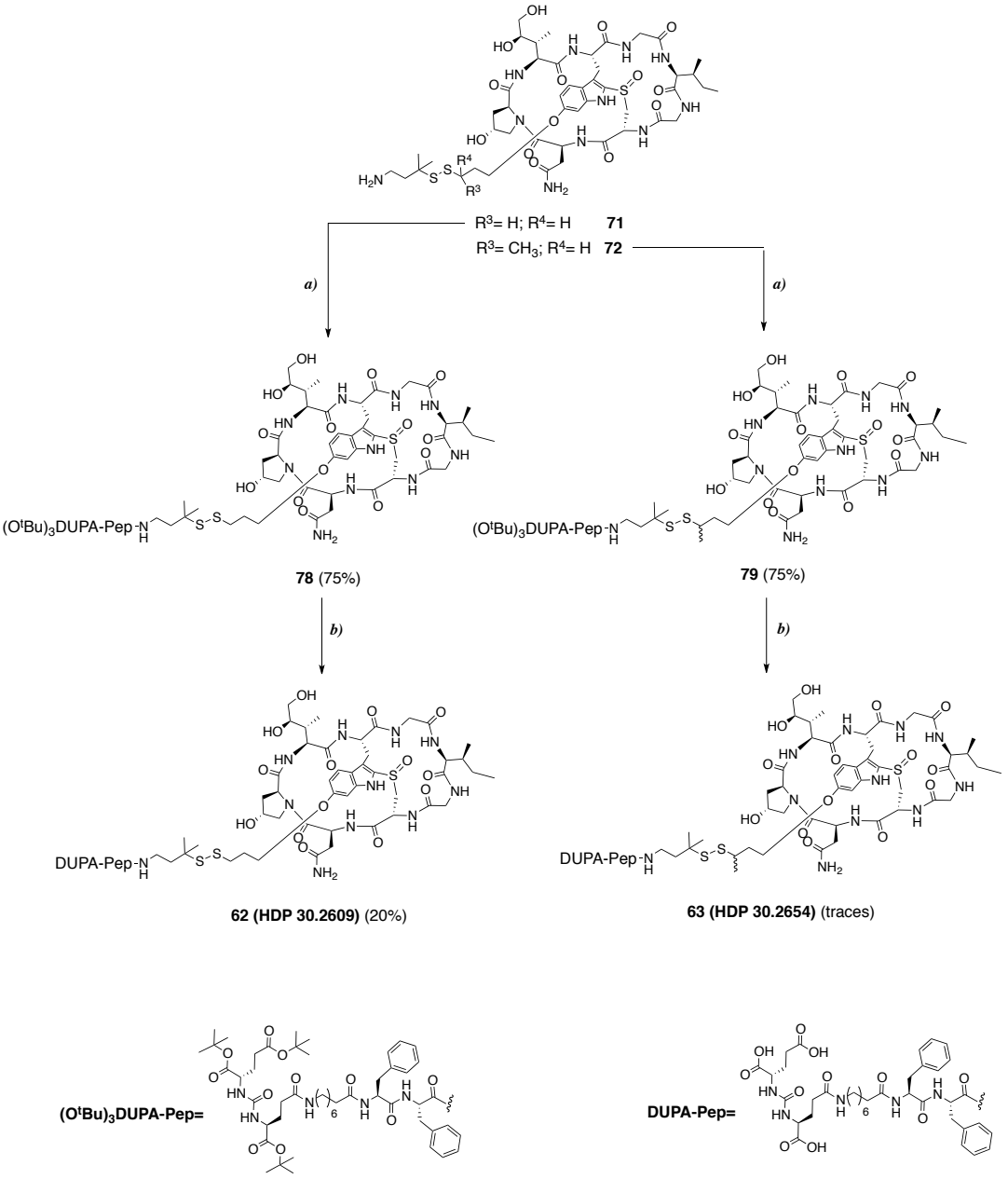

Reagents and conditions: ***a)*** **75**, $NaHCO_3$, H_2O/THF, 3 h; ***b)*** TFA, rt, 2 min (x 3).

While treatment of the (2:0) methylated disulfide drug-linker **71** with the NHS ester-activated DUPA-Pep reagent **75** afforded the *tert*-butyl protected SMDC **78**, reaction of the DUPA-Pep reagent **75** with the (2:1) methylated disulfide drug-linker **72** yielded the *tert*-butyl protected conjugates **79**. The *tert*-butyl protected groups were finally removed to afford the (2:0) disulfide-bridged DUPA-Pep-$(Me)_2$-SS-α-amanitin (**62**, **HD 30.2609)** and the (2:1) disulfide-bridged DUPA-Pep-$(Me)_2$-SS-(Me)-α-amanitin (**63**, **HD 30.2654)** SMDCs. However, this last step was plagued with inefficiencies, including incomplete deprotection or product degradation upon prolonged exposure to the strong acidic conditions. These issues may be attributed to the greater

steric hindrance surrounding the 2:0 and 2:1 methylated disulfide bonds, and account for the poor yields obtained.

All the final conjugates were isolated by preparative chromatography in a purity ≥ 95% considered sufficient for biological tests.

4.1.2 *In vitro* cytotoxic activity on human prostate cancer cell lines. The *in vitro* potency of the disulfide-bridged SMDCs **58**-**62** was evaluated against the PSMA$^+$ LNCaP and the PSMA$^-$ PC3 human prostate cancer cell lines, following the same procedure indicated in section 3.1.3. Dose-response curves and calculated EC_{50} values are shown in **Figure 40**. Data are also summarized in **Table 4**.

The unhindered and the most hindered disulfide-bridged conjugates **58** (0:0) and **62** (2:0) were the less potent on the PSMA$^+$ LNCaP cells, as indicated by the EC_{50} values of 103 and 61.3 nM, respectively.

The best performance was observed for the conjugates bearing disulfide bonds with an intermediate level of alkylation of the carbon atoms adjacent to the disulfide bond, i.e. conjugates **59** (0:1), **60** (1:0) and **61** (1:1), which showed EC_{50} values in the range 3.3-4.7 nM. This observation confirms that the stability in the extracellular environment against the rate of drug release inside the cells is a matter of balance. Indeed, the most effective compound on LNCaP cells, the monomethylated conjugate in format 0:1 (**59**), was approximately 320-fold more potent than the unhindered counterpart and approximately 18-fold more potent than the most hindered compound **62**.

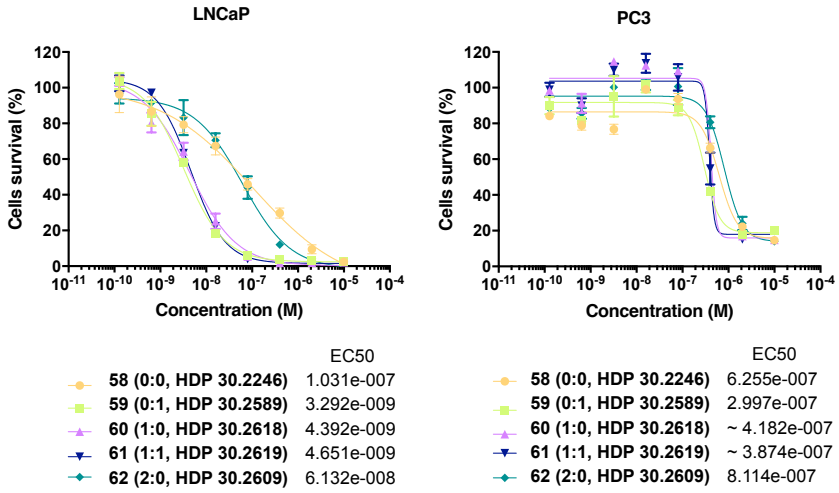

Figure 40. Dose-response curves for the disulfide-bridged DUPA-Pep-$(Me)_x$-SS-$(Me)_y$-α-amanitin (x= 0-2, y= 0-2) SMDCs (58-62). Curves were generated by using ATP cell viability assay (CellTiter Glo® 2.0) after 96 h incubation with PSMA$^+$ LNCaP (left panel) and PSMA$^-$ PC3 (right panel) cells of increasing concentrations (10^{-9}-10^{-5}) of each compound. Data points are average of triplicate wells compared to no treatment control.

		Format	EC_{50} (nM)		Stability in plasma	
			LNCaP	PC3	MP[a]	HP[a]
58	DUPA-Pep-SS-α–amanitin	0:0	103.1	625.5	––	––
59	DUPA-Pep-SS-Me-α–amanitin	0:1	3.3	299.7	+++ (72h)	+ (24h)
60	DUPA-Me-SS-α–amanitin	1:0	4.4	~ 418.2	+/- (6h)	+/- (6h)
61	DUPA-Me-SS-Me-α–amanitin	1:1	4.7	~ 387.4	+++ (72h)	+++ (72h)
62	DUPA-$(Me)_2$-SS-α–amanitin	2:0	61.3	811.4	–[b]	–[b]

Table 4. Calculated EC_{50} values and stability in mouse plasma (MP) and human plasma (HP) of the disulfide-bridged DUPA-Pep-$(Me)_x$-SS-$(Me)_y$- α -amanitin (x= 0-2, y= 0-1) SMDCs 58-62. +++ very stable; + stable; +/- moderately stable; –– very unstable; – not stable. [a] In brackets the time point up to when the cytotoxic potential of the compound is almost intact. [b] Slow drug release inside the cells due to the high steric hindrance around the disulfide bond rather than instability in plasma might be responsible for the low cytotoxic potential observed.

As expected, due to the targeting properties of the DUPA ligand, all the conjugates were not significantly toxic on the $PSMA^-$ PC3 cells. Essentially, the toxicity observed on this cell line can be purely attributed to the toxicity of α-amanitin.

4.1.3 *In vitro* plasma stability. Plasma stability of the disulfide-bridged SMDCs **58**-**61** was assessed as described in section 3.1.4. Dose-response curves and calculated EC_{50} values are shown in **Figure 41**. Data are summarized in **Table 4**.

While *in vitro* potency of the disulfide-bridged SMDCs **58**-**61** was not affected in PBS within the time points considered, compounds **58**-**61** exhibited variability in potency exposed to MP and HP, suggesting different degrees of stability of disulfides to plasma reductants.

Introduction of steric hindrance at one side of the disulfide bond in format 0:1 (**59**) and 1:0 (**60**) resulted in a significant increase of stability in MP and HP compared to the unhindered 0:0 conjugate (**58**), that lost most of its potency upon prolonged incubation in plasma matrices. This observation points out that lack of steric hindrance around the disulfide bond makes disulfide highly susceptible to thiol-exchange reactions with thiol-bearing species present in plasma.

Conjugate with hindrance on both sides of the disulfide bond (1:1, **61**) was more stable to premature reduction either in MP and HP even at the longest time points, compared to the unhindered 0:0 (**58**) conjugate and to conjugates with hindrance on one side of the disulfide bond (0:1, **59**; 1:0, **60**). Within the series of conjugates with intermediate level of steric hindrance surrounding the disulfide bond, while the 1:0 (**60**) and 1:1 (**61**) conjugates appeared to be equally stable in MP and HP, conjugate 0:1 (**59**) appeared to be more stable in MP than in HP up to the longest time points considered (48-72 h). The 2:0 conjugate (**62**) showed upon exposure to MP and HP potency in the range of the unhindered 0:0 conjugate (**58**). However, loss of potency due to prolonged exposure to plasma reductants was not as prominent as for the 0:0 conjugate (**58**). Additionally, the low cytotoxic potential showed by this conjugate also suggests that high degree of

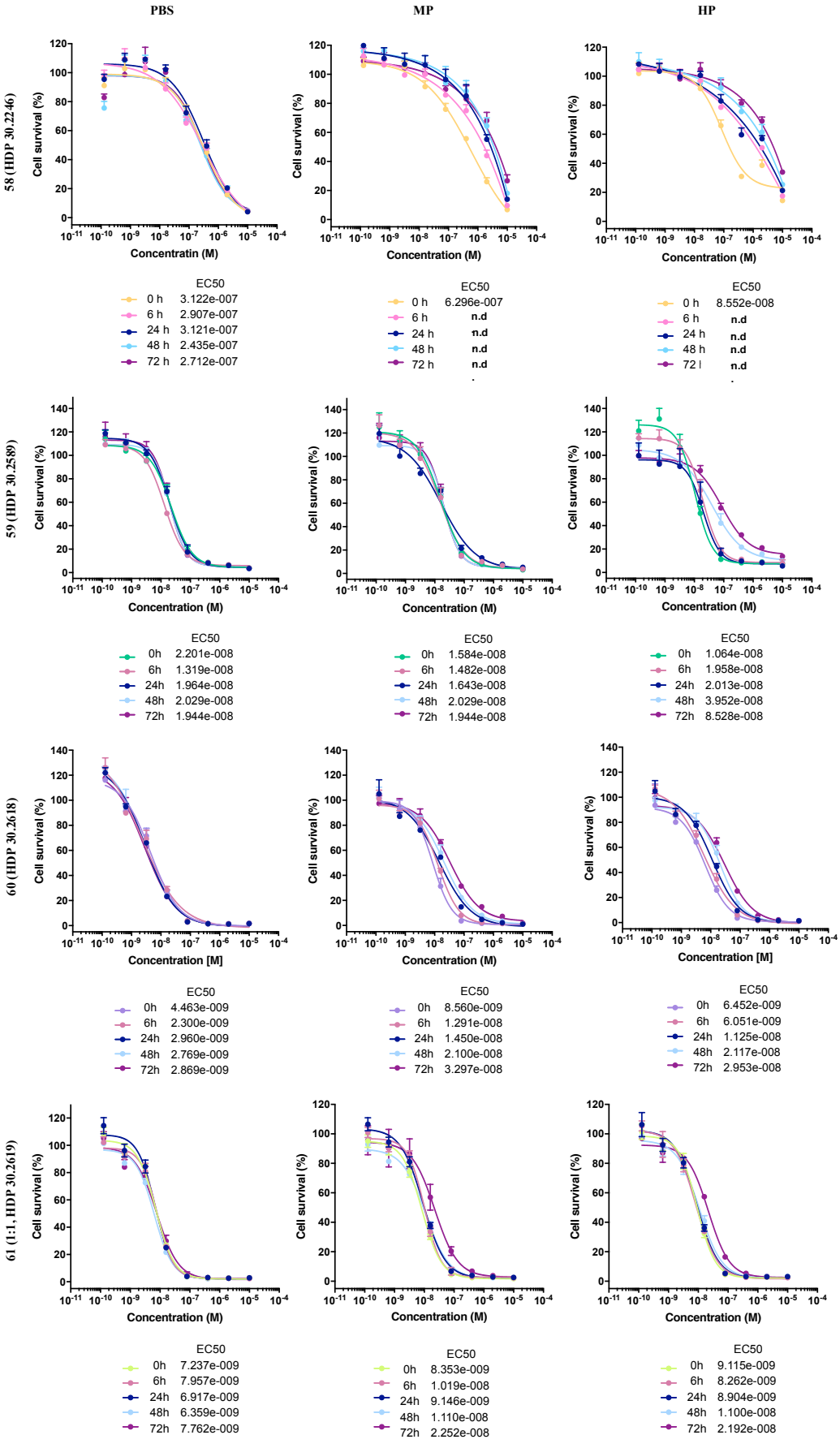
PBS
MP
HP
58 (HDP 30.2246)
59 (HDP 30.2589)
60 (HDP 30.2618)
61 (1:1, HDP 30.2619)
Cell survival (%)
Concentratin (M)
Concentration (M)
Concentration [M]
EC50
0 h 3.122e-007
6 h 2.907e-007
24 h 3.121e-007
48 h 2.435e-007
72 h 2.712e-007
0 h 6.296e-007
6 h n.d
24 h n.d
48 h n.d
72 h n.d
0 h 8.552e-008
6 h n.d
24 h n.d
48 h n.d
72 l n.d
0h 2.201e-008
6h 1.319e-008
24h 1.964e-008
48h 2.029e-008
72h 1.944e-008
0h 1.584e-008
6h 1.482e-008
24h 1.643e-008
48h 2.029e-008
72h 1.944e-008
0h 1.064e-008
6h 1.958e-008
24h 2.013e-008
48h 3.952e-008
72h 8.528e-008
0h 4.463e-009
6h 2.300e-009
24h 2.960e-009
48h 2.769e-009
72h 2.869e-009
0h 8.560e-009
6h 1.291e-008
24h 1.450e-008
48h 2.100e-008
72h 3.297e-008
0h 6.452e-009
6h 6.051e-009
24h 1.125e-008
48h 2.117e-008
72h 2.953e-008
0h 7.237e-009
6h 7.957e-009
24h 6.917e-009
48h 6.359e-009
72h 7.762e-009
0h 8.353e-009
6h 1.019e-008
24h 9.146e-009
48h 1.110e-008
72h 2.252e-008
0h 9.115e-009
6h 8.262e-009
24h 8.904e-009
48h 1.100e-008
72h 2.192e-008

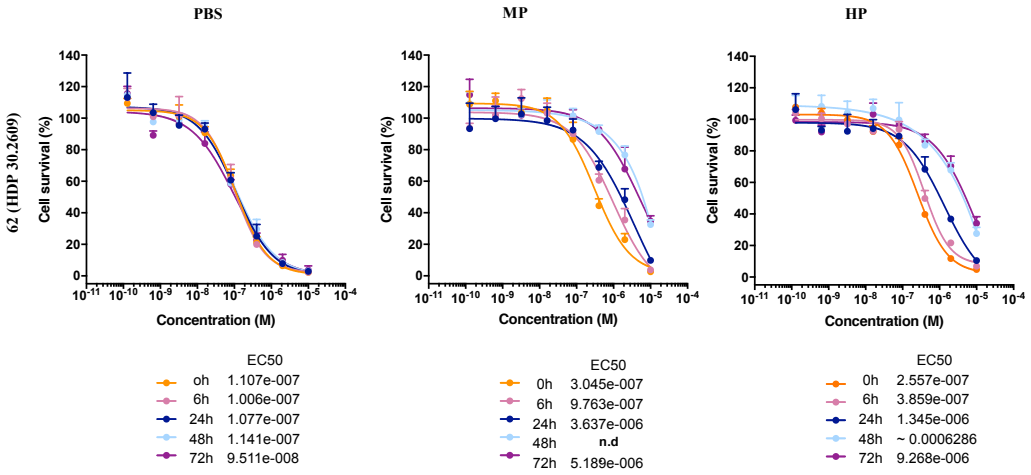

Figure 41. Plasma stability of the disulfide-bridged DUPA-Pep-$(Me)_x$-SS-$(Me)_y$- α -amanitin (x= 0-2, y= 0-1) SMDCs (58-62). Cytotoxic potential at time points 0-72 h was assessed by CellTiter Glo® 2.0 assay upon 96 h incubation with $PSMA^+$ LNCaP cells. Prior to cytotoxicity assay, compounds were incubated in PBS (left panel), mouse plasma (MP; middle panel) and human plasma (HP; right panel) for time points 0-72 h. n. d.= not determined

steric hindrance around the disulfide bond increases the stability in the extracellular environment but also hinders the drug release inside the cells.

4.2 Discussion

EC1169 (**35**; **Figure 35**), a disulfide-linked DUPA-TubH conjugate with sterically unhindered (0:0) self-immolative disulfide linker, has been studied in phase I clinical trials in patients with recurrent mCRPC. In preclinical models, EC1169 was able to induce tumor growth inhibition up to ca. 30 days post injection (p.i.).[122] Other promising DUPA-targeted SMDCs described in literature are also based on unhindered disulfide linkers,[127-129] as previuosly discussed.

To investigate whether the disulfide linkage was a suitable strategy to release α-amanitin inside the target cells, a first disulfide-bridged DUPA-Pep-α-amanitin SMDC with sterically unhindered disulfide linker (0:0, **58**) was generated.

Interestingly, while we had previously demonstrated that conjugates linked to α-amanitin using the maleimide chemistry (**37**-**39**; **Figure 34**) were highly active against the PSMA-expressing cells, the 0:0 disulfide-bridged DUPA-Pep-SS-α-amanitin conjugate (**58**) was not active below the range of activity of the unconjugated toxin. The hypothesis that the conjugate was not sufficiently stable exposed to reductants present in the culture medium, which is supplemented with fetal bovine serum (FBS), was confirmed by the evaluation of the stability upon incubation in plasma. Lack of stability led, reasonably, to the premature release in the culture medium of α-amanitin, that cannot passively diffuse into cells due to its hydrophilic nature.

The potent *in vitro* and *in vivo* activity observed for the 0:0 disulfide-linked DUPA conjugates [122] [127-129] featuring relatively hydrophobic payloads can be attributed to a self-amplifying effect,

known as bystander effect. Once extravasated, toxin is released upon disulfide cleavage in the tumor microenvironment, initiating cell death. Dying cells release reducing agents into the surrounding environment inducing additional drug release in a self-amplifying fashion.[152]

Lack of activity of the 0:0 conjugate (**58**) prompted us to investigate whether activity of the disulfide-bridged conjugates might be improved by increasing the stability of the disulfide bond to thiol-exchange reactions.

To this end, a small panel of disulfide-bridged conjugates with different degrees of steric hindrance around the disulfide bond was generated by introducing methyl groups on the carbons adjacent to the disulfide linkage. The panel lacked the 0:2, 2:2, and 1:2 disulfide formats. In fact, derivatization of α-amanitin with the thiol-reactive crosslinker bearing two methyl groups on the carbon next to the sulfur atom was not achievable perhaps due to the excessive steric hindrance provided by the two methyl groups.

Evaluation of the synthetic strategy demonstrated that the acidic treatment of the final conjugates with 2:0 or 2:1 disulfide linkage is not efficient and has a detrimental impact on the final yield. In particular, the 2:1 conjugate (**62**) was isolated in an amount not sufficient for the *in vitro* characterization.

Assessment of the *in vitro* activity of these conjugates showed that as the degree of steric hindrance around the disulfide bond increased the potency of the conjugate decreased, with the most hindered (2:0, **61**) being the less potent. It is likely that the enhanced stability to thiol-exchange reactions provided to the disulfide bond by the higher steric hindrance has parallely slowed down the drug release rate inside the cells.

The conjugates with an intermediate level of substitution around the disulfide bond were found to be the most active.

Overall, the observed order of activity was as follow: 0:1 (**59**) > 1:0 (**60**) ≈ 1:1 (**61**) > 2:0 (**62**) > 0:0 (**58**). Within the conjugates with the same level of substitution around the disulfide linkage, the conjugates 0:1 (**59**) and 1:0 (**60**), configuration of the steric hindrance appeared to have an impact on the conjugate potency. This might be due to the specific toxin metabolite released in the tumor cell upon cleavage of the disulfide bond and to its related activity. However, data regarding the activity of these specific α-amanitin metabolites are not available. It can be also argued that the reduced pK_a for the thiol in the cysteine-linked adducts **59** makes it a better leaving group than the alkyl thiol in **60** thus, facilitating the drug release inside the cell for the conjugate **59**.

Regarding the stability in mouse plasma compounds can be ranked as follow: 0:1 (**59**) ≈ 1:1 (**61**) > 1:0 (**60**) > 0:0 (**58**) ≈ 2:0 (**62**), and as follow considering the stability in human plasma: 1:1 (**61**) > 0:1 (**59**) > 1:0 (**60**) > 0:0 (**58**) ≈ 2:0 (**62**). Data obtained for SMDC **62** might be misleading. The low cytotoxic potential measured following exposure to plasma might suggest that SMDC **62** is quite unstable. However, the high steric hindrance reasonably resulted in a much slower and inefficient drug release, leading to the low cytotoxic potential observed.

Although conjugates **59**-**61** with an intermediate level of alkylation around the disulfide bond had cytotoxic activity in the same range, they were shown to possess different stability in mouse and in human plasma. Additionally, within this series, while the formats 1:0 (**60**) and 1:1 (**61**) had similar stability both in mouse and human plasma, format 0:1 (**59**) was more stable in mouse than in human plasma. All together these findings suggest that additional factors may contribute to the stability in plasma of these conjugates and that, therefore, the stability of the disulfide bond is not the only factor accounting for their activity *in vitro*.

Based on the ease of chemical synthesis, *in vitro* potency and stability in plasma, the 1:0 disulfide-linked DUPA-Pep-Me-SS-α-amanitin SMDC (**60**, **HDP 30.2618**) was selected as best in class for further *in vivo* characterization.

Chapter 5

In vivo profiling of the lead candidates

Based on the *in vitro* evaluation, DUPA-Pep-mc-va-α-amanitin (**37**, **HDP 30.2284**) bearing an enzyme-cleavable linker, its non-cleavable DUPA-Pep-mc-α-amanitin counterpart (**39, HDP 30.2301**) and the 1:0 disulfide-bridged DUPA-Me-SS-α-amanitin (**60, HDP 30.2618**) SMDCs were selected from the initial screening as lead therapeutic candidates.

5.1 Results

5.1.1 Maximum Tolerated Dose study. To define the dose for the efficacy study, a preliminary Maximum Tolerated Dose (MTD) study with the selected conjugates (**37**, **39**, **60**) was conducted in CB17-Scid male mice. The goal of this study was to define the highest dose that did not cause unacceptable side effects or overt toxicity for the study duration. To determine the MTD two endpoints were used: weight loss ≥ 20% and poor general conditions.

MTDs of conjugates were determined following intravenous (i.v.) administration of ascending/descending doses and evaluating the toxicity after administration over an observation period of at least one week.

A clear correlation between dose and weight loss was found for all the conjugates (**Figure 42**).

The established MTDs for a single dose were: DUPA-Pep-mc-va-α-amanitin (**37**) 0.046 mg/kg, DUPA-Pep-mc-α-amanitin (**39**) 2.56 mg/kg, DUPA-Pep-(Me)SS-α-amanitin (**60**) 1.2 mg/kg.

The starting dose (0.368 mg/kg) for the DUPA-Pep-mc-va-α-amanitin SMDC (**37**) was the equivalent of 150 μg/kg of α-amanitin, which is known from internal studies to be the MTD of unconjugated toxin in this mouse strain. However, this dose was not tolerated, as it caused severe toxicity and at day 5 p.i. all mice from this group were found dead. Doses were incrementally lowered by 50% until at 0.046 mg/kg (18.75 μg/kg of α-amanitin) a weight loss of approximately 20% was observed at day 7 and was completely regained in the follow-up period. The double-descending dose of 0.023 mg/kg was completely tolerated and therefore, the previous dose was set as the MTD.

Based on these data, the starting dose (0.02 mg/kg, 9.4 μg/kg of α-amanitin) for the related compound **39** was equivalent to the ½MTD of SMDC **37**. As this dose and the double-ascending dose (0.04 mg/kg) were well tolerated without significant toxicity, the following doses were incrementally escalated by a 50% factor until at 2.56 mg/kg (1.2 mg/kg of α-amanitin) at day 3 p.i. a marginal body weight loss was observed.

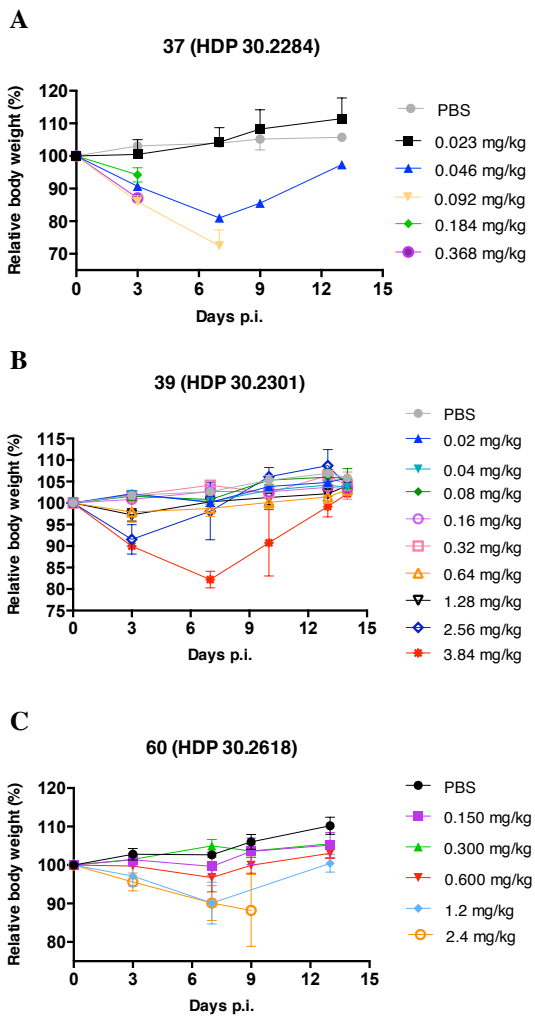

Figure 42. Maximum Tolerated Dose (MTD) study for A) DUPA-Pep-mc-va-α-amanitin (37); B) DUPA-Pep-mc-α-amanitin (39) and C) DUPA-Pep-Me-SS-α-amanitin (60). MTD was assessed by injecting CB17-Scid male mice with different intravenous (i.v.) doses of each compound, followed by observation for 15 days. Body weight was measured twice per week. Each data point represents the mean ± SEM of n= 3.

Such body weight loss returned to the baseline during the observation period. The following dose was escalated by a factor of 1.5 of the previous one. At this dose (3.84 mg/kg) the endpoints were met and the previous dose was established as the MTD.

The starting dose (0.150 mg/kg) for DUPA-Pep-Me-SS-α-amanitin SMDC (**60**) was equivalent to the ½MTD of α-amanitin. As no toxicities were observed the following doses were incrementally escalating by a 50% factor. A weight loss of approximately 10% was observed at day 7 after administration of 1.2 mg/kg and 2.4 mg/kg. Weight loss was completely recovered after day 7 following 1.2 mg/kg dose administration. The 2.4 mg/kg dose led instead to an extendend period (up to day 9) of weight loss. For one animal of this group the endpoints were met and the animal was euthanized. These observations led to set the 1.2 mg/kg (0.6 mg/kg of α-amanitin) dose as the MTD for the SMDC **60**.

5.1.2 Plasma pharmacokinetic study. In order to establish the dosing frequency, plasma concentration of the selected SMDCs was measured over a period of 48 h after a single i.v. administration of conjugate in LNCaP xenograft-bearing CB17-Scid male mice. Conjugates were administered at the following doses: of 0.182 mg/kg (4x MTD) for SMDC **37**, 1.28 mg/kg (½MTD) for SMDC **39** and 0.6 mg/kg (½MTD) for SMDC **60**. Concentrations were measured by anti-α-amanitin ELISA which determines the total concentration of α-amanitin-containing compounds, i.e. intact SMDC, SMDC-derived metabolites and releasead α-amanitin. The clearance curves are shown in **Figure 43**. Assuming a single compartmental first order pharmacokinetic model, all the DUPA-Pep-α-amanitin SMDCs evaluated in this study demonstrated similar clearance profile. Half-life ($t_{1/2}$) was determined as 44.2 min for DUPA-Pep-mc-va-α-amanitin (**37**, **Figure 43A**), 61.8 min for DUPA-Pep-mc-α-amanitin (**39**, **Figure 43B**) and 81.5 min for DUPA-Pep-Me-SS-α-amanitin (**60**, **Figure 43C**). As doses for DUPA-Pep-mc-α-amanitin (**39**) and DUPA-Pep-Me-SS-α-amanitin (**60**) were higher, the

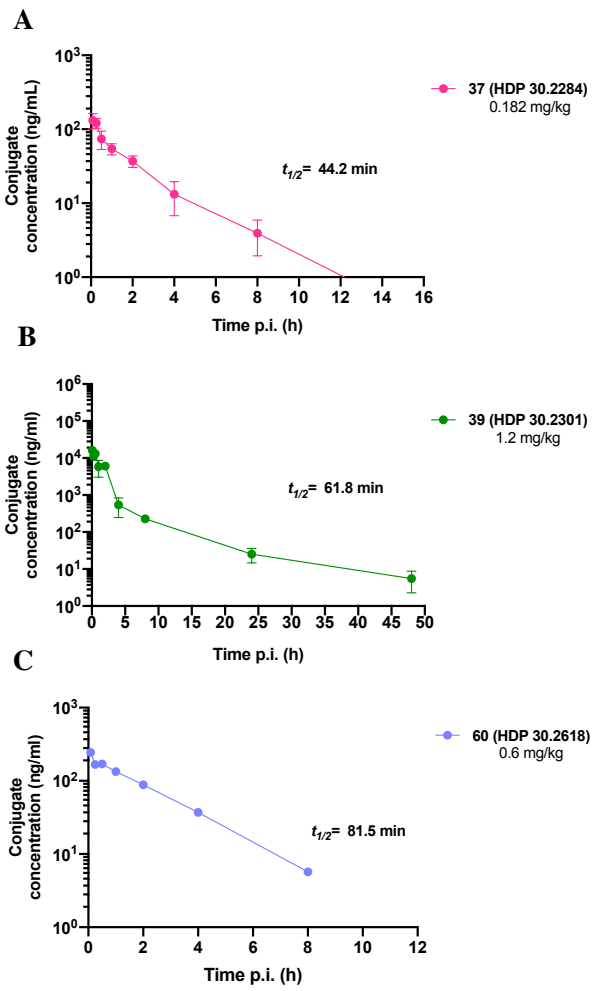

Figure 43. Pharmacokinetic (PK) study of A) DUPA-mc-va-α-amanitin (37); B) DUPA-mc-α-amanitin (39) and C) DUPA-(Me)SS-α-amanitin (60). Plasma concentration of α-amanitin-containing compounds in CB17-Scid male mice after a single intravenous (i.v.) dose was determined by anti-α-amanitin ELISA. Each data point represents the mean ± SEM of n= 3 mice.

slightly longer $t_{1/2}$ observed for these conjugates might be the result of dose-dependent pharmacokinetics due to saturation of the clearance processes.[153]

In general, the short half-life reported for all the three conjugates suggested that an important determinant of the efficacy might be the dosing frequency.

5.1.3 Biodistribution study. To assess the tissue distribution of the DUPA-Pep-α-amanitin SMDCs, SMDCs **37** and **39** were injected in CB17-Scid male mice bearing LNCaP xenografts at single dose of 0.182 mg/kg (4x MTD) to secure detectable conjugate concentrations in serum and extracts of organs, and 1.28 mg/kg (½MTD), respectively. The content of α-amanitin-containing compounds in tumor and tissue of excretory organs (liver and kidney) was determined using anti-α-amanitin ELISA.

There was a similar biodistribution pattern for the SMDCs with the dipeptide cleavable linker and the non-cleavable linker (**Figure 44A** and **B**).

Compounds gradually concentrated in the tumor, achieving maximum concentration of approximately 51 ng/g of tissue at 1 h p.i. for SMDC **37** and 2 µg/g at 0.5 h p.i. for SMDC **39.** Both compounds were still detectable 48 h after administration. Consistently to the rapid decrease over time of the blood concentration (**Figure 43A** and **B**), SMDCs **37** and **39** rapidly distributed to the kidneys, reaching a peak concentration of approximately 2 µg/g of tissue at 4 h p.i. for SMDC **37** and 5 µg/g of tissue at 2 h p.i. for SMDC **39**. SMDCs **37** and **39** persisted up to 48 h p.i. in the kidneys in relatively high concentration (approximately 0.6 and 3 µg/g of tissue, respectively).

A gradual decrease of the liver concentration over the study duration was observed for both SMDCs, reflecting the clearance profile from the circulation (**Figure 43A** and **B**).

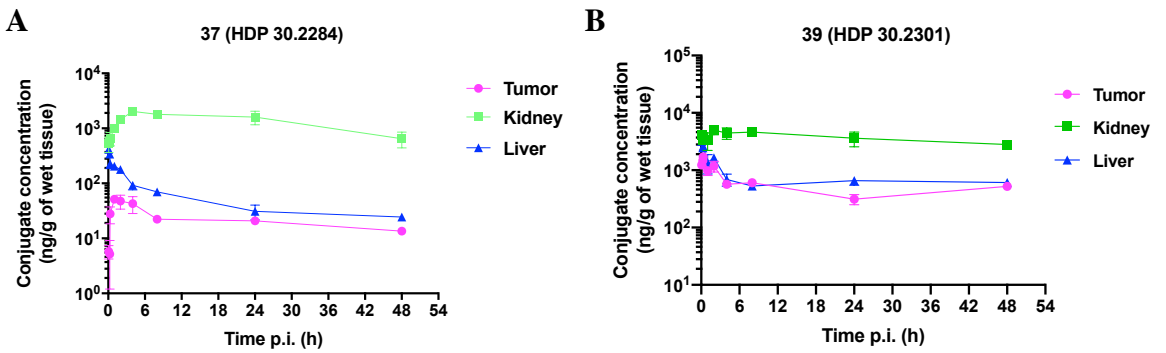

Figure 44. Biodistribution study of A) DUPA-Pep-mc-va-α-amanitin (37) and B) DUPA-Pep-mc-α-amanitin (39) SMDCs in LNCaP xenograft CB17-Scid male mice. Concentration of α-amanitin-containing compounds after a single intravenous (i.v.) dose (0.184 and 1.28 mg/kg for DUPA-Pep-mc-va-α-amanitin **37** and DUPA-Pep-mc-α-amanitin **39**, respectively) was determined by anti-α-amanitin ELISA by using a polyclonal rabbit anti-α-amanitin capture antibody biotinylated α-amanitin and a HRP(horseradish peroxidase)-streptavidin conjugate for detection. The results are expressed as nanograms per gram (ng/g) of wet tissue. Error bars represent the mean concentration ± SEM of n= 3 mice/group.

5.1.4 Renal uptake mechanistic study. PSMA is physiologically expressed in the kidney proximal tubules.[100,101] To elucidate whether the renal accumulation observed for the DUPA-Pep-α–amanitin SMDCs **37** and **39** was mediated by PSMA, blocking studies with the pre- (100-fold excess) and co-administration (50-fold excess) of the PSMA inhibitor 2-PMPA were performed in CB17-Scid male mice (**Figure 45A**). SMDCs **37** and **39** were administered at a single dose equivalent to 75 µg/kg of α-amanitin. Animals were sacrificed 6 h after administration and kidney tissues were analyzed by competitive anti-α-amanitin ELISA.

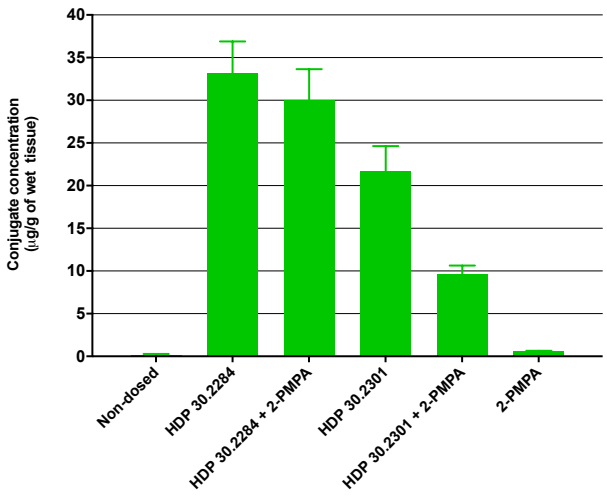

Figure 45. A) Renal uptake mechanistic study for DUPA-mc-va-α-amanitin (37, HDP 30.2284) and DUPA-mc-α-amanitin (39, HDP 30.2301) in CB17-Scid male mice. Blocking studies were perfomed with pre- (100-fold excess) and co-injections (50-fold excess) of the PSMA inhibitor 2-PMPA. Injected dose of compound: 0.182 mg/kg and 1.28 mg/kg for **37** and **39**, respectively. Concentrations of α-amanitin-containing compounds was determined in ethanol extracts of kidneys by competitive anti-α-amanitin ELISA using a polyclonal anti-α-amanitin antibody, biotinylated α-amanitin and HRP-streptavidin for detection. Error bars represent SEM of n= 3 mice.

Unblocked renal uptake was approximately 10% higher for SMDC **37** than for SMDC **39**. Upon pre- and co-administration of 2-PMPA the renal uptake of α-amanitin-containing compounds was only minimally reduced (< 5%) for the DUPA-mc-va-α-amanitin SMDC **37**. In contrast, the renal uptake for the DUPA-mc-α-amanitin SMDC **39** was reduced by a factor of approximately 50%, in comparison to the unblocked uptake.

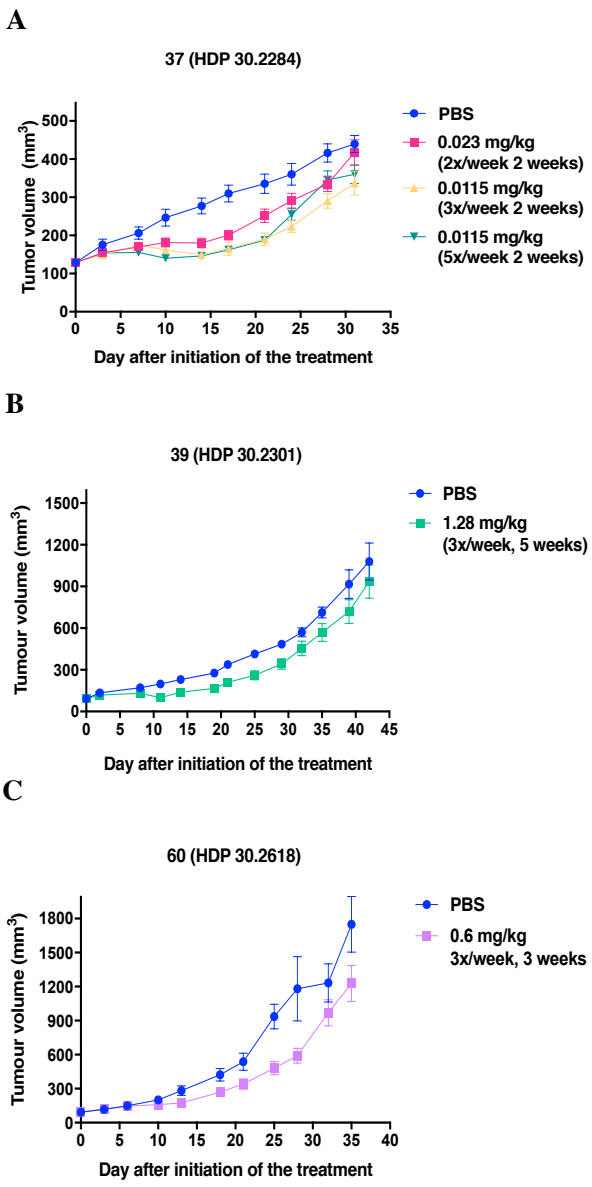

Figure 46. Antitumor efficacy of A) DUPA-mc-va-α-amanitin (37); B) DUPA-mc-α-amanitin (39) and C) DUPA-(Me)SS-α-amanitin (60) in LNCaP xenograft male CB17-Scid mice after multiple intravenous (i.v.) injections. Error bars in tumor volume curves represent SEM of n= 8-10. For HDP 30.2618 from day 25 onward results of minimal n= 4 are presented, remaining animals from this group were sacrified due to unacceptable tumor volume.

A comparative kidney accumulation study between unconjugated α-amanitin and SMDC **37** (data not shown) administered at the same equivalent dose of 75 μg/kg revealed no accumulation of the unconjugated toxin up to 24 h after administration corresponding to the study duration. These data suggest that the renal uptake of α-amanitin-containing compounds is enhanced when toxin is administered in the conjugated form.

Taken together, results of this study indicate that while the renal uptake for the DUPA-Pep-mc-α-amanitin SMDC **39** is partly mediated by PSMA, PSMA-specific uptake might not be the main uptake mechanism for the DUPA-Pep-mc-va-α-amanitin SMDC **37**.

5.1.5 Efficacy. *In vivo* antitumor activity of the thiosuccinimide-linked SMDCs **37** and **39**, and the 1:0 disulfide-linked SMDC **60** was evaluated in LNCaP xenograft models. LNCaP cells were implanted subcutaneously (s.c.) in CB17-Scid male mice and allow to grow to ~100 mm^3 prior to initiaton of the treatment.

In a pilot efficacy study, activity of the DUPA-Pep-mc-va-α-amanitin SMDC (**37**) was evaluated (**Figure 46A**). Because SMDCs **37**, **39**, and **60** displayed short PK half-life (**Figure 43A-C**), to define the optimal dosing, conjugate **37** was administered at different doses and dosing regimens.

As basis for the study a triweekly regimen of 0.023 mg/kg (½ MTD) administered twice per week was established and compared with the drug given at half dose (¼ MTD, 0.0115 mg/kg) but three or five times per week to mantain plasma drug concentration to optimal levels.

Untreated LNCaP tumors reached a volume of approximately 400 mm^3 within the termination of the study.

The level of efficacy of SMDC **37** varied depending on the dosing regimen, with half dose/high frequency-based regimen determining better antitumor activity. However, only a partial tumor growth inhibition effect was observed and the effect persisted only throughout the treatment period. Indeed, upon termination of the treatment, tumors started to regrow with a kinetics similar to that of the vehicle-injected group. Importantly, body weights remained unchanged during the course of the study, indicating that the therapy was well tolerated (data not shown).

Having assessed that short PK exposure is an important determinant of the antitumor activity, it was later investigated whether the dose-limiting toxicity (DLT) could also account for the limited *in vivo* efficacy of the DUPA-Pep-mc-va-α-amanitin SMDC (**37**). Therefore, the counterpart DUPA-Pep-mc-α-amanitin SMDC (**39**) containing the non-cleavable linker was also evaluated (**Figure 46B**). Indeed, the higher tolerability of SMDC **39** allowed the application of a high dose/high frequency regimen (1.28 mg/kg, three times per week) for an extendend period of five weeks.

The trend in body weight was similar in control and conjugate-treated animals at all dosing regimens, indicating that therapy was not grossly toxic (data not shown).

Despite the higher dose of toxin in conjugated form administered frequently, partial response to the therapy intended as tumor growth inhibition was achieved and sustained only during the period from day 10 to approximately day 20. SMDC **39**-treated mice stopped responding to the therapy approximately three weeks after initiation of the treatment and mean tumor volume for the treated and the control groups became less significantly different.

In the last efficacy study, the *in vivo* antitumor activity of DUPA-Pep-Me-SS-α-amanitin SMDC (**60**) was investigated (**Figure 46C**). At a dose of 0.6 mg/kg (½ MTD) administered three times per week for three weeks, SMDC **60** induced only a slight tumor growth delay, which was not sustained over the entire period of the study. As for the previous compounds, all mice mantained their normal body weights during the treament period indicating that the therapy with the DUPA-Pep-Me-SS-α-amanitin SMDC (**60**) was well tolerated (data not shown).

5.2 Discussion

A significant amount of effort has been spent on attaching different microtubule inhibitors to DUPA-based PSMA binding moiety through self-immolative disulfide linkers.[122, 128, 129]

Interestingly, there has been much less focus on systematic investigation of innovative payloads and impact of linker type on the efficacy and toxicity of DUPA-targeted SMDCs.

In this preliminary study a new linker-drug technology based on α-amanitin was developed for DUPA-targeted SMDCs. The primary question revolved around the impact of linker and release mechanism on the efficacy and toxicity of the DUPA-Pep-α-amanitin SMDCs. To address this question, peptide cleavable-, mc non-cleavable- and disulfide-linked DUPA-Pep-α-amanitin

SMDCs were developed. The peptide-linked SMDC (**37**) is expected to be cleaved by cysteine cathepsin B and to release the unmodified toxin in the lysosome. On the opposite, the non-cleavable linker relies on the scaffold degradation within the lysosome to release a toxin metabolite.

The selected 1:0 disulfide-bridged SMDC (**60**) relies on the steric hindrance of a methyl group for stabilization of the linkage exposed to plasma enzymes and on the cleavage and release of the toxin in the cellular reducing environment, upon internalization.

Having identified three DUPA-Pep-α-amanitin SMDCs exemplifying different linker-drug technologies with good *in vitro* profile, their *in vivo* efficacy and toxicity were compared.

Results from the safety studies in mice demonstrated that the most active *in vitro* dipeptide-linked SMDC (**37**) was less tolerated than the mc non-cleavable (**39**) and the disulfide-linked (**60**) SMDCs. When MTDs are expressed as drug equivalents the increased toxicity in this series DUPA-Pep-mc-α-amanitin (**39**) < DUPA-Pep-Me-SS-α-amanitin (**60**) < DUPA-Pep-mc-va-α-amanitin (**37**) suggests a relationship between linker cleavability and conjugate toxicity. For the thiosuccinimide adducts (**37**, **39**) different mechanisms that can impair the conjugate stability in systemic circulation, such as decoupling of maleimide-based linkage by *retro*-Michael addition or linker enzymatic degradation, may account for the reported toxicity. Premature degradation in mouse serum mediated by carboxylesterase 1C (Ces1C) of dipeptides has been recently reported for dipeptide drug-linker containing Val-Cit motif. Because Val-Ala dipeptides are susceptible to the same enzyme,[154] it is plausible that the enzyme activity in mouse serum determined premature loss of the α-amanitin payload in the cleavable DUPA-Pep-mc-va-α-amanitin SMDC (**37**). Thus, it may argue that the severe kidney toxicity observed in mice treated with high doses of DUPA-Pep-mc-va-α-amanitin (0.368 and 0.184 mg/kg equal to 150 and 75 μg/kg of α-amanitin, respectively) was due to the α-amanitin released from the conjugate. However, assuming that all the conjugated α-amanitin was released from the conjugate, concentrations achieved *in vivo* would be equal to or even lower than the MTD of α-amanitin for this mouse strain (150 μg/kg). Moreover, accumulation of toxic concentrations is not likely as α-amanitin is excreted by mammals very rapidly in urine with a half-life in mice of about 30 minutes.[73] This hypothesis is further supported by the comparative kidney accumulation study between unconjugated α-amanitin and DUPA-Pep-mc-va-α-amanitin SMDC (**37**), which showed no accumulation of toxin in the kidney over the course of the study when administered as unconjugated toxin compared to the toxin administered in the conjugated form. Biodistribution studies carried out with either the DUPA-Pep-mc-va-α-amanitin (**37**) and the DUPA-Pep-mc-α-amanitin (**39**) SMDCs demonstrated that, while concentration of the compounds in blood rapidly decreased, compounds distributed and accumulated in the kidneys. These results are in accordance with the plasma pharmacokinetic studies, which showed fast plasma clearance for the three SMDCs investigated ($t_{1/2}$ ca. 0.5-1.5 h). This is likely a consequence of the kidney glomerular filtration, which occurs readily within 15-25 min for molecules with

molecular weight (M_r) < 40 kDa. For instance, etarfolatide, a low molecular weight anticancer agent (M_r ca. 856 Da) has a $t_{1/2}$ of 27 min.[54]

Besides the rapid renal clearance, other mechanisms can affect the stability of the SMDCs in circulation and consequent low plasma exposure to the drug in the conjugated form.

Mc-derived SMDCs **37** and **39** can undergo to drug-linker loss by *retro*-Michael deconjugation and exchange with exogenous thiols, such as glutathione, cysteine and the serum albumin. In the context of ADCs, it has been demonstrated by Alley *et al*.[145] that the cysteine residue 34 on serum albumin exchanges with alkyl maleimides, which is also consistent with other studies related to systematically administered maleimido-containing anticancer drugs.[155] Exchange reactions with exogenous thiols in circulation can also cause premature drug-linker loss from the disulfide-linked SMDC **60**.

In 1988 Derenzini *et al*. reported that amatoxins covalently bound to albumin are preferentially taken up by cells involved in the protein turnover, such as macrophages, sinusoidal cells of the liver and protein-absorbing cells of kidney leading to increased toxin-related toxicity *in vivo*.[156] It cannot be ruled out that, upon thiol-exchange in circulation, albumin conjugates were taken up by the kidneys, where they were later processed to different α-amanitin metabolites with different levels of toxicity. However, the current method ELISA used in these studies, which detects only the α-amanitin component does not allow to detect differences in drug-linker metabolism in circulation neither possible albumin conjugates.

High and specific kidney uptake and retention are also described in literature for PSMA-targeted radioligands due to the PSMA physiological expression on the brush border of proximal tubules,[101,102] suggesting the involvement of PSMA in the kidney uptake of DUPA-Pep-α-amanitin SMDCs. PSMA blocking studies indicated that the kidney uptake was actually partly associated to the PSMA expression in the murine kidneys only for the DUPA-Pep-mc-α-amanitin SMDC **39**.

In contrast, uptake of the DUPA-Pep-mc-va-α-amanitin SMDC **37** in the kidneys could not be significantly blocked by pre- and co-injection of 2-PMPA, suggesting that kidney uptake for this conjugate was not primarily PSMA-mediated.

The different kidney uptake mechanism assumed for SMDCs **37** and **39** might be related to the different linker cleavability. SMDC **37** features an enzymatic cleavable linker. Linker cleavage in the kidneys would result in α-amanitin-containing metabolites devoid of the PSMA binding motif which would constitute the major component uptaken and retained by the kidneys. This hypothesis might explain why pre- and co-injection of the PSMA inhibitor 2-PMPA had no significant impact on the kidney uptake of SMDC **37**. On the opposite, the higher linker stability of SMDC **39** may have preserved the conjugate from premature degradation and loss of the targeting moiety. Hence, the PSMA-mediated uptake had a higher contribution to the kidney uptake of SMDC **39**. However, contribution from specific metabolites to the renal uptake of SMDCs **37** and **39** can not be demonstrated as measurements of metabolites in mice urines were not carried out in the present

study. Although expression of PSMA in the mouse kidneys was shown to be partly responsible for the kidney uptake of SMDCs **37** and **39**, it would not constitute the major pitfall for clinical translation of DUPA-Pep-α-amanitin SMDCs since human kidneys express PSMA at significantly lower levels than murine kidneys.[124]

Furthermore, contribution of other off-targets expressed in the mouse kidneys to the uptake of DUPA-Pep-α-amanitin SMDCs can not be totally ruled out.

Importantly, α-amanitin is known to cause severe liver injury in humans upon uptake in the hepatocytes mediated by the OATP1B3 transporter,[80,81] which is the ortholog of the Oatp1b2 expressed in the murine liver. Oatp1b2 transporter is thought to be one of the transporter systems involved in the α-amanitin uptake in the murine liver.[157] For the mc-linked DUPA-Pep-α-amanitin SMDCs **37** and **39**, accumulation of α-amanitin containing compounds in the liver was not observed, confirming that α-amanitin in the conjugated form is no longer a substrate for the liver transporters.[158]

Despite the different linker cleavability, the thiosuccinimide- (**37**, **39**) and the disulfide-linked (**60**) SMDCs provided similar efficacy. The dose frequency-dependent tumor growth inhibition observed during the therapy was not sustained after termination of the treatment. The reduced exposure to the drug in the conjugated form due to the fast renal clearance and/or metabolic instability prevented sufficient accumulation of the toxin in the tumor. This was confirmed by the tissue distribution studies of the thiosuccinimide-linked DUPA-Pep-α-amanitin SMDCs (**37**, **39**), which showed that at 8 h p.i. the tumor content was only 22 ng/g of tissue for the DUPA-Pep-mc-va-α-amanitin SMDC (**37**) and 0.6 μg/g of tissue for the DUPA-Pep-mc-α-amanitin (**39**), respectively.

Altogether, the results indicate that instability in plasma combined to fast renal clearance severely limit the therapeutic potential of the DUPA-Pep-α-amanitin SMDCs.

Chapter 6

The thioacetamide-linked SMDCs

The limited antitumor activity of the lead DUPA-Pep-α-amanitin SMDCs (**37, 39, 60**) was most probably the consequence of the poor toxin accumulation in the tumor, likely due to a combination of rapid renal clearance and low stability in circulation of the conjugates. Low stability of the conjugates in circulation can reduce exposure to the DUPA-conjugated form of α–amanitin and thus, affect the conjugates efficacy.

The structural feature shared by the DUPA-Pep-mc-va-α–amanitin (**37**) and DUPA-Pep-mc-α–amanitin (**39**) SMDCs is the thiosuccinimide linkage formed through the reaction between the alkyl maleimide handle on the drug-linker and the cysteine thiol on the DUPA-Pep motif.

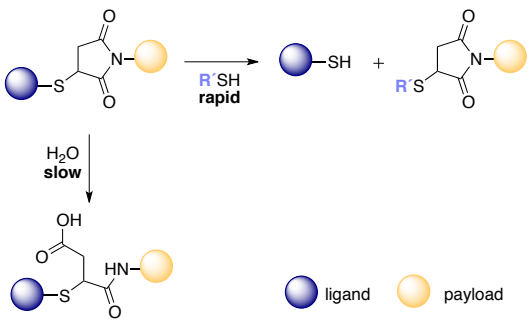

Figure 47. Mechanisms that can affect stability of the thiosuccinimide linkage. Thiosuccinimide adducts can undergo either rapid *retro*-Michael-addition reaction or slow hydrolysis.

As discussed in section 3.2, it has been recognized that this conjugation chemistry is reversible in thiols-enriched environments.[145] The thiosuccinimide is susceptible *in vivo* to rapid exchange with thiols present in plasma through the *retro*-Michael addition reaction (**Figure 47**). This leads to the premature loss of the drug payload, thereby reducing the circulating amount of drug in the conjugated form and rising risks of off-site toxicities.[145]

In addition to the *retro*-Michael reaction, the succinimide ring may also undergo irreversible hydrolysis, forming an elimination-resistant product (**Figure 47**). However, the kinetics of the ring opening reaction is considerably slower with reaction rate ≥ 200 h under physiological conditions.[159] In animal models DUPA-targeted conjugates were found to be cleared from circulation in less than 1 h, suggesting that ring opening reaction is not likely to have an impact on the stability of the conjugates.

In the context of ADCs, Alley and co-workers demonstrated that replacement of thiosuccinimide with thioacetamide linkage increased significantly the *in vivo* stability of the thioether product, leading to higher intratumoral drug exposure compared to the succinimide counterpart.[145]

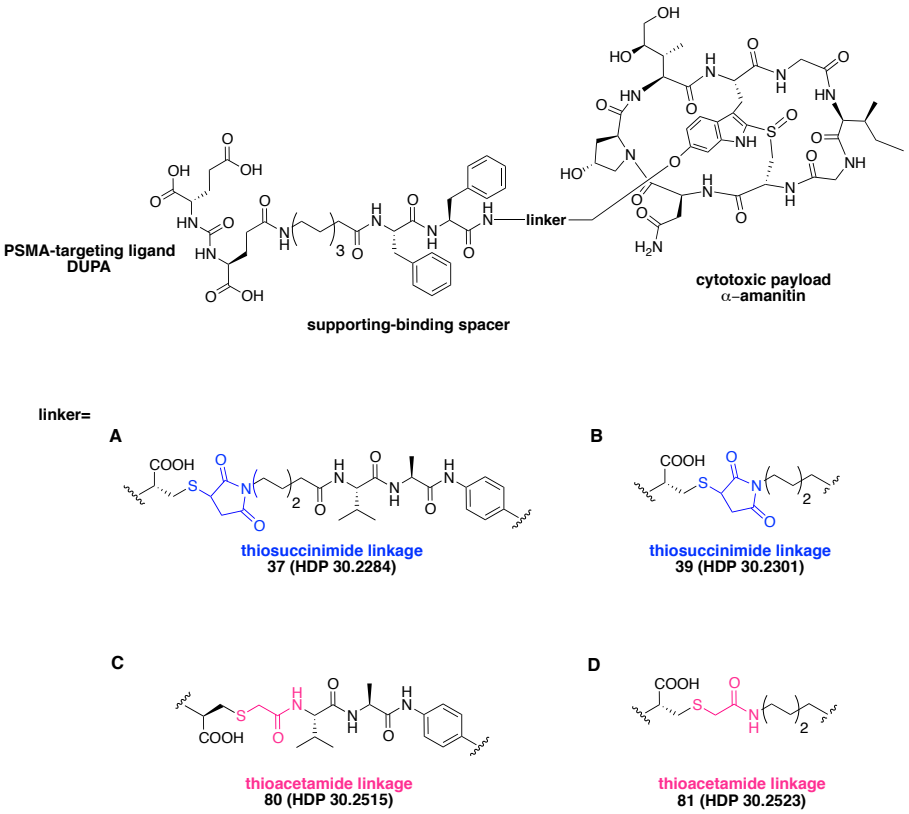

Figure 48. Structures of the thioacetamide-based DUPA-Pep-α-amanitin SMDCs (C, D) compared to the previuosly reported thiosuccinimide-linked SMDCs (A, B). Thiosuccinimide-linked SMDCs bearing**: A**) cathepsin B-sensitive self-immolative va-PAB linker DUPA-Pep-mc-va-α-amanitin (**37, HDP 30.2284**); **B**) alkyl non-cleavable linker DUPA-Pep-mc-α-amanitin (**39, HDP 30.2301**). Thioacetamide-linked SMDCs bearing: **C**) cathepsin B-sensitive self-immolative va-PAB linker DUPA-Pep-ac-va-α-amanitin (**80, HDP 30.2515**) and **D**) alkyl non-cleavable linker DUPA-Pep-ac-α-amanitin (**81, HDP 30.2523**).

Aiming at extending the plasma stability of the thioether bond, thioacetamide (ac)-linked analogues (**80**-**81**; **Figure 48**) of the previously described thiosuccinimide-linked SMDCs (**37**, **39**; **Figure 34**) were synthesized. To evaluate the effectiveness of this approach, plasma stability of the thioacetamide adducts (**80**-**81**) was evaluated in comparison to the parent thiosuccinimide adducts (**37**, **39**).

6.1 Results

6.1.1 Chemistry. The DUPA-Pep-ac-va-α–amanitin (**80**) was synthesized according to the procedure illustrated in **Scheme 11**.

Primary amine incorporated into the va-α–amanitin drug-linker **47a**, synthetized as described in section 3.1.1 **(Scheme 3)**, easily reacted with the bromoacetic acid NHS-ester furnishing the bromoacetamide (bac)-va-α–amanitin drug-linker **82**. This derivative was designed to react with the thiol-bearing DUPA-Pep sequence **44** (section 3.1.1, **Scheme 2**). As well established procedure, conjugation was run at controlled pH (~ 8-9) generating the desired thioacetamide adduct **80 (HDP 30.2515**).

Scheme 11. Synthesis of the ac-derived DUPA-Pep-ac-va-α-amanitin SMDC (80).

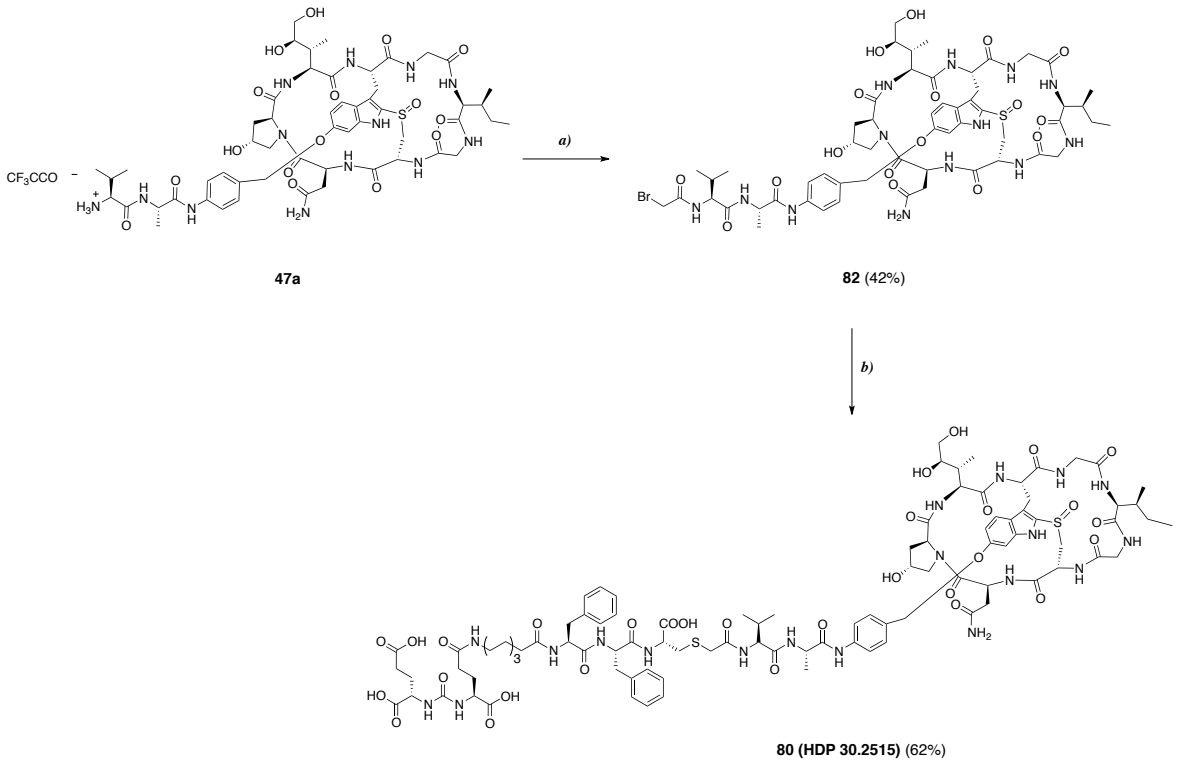

Reagents and conditions: ***a)*** bromoacetic acid NHS ester, DIPEA, DMF, rt, 1 h; ***b)*** **44**, Na_2CO_3/$NaHCO_3$ pH 9.3, ACN/H_2O, rt, 1.5 h.

For the preparation of the DUPA-Pep-ac-α–amanitin (**81**; **Scheme 12**) following the standard procedure, α–amanitin was alkylated in position 6'-OH with the commercially available Boc-protected carboxylate- and phenol-reactive crosslinker 6-(Boc-amino)hexyl bromide. Boc deprotection upon short exposure to acidic conditions yielded the intermediate **84** containing the free primary amine as trifluoroacetate salt. Carboxylate-reactive intermediate **84** was coupled to the NHS ester-activated bromoacetic acid, leading to the bac-α–amanitin drug-linker **85**. Similarly to

the procedure described above, conjugation of the resulting thiol-reactive bac-α-amanitin drug-linker **85** to the cysteine thiol of the DUPA-peptide reagent **44** was carried out at controlled pH yielding the final thioacetamide analogue **81** (**HDP 30.2523**). Both ac-linked SMDCs (**80**-**81**) were isolated by preparative chromatography in purity ≥ 95% prior their usage in biological assays.

Scheme 12. Synthesis of the ac-derived DUPA-Pep-ac-α-amanitin SMDC (81).

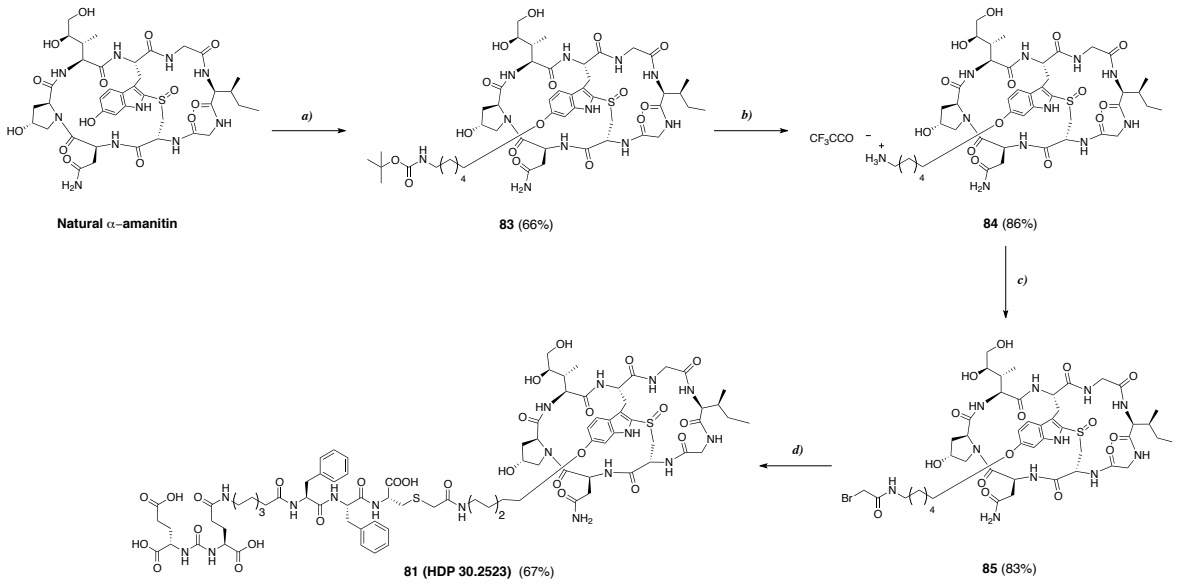

Reagents and conditions: ***a)*** 6-(Boc-amino)hexyl bromide, 2M LiOH, DMSO, rt, 40 min; ***b)*** TFA, rt, 2 min; ***c)*** bromoacetic acid NHS ester, DIPEA, DMF, rt, 1 h; ***d)*** **44**, Na_2CO_3/$NaHCO_3$ pH 9.3, ACN/H_2O, rt, 1.5 h.

6.1.2 *In vitro* cytotoxicity. Following the same protocol described previously (section 3.1.3), *in vitro* potency of the thioacetamide-linked SMDCs (**80**-**81**) was determined against the $PSMA^+$ LNCaP and $PSMA^-$ PC3 human prostate cancer cell lines. Dose-response curves and calculated EC_{50} values are shown in **Figure 49** in comparison to the outcomes obtained for the parent thiosuccinimide-linked SMDCs **37** and **39**.

DUPA-Pep-ac-va-α-amanitin SMDC (**80**) exhibited a cytotoxic profile comparable to that of the mc-linked DUPA-Pep-mc-va-α-amanitin counterpart (**37**) against the $PSMA^+$ LNCaP cells, with an estimated EC_{50} value of 2.57 nM. Not surprisingly, the thioacetamide-linked SMDC **80** was almost as potent as the parent thiosuccinimide-linked SMDC **37**. Indeed, SMDCs **37** and **80** are both supposed to release α-amanitin upon cleavage and self-immolation of the dipeptide Val-Ala-PAB linker.

Despite the DUPA-Pep-mc-α-amanitin (**39**) and the DUPA-Pep-ac-α-amanitin (**81**) SMDCs release, upon lysosomal degradation of the scaffold, presumably chemically different drug-linker, they are equally potent against the $PSMA^+$ LNCaP cells, and both are less active than the corresponding SMDCs bearing the dipeptide cleavable linker Val-Ala-PAB.

As expected, potency displayed against the PSMA$^-$ PC3 cells by both the DUPA-Pep-ac-va-α-amanitin (**80**) and the DUPA-Pep-ac-α-amanitin (**81**) SMDCs was in the activity range of unconjugated α-amanitin (10^{-7}-10^{-6} M). This observation remarks that the greater potency reported on the PSMA$^+$ LNCaP cells is the consequence of the PSMA-mediated cell internalization properties of the DUPA-Pep-α-amanitin conjugates.

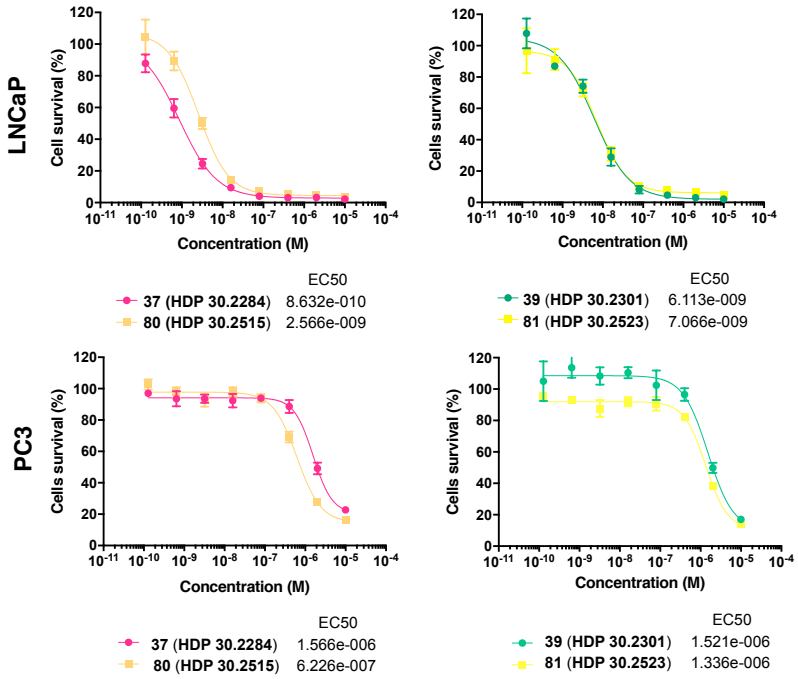

Figure 49. **Dose-response curves for DUPA-Pep-ac-va-α-amanitin (80; left panel) and DUPA-Pep-ac-α-amanitin (81; right panel).** Curves were generated by using ATP cell viability assay (CellTiter Glo® 2.0) after 96 h incubation with PSMA$^+$ LNCaP (top panel) and PSMA$^-$ PC3 (lower panel) cells of increasing concentrations (10^{-10}-10^{-5}) of each compound in comparison to the parent thioacetamide-linked DUPA-Pep-mc-va-α-amanitin (**37**; left panel) and DUPA-Pep-mc-α-amanitin (**39**; right panel) SMDCs. Data points are average of triplicate wells compared to no treatment control.

6.1.3 *In vitro* plasma stability. To confirm the greater chemical stability expected for the thioacetamide-linked SMDCs (**80-81**) compared to the parent thiosuccinimide-linked SMDCs (**37**, **39**), plasma stability of conjugates **80**-**81** was assessed as described in section 3.1.4. The dose-response curves and the calculated EC_{50} values are reported in **Figures 50-51**. Data obtained for the parent thiosuccinimide-linked SMDCs (**37**, **39**) shown in sections 3.1.4 are also reported as thiosuccinimide-linked SMDCs (**37**, **39**) serve as reference conjugates in the present study.

As mentioned in section 3.1.4, thiosuccinimide-linked DUPA-Pep-mc-va-α-amanitin (**37**) and DUPA-Pep-mc-α-amanitin (**39**) SMDCs retained intact their activity within 6 h incubation in either MP and HP. For time points longer than 6 h, curves tend progressively to flatten indicating loss of activity due to increased instability in plasma with a more pronounced effect in HP than in MP.

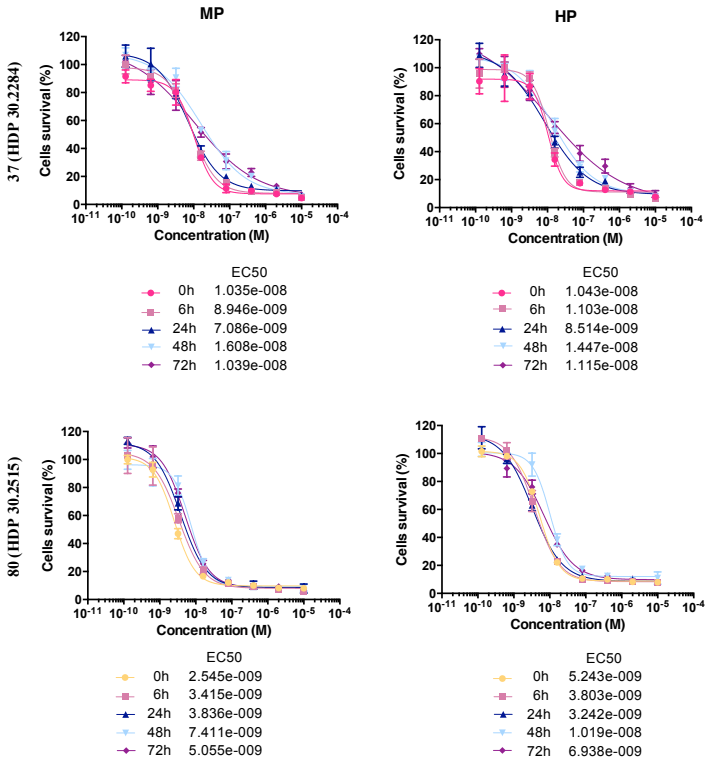

Figure 50. Plasma stability of the of the thiosuccinimide-linked DUPA-Pep-mc-va-α-amanitin SMDC (37) (top panel) and the thioacetamide-linked DUPA-Pep-ac-va-α-amanitin SMDC (80) (lower panel). Cytotoxic potential at time points 0-72 h was assessed upon 96 h incubation with PSMA$^+$ LNCaP cells. Prior to cytotoxicity assay, compounds were incubated in mouse plasma (MP; left panel) and human plasma (HP; right panel) for time points within 0 to 72 h.

As for the reference conjugates (**37**, **39**), different linker cleavability did not translate into a remarkable difference in terms of stability in MP and HP between the conjugate containing the dipeptide cleavable linker (**80**) and its non-cleavable counterpart (**81**).

In contrast to the reference compounds (**37**, **39**), the thioacetamide-linked SMDCs (**80**-**81**) did not display significant reduction of potency after being stressed in MP for 0 to 72 h. At concentrations ≥ 100 nM potency was slightly diminished by approximately 10-20% for samples incubated in HP for time points longer than 6 h, as shown by the flattening of the curves.

This finding suggests greater stability of the thioacetamide-linked SMDCs (**80**-**81**) in MP than in HP, in line to what was observed for the parent thiosuccinimide-linked SMDCs (**37**, **39**).

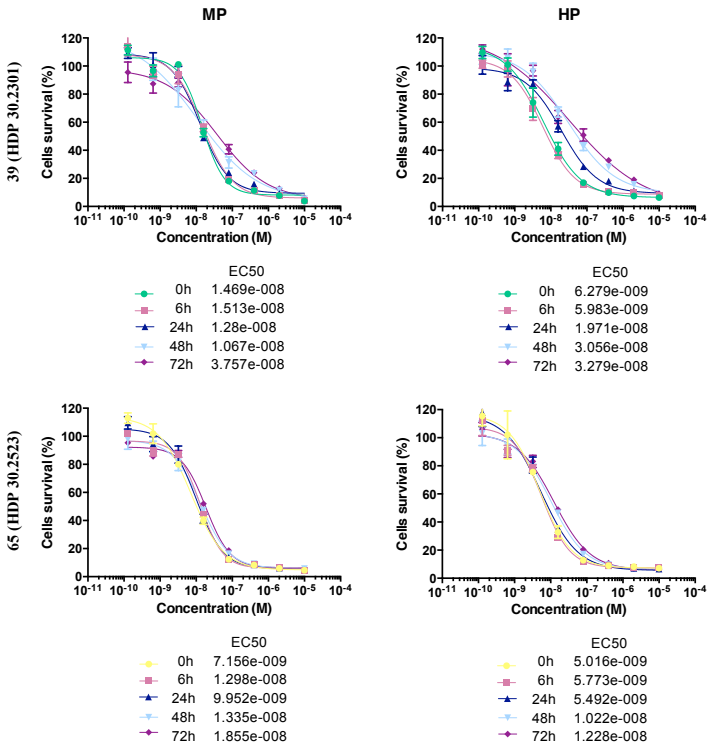

Figure 51. Plasma stability of the thiosuccinimide-linked DUPA-Pep-mc-α-amanitin SMDC (39) (top panel) and the thioacetamde-linked DUPA-Pep-ac-α-amanitin SMDC (81) (lower panel). Cytotoxic potential at time points 0-72 h was assessed upon 96 h incubation with $PSMA^+$ LNCaP cells. Prior to cytotoxicity assay, compounds were incubated in mouse plasma (MP; left panel) and human plasma (HP; right panel) for time points within 0 to 72 h.

6.2 Discussion

In an effort to address the stability issue of the thiosuccinimide linkage, second generation DUPA-Pep-α-amanitin SMDCs were developed by replacing the alkyl maleimide drug-linkers with the acetamide analogues.

Regarding the synthesis, the thiosuccinimide chemistry is more attractive because reaction occurred in a highly selective manner without usually the careful control of the reaction conditions. Nevertheless, with a slightly alkaline buffer and control of the reaction stoichiometry, the thioacetamide conjugation was successfully achieved with the exclusive modification of the cysteine residue.

Replacement of the thiosuccinimide with the thioacetamide resulted in the increased stability of the SMDCs over the time. The resulting thioacetamide-linked SMDCs (**80**-**81**) retained intact the *in vitro* potency of the parent thiosuccinimide-linked SMDCs (**37**, **39**). In spite of the similar cytotoxic potency, the thioacetamide-linked derivatives displayed no apparent loss of activity upon prolonged exposure to plasma proteins (up to 72 hours) compared to the parent conjugates.

The pharmacological consequences of extending the linker half-life could not be investigated within the time frame of this project. However, taking into account that the thiosuccinimide-linked SMDCs were found to be stable up to 6 hours, it is reasonable that chemical linker stability was not

the main factor limiting the therapeutic efficacy of the DUPA-Pep-α-amanitin conjugates tested so far, but rather the very short clearance half-life displayed *in vivo*. Therefore, extending the linker stability beyond the clearance half-life is not likely to have a significant impact on the drug efficacy, due to the reduced compound concentration over time. Nonetheless, this finding appears to be significant in the context of the half-life extension strategies, where increasing the linkage stability over prolonged period of time can make the difference.

Chapter 7

Improving the pharmacokinetics with a PKM linker

Biodistribution profile of the DUPA-Pep-mc-va-α–amanitin (**37**) and DUPA-Pep-mc-α-amanitin (**39**) SMDCs showed high uptake and retention in the kidneys, which was the dose-limiting toxicity organ. It was later shown that the PSMA expression in the murine kidney tubules was not the main factor determining the kidney uptake of the DUPA-Pep-α–amanitin SMDCs (section 5.1.4).

Nephrotoxicity due to the kidney uptake and accumulation of radiolabeled peptides and antibody fragments is widely documented in literature.[160]

Small biomolecules in plasma are rapidly cleared through glomerular filtration, which occurs freely at sizes below approximately 60 to 70 kDa, and apparently this process is more efficient for cationic and neutral solutes than for the anionic ones.[161a-b]

Following glomerular filtration, most peptides and proteins are almost quantitatively reabsorbed in the proximal tubules mainly through receptor-mediated endocytosis, resulting in the effective renal trapping and retention of related metabolites.[162] The negatively charged scavenger receptors megalin and the megalin-dependent cubilin receptors, both expressed on the apical membrane of the proximal tubules, have been recognized as involved in the proximal tubular reabsorption of structurally different molecules.[162] For example, it has been proved in kidney-specific megalin-deficient mice that megalin is responsible for the kidney uptake of radiolabeled octreotide and neurotensin peptides, both containing basic lysine amino acid residues.[163]

Different strategies have been proved effective in reducing the kidney uptake and retention of radiolabeled peptides, such as coadministration of charged amino acids[164a-b] or incorporation in the structure of negatively charged linker or single amino acids, known as pharmacokinetics-modifying (PKM) linkers, in order to interfere with the negatively charged sites of the glomerular filtration barrier[165,166] and the membrane of renal tubular cells at physiological pH.

For example, the $(EH)_3$-tag was shown to have a positive impact on reducing the kidney uptake of the radiolabeled PSMA inhibitor ACUPA(Ahx)-HBED-CC (**86**; **Figure 52**) by a factor of 2.8 (from 139.44 ± 21.40 to 49.03 ± 16.34 %ID/g), without affecting the tumor uptake.[167] In 2016 Eder *et al*. described the incorporation of a $(HE)_2$ linker into a heterodimeric PSMA/GRPr (Gastrin releasing peptide receptor)-targeting radiolabeled agent (**87**; **Figure 52**). The peptide with increased negative net charge at physiological pH showed improved tumor uptake and ca. 50-fold

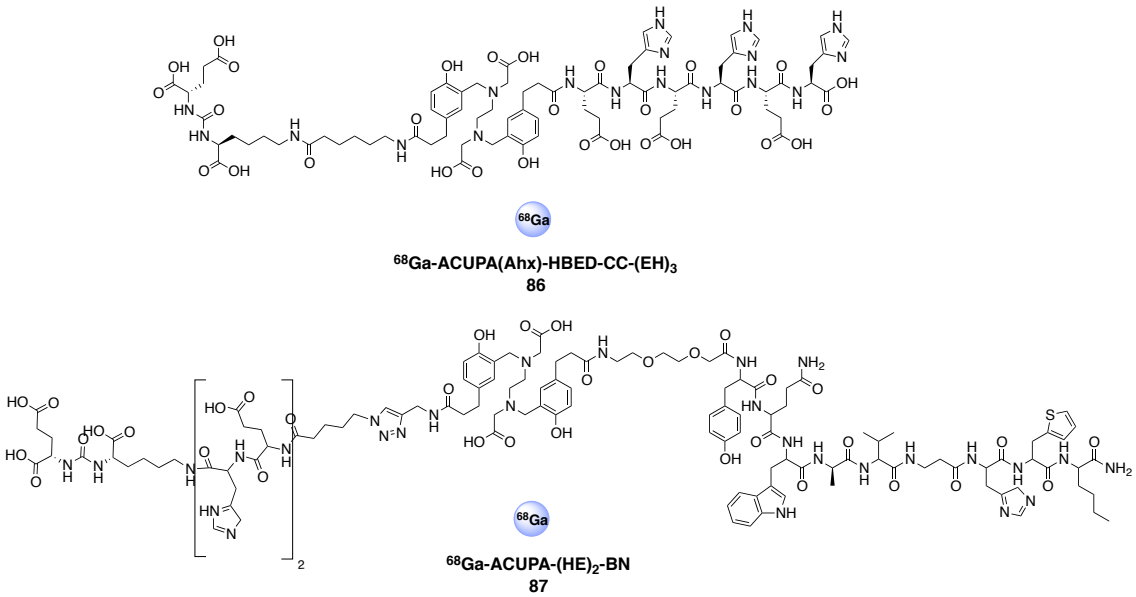

Figure 52. Structures of selected radiolabeled peptides incorporating PKM linkers. The ^{68}Ga-radiolabeled PSMA-targeting ACUPA(Ahx)-HBED-CC-$(EH)_3$ including the $(EH)_3$ PKM linker (**86**; top panel) and the PSMA/GRPr-targeting ACUPA-$(HE)_2$-BN peptide including the (HE_2) PKM linker (**87**; lower panel).

reduced kidney uptake at 60 min p.i. compared to the analogous peptide lacking the PKM linker.[168]

In an attempt to optimize the PK properties of the DUPA-Pep-α-amanitin SMDCs regarding the high kidney uptake and retention, the effect of the $(HE)_2$ PKM linker on clearance half-life and renal uptake was evaluated. As longer clearance half-life was expected, for this proof of concept study the maleimide conjugation chemistry was replaced by the bromoacetamide conjugation chemistry, which was demonstrated in the previous chapter to confer higher stability in plasma to the construct. The structure of the DUPA-Pep-$(HE)_2$-ac-va-α-amanitin SMDC (**88**) is shown in **Figure 53**.

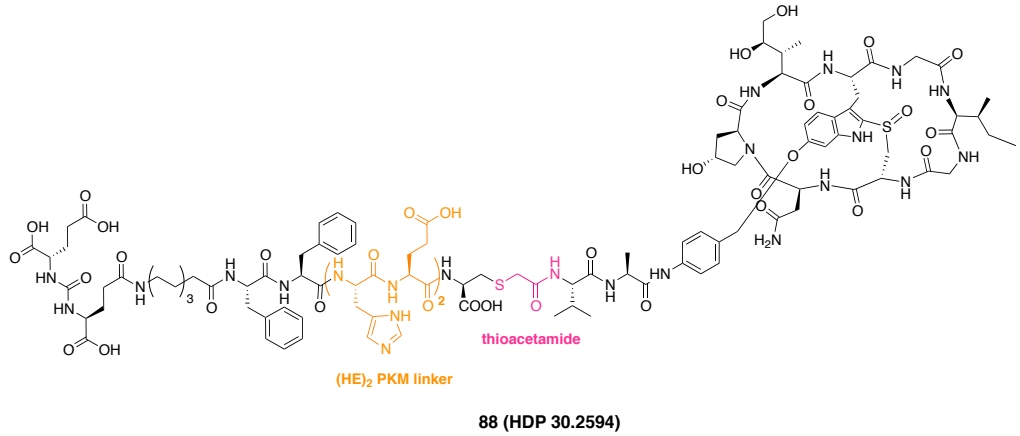

Figure 53. Structure of the DUPA-Pep-$(HE)_2$-ac-va-α-amanitin (88, HDP 30.2594). The $(HE)_2$ PKM linker and the plasma stable thioacetamide linkage are shown in cyan and magenta, respectively.

7.1 Results

7.1.1 Chemistry. The $(HE)_2$ PKM linker was introduced between the DUPA-8-Aoc-Phe-Phe pharmacophore sequence and the *C*-terminal conjugation site. The whole sequence was assembled by SPPS according to the standard Fmoc peptide protocol on trityl-protected cysteine-preloaded chlorotrityl resin (**Scheme 13**).

Scheme 13. Synthesis of the $(HE)_2$-incorporating DUPA-Pep-$(HE)_2$-va-α-amanitin SMDC (88).

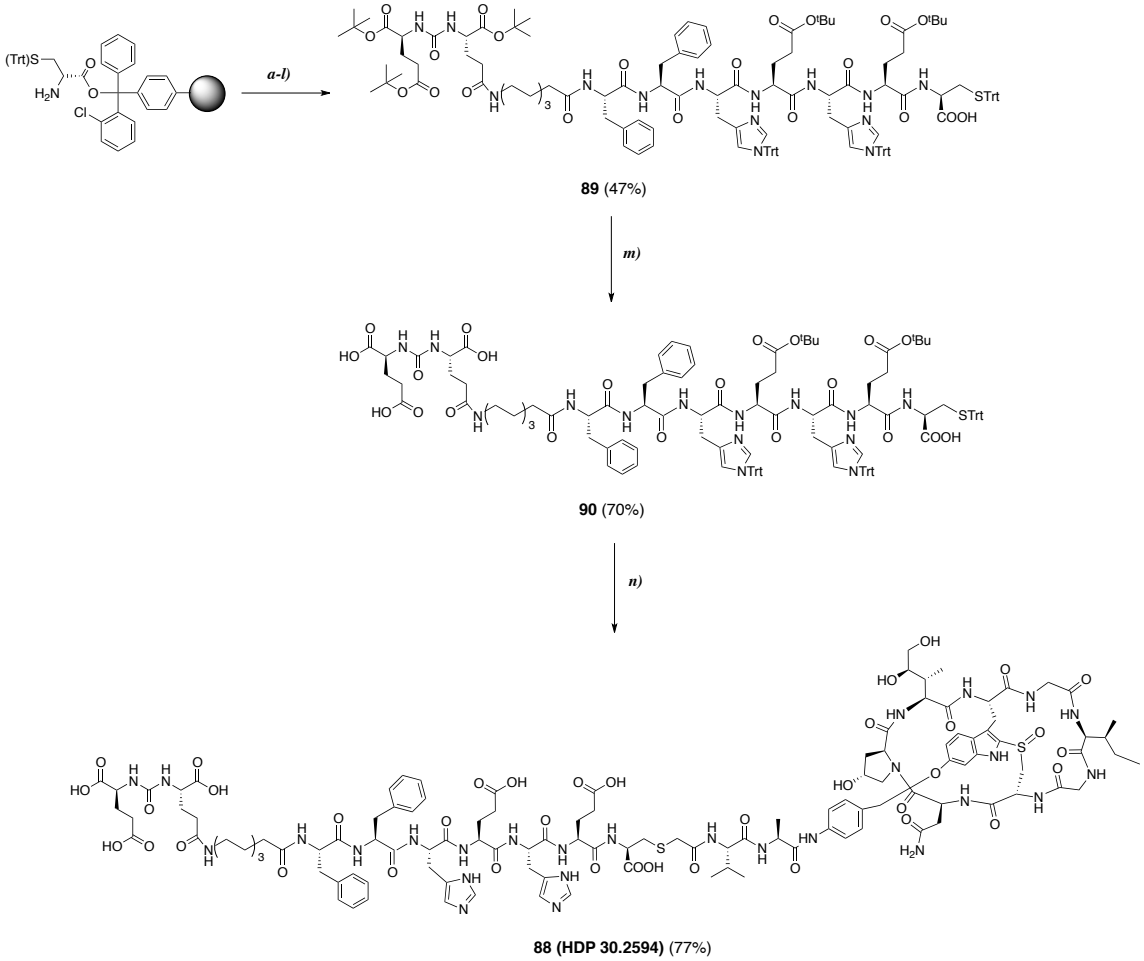

Reagents and conditions: ***a-h)*** i. Fmoc-AA-OH, HOBt, HBTU, DIPEA, DMF, 60 °C, 40 W, 10 min; ii. 20% piperidine/DMF, 60 °C, 40 W, 3 min; ***i)*** **42**, HOBt, HBTU, DIPEA, DMF, 60 °C, 40 W, 10 min; ***l)*** TFE/AcOH/DCM (1:1:8, v:v.v), 23 °C, 1.5 h; ***m)*** TFA/TIS/H_2O (95:2.5:2.5, v:v:v), DTT; ***n)*** **82**, Na_2CO_3/$NaHCO_3$ pH 9.0, ACN/H_2O (1:1, v:v), rt, 1.5 h.

Once cleaved from the resin under mild acidic conditions, the fully protected DUPA-Pep-$(HE)_2$-SH reagent **89** was totally deprotected. The intermediate **90** was reacted with the bac-va-α-amanitin drug linker **82** according to the protocol described in section 6.1.1 for the thiol-bromoacetamide conjugation chemistry, affording the final product **88** (**HDP 30.2594**). Preparative chromatography

was used to isolate ≥ 95% pure DUPA-Pep-$(HE)_2$-ac-va-α-amanitin (**88**) to be used in biological assays.

7.1.2 *In vitro* cytotoxicity. In order to evaluate the *in vitro* potency and selectivity, $(HE)_2$-incorporating SMDC **88** was incubated with $PSMA^+$ LNCaP and $PSMA^-$ PC3 cells in presence and absence of an excess of the PSMA inhibitor 2-PMPA, according to the protocol described already in section 3.1.3. In this assay unconjugated α-amanitin was used as reference compound. The dose-response curves are shown in **Figure 54**. The calculated EC_{50} values for conjugate **88** and the lead DUPA-Pep-mc-va-α-amanitin SMDC (**37**) are presented in **Table 5**.

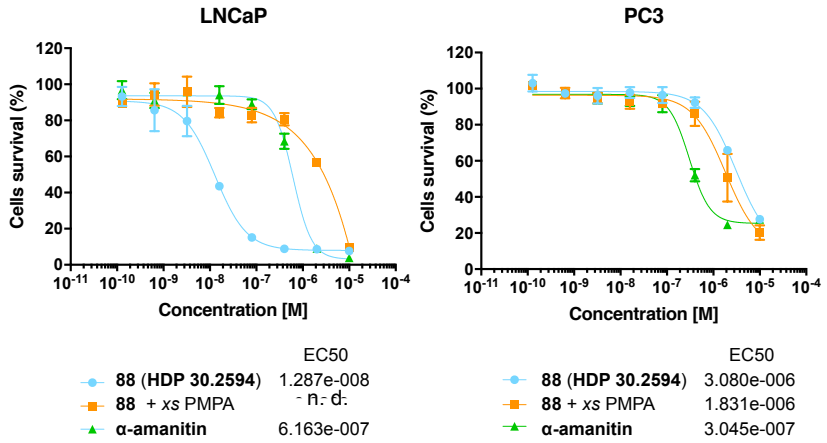

Figure 54. Dose-response curves for the DUPA-Pep-$(HE)_2$-ac-va-α-amanitin SMDC (88). Curves were generated by using ATP cell viability assay (CellTiter Glo® 2.0) after 96 h incubation with $PSMA^+$ LNCaP (left panel) and $PSMA^-$ PC3 (right panel) cells of increasing concentrations (10^{-10}-10^{-5}) of each compound, in presence and absence of a 100-fold molar excess (*xs*) of the PSMA inhibitor 2-PMPA (PMPA). Data points are average of triplicate wells compared to no treatment control.

		EC_{50} (nM)	
		LNCaP	**PC3**
37	DUPA-Pep-mc-va-α–amanitin	0.9	[a]*none*
88	DUPA-Pep-$(HE)_2$-ac-α–amanitin	12.9	[a]*none*

[a]*none*= not active within 100 pM to 1 μM.

Table 5. Summary of the EC_{50} values calculated for the PKM linker-incorporating DUPA-Pep-$(HE)_2$-ac-va-α-amanitin SMDC (88) compared to the lead DUPA-Pep-mc-va-α-amanitin SMDC (37).

Although the potency of the DUPA-Pep-$(HE)_2$-ac-va-α-amanitin SMDC (**88**) on $PSMA^+$ LNCaP cells was approximately 48-fold greater than that of unconjugated α-amanitin (EC_{50} 12.8 and 616.3 nM for SMDC **88** and α-amanitin, respectively), a slight reduction of potency compared to the

PKM-non incorporating counterpart **37** was observed. Potency on the $PSMA^+$ cells was nearly quantitative inhibited in the competitive binding assay, demonstrating that the PSMA-mediated internalization properties of the DUPA-Pep-α–amanitin SMDCs were not affected by the introduction of the PKM $(HE)_2$ linker. This conclusion is further supported by lack of significant toxicity on the $PSMA^-$ PC3 cells.

7.1.3 *In vivo* serum pharacokinetics and kidney uptake study. Studies comparing the serum clearance and kidney uptake of the DUPA-Pep-mc-va-α-amanitin SMDC (**37**) and DUPA-Pep-$(HE)_2$-ac-va-α-amanitin SMDC (**88**) were conducted in mice after i.v. administration of a single dose of conjugates corresponding to 75 µg/kg of α-amanitin. Concentration of α-amanitin-containing compounds was determined by anti-α-amanitin ELISA.

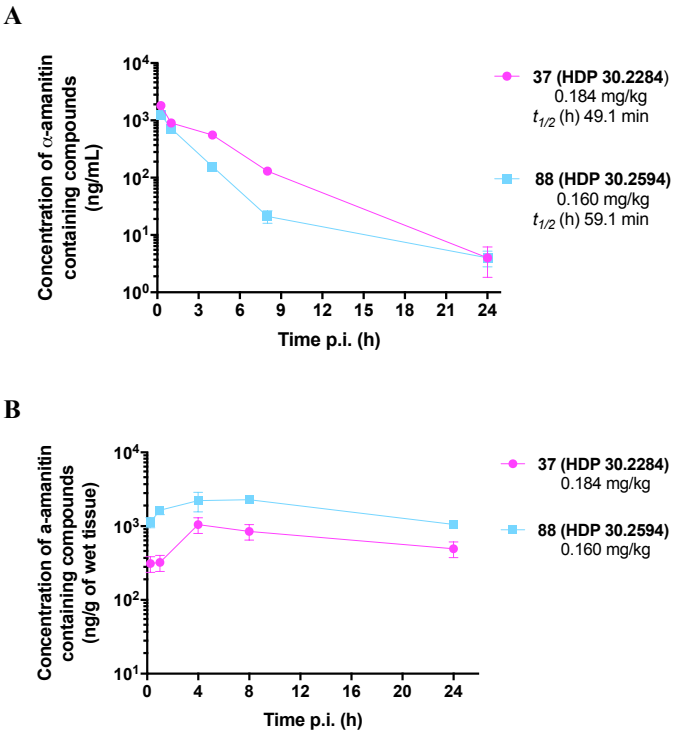

Figure 55. Comparative A) serum pharmacokinetics and B) kidney uptake studies between DUPA-Pep-$(HE)_2$-ac-va-α-amanitin SMDC (88; cyan) and lead DUPA-Pep-mc-va-α-amanitin SMDC (37; magenta). Studies were carried out following intravenous injection (i.v.) of a single dose corresponding to 75 µg/kg of α-amanitin. Concentrations were determined by anti-α-amanitin ELISA by using a polyclonal rabbit anti-α-amanitin antibody, biotinylated α-amanitin and a HRP(horseradish peroxidase)-streptavidin conjugate for detection. The results are expressed as nanograms per gram (ng/g) of wet tissue. Single points are average of data ± SEM from n= 3 mice.

Analysis provided a $t_{1/2}$ for clearance of approximately 49 minutes for the lead SMDC **37**, which is consistent with the value reported in the previous study (section 5.1.2), and 59 minutes for the SMDC **88** incorporating the $(HE)_2$ PKM linker (**Figure 55A**).

Results from the kidney uptake study are shown in **Figure 55B**. DUPA-Pep-mc-va-α-amanitin SMDC (**37**) presented maximal kidney uptake at 4 h p.i. and persisted up to 24 h p.i., in accordance to the data reported previously (section 5.1.3).The DUPA-Pep-$(HE)_2$-ac-va-α-amanitin SMDC (**88**) showed a renal uptake and retention profile similar to that of the DUPA-Pep-mc-va-α-amanitin SMDC (**37**), with a peak concentration reached at 4 h following administration. These data showed that, despite the incorporation of the $(HE)_2$ PKM linker, the pharmacokinetics and biodistribution profile of the DUPA-Pep-α-amanitin SMDCs were not improved.

7.2 Discussion

High kidney uptake of the DUPA-Pep-α-amanitin SMDCs caused dose-limiting nephrotoxicity, as in the case of the most *in vitro* active conjugate, the DUPA-Pep-mc-va-α-amanitin SMDC (**37**). Reduction of the kidney uptake could allow administration of higher doses, which might improve the therapy effectiveness.

Different strategies have been successfully applied in the peptide-receptor radionuclide therapy (PRRT) to reduce the kidney uptake of radiolabeled peptides and antibody fragments.[164a-b] Coadministration of cationic amino acids (Lys and Arg) intereferes with the renal uptake of radiolabeled antibody fragments and cationic peptides like octreotide, while negatively charged poly-glutamic acid chains can reduce renal uptake of anionic peptides, such as the minigastrin peptide MG0. These findings suggest that factors such as total charge and charge distribution of the molecule might play a role in the peptides uptake into proximal tubular cells.

Other strategies to influence interactions with kidney compartments, such as glomeruli and proximal tubules, consist in structural modifications. As the glomerular filtration barrier has an overall negative charge at physiological pH[165] and the membrane of renal tubular cells contains negatively charged sites, incorporation of negatively charged PKM linkers might reduce the renal filtration and uptake.[166]

Recently, Liolios *et al*. reported the incorporation of the charged $(HE)_2$ PKM linker in the structure of a PSMA/GRPr-targeting radiolabeled heterodimer, which led to a significant reduction of the kidney uptake.[168]

In this initial study, the effect of the $(HE)_2$ PKM linker in combination with the bromoacetamide linkage chemistry on serum clearance and renal uptake of the DUPA-Pep-α-amanitin SMDCs was investigated. *In vitro* analyses of the $(HE)_2$-incorporating conjugate, DUPA-Pep-$(HE)_2$-ac-va-α-amanitin SMDC (**88**), in comparison to the $(HE)_2$-non incorporating counterpart **37** revealed similar activity profile against the panel of the tested cell lines. However, remarkably, the potency of the $(HE)_2$-incorporating conjugate **88** on the PSMA-expressing LNCaP cells was reduced by a factor of approximately 14 compared to the $(HE)_2$-non incorporating counterpart **37**.

Former studies[167] described a worsening of the binding affinity for PSMA of radiolabeled peptides incorporating such PKM linkers. Affinity of the ACUPA(Ahx)-HBED-CC-$(EH)_3$ (**87**; **Figure 52**) reported by Eder et *al*., for example, was reduced by a factor of 3 from 10.33 ± 1.2 to 31.80 ± 1.2 nM. Binding affinity of the DUPA-Pep-mc-va-α-amanitin (**37**) and DUPA-Pep-$(HE)_2$-ac-va-α-amanitin (**88**) SMDCs was not determined. Nevertheless, it is reasonable that a reduction of the binding affinity accounts for the decreased activity observed on PSMA-expressing cells for the $(HE)_2$-incorporating SMDC **88**. It is known that negatively charged molecules, such as phosphatidylserine, heparin sulfate and sialic acid are more abundantly expressed on tumor cells than on normal cells. Thus, it is plausible that electrostatic repulsion occurred between the

negatively charged conjugate and the negative charges on the membrane of tumor cells, hampered the binding affinity of the $(HE)_2$-incorporating SMDC **88**.

Comparative serum pharmacokinetics and kidney uptake studies showed that the DUPA-Pep-$(HE)_2$-ac-va-α-amanitin conjugate (**88**) combining the charged $(HE)_2$ PKM linker and the stable thioacetamide linkage retained the unfavourable characteristics of the first generation SMDCs with regards to their fast serum clearance and accumulation in excretory organs, i.e. the kidney.

It has been shown that coadministration of cationic peptides is not effective in reducing the renal uptake of anionic peptides, like MG0, which has a net negative charge of -7. In this latter case, a different uptake mechanism based on OAT transporters has been proposed.[160] A similar mechanism mediated by an OAT transporter system might have contributed to the kidney uptake of the DUPA-Pep-α-amanitin SMDCs, which display at physiological pH negatively charged carboxylates, and the negative net charge is further increased in the SMDC **88** by incorporation of the $(HE)_2$ PKM linker. However, further investigations are required in order to fully elucidate the kidney uptake mechanism of the DUPA-Pep-α-amanitin SMDCs.

Because the DUPA-Pep-$(HE)_2$-ac-va-α-amanitin SMDC (**88**) did not show improved PK properties, it was not further developed.

Chapter 8

A multivalent approach to improve the tumor uptake and retention

In vivo profiling of the DUPA-Pep-α-amanitin SMDCs developed so far pointed out that the rapid blood clearance along with the low tumor uptake and the short retention time severely limit their potential development as successful therapeutics.

Compared to antibodies as targeting agents, small ligands typically display lower tumor affinity and short retention time.

High tumor retention of antibodies is achieved through multivalent interactions. Mutivalent interactions are involved in several biological processes, including cell recognition and signal transduction.[169] Since they are stronger than bonding of an equivalent number of ligands, multivalent interactions lead to an overall higher binding affinity (**Figure 56**).[170, 171] Enhancement of the interaction strength can derived from different mechanisms, such as: a) clustering of soluble partners; b) chelation and c) statistical rebinding or proximity effects (**Figure 57**).[172]

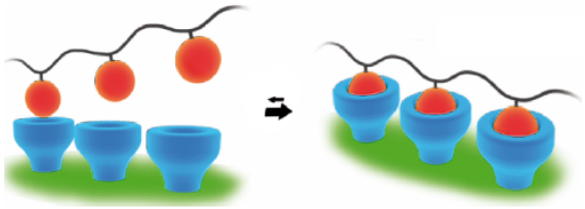

Figure 56. Multivalent interactions shift the equilibrium enhancing the binding strength. Reprinted with permission from Fasting, C. *et al. Angew. Chem.* 2012, *124*, 10622-10650, Copyright 2012 Wiley-VCH.

Multivalency approach has been often applied to enhance the affinity of molecular probes.

It has been previously reported that multivalent DUPA-based radiolabeled agents exhibited higher tumor uptake and prolonged retention as compared to their monovalent analogues.

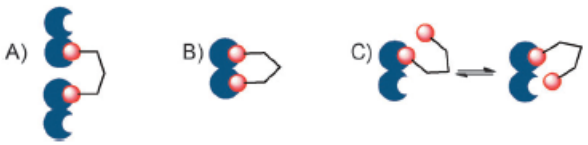

Figure 57. Modes of multimeric ligand binding. A multivalent ligand (red): A) clustering a soluble protein (blue); B) chelating a divalent protein; C) binding to a protein exploiting the statistical rebinding (proximity) effect. Reprinted from Ordanini, S. *et al. Chem. Comm.* 2015, *51*, 3816-3819. Published by The Royal Society of Chemistry.

Pomper *et al.* compared the PSMA binding affinity of ACUPA-based monovalent (**91**), bivalent (**92**) and DOTA-chelated bivalent (**93**) agents (**Figure 58**). It was observed that binding affinity of the bivalent (**92**) and DOTA-chelated bivalent (**93**) agents was 5- and 11-fold higher, respectively, than that of the monovalent agent (**91**).

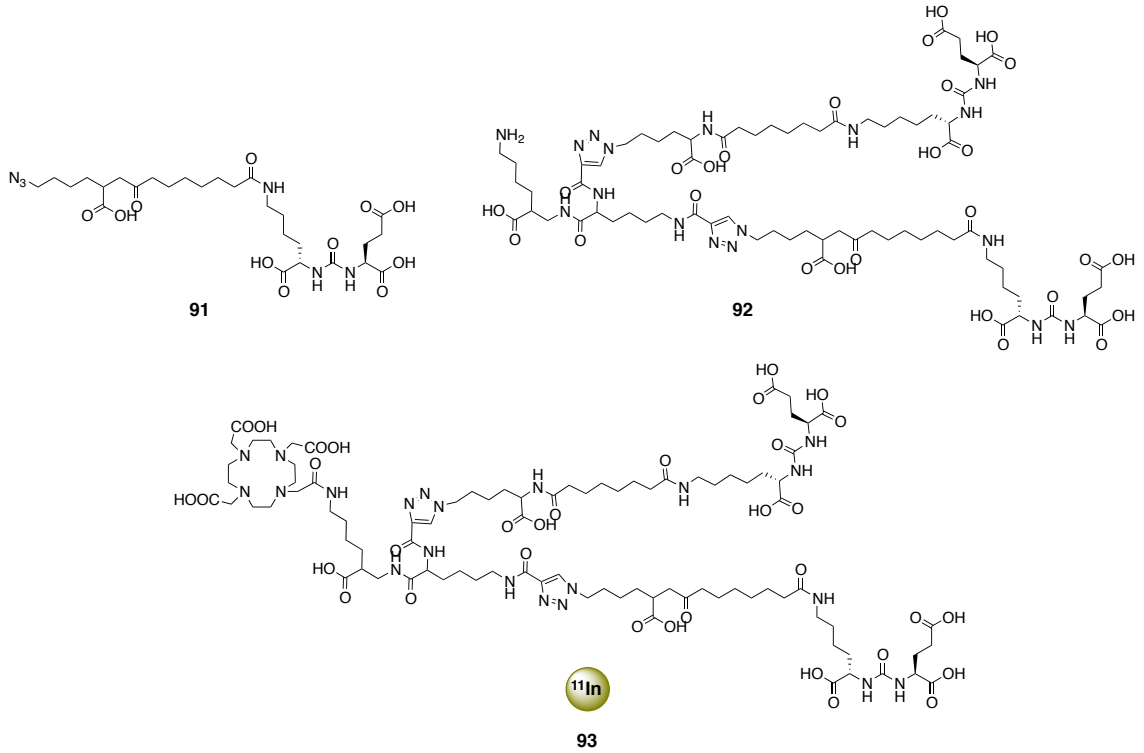

Figure 58. Structure of the PSMA-targeting ACUPA-based monovalent (91), bivalent (92) and DOTA-chelated bivalent agents (93).[173]

A SPECT-CT imaging study of the ^{11}In-labeled DOTA-chelated bivalent agent **93** revealed high and specific uptake in PSMA^{+} PC3 PIP tumor which was imaged out to eight days post injection. Rapid clearance from non-targeted tissues, included kidneys, was also observed. Imaging data were further validated by biodistribution studies which demonstrated continuous accumulation at the tumor site out to 24 h p.i. (34.0 ± 7.5 % ID/g).[173]

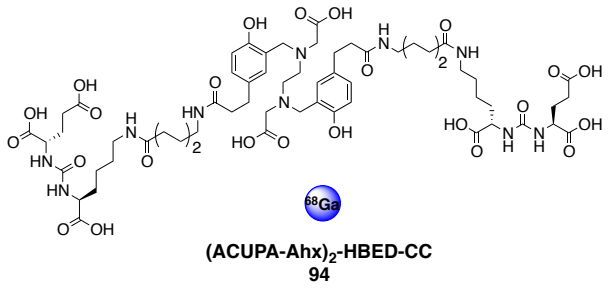

Figure 59. Structure of the ^{68}Ga-labeled divalent ACUPA(Ahx)-HBED-CC (**94**).[175]

Dimerization of the ACUPA pharmacophore via the ^{68}Ga HBED-CC chelator increased significantly the binding properties of the imaging probe **94** (**Figure 59**) compared to the monomeric one (IC_{50}(dimer)= 3.9 ± 1.8 nM *vs*. IC_{50}(monomer)= 12.1 ± 2.1 nM on LNCaP cells), and enhanced the tumor-to-background (T/B) ratio (T/B(monomer)= 9.2, T/B(dimer)= 26.5).[174]

Based on these findings, in the present study dimerization of the DUPA-Pep binding motif was explored as strategy to improve the tumor uptake and retention of the DUPA-Pep-α-amanitin SMDCs. Crystal structure of PSMA revealed that the two catalytic binding sites face opposite to each other with a distance between two similar zinc ions in the catalytic site of each monomer of 56 Å.[175]

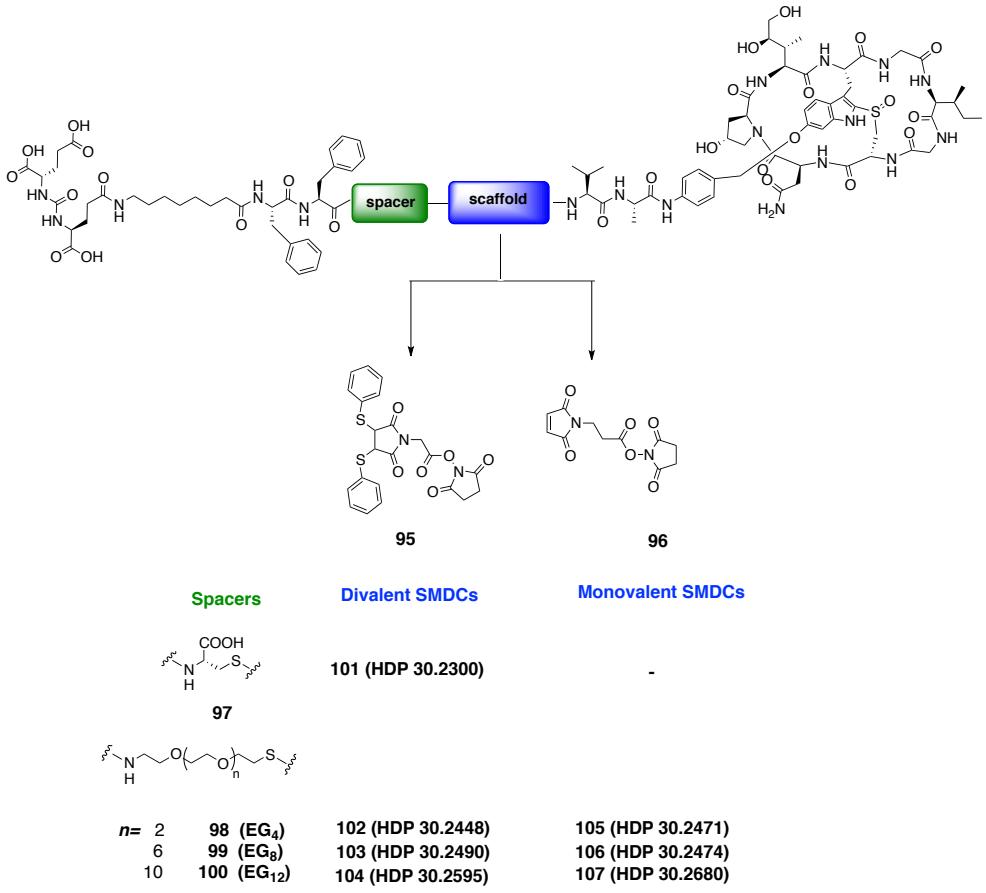

Figure 60. Schematic structure representation of the bivalent (DUPA-Pep-spacer)$_2$-maleimidoacetyl(ma)-va-α-amanitin SMCDs (102-104) and monovalent DUPA-Pep-EG$_n$-mp-va-α-amanitin SMDCs (105-107).

To investigate the spacer length and flexibility to which the ligand-receptor system responds optimally, bivalent DUPA-Pep-α-amanitin SMDCs with or without various oligo(ethylene glycol) spacers EG$_n$ were generated (**Figure 60**). For this proof-of-concept study, the va-PAB linker was selected as toxin-releasing system. In order to set a general synthetic strategy, a 3,4-disubstituted maleimide was used as central bifurcated scaffold and connected to the *N*-terminus of the va-α-amanitin drug-linker payload. The commercially available 3-(maleimido)propionic acid was used as scaffold for the preparation of the corresponding flexible monovalent conjugates to be used as reference compounds in the biological evaluation of the bivalent SMDCs.

8.1 Results

8.1.1 Chemistry. Bivalent SMDCs (**102-104**) were prepared by assembling two modules: a "Y" shaped branched drug–linker payload in the form of [3,4-*bis*(phenylthio)]-maleimidoacetyl (ma)-va-α-amanitin (**109**) and a thiol-bearing DUPA-Pep-spacer (**97**-**100**), as outlined in **Scheme 14**. [3,4-*bis*(phenylthio)]-ma-α-amanitin derivative **108** was achieved via coupling the va-α-amanitin drug-linker **47a** (section 3.1.1, **Scheme 5**) to the NHS ester-activated [3,4-*bis*(phenylthio)] maleimide *N*-acetic acid building block (**95**).

Scheme 14. Synthesis of bivalent (DUPA-Pep-spacer)$_2$-ma-va-α-amanitin SMDCs (102-104).

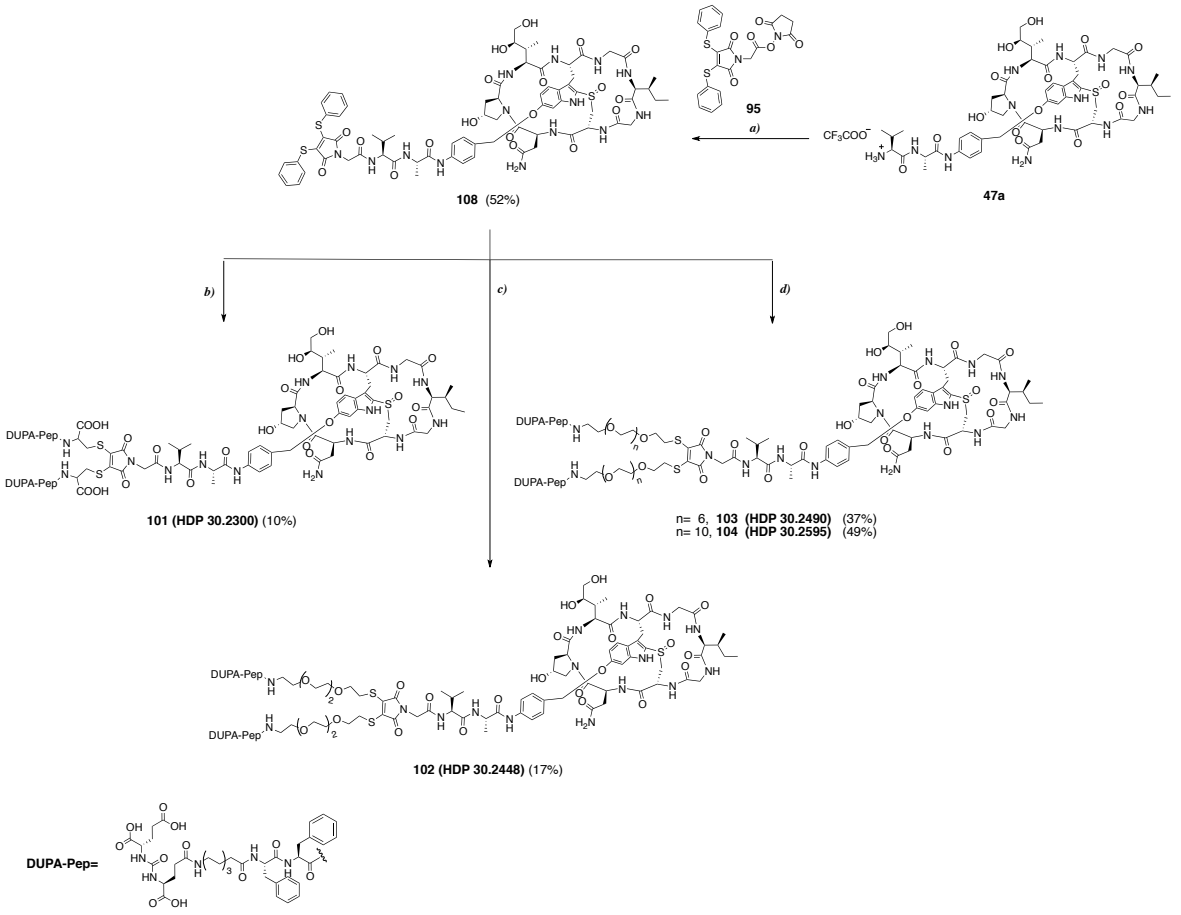

Reagents and conditions: ***a)*** **95**, DIPEA, DMF, rt, 2 h; ***b)*** **97**, DIPEA, DMSO, 48 h; ***c)*** **98**, TEA, rt, 48 h; ***d)*** **99** or **100**, NaOMe, MeOH, rt, 20 h.

The initial procedure investigated for the reaction of the thiol-bearing DUPA-based binding sequence with the [3,4-*bis*(phenylthio)]-ma-va-α-amanitin drug-linker **108** involved the addition of an organic base to the mixture of reagents. This procedure applied for the preparation of the rigid bivalent (DUPA-Pep-Cys)$_2$-ma-va-α-amanitin SMDC (**101**) from the DUPA-Pep sequence **44** (section 3.1.1, **Scheme 2**) led to a very poor yield of the final product due to the formation of by-

products. The same outcome was obtained by using the less steric hindered triethylamine (TEA) base for the preparation of the flexible bivalent (DUPA-Pep-EG_4)$_2$-ma-va-α-amanitin SMDC (**102**). A careful examination of the reaction by-products provided a deeper insight into the low yield obtained for the entries **101**-**102**. The low yield came from unconversion or partial conversion to the monosubstituted product of the [3,4-*bis*(phenylthio)]-ma-va-α-amanitin drug-linker **108**.

Therefore, for the preparation of the structurally more flexible conjugates **103**-**104** alternative reaction conditions were explored. Addition of a solution of the strong base sodium methylate (NaOMe; pK_a ~ 16) in methanol (MeOH) and a large excess of the respective DUPA-Pep-EG_n motifs (**99**-**100**) allowed to maintain the formation of the monosubstituted side product at a low level and consequently to achieve higher yields for the desired conjugates **103**-**104**.

The flexible DUPA-Pep-EG_n motifs (**98**-**100**) were synthesized as illustrated in **Scheme 15**.

Scheme 15. Synthesis of the flexible DUPA-Pep-EG_n motifs (98-100).

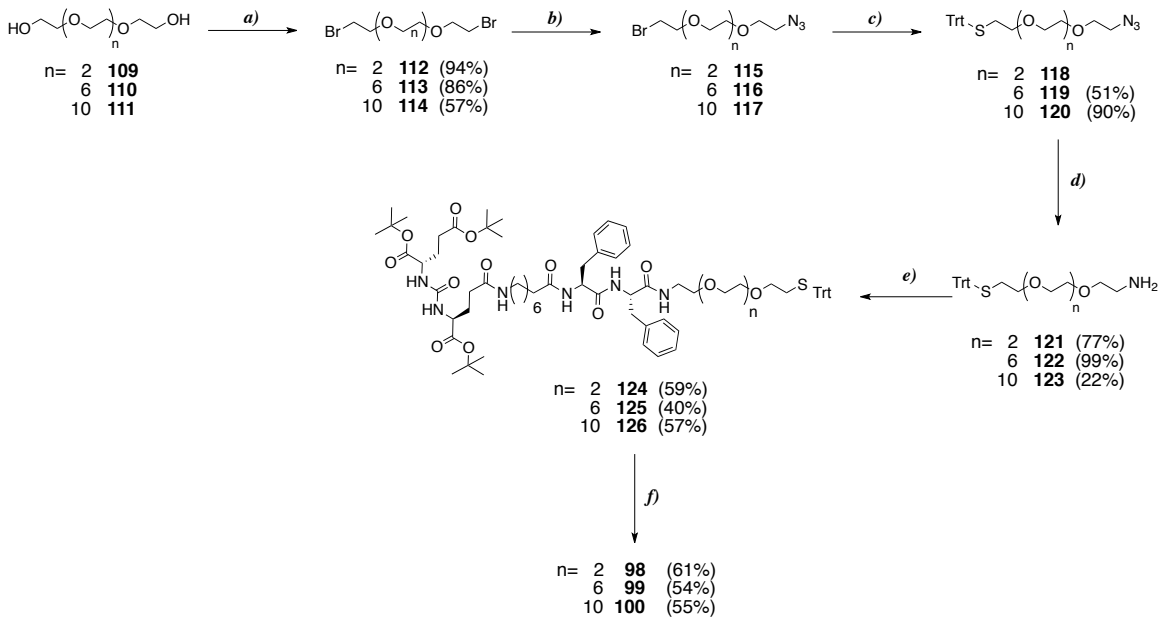

Reagents and conditions: ***a)*** Br_2, PPh_3, DCM, rt, 72 h; ***b)*** NaN_3, DMF, rt, 21 h; ***c)*** Ph_3CSH, NaOMe, rt, 1.5 h; ***d)*** Ph_3P, H_2O/THF, rt, 42 h; ***e)*** **75**, $NaHCO_3$, H_2O/THF, rt, 1h; ***f)*** TFA/TIS/H_2O (95:2.5:2.5, v:v:v), DTT; rt, 1.5 h.

The thiol-protected bifunctional carboxylate-reactive EG_n crosslinkers (**121**-**123**) were prepared from the corresponding commercially available EG_n **109**-**111**. First, the Appel reaction converted the alcohols into bromides by using triphenylphosphine (PPh_3) and dibromine (Br_2) as source of bromine. Intermediates **112**-**114** were then converted to the respective monoazide derivatives **115**-**117**. Substitution of the second bromine with the triphenylmethanthiol (Ph_3CSH) yielded the intermediates **118**-**120**. At this stage an easy separation of the co-formed diazide or dithioether by flash chromatography was possible. The Staudinger reaction was applied to reduce the azide group to the primary amine under mild conditions, affording the desired thiol-protected carboxylate-

reactive EG_n crosslinkers **121**-**123**. The crosslinkers **121**-**123** were coupled to the NHS ester-activated fully protected DUPA-Pep sequence **75** (section 4.1.1, **Scheme 9**). Final deprotection under acidic conditions of the resulting *tert*-butyl- and trytil-protected DUPA-Pep-EG_n motifs (**124**-**126**) yielded upon purification the maleimide-reactive DUPA-Pep-EG_n-SH motifs **98**-**100**.

While the lead compound DUPA-Pep-mc-va-α-amanitin **37** can be considered as the direct monovalent analogue of the rigid bivalent $(DUPA\text{-}Pep\text{-}Cys)_2$-ma-va-α-amanitin SMDC (**100**), monovalent analogues (**105**-**107**) of the flexible bivalent $(DUPA\text{-}Pep\text{-}EG_n)_2$-ma-va-α-amanitin SMDCs (**102**-**104**) were prepared as illustrated in **Scheme 16**. The va-α-amanitin drug-linker **47a** (section 3.1.1, **Scheme 5**) was easily reacted with the commercially available 3-(maleimido)propanoic acid NHS-ester (BMPS) building block (**96**), leading to the maleimidopropyl (mp)-va-α-amanitin drug linker **127**. This latter was coupled to the maleimide-reactive DUPA-Pep-EG_n-SH crosslinkers **98**-**100**, affording the final SMDCs **105**-**107**, which were purified by preparative chromatography prior to their application in biological assays.

Scheme 16. Synthesis of monovalent DUPA-Pep-EG_n-mp-va-α-amanitin SMDCs (105-107).

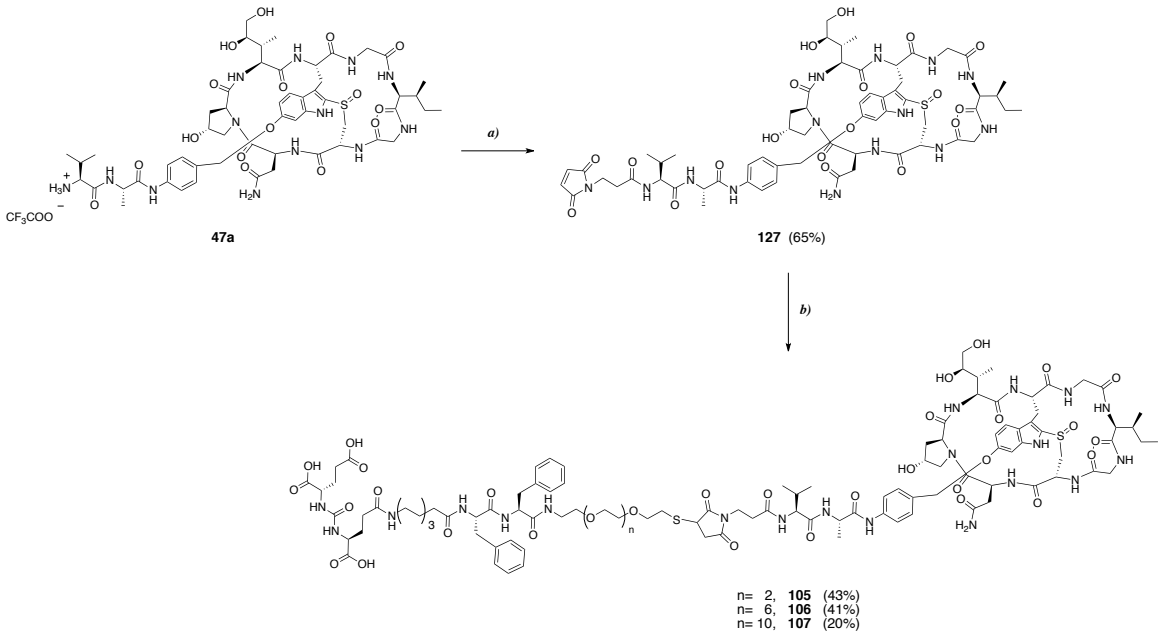

Reagents and conditions: ***a)*** 3-(maleimido)propanoic acid NHS-ester (BMPS), DIPEA, DMF, rt, 1.5 h; ***b)*** **98**, **99**, or **100**, DIPEA, DMSO, rt, 24 h.

8.1.2 *In vitro* cytotoxicity. Bivalent $(DUPA\text{-}Pep\text{-}spacer)_2$-ma-va-α-amanitin SMDCs (**101**-**104**) were tested against the $PSMA^+$ LNCaP and $PSMA^-$ PC3 human prostate cancer cells, following the protocol described in section 3.1.3. The monovalent flexible DUPA-Pep-EG_n-mp-va-α-amanitin SMDCs (**105**-**107**) and the unconjugated α-amanitin were also included in the assay as reference compounds. Specific cellular uptake was determined by competitive blocking with 200-fold molar

excess of the PSMA inhibitor 2-PMPA. Dose-response curves are shown in **Figure 61** and data are summarized in **Table 6**.

Data reported for the rigid bivalent (DUPA-Pep-Cys)$_2$-ma-va-α-amanitin SMDC (**101**) on PSMA$^+$ cells showed a 189-fold decrease of cytotoxicity in comparison to the lead DUPA-Pep-mc-va-α-amanitin SMDC (**37**). The EC_{50} value (170.2 nM) calculated for the SMDC **101** was essentially in the activity range of unconjugated α-amanitin (EC_{50} 721.7 nM) and comparable to the activity of the SMDC observed in presence of the excess of 2-PMPA (EC_{50} 625.6 nM), suggesting partial loss of the active targeting and internalization properties.

Introduction of flexible EG_n spacers considerably improved the potency of the bivalent systems compared to the rigid bivalent SMDC (**101**), and this effect was even more pronounced with the SMDCs incorporating the EG_4 and EG_8 spacers. The related SMDCs, (DUPA-Pep-EG_4)$_2$-ma-va-α-amanitin (**102**) and (DUPA-Pep-EG_8)$_2$-ma-va-α-amanitin (**103**) (EC_{50} 2.9 and 7.7 nM, respectively) were one magnitude order more active than the monovalent analogues **105** and **106** (EC_{50} 16.3 and 20.9 nM, respectively).

In the series of the bivalent SMDCs with flexible EG_n spacers, (DUPA-Pep-EG_{12})$_2$-ma-va-α-amanitin SMDC (**104**) incorporating EG_{12} spacers was the less potent (EC_{50} 29.6 nM) and its potency was in the same range of the corresponding monovalent DUPA-Pep-EG_{12}-mp-va-α-amanitin (**107**; EC_{50} 52.4 nM). While cytotoxicity on PSMA$^+$ LNCaP cells of the EG_8- and EG_{12}-incorporating bivalent SMDCs (**103**, **104**) could be significantly inhibited by excess of the PSMA competitor 2-PMPA, cytotoxicity of the EG_4-incoporating bivalent, (DUPA-Pep-EG_4)$_2$-ma-va-α-amanitin SMDC (**102**) could be only partly affected under the same conditions. These results indicated that a mechanism other than the PSMA-mediated one might contribute to the uptake of the (DUPA-Pep-EG_4)$_2$-ma-va-α-amanitin SMDC (**102**).

All the compounds evaluated in this study exhibited significantly lower activity (EC_{50}: **101** 5.1 mM, **103** 403.7, **104** 288.1, **105** 416.6, **106** 338.6, **107** 480.0 nM) on the PSMA$^-$ PC3 cells either in absence or in presence of excess of 2-PMPA, supporting the hypothesis of the PSMA-mediated uptake. Only the EG_4-incorporating bivalent SMDC **102** resulted to be toxic against the PSMA$^-$ PC3 cells with an EC_{50} value of 47.6 nM and 37.8 nM in absence and presence of excess of 2-PMPA, respectively, confirming the hypothesis of a nonspecific uptake mechanism for this SMDC.

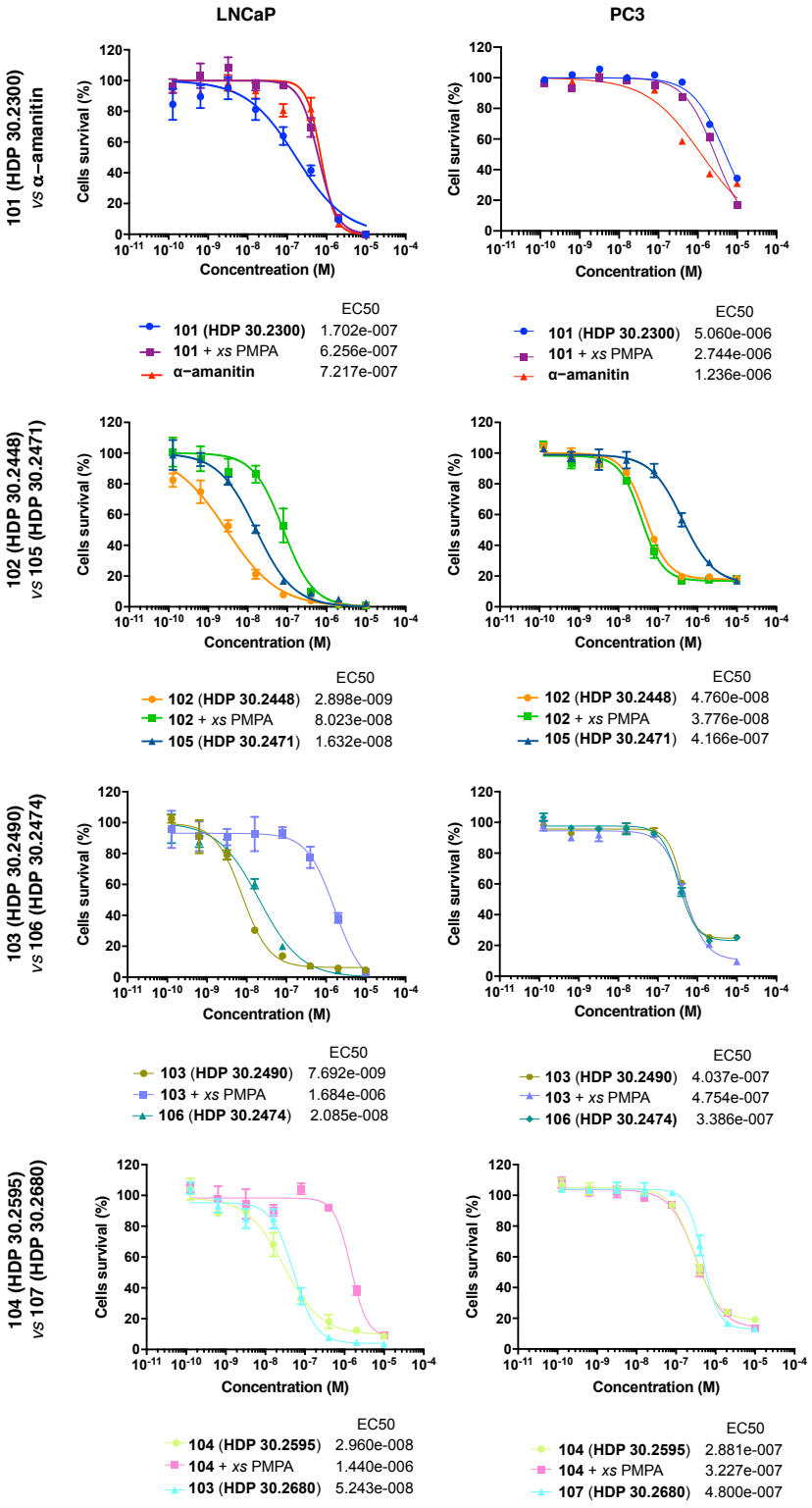

Figure 61. Dose-response curves for the bivalent (DUPA-Pep-spacer)$_2$-ma-va-α-amanitin SMDCs (101-104). Curves were generated by using ATP cell viability assay (CellTiter Glo® 2.0) after 96 h incubation with PSMA$^+$ LNCaP (left panel) and PSMA$^-$ PC3 (right panel) cells in absence and in presence of 200-fold molar excess (*xs*) of the PSMA inhibitor 2-PMPA (PMPA). Each flexible bivalent (DUPA-Pep-EG$_n$)$_2$-ma-va-α-amanitin SMDC was evaluated in comparison to the corresponding monovalent DUPA-Pep-EG$_n$-mp-va-α-amanitin SMDC (**105**-**107**). Data point are average of triplicate wells compared to no treatment control.

		EC_{50} (nM)			
		LNCaP	**LNCaP** *xs* PMPA	**PC3**	**PC3** *xs* PMPA
-	α–amanitin	721.7	-	*none*[a]	
37	DUPA-Pep-mc-va-α–amanitin	0.9	540.2	*none*[a]	*none*[a]
101	$(DUPA\text{-}Pep\text{-}Cys)_2$-mp-va-α-amanitin	170.2	625.6	*none*[a]	*none*[a]
102	$(DUPA\text{-}Pep\text{-}EG_4)_2$-ma-va-α-amanitin	2.9	80.2	47.6	37.8
105	DUPA-Pep-EG_4-mp-va-α–amanitin	16.3	-	417.0	-
103	$(DUPA\text{-}Pep\text{-}EG_8)_2$-ma-va-α–amanitin	7.7	*none*[a]	403.7	475.4
106	DUPA-Pep-EG_8-mp-va-α–amanitin	20.9	-	338.6	-
104	$(DUPA\text{-}Pep\text{-}EG_{12})_2$-ma-va-α–amanitin	29.6	*none*[a]	288.1	322.7
107	DUPA-Pep-EG_{12}-mp-va-α–amanitin	52.4	-	480.0	-

none[a], not active within 100 pM to 1 μM range.

Table 6. Summary of the EC_{50} values of bivalent $(DUPA\text{-}Pep\text{-}spacer)_2$-ma-va-α-amanitin SMDCs (101-104) in absence or in presence of 200-fold molar excess (*xs*) of the PSMA inhibitor 2-PMPA (PMPA) and monovalent DUPA-Pep-EG_n-mp-va-α-amanitin SMDCs (105-107). EC_{50} data of α-amanitin and lead DUPA-Pep-mc-va-α-amanitin SMDC (**37**) are also reported as comparison.

8.2 Discussion

Multimerization has been proved a suitable strategy to improve tumor uptake and prolong retention of tracers by enhancing the binding affinity. For example, multivalent PSMA urea-based radioligands were developed as diagnostic tools with improved binding and imaging properties.[173,174]

Because PSMA exists as homodimer on the cell surface, scope of the present study was to design a bivalent DUPA-Pep-α-amanitin SMDC able to simultaneously bind both PSMA catalytic binding pockets thus, leading to improved binding affinity.

The key factor determining the capability of chelating more than one binding sites is the spacer which separates the binding units. The spacer should be carefully designed in respect to its length, flexibility and to receptor density.[177] Optimal spacer length ideally spans the distance between two adjacent binding sites. Below the optimum ligands might be not able to bind multiple binding sites at once, while beyond the optimum the conformational entropy of the system would increase making less likely that the ligand will locate and bind to its corresponding receptor. Optimal flexibility is then necessary to ensure that ligand will be capable to reach and interact with the binding site and to constrain the freedom of the bound system.

Aiming to design the optimal bivalent system in respect to spacer length and spacer-depending flexibility, bivalent DUPA-Pep-based SMDCs with and without EG_n spacers were generated.

Assuming that a greater binding affinity leads to enhanced potency of the conjugate, the cytotoxicity outcomes were used to evaluate the effectiveness of the multivalency approach. The EG-non incorporating bivalent, $(DUPA\text{-}Pep\text{-}Cys)_2$-ma-va-α-amanitin SMDC (**101**) displayed a remarkable weakening of the potency against the PSMA-expressing LNCaP cells as compared to the reference monovalent DUPA-Pep-mc-va-α-amanitin SMDC (**37**). Potency of the bivalent SMDC **101** and unconjugated toxin were comparable, suggesting the partial loss of targeting and internalization properties for SMDC **101**. This was likely the consequence of lack of flexible spacers between the binding moieties and the central branched scaffold, which may have caused steric hindrance and reduced the spatial flexibility required for the binding moieties to reach and bind the PSMA binding sites.

By introducing the EG_n spacers activity of the bivalent SMDCs significantly improved compared to the rigid bivalent SMDC **101**. The EG_n-incorporating bivalent $(DUPA\text{-}Pep\text{-}EG_n)_2$-ma-va-α-amanitin SMDCs (n= 4 **102**; 8 **103**; 12 **104**) were 59-, 22- and 5.8-fold more potent than the rigid bivalent SMDC **101**. Additionally, they were found to be six-, three- and twice-fold as potent as their corresponding monovalent analogues **105**, **106** and **107**, respectively.

The EC_{50} values rose with the spacer length and flexibility throughout the EG_n-incorporating mono- and bivalent conjugates and the effect was more prominent in the case of the EG_{12}-incorporating bi- and monovalent systems (**104**, **107**). It may be argued that the greater spacer length and flexibility featured by the EG_{12} spacer increased the conformational entropy of the systems inducing conformations less suitable for binding.[170]

It is worth to be mentioned that in the series of the EG_n-incorporating bivalent SMDCs, the most active against the PSMA-expressing cells, the $(DUPA\text{-}Pep\text{-}EG_4)_2$-ma-va-α-amanitin SMDC (**102**), was slightly toxic even against the PSMA-nonexpressing cells and its toxicity was not quantitatively inhibited by excess of the PSMA competitor 2-PMPA. This observation supports the hypothesis that mechanisms other than the specific PSMA-mediated uptake are responsible for the toxicity issue reported for this conjugate, and that deeper investigations are needed to elucidate the exact mechanism.

However, none of the bivalent SMDCs evaluated in the present study showed significant improvements over the reference monovalent conjugate **37** in terms of *in vitro* activity. Assuming a maximal distance of 5.2 Å for one ethylene glycol unit [178] and an average distance of 4.8 Å for the central scaffold, the following maximal distances between two binding motifs in the bivalent systems can be calculated as follows: 25.6 Å, 46.4 Å and 67.2 Å for SMDCs **102**, **103** and **104**, respectively. Thus, orientation of the binding sites of the PSMA homodimer and distance between them suggests that bivalent systems are hardly able to bind both PSMA monomers simultaneously, but rather that they bind in the proximity of only one catalytic site in the PSMA dimer. This would

explain why bivalent conjugates (**101**-**104**) did not display any improvement compared to the lead SMDC **37**.

Collectively, these findings suggest that dimerization is not the optimal modality for improving the tumor uptake and retention of the DUPA-Pep-α-amanitin SMDCs. Despite these results, *in vivo* analysis may show advantages of incorporating EG_n spacers in terms of PK. Therefore, it would be of particular interest to pursue in the future the *in vivo* development of these EG_n-incorporating systems to fully investigate their potential favourable properties.

Chapter 9
Small Molecule-Fc-Drug Conjugate: a viable alternative to SMDCs

In vivo profiling of the lead SMDCs **37**, **39** and **60** demonstrated that a key challenge in developing the DUPA-Pep-α-amanitin SMDCs is achieving adequate systemic exposure to the drug in the conjugated form to support durable therapeutic response.

The small size of the DUPA-Pep-α-amanitin SMDCs (lower than 4 kDa) reasonably highly predisposed them to the kidney glomerular filtration. Instability and fast renal clearance affected the biodistribution of the DUPA-Pep-α-amanitin SMDCs into tissues, reducing their therapeutic efficacy at the target site. These issues impose frequent administration to keep concentrations within the effective range, which would be undesirable in a clinical setting.

In contrast to small-sized molecules, immunoglobulin G (IgG) proteins (**Figure 62A**) are protected from degradation and fast elimination through the neonatal Fc receptor (FcRn) recycling process (**Figure 62B**).[178] Widely expressed in vascular epithelial cells, endothelial cells, macrophages, dendritic cells and leukocytes,[179] FcRn binds in the acidic endosomes the Fc domain of IgG molecules (more efficiently isotypes 1, 2 and 4) after they have been internalized from the bloodstream by fluid phase pinocytosis. IgGs bound to FcRn are able to escape lysosomal degradation, to be trafficked back to the cell surface where the neutral pH facilitates their release

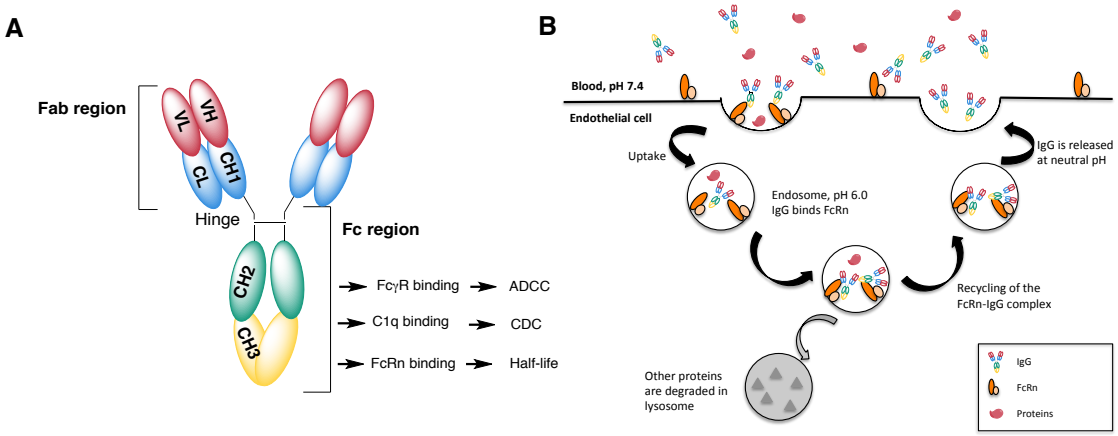

Figure 62. Structure of immunoglobulins G (IgGs) and recycling process mediated by the FcRn. A) Structure of an IgG can be divided in two regions: the Fab (antigen binding fragment), and the Fc (fragment crystallizable). The Fc region mediates the effector functions, such as the antibody-dependent cellular cytotoxicity (ADCC) and the complement-dependent cytotoxicity (CDC) and the FcRn recycling process. **B)** Upon internalization by fluid-phase pinocytosis, in the early endosome IgG interacts with FcRn at pH 6.0. The FcRn-IgG complex is then recycled back to the cell surface and the IgG is released at neutral pH thus, rescuing the IgG from lysosomal degradation.

back into the bloodstream.[180] Due to the FcRn recycling process IgG molecules have a mean half-life in humans of approximately 23 days.[181] Covalent association of small molecules to the Fc domain of IgGs allows to reduce the impact of the aforementioned clearance mechanisms on the efficacy of small molecules by increasing the size to approximately 60 to 70 kDa, the threshold for the renal filtration, and by protecting them from proteolytic degradation through the FcRn salvage pathway.[182]

The prolonged half-life, compared to small-sized therapeutics, permits less frequent dose administration, which is clinically relevant.[181] Small molecules conjugated to a Fc domain usually retained their therapeutic activity. Due to the strong interactions of the CH3 domains which induce the homodimerization of two Fc molecules, each construct features a minimum of two molecules, resulting in an increased avidity for the target and in an enhanced therapeutic activity of the molecule.[181]

In an effort to blend the PK properties of IgGs with the therapeutic potential of PSMA-targeting α-amanitin-based SMDCs, the DUPA-Pep-α-amanitin moiety was grafted onto an IgG_1-Fc scaffold. The resulting PSMA-targeting α-amanitin-based Small Molecule-Fc-Drug Conjugate (Fc-SMDC; **128**, **Figure 63**) combines in a single platform: 1) extended serum half-life due to larger size and the FcRn-mediated recycling process; 2) selective targeting of PSMA-expressing PCa cells by virtue of the DUPA-Pep binding motif and 3) cell-killing function exerted by α-amanitin.

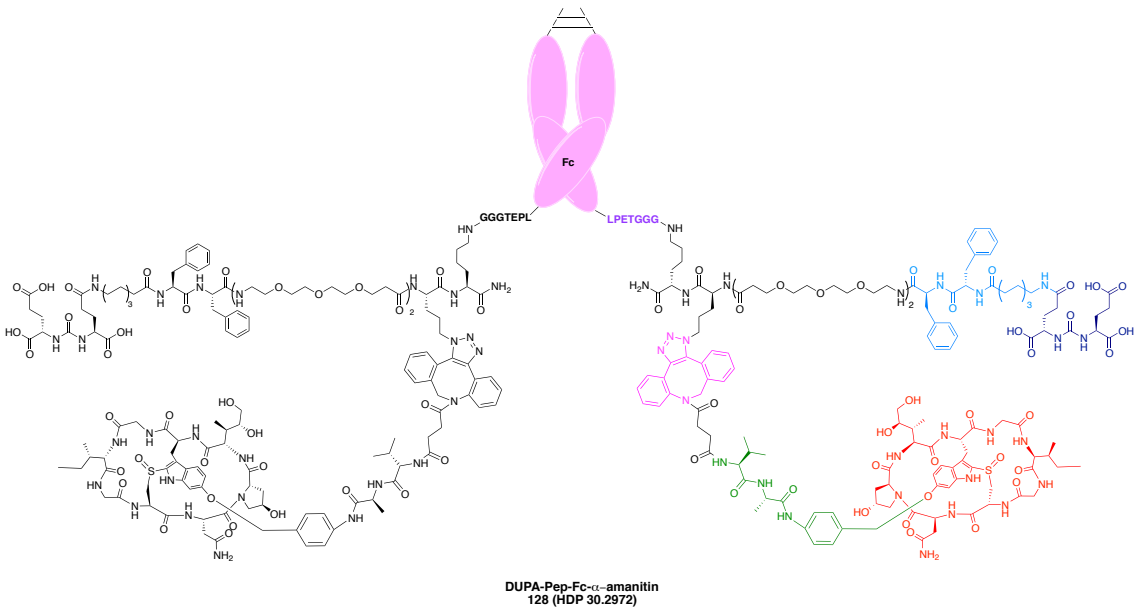

Figure 63. Structure of the PSMA-targeting α-amanitin-based Fc-SMDC (128, HDP 30.2972) with a molecular weight of ~ 61 kDa. The construct comprises the PSMA-targeting ligand DUPA (blue), the supporting PSMA binding spacer (cyan), the toxin warhead α-amanitin (red), the cleavable dipeptide self-immolative va-PAB linker (green). Conjugation to the Fc fragment (purple) and to the drug-linker payload (magenta) are also highlighted.

9.1 Results

9.1.1 General strategy. Based on the work of Thomas *et al.*,[184a,b] a two-step "program and arm" strategy was developed for grafting the DUPA-Pep-α-amanitin moiety onto a human IgG_1-Fc scaffold (**Figure 64**).

The IgG_1-Fc scaffold was first programmed to selectively recognize the PSMA-expressing cells by attaching via sortase A (SrtA)-mediated ligation (**Figure 64**, **step *a***) a trifunctional linker (**130**, **Figure 65**), that simultaneously displayed 1) the cell-specific targeting motif, 2) the oligoglycine substrate for the regiospecific labeling of the Fc scaffold and 3) a clickable handle for chemoselective conjugation to the toxin warhead. To avoid steric interference from the large Fc protein, a flexible and long EG_3 dimer was introduced as spacer between the targeting motif and the *C*-terminal end of the trifunctional linker **130**.

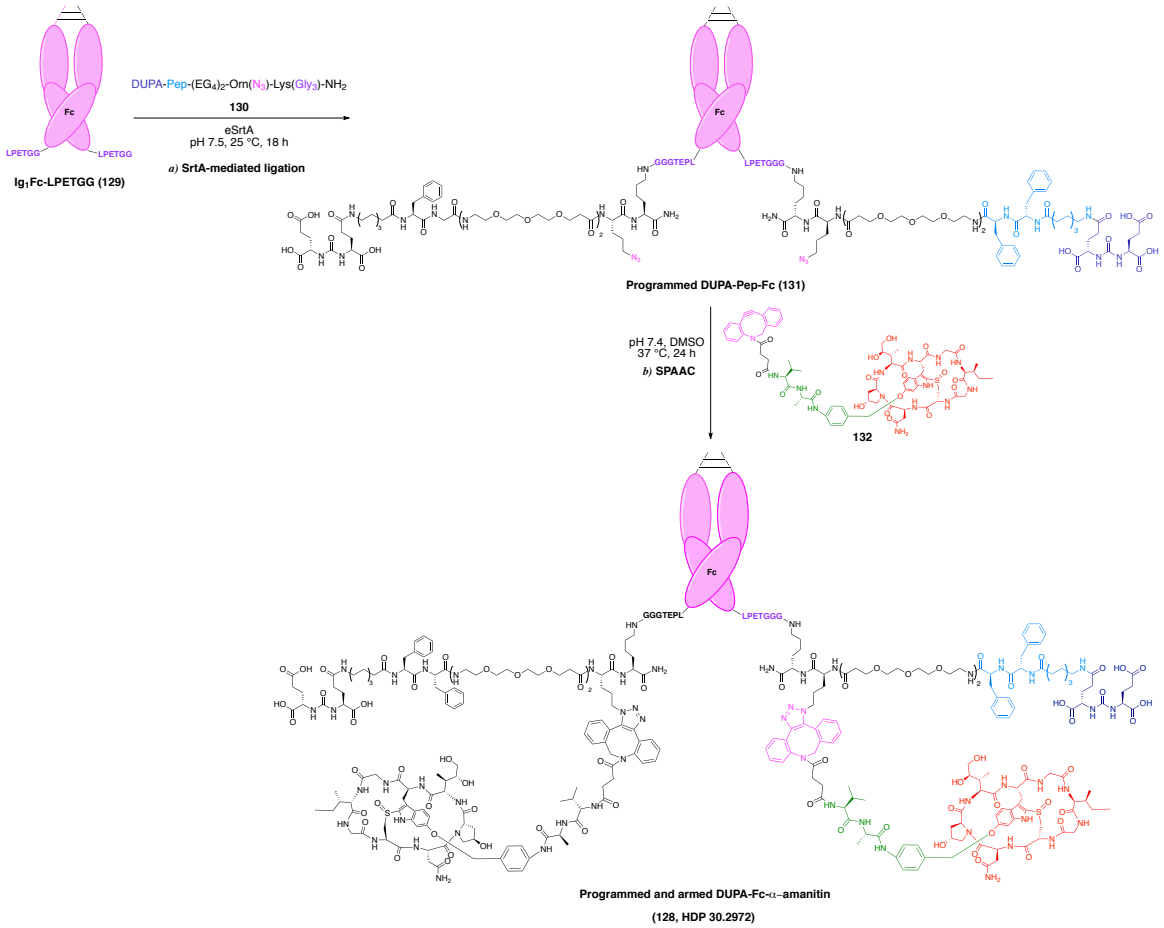

Figure 64. **General strategy for producing the DUPA-Pep-Fc-α-amanitin Fc-SMDC (128, HDP 30.2972).** *a*: IgG_1-Fc scaffold (**129**, **Fc-LPETGG**) is programmed by attaching at the *C*-termini through sortase A (eSrtA)-mediated ligation the trifunctional linker (**130**) containing the DUPA-Pep PSMA binding motif and an azide as "clickable" handle; *b*: programmed DUPA-Pep-Fc (**131**) is armed with the dibenzocyclooctine (DBCO)-bearing drug linker (**132**) via strain-promoted azide-alkyne cycloaddition (SPAAC). Pep= 8-Aoc-Phe-Phe.

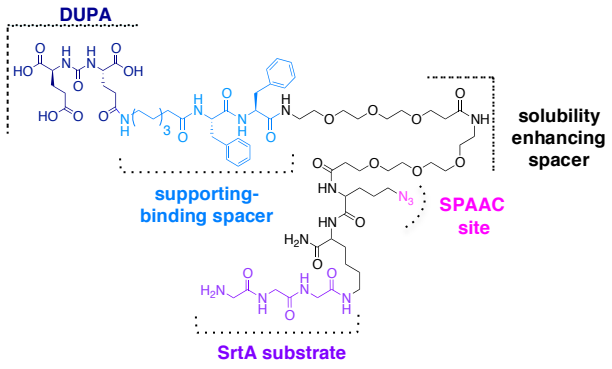

130

Figure 65. Structure of the trifunctional linker 130. The linker displays: the PSMA-binding motif constituted of the DUPA ligand (blue) and the supporting binding spacer (cyan); the EG_3 dimer as solubility-enhancer spacer (black); the azido moiety (magenta) for conjugation by strain-promoted azide-alkyne cycloaddition (SPAAC) to the toxin warhead; the triglycine substrate for the regiospecific sortase A (SrtA)-mediated ligation to the IgG_1- Fc scaffold.

The hydrophilicity of the $(EG_3)_2$ spacer provided an additional advantage by increasing the water solubility of the synthetic component allowing later to perform the conjugation reactions in aqueous media. SrtA is a transpeptidase from *Staphilococcus aureus* widely used for site-specific modifications of antibody and antibody fragments.[185a-d] The reaction catalyzed by SrtA leads to the formation of a new amide bond between a *C*-terminal sorting motif LPXTG (where X is equal to any amino acid) and a *N*-terminal oligoglycine $(G)_n$ (n= 3-5) (**Figure 66**).[186] To allow the site-specific attachment of the synthetic component by SrtA-mediated ligation, the IgG_1-Fc scaffold was initially engineered at the *C*-terminus with the peptide tag LPETGG.

Following the SrtA-mediated ligation, the strain-promoted azide-alkyne cycloaddition (SPAAC; **Figure 64**, **step *b***) was explored for conjugation of the drug-linker component (**132**, **Figure 64**). Due to the chemoselectivity and the mild conditions required, click reactions allow to attach the drug cargo to the protein scaffold without altering the stoichiometry and residue specificity of the Fc scaffold.[184a] Also, the copper-free click chemistry was chosen in order to minimize protein oxidation by reactive oxygen species and to avoid residual copper in the final product, therefore preventing potential copper-related cytotoxicity.

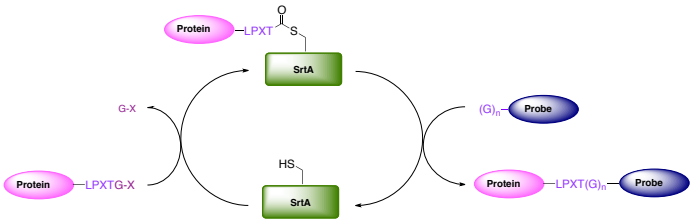

Figure 66. Site-specific *C*-terminal labeling of protein by sortase A (SrtA)-mediated ligation. The catalytic mechanism involves the nucleophilic attack by the cysteine residue in the actve site of the enzyme to the carbonyl of the threonine in the recognition sequence LPXTG, leading to the formation of a thioester-acyl intermediate. This intermediate is then resolved by the nucleophilic attack of the amine group from an oligoglycine motif.

9.1.2 Fc-LPETGG production. An expression plasmid encoding human IgG_1-Fc domain embedding the SrtA LPETGG tag at the *C*-terminus was cloned and used for transient expression in Expi293F™ cells. To prevent formation of *N*-terminal truncations, an additional TEV protease

(Tobacco Etch Virus nuclear-inclusion-a endopeptidase) cleavage site was introduced at the *N*-terminus. The Asn[297] glycosylation site in the CH2 domain was removed by mutation to alanine, a common strategy to reduce the IgG1 binding to FcγRI and C1q.[187a-b] Aglycosylation was achieved also to avoid the heterogeneity issue which occurs when mammalian cells are used as production system and thereby, to simplify the manufacturing and analysis process.[188] The engineered protein, designated as Fc-LPETGG (**129**, **Figure 64**) was purified prior to its chemical modification, and analyzed by gel filtration chromatography (**Appendix**, **Figure A19**).

9.1.3 Chemistry. For the IgG_1-Fc chemical programming and arming strategy, the trifunctional linker **130** was designed (**Figure 65**) and assembled by SPPS on AmphiSphere® 40 RAM resin using standard Fmoc chemistry (**Scheme 17**).

Scheme 17. Synthesis by SPPS of the trifunctional linker (70).

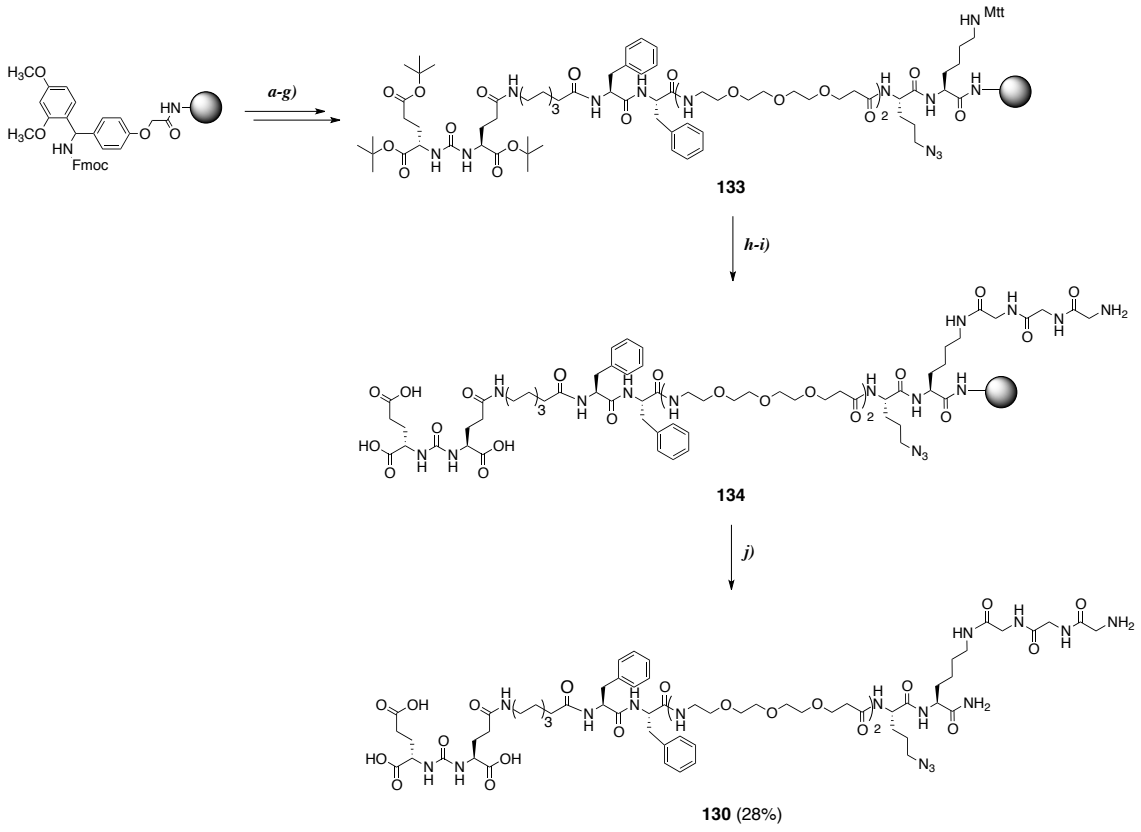

Reagents and conditions: ***a)*** i. 20% piperidine in DMF, rt, 30 s (x1), 30 W, 50 °C, 3 min (x2), ii. Fmoc-Lys(Mtt)-OH, TBTU, DIPEA, rt, 1 h, 30 W, 50 °C, 3 min (x 1); iii. 20% piperidine in DMF, rt, 30 s (x1), 30 W, 50 °C, 3 min (x2); ***b-f)*** i. Fmoc-AA-OH, TBTU, DIPEA, 30 W, 50 °C, 3 min (x 3); ii. 20% piperidine in DMF, rt, 30 s (x1), 30 W, 50 °C, 3 min (x2); ***g)*** **42**, TBTU, DIPEA, 30 W, 50 °C, 3 min (x 3); ***h)*** TFA/TIS/DCM (1:2:97, v:v:v, 4 ml), rt, 10 min (x 20); ***i)*** i. Fmoc-Gly-Gly-Gly-OH, TBTU, DIPEA, 1 h, rt and 30 W, 50 °C, 3 min (x 3), ii. 20% piperidine in DMF, rt, 30 s (x1), 30 W, 50 °C, 3 min (x 2) [x 3]; ***j)*** TFA/anisole/TIS/H_2O (94:2:2:2, v:v:v, 20 ml), rt, 2 h.

Once the linear sequence (**133**) was assembled, removal of the Mtt protecting group from the lysine side chain was performed by repeatedly treating the resin-bound peptide with a mild acidic cleavage cocktail and monitoring the reaction by HPLC to ensure the complete removal of the Mtt group. The ε-amine of the *C*-terminal lysine was then coupled to a $(Gly)_3$ motif and the resulting resin-bound peptide (**134**) was fully deprotected and cleaved from the resin under strong acidic conditions, yielding the trifunctional linker (**130**). The final product (**130**) was purified by preparative chromatography to achieve high-purity substance prior to its usage in the bioconjugation reaction.

To arm the DUPA-Pep-Fc scaffold **131** (**Figure 64**) with the toxin warhead by SPAAC, the va-α-amanitin drug-linker **47a** (section 3.1.1, **Scheme 2**) was functionalized with a dibenzocyclooctine (DBCO) group by reacting with the DBCO *N*-hydroxysuccinimide ester (DBCO-SU) reagent, as outlined in **Scheme 18**.

Scheme 18. Synthesis of the DBCO-va-α-amanitin drug linker (72).

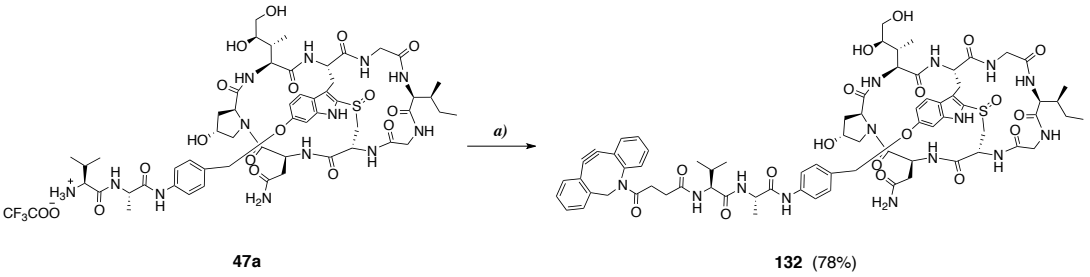

Reagents and conditions: ***a)*** DBCO-SU, DIPEA, DMF, rt, 2.5 h.

9.1.4 SrtA-mediated ligation. The Fc-LPETGG protein (**129**) was reacted with the trifunctional linker **130** under the catalysis of an activity-optimized SrtA (eSrtA, a pentamutant SrtA variant from *Staphilococcus aureus*), which offers the advantage of enhanced reaction rate over the wild-type enzyme.[189] Ligation conditions were optimized to ensure maximum conjugation yield and minimize reversed reaction.

Optimization of reaction conditions was performed on sub-milligram scale before determining optimal conditions for large-scale reactions. Systematically, concentration of the triglycine probe (**130**) and reaction time were varied (**Figure 67**). Experimentally, low excess of triglycine probe (**130**) over the Fc-LPETGG protein (**129**) led to conversion within 1 to 2 h. However, two higher molecular weight bands were seen in the SDS-PAGE analysis (**Figure 67A**). Heterogeneity was assumed to be due to formation of species with LPR (linker-to-protein ratio) ranging from one to two. At longer time points, a decrease in product was observed probably because of the competitive hydrolysis reaction, where the enzyme irreversibly hydrolyzes the LPETGG motif present in the product as well. According to the SDS-PAGE analysis, with higher excess of triglycine substrate

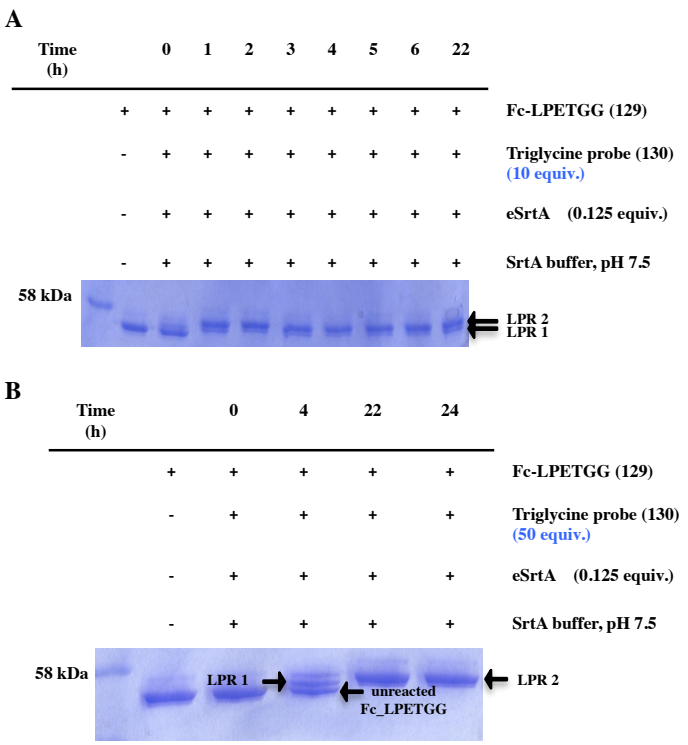

Figure 67. Optimization of the eSrtA-mediated reaction conditions for the Fc labeling. Reaction was performed with **A)** 10-, **B)** 50-fold excess of triglycine probe (**130**) over the Fc-LPETGG protein (**129**) at different time points. Highest conversion to Fc protein labeled at both *C*-termini with linker molecules (LPR 2) was achieved by using 50-fold excess of triglycine probe (**130**) over Fc-LPETGG protein (**129**) within 22 h. Protein loading: 5 µg. LPR= linker-to-protein ratio.

(50-fold over the Fc-LPETGG **129**) and 22 h incubation time (**Figure 67B**), formation of heterogenous species with LPR 1-2 could not be completely avoided. However, under these conditions the highest molecular weight band presumably corresponding to the DUPA-Pep-Fc conjugate (**131**, **Figure 64**) with LPR 2 was the most intense. Therefore, these conditions were set for the large scale reaction.

Under these conditions, large scale reaction proceeded smoothly with nearly full conversion, based on the visual analysis of the SDS-PAGE gel (**Figure 68B**). Excess of reagents was removed by size exclusion chromatography (SEC) under native, non-reducing conditions (**Appendix**, **Figure A20**). Programmed DUPA-Pep-Fc conjugate (**131**, **Figure 64**) was confirmed to be a disulfide-linked Fc dimer by SDS-PAGE under reducing and non-reducing conditions (**Figure 68B**). HRESI-MS analysis under non-reducing conditions (**Figure 68A**, panel **b**) further confirmed the expected molecular weight for a Fc dimer. As expected, deconvolution results revealed two different peaks, which were assigned to versions of the Fc dimer modified with one to two molecules of trifunctional linker **130**, resulting in an average LPR of 1.62 (**Figure 68A**, panel **b**).

9.1.5 SPAAC. Following the SrtA-mediated conjugation, the DUPA-Pep-Fc scaffold (**131**) was armed with the DBCO-va-α-amanitin drug linker (**132**) by SPAAC (**Figure 64**, **step b**). To afford the programmed and armed DUPA-Pep-Fc-α-amanitin Fc-SMDC (**128**), the azido functional group in DUPA-Pep-Fc scaffold (**131**) was reacted with the DBCO-va-α-amanitin drug-linker (**132**). Incorporation of α-amanitin in the Fc-SMDC product (**128**) was confirmed by SDS-PAGE under non-reducing conditions (**Figure 68B**), showing band migration to higher molecular weight (lane 3) in comparison to DUPA-Pep-Fc (**131**; lane 2) and by Western blot analysis with immunodetection of α-amanitin performed under non-reducing conditions (**Figure 68C**).

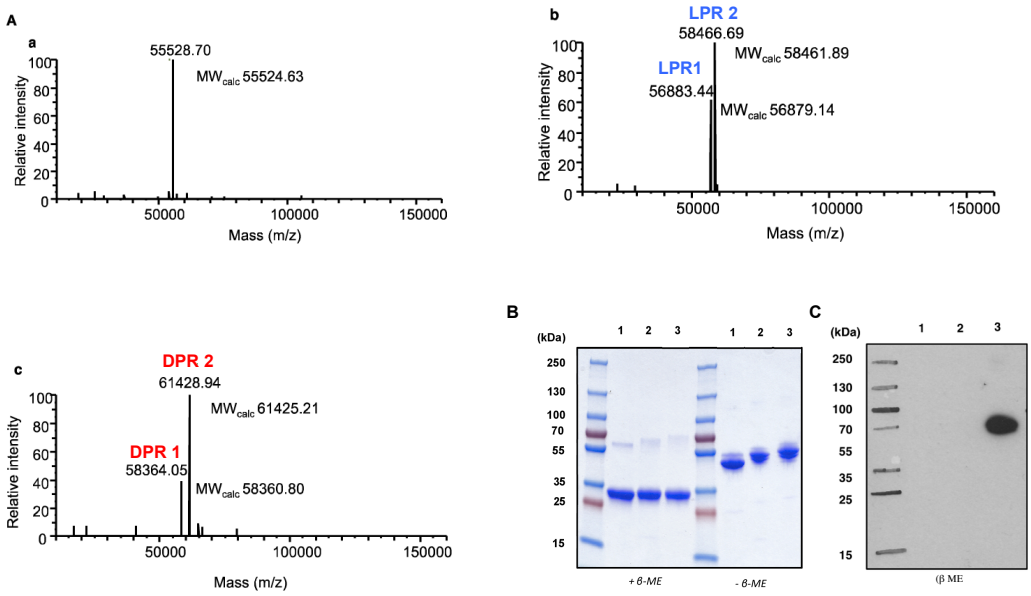

Figure 68. Characterization of the DUPA-Pep-Fc-α-amanitin Fc-SMDC (128, HDP 30.2972). A) HRESI-MS analysis after deconvolution of Fc-LPETGG (**129**; panel **a**), DUPA-Pep-Fc (**131**; panel **b**) and DUPA-Pep-Fc-α-amanitin (**128**; panel **c**). **B)** SDS-PAGE analysis under reducing (*+β-ME*) and non-reducing (*-β-ME*) conditions. **C)** Anti-α-amanitin Western blot under non-reducing conditions (*-β-ME*). SDS-PAGE was performed on Fc-LPETGG (**129**; lane 1), DUPA-Pep-Fc (**131**; lane 2) and DUPA-Pep-Fc-α-amanitin (**128**; lane 3) under non-reducing conditions followed by staining with Comassie blue or Western blot analysis with immunodetection of α-amanitin. LPR= linker-to-protein ratio; DPR= drug-to-protein ratio.

Heterogeneity from the DUPA-Pep-Fc precursor (**131**) with respect to number of attached linker molecules led to the formation of heterogenous species with a drug-to-protein ratio (DPR) ranging from one to two, as confirmed by the deconvoluted mass spectrum, with the content of the species with DPR 2 calculated as equal to 76%.

The average DPR was calculated to be 1.72, consistent to the LPR value reported for the precursor **131** (**Figure 68A**, panel **c**). Importantly, species with DPR 0 which might compete with the α-amanitin-loaded species for binding to the target were not detected.

9.1.6 *In vitro* cytotoxicity. Survival of human prostate cancer $PSMA^+$ LNCaP and $PSMA^-$ PC3 cells upon incubation with increasing concentrations (10^{-11}-10^{-6} M) of DUPA-Pep-Fc-α-amanitin Fc-SMDC (**128**) was assessed according to the procedure described in section 3.1.3.

In a first experiment (**Figure 69A**), potency of the Fc-SMDC (**128**) was assayed in presence and absence of an excess of the PSMA inhibitor 2-PMPA and compared with the effects on cells treated with the DUPA-Pep-Fc scaffold (**131**), which served as control compound.

Either on LNCaP and PC3 cells treatment with the DUPA-Pep-Fc alone did not exhibit any effects on cell survival over the entire range of tested concentrations. Similar results were observed when cells were treated with the DUPA-Pep-Fc-α-amanitin Fc-SMDC product (**128**) coadministered with 200-fold molar excess of 2-PMPA.

On the contrary, the highest inhibition of cell survival occurred upon treatment of the $PSMA^+$ LNCaP cells with the DUPA-Pep-Fc-α-amanitin Fc-SMDC (**128**), which was associated to an EC_{50}

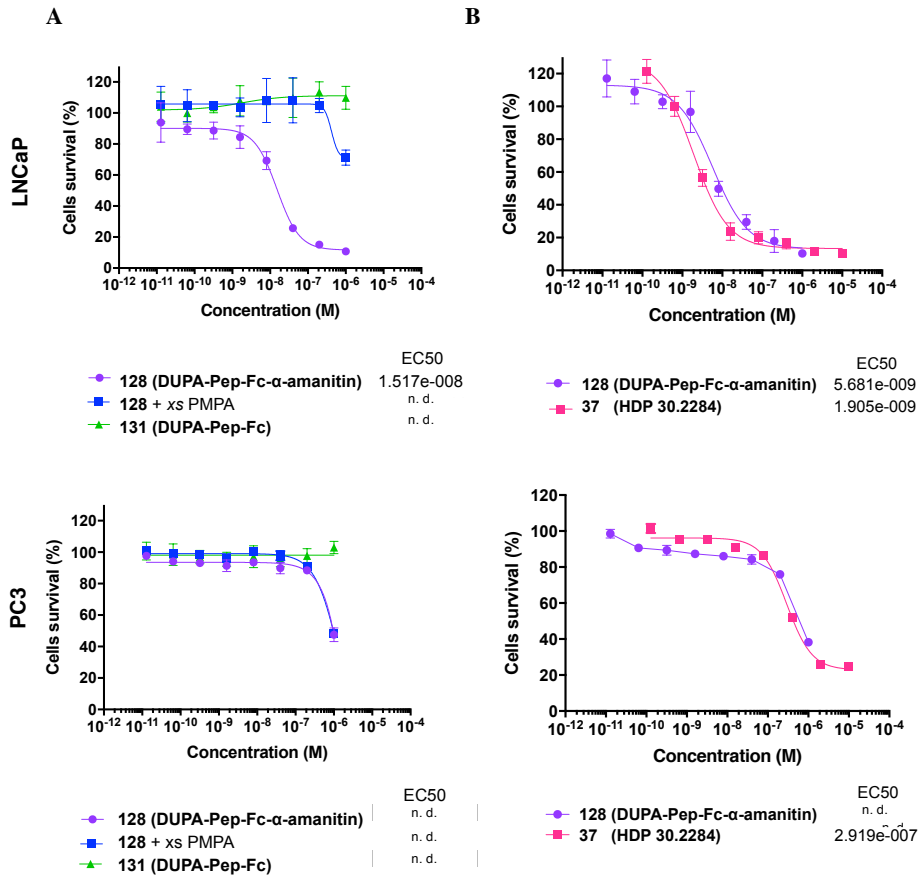

Figure 69. Dose-response curves for DUPA-Pep-Fc-α-amanitin Fc-SMDC (128, HDP 30.2972). Curves were generated by using ATP cell viability assay (CellTiter Glo® 2.0) after 96 h incubation with PSMA$^+$ LNCaP (top panel) and PSMA$^-$ PC3 (lower panel) cells. DUPA-Pep-Fc-α-amanitin (**128**) was tested **A)** in presence and absence of 200-fold molar excess (*xs*) of the PSMA inhibitor 2-PMPA (PMPA) and in comparison to the DUPA-Pep-Fc scaffold (**131**) lacking the toxin warhead α-amanitin as control; **B)** in comparison to the lead DUPA-Pep-mc-va-α-amanitin SMDC (**37**). Data points are average of triplicate wells compared to no treatment control.

of 15.2 nM in the present experiment.

Collectively, these results proved the specific PSMA-targeting delivery of α-amanitin mediated by the Fc-SMDC **128** and suggest that conjugation to the Fc scaffold bearing the targeting sequence DUPA-Pep is necessary to α-amanitin in order to exert its cytotoxic effect. Fc-SMDC **128** was not toxic on PSMA$^-$ PC3 cells thus, supporting that its potency depends on the PSMA-mediated cell internalization. In a second experiment (**Figure 69B**), the effect of the DUPA-Pep-Fc-α-amanitin Fc-SMDC (**128**) treatment on cell survival was compared to that of the lead DUPA-Pep-mc-va-α–amanitin SMDC (**37**), which served as reference compound. The Fc-SMDC **128** showed potency in the same range as the SMDC **37** on PSMA$^+$ LNCaP cells (EC_{50}= 5.7 nM for **128**; 1.9 nM for **37**), demonstrating that grafting the DUPA-Pep-α-amanitin SMDC onto an IgG_1-Fc scaffold does not alter significantly its potency.

9.1.7 *In vitro* plasma stability. Stability of the DUPA-Pep-Fc-α-amanitin Fc-SMDC (**128**) upon incubation in PBS, MP and HP was assessed by western blot analysis (**Figure 70**) and cytotoxicity assay (**Figure 71**). WB analysis was performed with immunodetection of α-amanitin following incubation of Fc-SMDC **128** in PBS, HP and MP for time points within 0 to 5 days. Results showed that, while no degradation occurred in PBS, Fc-SMDC **128** exhibited different degree of stability in mouse and human plasma.

For incubation time longer than 3 days either in mouse and human plasma, intensity of the band corresponding to the Fc-SMDC **128** progressively decreased. This can be due to the loss of drug or drug-linker payload as well as to the parallel formation of aggregates, as indicated by the appearance of higher molecular weight bands. However, the effect is more prominent for the conjugate incubated in mouse plasma (**Figure 70C**), where aggregates formation already appeared at day zero and band almost completely faded away from day three onward, indicating that DUPA-Pep-Fc-α-amanitin Fc-SMDC (**128**) is more stable in human than in mouse plasma. Cytotoxicity assay after 96 h incubation with PSMA$^+$ LNCaP cells was carried out to evaluate the residual potency of the DUPA-Pep-Fc-α-amanitin Fc-SMDC (**128**) upon incubation in PBS, HP and MP for the time range from 0 h to 11 days. Results from this experiment (**Figure 71**) confirmed that Fc-SMDC **128** is overall more stable in human than in mouse plasma. In human plasma Fc-SMDC **128** retained much of its cytotoxic potential up to three days. From the day 4 onward, dose-response curves progressively flattened and offset increased, indicating a reduction of activity. These results are consistent with the western blot analysis showing for these time points increasing fading of the band corresponding to the conjugate **128** and formation of aggregates. However, significant loss of potency appeared only after nine day incubation in human plasma. Exposed to mouse plasma, Fc-SMDC **128** exhibited reduction of potency already at day one as suggested by curve flattening and

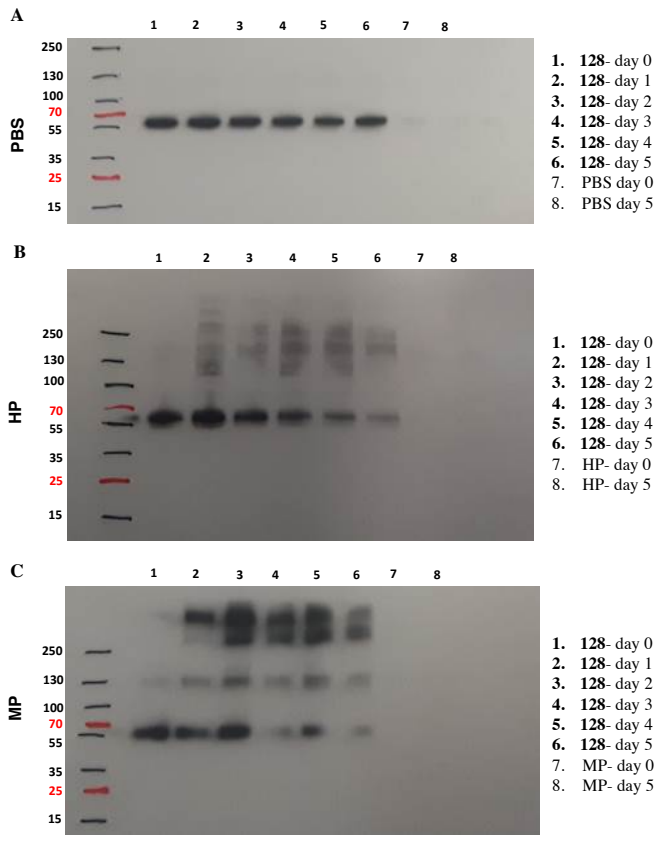

Figure 70. Anti-α-amanitin Western blot under non-reducing conditions. SDS-PAGE was performed on DUPA-Pep-Fc-α-amanitin (**128**) under non-reducing conditions following incubation in **A**) phosphate-buffered saline (PBS); **B**) human plasma (HP) and **C**) mouse plasma (MP) for time points within 0 to 5 days (lanes 1-6).

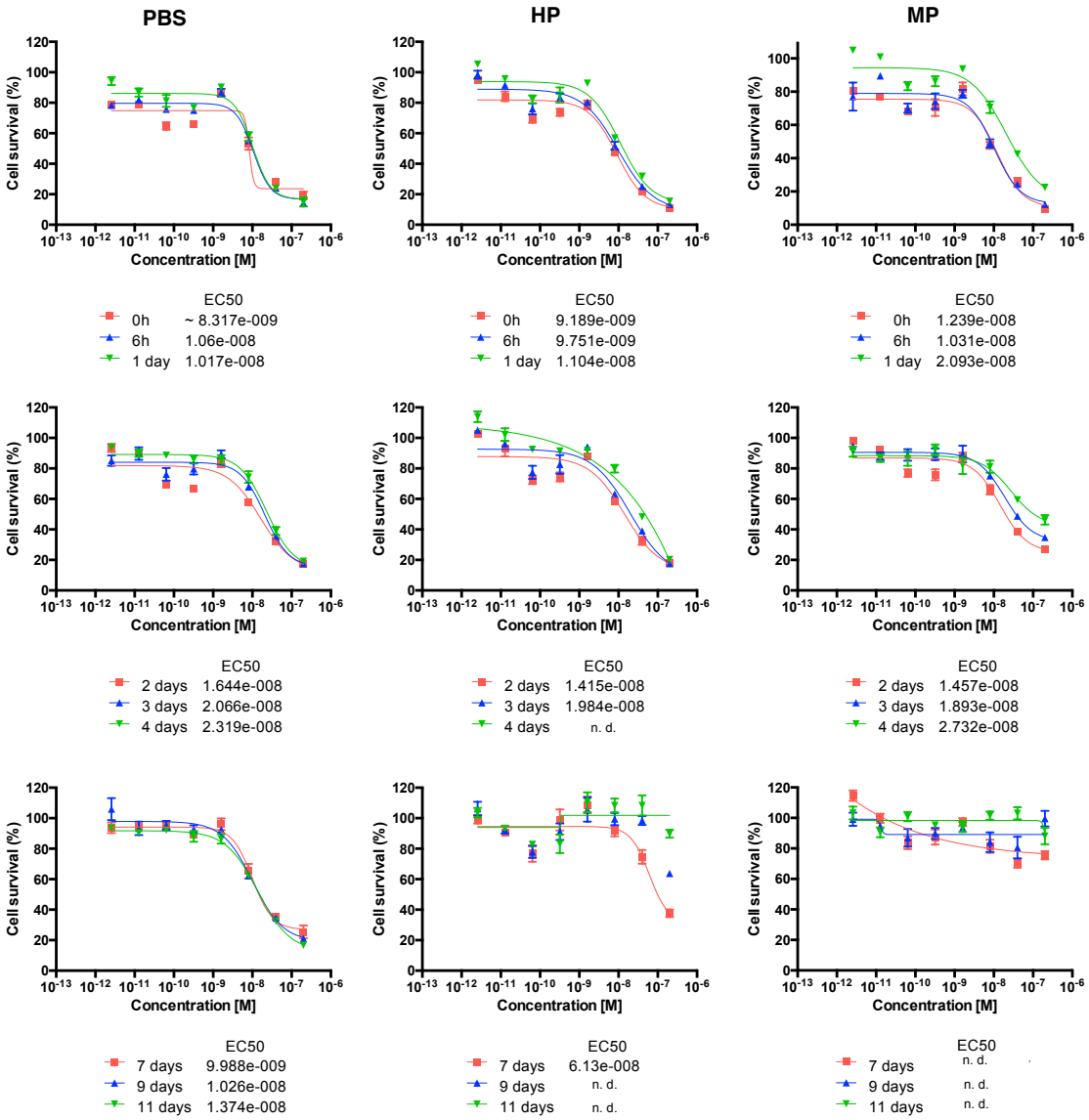

Figure 71. **Dose-response curves for the DUPA-Pep-Fc-α-amanitin Fc-SMDC (128)**. Curves were generated following 96 h incubation with PSMA$^+$ LNCaP cells. Prior to cytotoxicity assay, conjugate was incubated in phosphate-buffered saline (PBS; left panel); human plasma (HP; middle panel) and mouse plasma (MP; right panel) for time points within 0 h to 11 days.

increasing curve offset, which is consistent with the band fading observed in western blot analysis. Potency of the conjugate resulted totally impaired after being incubated in mouse plasma for seven days or longer time.

9.1.8 Maximum tolerated dose study. MTD study (**Figure 72**) was conducted in CB17-Scid mice. The study aimed at defining the highest dose of conjugate **128** that did not cause unacceptable side effects or overt toxicity for the study duration. The primary endpoints for MTD determination were: body weight loss ≥ 20% and general poor conditions.

MTD of conjugate was determined following i.v. administration of descending doses and evaluating toxicity after administration over an observation period of two weeks.

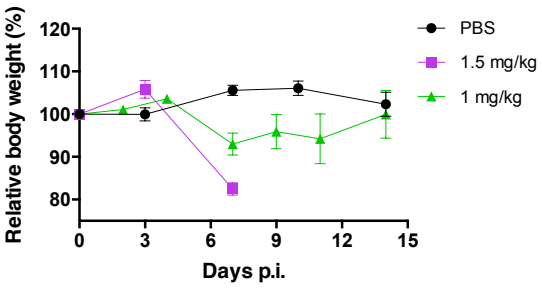

Figure 72. Maximum Tolerated Dose (MTD) study for DUPA-Pep-Fc-α–amanitin Fc-SMDC (128). MTD was assessed by injecting CB17-Scid male mice with different intravenous (i.v.) doses of conjugate followed by observation for 15 days. Body weight was measured twice per week. Each data point represents the mean ± SD of n= 3 mice.

A single dose of 1.5 mg/kg of DUPA-Fc-α-amanitin (**128**) corresponding to 38.7 mg/kg of α-amanitin caused unacceptable toxicity. As the primary endpoints were achieved, at day seven mice were euthanized. Dose was lowered to 1 mg/kg (25.7 mg/kg of α-amanitin). At this dose a partial body weight loss lower than 10% was completely recovered from day seven. Therefore, this dose was set as the MTD for the DUPA-Pep-Fc-α-amanitin Fc-SMDC (**128**).

9.1.9 Plasma pharmacokinetic study. Serum levels at time points between 5 minutes to 14 days of Fc-SMDC **128** following single i.v. injection of 0.5 mg/kg (1/2 MTD) in LNCaP xenograft CB17-Scid mice were measured using anti-α-amanitin ELISA. Serum concentration-time profile is depicted in **Figure 73**.

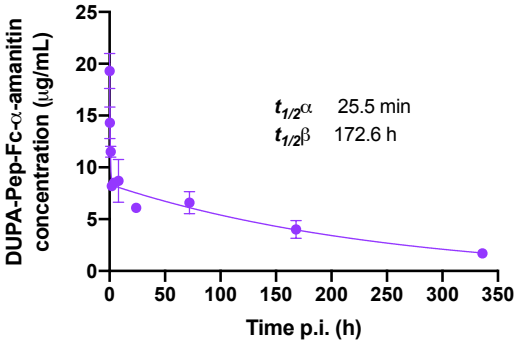

Figure 73. Pharmacokinetic (PK) study of DUPA-Pep-Fc-α–amanitin Fc-SMDC (128). Plasma concentration of α–amanitin-containing compounds in CB17-Scid male mice after a single intravenous (i.v.) dose of conjugate was determined by anti-α–amanitin ELISA. Each data point represents the mean ± SEM of n= 3 mice.

A two-compartment 1st-order PK model with a 1st-order elimination rate was considered as the best fit to explain the generated data. The distribution ($t_{1/2}\alpha$) and elimination ($t_{1/2}\beta$) half-life were found to be 25.5 min and 172.6 h (7.2 days), respectively.

9.1.10 Biodistribution study. The tissue distribution of the DUPA-Pep-Fc-α-amanitin Fc-SMDC (**128**) and the released toxin α-amanitin was evaluated following single dose i.v. application of 1 mg/kg in LNCaP xenograft CB17-Scid male mice. At each time point within the range from 5 minutes to 14 days, three mice were euthanized and liver, kidney and tumor were collected and analyzed. Concentration of conjugate **128** and released toxin α-amanitin in liver, kidney and tumor over the time course of the study is shown in **Figure 74**. DUPA-Pep-Fc-α-amanitin (**128**) was rapidly distributed to the liver reaching a concentration of approximately 4 µg/g of wet tissue at time point 5 min after dose administration. The liver uptake declined with time with a transient increase to approximately 5 µg/g of wet tissue detected after 168 h (7 days) following administration.

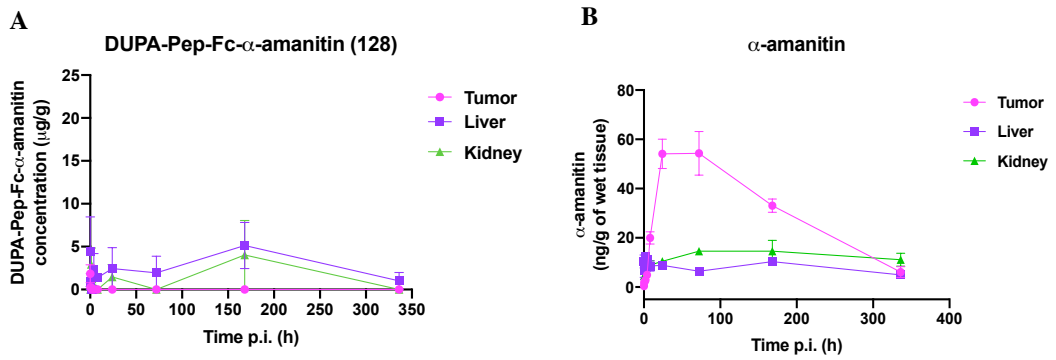

Figure 74. Biodistribution study of DUPA-Pep-Fc-α-amanitin DC (128) and the released toxin α-amanitin after a single i.v. administration of 1 mg/kg to CB17-Scid mice bearing subcutaneous LNCaP xenografts. A) Concentration of DUPA-Pep-Fc-α-amanitin DC (**128, HDP 30.2972**)) at time points within 5 min to 336 h (14 days) was determined by ELISA using a polyclonal anti-α-amanitin antibody as capture antibody and an anti-human Fc antibody for detection. **B)** Concentration of the released toxin α-amanitin at time points within 5 min to 336 h was determined by a competitive ELISA with a monoclonal anti-α-amanitin antibody, biotinylated α-amanitin and HRP-streptavidin for detection. Each data point represents the mean ± SEM of n= 3 mice.

A similar concentration-time profile was observed in the kidneys. After the initial peak of 3 μg/g of wet tissue reached at 1 h post administration, the concentration of the conjugate **128** dropped off and transiently increased to around 4 μg/g of wet tissue at time point 168 h upon injection. In the tumor, conjugate **128** was detectable only at the earliest time points (5-15 min). For the following time points concentration of the conjugate **128** was below the detection limit. Concentration of the released α-amanitin was measured by competitive anti-α-amanitin ELISA (**Figure 74B**).

Levels of released toxin in the serum were below the detection limit for all the evaluated time points. The toxin reached the maximum liver uptake of approximately 12 ng/g of wet tissues at 2 h p.i., which decreased continously over the time, with a transient increase at 168 h post administration. Kidney uptake showed an increase up to 14.5 ng/g of wet tissue at 72 h, followed by a steady wash-out to ~ 11 ng/g of wet tissue at time point 336 h (14 days) after administration. Toxin concentration in the tumor gradually increased to ~ 54 ng/g of wet tissue at 24 h p.i. and dropped off to ~ 6 ng/g of wet tissue after 336 h.

9.1.11 Efficacy study. Next, DUPA-Pep-Fc-α-amanitin Fc-SMDC (**128**) was tested for its antitumor activity in LNCaP xenograft models. CB17-Scid male mice (n= 8 to 10 per treatment and control groups) were injected with LNCaP cells and tumors were allowed to reach an average size of 100 mm^3 before initiation of the treatment. Different dosing regimens of conjugate **128** administered via i.v. injection were evaluated: 1 mg/kg once per week, 0.5 mg/kg (½MTD) once or twice per week, 0.25 mg/kg (⅓MTD) once, twice or three times per week, for a total of three weeks of treatment. Day 42 after initiation of the treatment was chosen for statistical comparison among the treated groups, as it was the final day of the study with at least eight animals per group included (**Figure 75A**). A dose-dependent effect on tumor regression was observed.

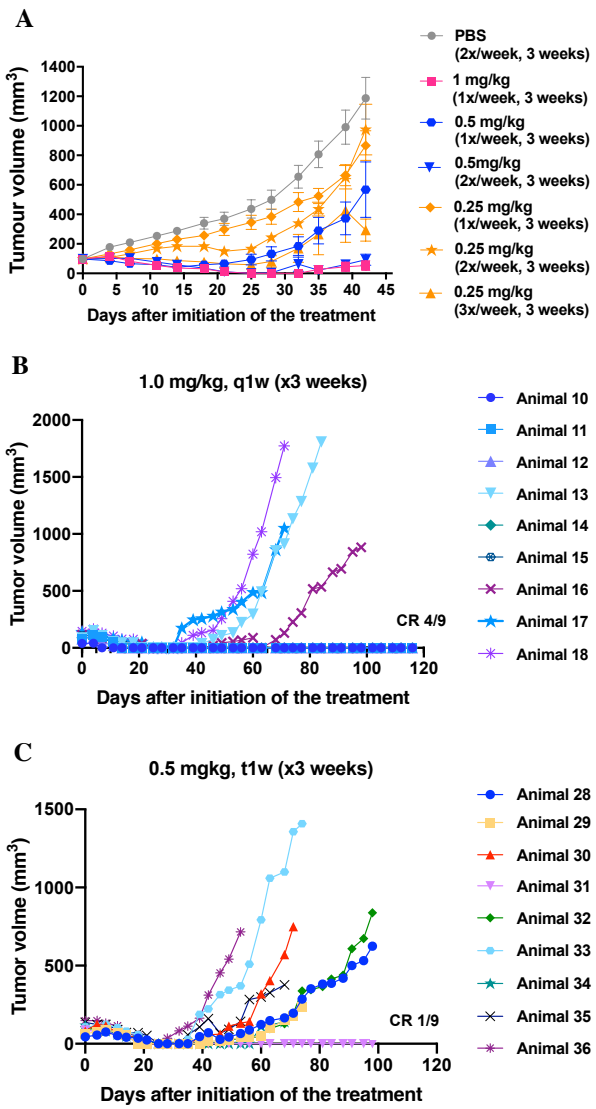

Figure 75. Efficacy study of DUPA-Pep-Fc-α-amanitin Fc-SMDC (128, HDP 30.2972). A) Antitumor efficacy of conjugate **128** in LNCaP xenograft male CB17-Scid mice after multiple intravenous (i.v.) injections over a period of 42 days. **B-C**) Follow-up of antitumor efficacy in groups dosed with 1 mg/kg once weekly (q1w) x3 weeks (**B**) or 0.5 mg/kg twice weekly (t1w) x3 weeks (**C**) over the entire study duration (116 days). Error bars in tumor volume curves represent SEM of n= 8 to 10. Tumor size across the groups on day 42 was analyzed using a one-way ANOVA.

When tumor size in the treated groups is compared with the untreated control at day 42, a statistically significant effect ($P<$ 0.0001) on tumor regression was observed in groups dosed with 1 mg/kg weekly and 0.5 mg/kg twice weekly (**Figure 75A**), Complete response was observed in these groups (**Figure 75B-C**). While in the long-term follow-up 8/9 animals from the group administered with 0.5 mg/kg twice per week had tumor relapse (**Figure 75C**) and at day 98 all animals had been euthanized, at the last day of the follow-up period (day 116 after treatment initiation) 4/8 animals dosed with 1 mg/kg once weekly were still alive and tumor free (**Figure 75B**).

At day 42, animals given 0.5 mg/kg once weekly showed a moderate but statistically significant ($P=$ 0.0050) tumor regression compared to the untreated control group.

Response to the treatment of groups dosed with 0.25 mg/kg was different according to the dosing frequency. No significant effect on tumor size as compared to the untreated control group at day 42 was seen in the groups dosed once ($P=$ 0.3096) or twice weekly ($P=$ 0.6790). In contrast, the 0.25 mg/kg dose of conjugate **128** administered three times per week was effective at inducing significant ($P<$ 0.0001) tumor growth inhibition.

9.2 Discussion

In present study the DUPA-Pep-α-amanitin SMDC was successfully grafted onto a human IgG_1-Fc fragment which served as scaffold to achieve an ADC-like therapeutic with a serum half-life close to that of full size antibodies, but yet much smaller in size (~ 61 kDa *versus* ~ 150 kDa for ADCs).

For conjugation of the DUPA-Pep-α-amanitin moiety to the Fc domain, a two step chemo-enzymatic strategy was set out. The initial attachment of the trifunctional linker (**130**) via sortase A-mediated ligation was the critical step. Despite efforts to optimize the reaction conditions, the large scale conjugation was not efficient probably due to the occurence of reversed hydrolysis reaction during the long incubation time. The final product was obtained, therefore, as heterogenous mixture of species with an average DPR of 1.72, stressing the importance of further tuning the reaction conditions in order to achieve a homogenous product with DPR 2.

Assessment of the *in vitro* activity showed that, in spite of the bulky Fc scaffold, the Fc-SMDC **128** preserved the *in vitro* profile of the DUPA-Pep-α-amanitin SMDCs, as the level of activity on and selectivity for the PSMA-expressing cells was in the range reported for the DUPA-Pep-α-amanitin SMDCs. This observation suggests that the targeting properties of the DUPA-Pep moiety are not affected by the presence of the bulky Fc scaffold. The EG_3 dimer within the trifunctional linker (**130**) provided sufficient spacing from the Fc scaffold, enabling the targeting moiety still to reach and bind to PSMA and thus, the conjugate to be efficiently internalized and deliver adequate amount of toxin inside the cell.

In contrast to the SMDC counterpart (**37**), for the Fc-SMDC **128** the high *in vitro* activity translated into an outstanding *in vivo* efficacy. Durable complete response was reported in LNCaP xenograft models at full MTD and half MTD administered once and twice weekly, respectively, for three weeks. Four out of nine animals in the first group remained tumor-free as long as 116 days after initiation of the treatment. PSMA-targeted ADC Thiomab-30.1699 (**29**, **Figure 25**) at the equivalent dose of 2 mg/kg administered once weekly for four weeks showed sustained tumor regression in six out of eight animals.[118] Despite results of this study can not be directly compared with Fc-SMDC **128**, they provide further evidence that the PSMA-targeting α-amanitin-based Fc-SMDC **128** features ADC-like properties and might be a viable alternative to ADCs and SMDCs.

Also, as small-sized therapeutic combining a small organic molecule as tumor-homing vehicle, a hydrophilic toxin with a novel mode of action and a Fc portion providing extended circulatory half-life, DUPA-Pep-Fc-α-amanitin **128** is, to the best of our knowledge, unique in its ability to induce such a therapeutic response so far.

In 2016 Cochran *et al.*[190] described an integrin-targeting knottin fused to a human Fc domain (Knottin-Fc-Drug Conjugate, KFDC), the 2.5F-Fc-MMAF, that was evaluated as vehicle for the targeted delivery of MMAF to tumors. Similarly to the DUPA-Pep-Fc-α-amanitin **128**, the 2.5F-Fc-MMAF is based on an alternative scaffold embedding a Fc portion approximately 60% smaller than a conventional ADC conjugated to a hydrophilic drug payload. However, the 2.5F-Fc-MMAF KFDC demonstrated only modest antitumor activity in glioblastoma xenograft tumor models, probably as consequence of the limited amount of drug delivered to the cells, the inefficient processing of the conjugate in the lysosomes or the low potency of the drug attached to the non-cleavable linker which is supposed to be the active compound released inside the cells. Results of

this study cannot be head-to-head compared to the DUPA-Pep-Fc-α-amanitin **128** since targeting agents, linkers, toxin warheads and tumor models are different. However, they suggest that conjugate size, target, tumor-homing vehicle, linker and drug payload properties play a concerted role in determining the efficacy of the α-amanitin-based Fc-SMDC **128**.

In contrast to the SMDC counterpart **37** that, due to the short half-life of ~ 44 min required frequent dose administration without exerting significant anti-tumor activity, the weekly dosing of the Fc-SMDC **128** was supported by the longer elimination half-life ($t_{1/2}\beta$) of ~ 7 days displayed in murine models.

As its molecular weight is at the threshold of the renal cutoff (60-70 kDa), contribution of renal filtration to the clearance of Fc-SMDC **128** is supposed to be lower. However, it should be considered that factors other than size, such as charge, lipophilicity, liability to protease degradation, contribute as well to the efficiency of the renal filtration and thus, they can have also an impact on the clearance of the conjugate **128**.

Several preclinical studies have demonstrated that clearance of peptibodies, bioactive peptides fused to an IgG-Fc domain which can be considered as analogues of our platform, such as romiplostin and trebananib, is 14- to 24-fold increased in FcRn-knockout mice than in wild-type animals.[191,192] These studies points out that FcRn likely plays a crucial role on the disposition of the Fc-SMDC **128** by preventing it from undergoing lysosomal degradation, thereby extending its circulatory half-life. Although interaction of the human FcRn with the human IgG-Fc domain is species-specific, residues on the murine FcRn responsible for IgG binding are conserved across the species,[193] supporting the murine model as appropriate for the assessment of the pharmacokinetics of Fc-SMDC **128**.

The greater stability of the triazole linkage, which anchors the α-amanitin warhead to the DUPA-Pep-Fc scaffold until the conjugate is internalized and the toxin is released inside the cell by virtue of secreted proteases might have contributed to increase the plasma exposure of the α-amanitin-based Fc-SMDC **128**. Indeed, the biodistribution data showed that no premature drug loss occurred in circulation, suggesting that the stable conjugation chemistry can preserve the potency of the Fc-SMDC **128**. Expressing the MTDs as drug equivalents, the safety studies in mice revealed a slightly higher tolerability for the Fc-SMDC **128** than for the SMDC counterpart **37** (25.7 *vs*. 18.7 μg/kg of α-amanitin, respectively). Following the hypothesis of enhanced kidney toxicity of amanitin-albumin conjugates forming upon *retro*-Michael deconjugation of thiosuccinimide adducts outlined in section 5.2, replacement of the thiosuccinimide with the stable triazole linkage might have contributed to lower the overall toxicity for the Fc-SMDC **128**.

The main issues in the development of the α-amanitin-based SMDCs as effective therapeutics were the low stability and short half-life displayed in circulation, which prevented the drug from accumulating in the tumor at sufficient levels to be effective. In this perspective, the extended linkage stability coupled to the prolonged PK half-life of the Fc-SMDC **128** sustained increased

exposure to the drug in conjugated form, allowing increasing accumulation over time of α-amanitin in the tumor tissue (**Figure 74B**), with the healthy tissues (i.e. kidneys and liver) being essentially spared.
Altogether these proof-of-concept studies validate the tumor targeting and drug delivery properties of the novel α-amanitin-based Small Molecule-Fc-Drug Conjugate platform (**128**).

Within a size approximately equal to the 40% of a conventional ADC, the platform developed merges the favorable properties of a small-sized therapeutic with the PK properties of an ADC. As alternative to the genetic fusion, the two-step strategy employed for chemically programming and arming the Fc scaffold allows to programm a single generic Fc-LPETGG fragment against a variety of targets without requiring extensive protein engineering project customed for each target and being accessible even to chemically synthetised ligands not suitable to genetic fusion. Additionally, different targeting ligands can be combined with a variety of linkers, toxic warheads and conjugation chemistries, thereby expanding the landscape of the tumor targeted technologies.

Chapter 10
Conclusions and Outlooks

Despite being a promising target no PSMA-targeted ADCs have reached the late phase clinical trial so far. Indeed, challenges still remain for application of ADCs to the more difficult-to-treat solid tumors.[194] The specific physiology of the tumor environment and the large size of ADCs can result in the limited and uneven distribution of the ADC in the tumor tissues compromising the clinical outcome. In this perspective, SMDCs hold the potential to achieve rapid and uniform distribution in the tumor tissue.
Additionally, discontinuation of the clinical development for solid cancer indications of some microtubule inhibitors-based targeted conjugates,[195] which still constitute the majority of ADC and SMDC payloads, stresses out that further refinements of the design of targeted conjugates are needed. Incorporation of novel payloads with alternative mode of action and more favorable physiochemical properties may be crucial to a conjugate to eradicate the tumor and overcome tumor-resistance and toxicity issues.

The current project aimed at combining the tumor-targeting and -penetrating properties of a small-sized binding ligand with the novel mode of action of α-amanitin, a potent inhibitor of eukaryotic RNA polymerase II, for the treatment of prostate cancer.

In order to assess the optimal approach for distribution of the conjugate to the tumor and payload release inside the tumor cells, different linkers and release strategies were borrowed from the ADC technology. Thiosuccinimide-linked SMDCs (SMDCs **37**-**39**; **Chapter 3**) with self-immolative peptide cleavable (Val-Ala, **37;** Val-Cit, **38**), and non-cleavable (**39**) linkers and a panel of disulfide linkers with different degree of steric hindrance around the disulfide bond (SMDCs **58**-**62**; **Chapter 4**) were developed as first generation of PSMA-targeting α-amanitin-based SMDCs.
The majority of the PSMA-targeted SMDCs described in literature feature hydrophobic payloads linked via unhindered disulfide linker which display a cytotoxic potential in the range of activity of unconjugated toxin. In contrast, the α-amanitin-based thiosuccinimide-linked SMDCs (**37**-**39**) and the disulfide-bridged SMDCs with an intermediate level of steric hindrance around the disulfide bond (**58**-**60**) showed increased *in vitro* potency and selectivity against the PSMA-expressing cells compared to the unmodified α-amanitin. These findings offered proof-of-concept of the targeting

and internalization properties of DUPA-Pep-α-amanitin SMDCs, which are key requirements for a hydrophilic toxin, like α-amanitin, to be uptaken by the cells and exert its killing activity.
The thiosuccinimide-linked SMDCs bearing the self-immolative cathepsin B-cleavable linker Val-Ala (**37**) or the non-cleavable maleimidocaproyl linker (**39**), and the monoalkylated disulfide bridged SMDC (1:0, **60**) were selected as best in the class for further characterization in murine models (**Chapter 5**).
The limited therapeutic activity of the DUPA-Pep-α-amanitin SMDCs observed *in vivo* over the range of tolerated doses did not correlate with the potent activity observed *in vitro*.
An insight in the pharmacokinetics of the DUPA-Pep-α-amanitin SMDCs showed that they were featured with short half-life ($t_{1/2}$ < 1 h) and as consequence of the rapid renal clearance which occurs freely for low molecular weight (< 60-70 kDa) compounds upon intravenous administration. Multiple weekly administrations of a large dose would be required in order to achieve the desired therapeutic effect. However, this approach would not be applicable due to the identified kidney DLT. Uptake and accumulation of α-amanitin or α-amanitin-containing metabolites in the kidney was showed to be related to some extent to the linker cleavability of the SMDCs **37** and **39** investigated for the tissue distribution, and only partly associated to the PSMA physiological expression in the proximal renal tubules. However, future studies will seek to elucidate the SMDC metabolites in order to identify the exact cause behind this off-target toxicity issue. Such tissue exposure information are needed in order to define strategies to overcome the DLT thus, expanding the therapeutic index of the DUPA-Pep-α-amanitin conjugates.

The problem of the poor pharmacokinetic properties spurred research into strategies to confer improved PK properties to the DUPA-Pep-α-amanitin SMDCs (**Chapters 6-9**). Replacement of the thiosuccinimide with the thioacetamide linkage (SMDCs **80**-**81**; **Chapter 6**) was effective at increasing the stability of the conjugates exposed to the plasma proteins from 6 to 72 hours. Despite the pharmacological consequences of modifying the linkage chemistry were not investigated, these observations suggested that the linkage chemistry is a critical structural feature that might compromise the exposure to the drug in the conjugated form. Thus, optimization of the linkage chemistry appeared to be crucial in the context of half-life extension strategies. Therefore, the thioacetamide linkage was explored as conjugation chemistry for the SMDC **88** (**Chapter 7**) bearing a His-Glu dimer as pharmacokinetics-modifying spacer. The increased net negative charge at physiological pH provided by the His-Glu dimer was expected to reduce the renal filtration and uptake of the conjugate due to the repulsion with the negatively charged sites of the glomerular filtration barrier and the renal tubular cells membrane, reducing the clearance rate and the kidney uptake. However, comparative studies with the reference SMDC **37** did not reveal any improvements in terms of pharmcokinetics and accumulation in the kidney, suggesting that other mechanisms might be involved in the kidney uptake of the DUPA-Pep-α-amanitin SMDCs. The

alternative strategy pursued to improve the tumor uptake and retention of the DUPA-Pep-α-amanitin SMDCs was enhancing the binding affinity via dimerization of the binding moiety (SMDCs **101**-**104**; **Chapter 8**). By using a central bifurcated scaffold two DUPA-Pep binding moieties were attached to the Val-Ala-PAB-α-amanitin prodrug moiety through EG_n spacers of different length (n= 0, 4, 8, 12). Assuming that a greater binding affinity would lead to potency enhancement, evaluation of the *in vitro* activity did not show significant improvements compared to the reference conjugate **37**, suggesting that dimerization may not be the optimal modality to improve the tumor uptake and retention of DUPA-Pep-α-amanitin SMDCs.

Attempts to improve the PK properties led ultimately to the unprecedented grafting of the SMDC onto an IgG_1-Fc scaffold leading to the new Small Molecule-Fc-Drug Conjugate (Fc-SMDC) format **128** (**Chapter 9**). While the *in vitro* profile of the Fc-SMDC **128** and the small-sized counterpart **37** was comparable, modulation of the PK properties dramatically affected the anti-tumor efficacy. Reduction of renal filtration due to the increased size and the FcRn recycling process conferred extended half-life to the Fc-SMDC **128** ($t_{1/2\beta}$ ~ 7.2 days). The prolonged half-life translated into a complete response achieved at the MTD given once weekly and at half MTD given twice weekly with ~ 50% of animals treated with the highest dose remaining tumor free 116 days after initiation of the treatment. The data generated in this study confirmed that prolonged exposure to the drug conjugated to the tumor-homing vehicle is essential for a membrane-impermeable payload, like α-amanitin, to be accumulated and internalized at adequate levels in the tumor for a durable therapeutic effect. In opposite to the SMDC counterpart **37**, which was detectable in the tumor only at very low concentration, even lower doses of Fc-SMDC **128** led to a constant accumulation over time of toxin in the tumor.

Considering the limitations in treating solid tumors with ADCs due to their large size and with SMDCs due to the large dose and the high dosing frequency required, our Fc-SMDC **128** merging together in the same platform the best of the two technologies has the potential to be developed as an effective ADC-like anti-tumor therapeutic. The flexibility of the chemo-enzymatic strategy herein developed for the graftment of the SMDC onto the IgG_1-Fc scaffold allows to investigate different combinations of targeting ligands, toxin payloads and linkers to validate the platform tumor targeting and drug delivery properties for cancer indications other than PCa.

Chapter 11

Summary

Conjugation of cytotoxic drugs to tumor-homing vehicles, including monoclonal antibodies for antibody-drug conjugates (ADCs) and small molecules for small molecule-drug conjugates (SMDCs), allows the selective delivery of cytotoxic agents to the tumor site thus, reducing the systemic toxicity often associated to conventional chemotherapy.

The present project describes the development of small format-drug conjugates for the treatment of prostate cancer (PCa). The products herein presented were designed to: 1) selectively recognize the PCa cells by means of a small organic ligand, known as DUPA (2-[3-(1,3-dicarboxylpropyl)-ureido]pentanedioic acid), which binds with high affinity to the Prostate Specific Membrane Antigen (PSMA) overexpressed by PCa cells; 2) exert cytotoxic activity by shuttling inside the cells a hydrophilic toxin, named α-amanitin, which is a potent inhibitor of RNA polymerase II.

First, a small library of α-amanitin-based SMDCs was initially generated by varying the linker structure and the conjugation chemistry connecting the targeting moiety constituted of DUPA and a peptide supporting-binding spacer to the drug payload (**Figure 76**).

A modular approach with the initial synthesis and assembly of the targeting moiety bearing a conjugation site, the construction of the distinct linker-α-amanitin payloads and the assembly of the entire constructs occurring as final step of the synthetic process was set out as general synthetic strategy.

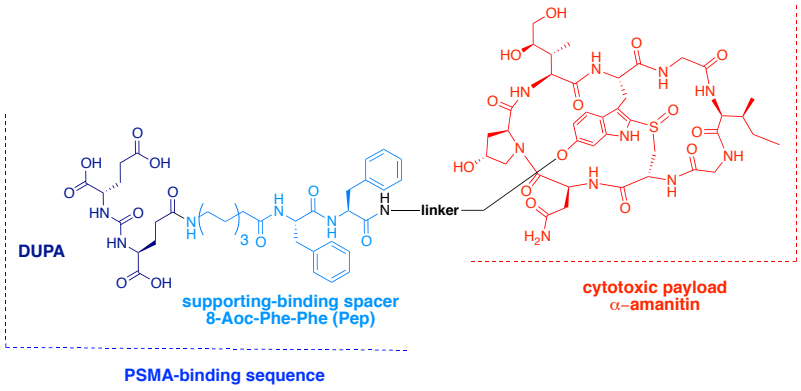

Figure 76. Schematic representation of the PSMA-targeting α-amanitin-based SMDCs. Modules are color coded as follows: the PSMA-targeting glutamate-urea-based ligand DUPA (dark blue) and the PSMA-supporting binding spacer (cyan) constituting the PSMA-binding sequence are circled in blue; the variable linker structure is shown in black, while the toxin warhead α-amanitin is shown in red.

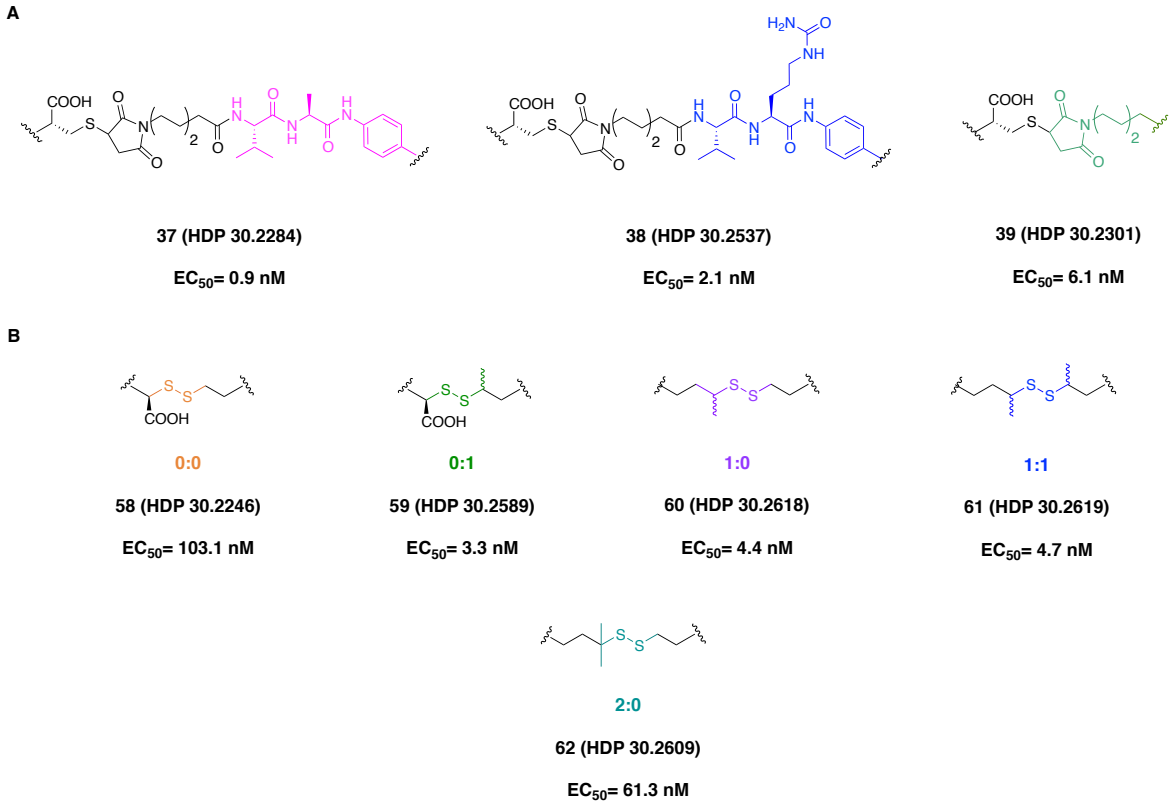

Figure 77. Linker structures of the first generation PSMA-targeting α-amanitin-based SMDCs: A) the thiosuccinimide-linked and B) the disulfide-bridged SMDCs. The steric hindrance around the disulfide bond is indicated with the notation *x*:*y*, where *x* corresponds to the number of methyl groups on the carbon adjacent to the sulfur on the binding sequence side of the disulfide bond, while *y* is equal to the number of methyl groups next to the sulfur on the α-amanitin side of the disulfide bond. EC_{50} on PSMA-expressing LNCaP cells.

In the thiosuccinimide-linked SMDCs (**Chapter 3**, **Figure 77A**) α-amanitin was conjugated via thiol-maleimide Michael addition to the targeting moiety through a self-immolative cathepsin B-cleavable Val-Ala (**37**) or Val-Cit linker (**38**), and a non-cleavable alkyl linker (**39**). In the disulfide-bridged SMDCs (**Chapter 4**, **Figure 77B**) the targeting moiety and the drug payload were conjugated through non-immolative disulfide linkers with different level of alkylation around the disufide bond (0:0, **58**; 0:1, **59**; 1:0, **60**; 1:1, **61**; 2:0, **62**). Cytotoxicity and selectivity of SMDCs were evaluated on PSMA-positive LNCaP and PSMA-negative PC3 cell lines. The thiosuccinimide-linked SMDCs resulted 555-fold to 90-fold more potent than unconjugated α-amanitin on LNCaP cells, with EC_{50} values in the picomolar or low nanomolar range (**Figure 77**). Competitive binding assay in presence of a molar excess of the PSMA inhibitor 2-PMPA, and lack of significant toxicity on the PSMA-negative PC3 cells further proved the targeting and internalization properties of our constructs. Cytotoxicity of the most potent SMDC **37** and its non-cleavable counterpart **39** was measured also upon stressing the conjugates in mouse and human plasma. Conjugates retained almost intact their potency up to 6-24 h, with a more pronounced stability in mouse plasma rather than in human plasma. For the disulfide-bridged SMDCs a strong dependance of potency on the level of steric hindrance around the disulfide bond was observed.

	MTD (mg/kg)		$t_{1/2}$ (min)
37	0.046	0.019[a]	44.2
39	2.56	1.20[a]	61.8
60	1.2	0.600[a]	81.5

Table 7. MTD (Maximum Tolerated Dose) and half-life ($t_{1/2}$) of the selected PSMA-targeting α-amanitin-based SMDCs. [a] equivalent dose of α-amanitin.

While a dramatic loss of activity was reported for the unhindered (**58**) and the most hindered disulfide-bridged SMDC (**62**), the SMDCs with an intermediate level of alkylation were found to be the most potent (**59**-**61**). SMDCs **59**-**61** also retained much of their activity for time points up to 24-72 h upon incubation in plasma matrices. These results suggested that for the disulfide-bridged SMDCs a critical balance must be found between conjugate stability and drug release.

Based on ease of chemical synthesis and *in vitro* data, SMDC **37** bearing the cathepsin B-cleavable linker, its non-cleavable counterpart **39** and the 1:0 disulfide-bridged SMDC **60** were selected for further chracterization *in vivo*, as discussed in **Chapter 5**.

From the toxicity study in CB17-Scid male mice, SMDC **37** bearing the self-immolative cathepsin B-cleavable linker resulted the least tolerated, followed by the non-immolative disulfide-bridged SMDC **60** and the thiosuccinimide-linked SMDC **39** containing the non-cleavable linker, suggesting a relationship between linker cleavability and tolerability (**Table 7**). Assessment of the *in vivo* pharmacokinetics demonstrated that SMDCs **37**, **39** and **60** were featured with a short half-life ($t_{1/2}$ ≈ 1-1.5 h, **Table 7**), likely due to their low molecular weight and consequent high rate glomerular filtration. Next, the therapeutic activity of SMDCs was assesed in LNCaP-xenografted mice at different dosing regimens over the range of tolerated doses (**Figure 78**). As expected due to their short half-life, high frequency-dosing regimens were the most effective at inducing tumor growth delay. However, this effect was not sustained upon termination of the treatment.

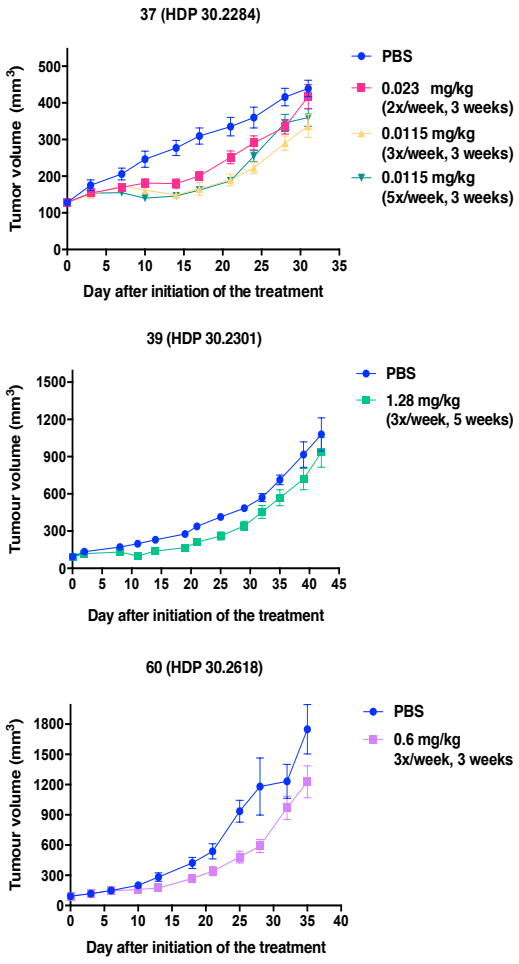

Figure 78. Efficacy study of the selected PSMA-targeting α-amanitin-based SMDCs in CB17-Scid mice bearing LNCaP tumors.

Based on these findings, subsequent efforts were dedicated to tuning the SMDC pharmacokinetic

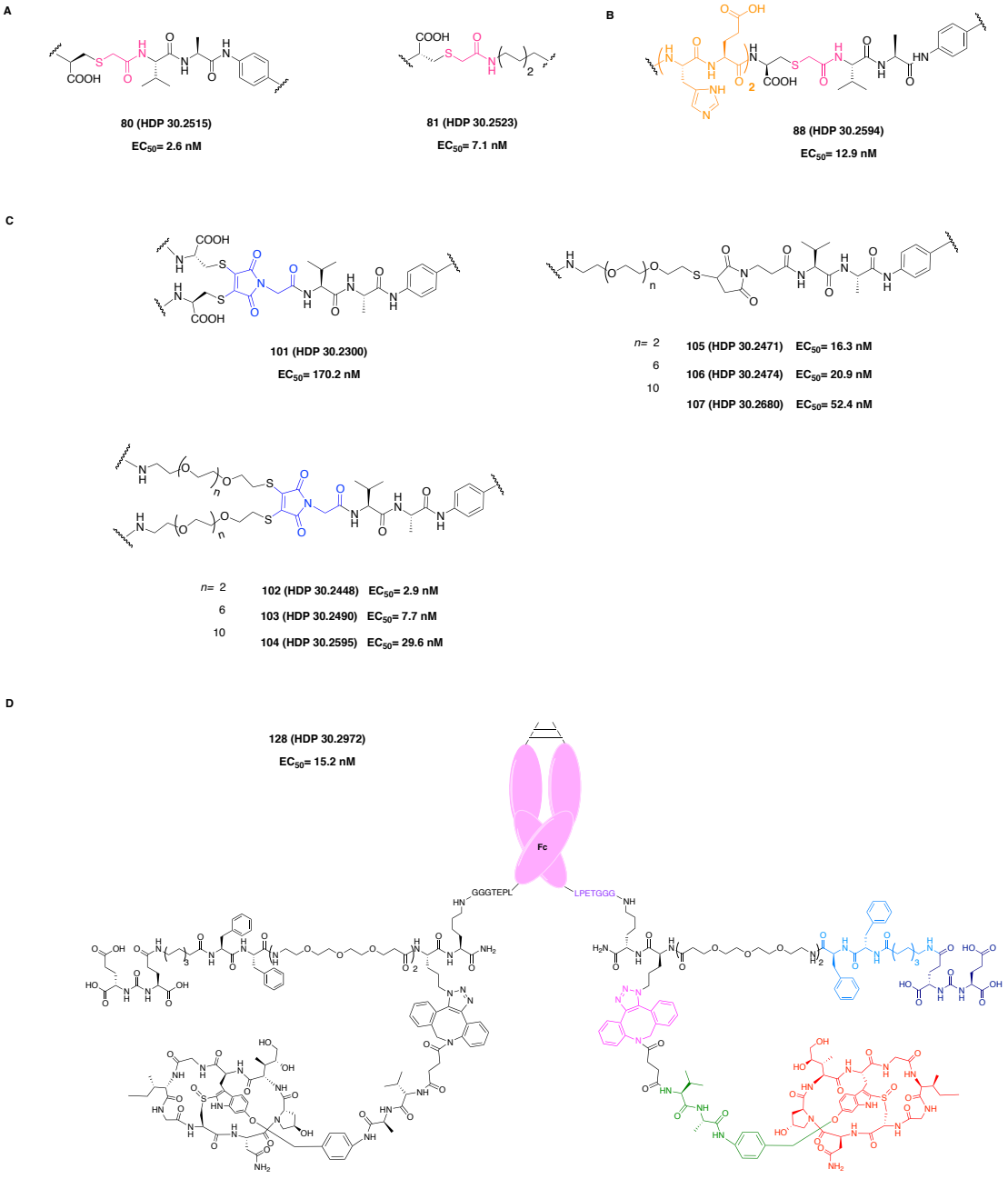

Figure 79. Schematic representation of the strategies pursued to improve the pharmacokinetic properties of the PSMA-targeting α-amanitin-based SMDCs. A) Thioacetamide-linked SMDCs **80**-**81**; **B)** pharmacokinetics-modifying linker-containing SMDC **88**; **C)** bivalent SMDCs **101**-**104** and corresponding monovalent **105**-**107**; **D)** SMDC grafted onto a human IgG_1-Fc fragment, Fc-SMDC **128**. EC_{50} on PSMA-expressing LNCaP cells.

properties in order to ensure prolonged tumor exposure to the drug in conjugated form thus, allowing accumulation of α-amanitin therein at sufficient level to exert durable therapeutic effect (**Chapters 6-9**). The following strategies were pursued: *a)* substitution of the thiol-maleimide linkage chemistry with the more stable thiol-acetamide chemistry (**Chapter 6**, **Figure 79A**); *b)* introduction in the SMDC structure of a pharmacokinetics-modifying (PKM) linker to reduce the glomerular filtration (**Chapter 7**, **Figure 79B**); *c)* dimerization of the binding moiety to increase tumor uptake and retention (**Chapter 8**, **Figure 79C**); *d)* grafting of the SMDC onto a human IgG_1-

Fc scaffold to reduce glomerular filtration and protect the construct from lysosomal degradation (**Chapter 9**, **Figure 79D**).

Thiol-maleimide adducts are known to be susceptible to *retro*-Michael addition in thiol-enriched environment. This mechanism was supposed to lead to the uncoupling of drug payload from the targeting moiety thus, compromising the exposure of the drug in conjugated form and rising risks of off-site toxicity. Supported by this hypothesis, thioacetamide analogues of lead SMDCs **37** and **39** were prepared (SMDCs **80**-**81**; **Chapter 6**, **Figure 79A**). SMDCs **80**-**81** were prepared by conjugating a self-immolative cathepsin B-cleavable or alkyl non-cleavable linker-α-amanitin payloads bearing a bromoacetamide handle to the thiol-containing binding sequence. This strategy was effective at increasing the *in vitro* plasma stability of SMDCs up to 72 h, suggesting that linkage chemistry is a critical structural feature to take into account in the context of half-life extension technologies. Therefore, thioacetamide linkage was exploited for conjugation of the α-amanitin payload bearing a self-immolative cathepsin B-cleavable linker to the binding sequence through a His-Glu dipeptide dimer, which served as PKM linker (SMDC **88**, **Chapter 7**). It was expected the increased negative net charge at physiological pH provided by the PKM linker to induce repulsion with the negatively charged sites of the glomerular filtration barrier and the renal tubular cells membrane, reducing the clearance rate and the kidney uptake. However, from comparative studies with the analogue lead SMDC **37**, it was not observed any significant improvement in terms of PK half-life ($t_{1/2}$ 59.1 min for SMDC **88** *vs*. 49.1 min for SMDC **37**) and kidney uptake profile.

In **Chapter 8** generation of bivalent SMDCs to increase tumor uptake and retention is described. The α-amanitin payload bearing a self-immolative cathepsin B-cleavable linker was equipped with an *N*-terminal [3,4-*bis*(phenylthio)]-maleimidoacetyl group, which served as central bifurcated scaffold for attaching the binding sequences through EG_n spacers of different length (n= 0, 4, 8, 12, SMDCs **101**-**104**). Based on the assumption that a greater binding affinity would lead to enhanced potency, effectiveness of this strategy was evaluated via *in vitro* cytotoxicity assays. Each bivalent conjugate was compared to the corresponding monovalent bearing an EG_n spacer (n= 0, 4, 8, 12, SMDCs **37** and **105**-**107**). With the exception of the rigid SMDC **101** (EG_n, n= 0; EC_{50} 170.2 nM), all the other bivalent SMDCs were more active than the corresponding monovalent, with the conjugate **103** (EG_n, n= 8) being the most active in the bivalent SMDCs series (EC_{50} 7.7 nM) and the SMDC **104** (EG_n, n= 12) showing an intermediate level of activity (EC_{50} 29.6 nM). However, since no great benefits were achieved in comparison to the lead SMDC **37**, the multivalent approach was not further developed.

In the last **Chapter 9**, graftment of an α-amanitin-based SMDC onto a human IgG_1-Fc scaffold, resulting in the novel Small Molecule-Fc-Drug Conjugate (Fc-SMDC **128**) format, is reported. By

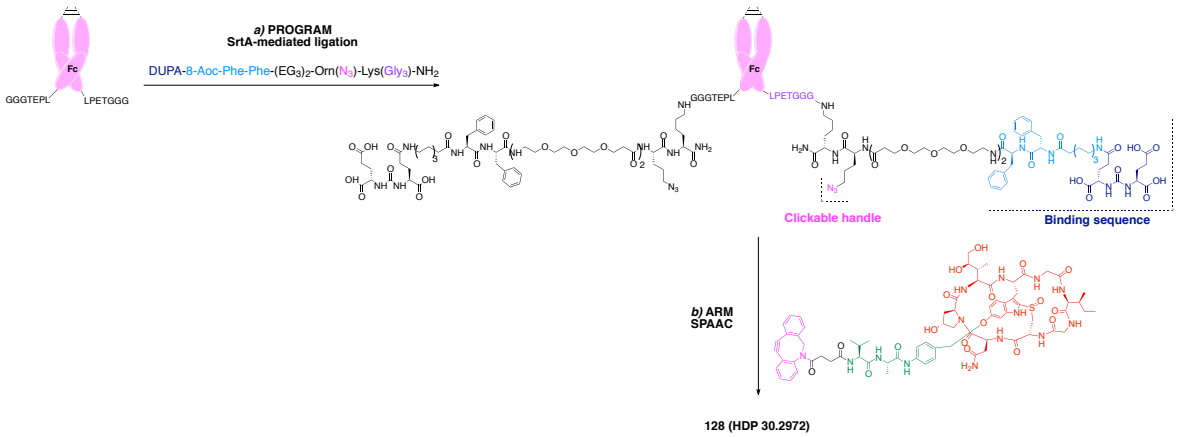

Figure 80. Two-step "program and arm" chemoenzymatic strategy used to graft the PSMA-targeting α-amantin-based SMDC onto the human IgG_1-Fc fragment.

means of a two-step "program and arm" strategy (**Figure 80**) the Fc scaffold was: 1) first programmed to selectively target the PCa cells. The *C*-termini were labeled via sortase A-mediated ligation with a trifunctional linker bearing the PSMA binding sequence and a clickable handle for conjugation to the toxin warhead; 2) subsequently armed via strain-promoted azide-alkyne cycloaddition (SPAAC) with the α-amanitin payload bearing a self-immolative cathepsin B-cleavable linker. Despite the Fc-SMDC **128** was slightly less toxic than the analogue small-sized counterpart **37** on LNCaP cells (EC_{50} 15.7 vs. 1.9 nM for Fc-SMDC **128** and SMDC **37**, respectively), the prolonged PK half-life of ~ 7.2 days turned out in an outstanding therapeutic activity *in vivo* (**Figure 81**). Indeed, the Fc-SMDC **128** was effective at inducing complete tumor response in LNCaP xenograft mouse models administered with doses corresponding to the MTD (1 mg/kg = 25.7 μg/kg of α-amanitin) given once weekly and to the half MTD (0.5 mg/kg) given twice weekly for a three weeks treatment period. In the group treated with the highest dose ~ 50% of animals remained tumor free 116 days after initiation of the treatment. The greater stability of the triazole linkage coupled to the prolonged PK half-life contributed to the constant over time accumulation of α-amanitin in the tumor avoiding undesired accumulation in the healthy tissues (i.e. kidneys and liver) and in circulation, as shown by biodistribution studies.

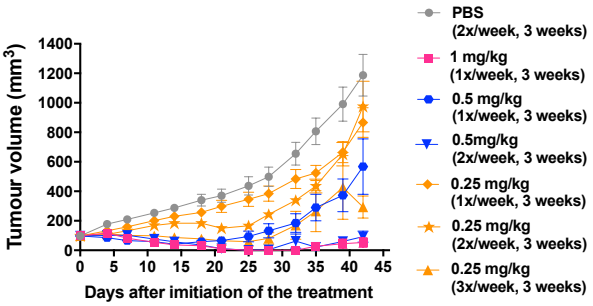

Figure 81. Efficacy study of the α-amanitin-based Fc-SMDC 128 in CB17-Scid mice bearing LNCaP tumors.

Collectively, findings of this study demonstrated that SMDC is not a suitable format for the targeted delivery of a hydrophilic toxin, like α-amanitin, to the site of action. As a membrane-impermeable toxin, prologend exposure of the target tissue to the drug conjugated to the target-homing vehicle is required for the toxin to be internalized and accumulated in the target tissue at sufficient levels to exert durable therapeutic effect.

Experimental part

1. General methods

Solvents and reagents were purchased from commercial vendors and used without further purification. ESI-MS studies were performed using a Thermo Orbitrap LTQ XL™ mass spectrometer (Thermo Scientific™) connected to an Agilent 1200 series high performance liquid chromatography (HPLC) system (isocratic mode; mobile phase composition: methanol:acetonitrile:water, 40:40:20; flow rate: 0.25 ml/min) at Heidelberg Pharma Research GmbH, dept. of Bioanalytic. HRESI-MS studies were performed at Immunodiagnostik AG (Bensheim, Germany) using an Orbitrap Elite™ mass spectrometer interfaced with Ion Max Source (HESI-II probe) (Thermo Scientific™) via reverse-phase liquid-chromatography (RP-LC) gradient separation. Deconvolution of isotopically unresolved spectra was performed with ReSpect™ algorithm using Biopharma Finder 3.0 (Thermo Scientific™). Analytical thin layer chromatography (TLC) was performed on POLYGRAM® SIL G/UV polyester pre-coated plates (40x80 mm, 0.20 mm silica gel 60) and compounds visualization was accomplished with UV light, 1% cinnamaldehyde, ninhydrin or Vaughn´s staining reagents depending on the functional groups to be detected. Flash chromatography was carried out by using Teledyne ISCO CombiFlash® RF system on Silica RediSep® Rf disposable columns. SPPS was performed using the automated microwave peptide synthesizer Liberty Blue™ (CEM Corporation) or the manual microwave peptide synthesizer Discover System (CEM Corporation). All peptides and conjugates were purified by preparative RP-HPLC (VWR LaPrep Sigma LP1200 pumps, VWR LaPrep Sigma 3101 UV detector; column: Phenomenex Luna® 10 μm C18(2) 100Å, 250 x 21.2 mm) and analyzed by analytical RP-HPLC (VWR HITACHI Chromaster 5110 binary HPLC pump, VWR HITACHI Chromaster 5430 diode array detector (DAD); column: Phenomenex Luna® 10 μm C18(2) 100Å, 250 x 4.6 mm). Fc protein was purified by Protein A-based affinity chromatography (Bio-rad NGC™ 100 Medium-Pressure Chromatography system; column: Tosoh Bioscience ToyoScreen® AF-rProtein A HC-650F 5 ml) and dyalized in Thermo Fisher Scientific Slide-A-Lyzer™ cassettes (MWCO 20000, 12-30 ml). Fc-conjugates were purified by preparative size exclusion fast-protein liquid chromatography (SEC-FPLC, ÄKTA™ Start system) and analyzed by analytical SEC (Knauer PLATINblue HPLC with DAD, column: Tosoh Bioscience TSKgel® UP-SW3000, 2 μm, 4.6 mm ID x 30 cm). Fc protein and Fc-conjugates were concentrated by using Amicon® Ultra-15 Centrifugal Filters MWCO 50000 (Millipore) and filtered through disposable sterile Millex®-GV syringe filters (Millipore). Concentration measurements were carried out with Thermo Fisher Scientifc NanoDrop™ 2000

spectrophotometer (λ= 280, 310 nm, sample size 2 μl). SDS-PAGE analysis were peformed on 4-20% precast polyacrylamide gels (Mini-PROTEAN® TGX® precast protein gel, Bio-rad) in Mini-PROTEAN® electrophoresis cells (Bio-rad). Marker PageRuler™ Plus Prestained Protein Ladder was purchased from Thermo Scientific. Western-blot analysis were run by using a primary rabbit α-amanitin polyclonal antibody (produced at Heidelberg Pharma Research GmbH) probed with an anti-rabbit IgG HRP-linked antibody (Cell Signaling Technology®). For chemoluminescent detection Clarity western ECL substrates (Bio-rad) were used.

2. General procedures

GP 1. General procedure for automated MW-assisted solid phase peptide synthesis on preloaded 2-chlorotrityl chloride (CTC) resins.

Resin was swollen in DMF:DCM (1:1, v:v; 10 ml) for 30 minutes prior to its use. For each coupling, the Fmoc-protected amino acid (2.5 equiv.), HBTU (4.25 equiv.), 4 HOBt (2.5 equiv.) and DIPEA (8.5 equiv.) were used. Each coupling reaction was carried out at 60 °C, 40 W for 10 min. After each coupling reaction, resin was washed with DMF (x3), and then a 20% solution of piperidine in DMF was added to the reaction vessel and two deprotection cycle (60 °C, 40 W, 30 s [x1]; 60 °C, 40 W, 2.5 min [x1]) were performed. Following deprotection, resin was thoroughly washed with DMF (x3).

GP 2. Two-stage general procedure for detachment/deprotection of peptides from CTC resin.

GP 2a. General procedure for detachment of peptides from CTC resin. Resin-bound peptide was suspended in a trifluoroethanol (TFE):acetic acid (AcOH):DCM (1:1:8, v:v:v; approximately 10 ml per 0.25 mmol of resin) mixture and shaken at rt for 1.5 h. Resin was then filtered and washed with freshly prepared TFE:AcOH:DCM mixture (1:1:8, v:v:v; 10 ml per 0.25 mmol of resin, 2 min), DCM (10 ml, 2 min) and MeOH (10 ml, 2 min) in sequence. The filtrates were collected and the solvents were removed under reduce pressure and residue dried in vacuo.

GP 2b. General procedure for deprotection of peptides. Deprotection was completed by taking up the residue in a TFA:triisopropylsilane (TIS):H_2O (95:2.5:2.5, v:v:v, 10 ml per 0.25 mmol of resin) or TFA:TIS:H_2O:DTT (94:2:2:2, v:v:v:w, 10 ml) if the peptide contained Cys. Mixture was shaken for 1.5 h at room temperature. TFA was removed under reduced pressure and co-evaporated twice with toluene.

GP 3. General procedure for post-cleavage/deprotection work-up.

Peptide isolation and work-up was achieved by adding to the crude peptide in a centrifuge tube a small volume of MTBE precooled on ice and triturated thoroughly until a precipitate was

formed. The precipitate was centrifuged at 0 °C (4500 rpm, 4 min). MTBE was carefully decanted from the tube and the MTBE washing was repeated. Residual solid was collected and dried in vacuo.

GP 4. General procedure for the synthesis of Boc-protected dipeptide Val-X (X= Ala or Cit) *p*-aminobenzylbromides.

GP 4.1- Boc-Val-X-PAB-OTBDMS

Boc-Val-Ala-PAB-OH was dissolved in DMF (2 ml per mmol of reagent) and DIPEA (2.5 equiv.) and *tert*-butyldimethyl-chlorosilane (TBDMSCl) (1.5 equiv.) were added. The reaction mixture was stirred at room temperature for 30 min, and then DMF was removed in vacuo. The residue was taken up in EtOAc, and washed with 0.2 M citric acid solution, water, saturated $NaHCO_3$ solution, and saturated NaCl solution. The organic layer was dried over $MgSO_4$, and solvents were removed under reduced pressure. The crude product was purified by flash chromatography on a silica gel column. Eluent composition was determined according to the amino acid composition. Following purification, solvents were removed by rotary evaporation.

GP 4.2- Boc-Val-X(SEM)-PAB-OTBDMS

Boc-Val-X-PAB-OTBDMS was dissolved in THF (5.6 ml per mmol of reagent) and 1 M solution of lithium bis(trimethylsilyl) amide (LiHMDS) in THF (1.5 equiv.) was added at 0 °C. The reaction mixture was stirred for 10 min and then neat 2-(trimethylsilyl)-ethoxymethyl chloride (SEMCl) (2 equiv.) was added at 0 °C.

GP 4.3- Boc-Val-X(SEM)-PAB-OH

Boc-Val-X(SEM)-PAB-OTBDMS was dissolved in THF (16.7 ml per mmol of reagent) and 1 M solution of n-tetrabutylammonium fluoride (TBAF) in THF (1.2 equiv.). Reaction mixture was stirred at room temperature for 20-45 min, and diatomaceous earth (approximately 1.7 g per mmol of starting material) was added to the reaction mixture and the volatiles were removed under reduced pressure. The remaining solid was applied on the top of a silica gel column and eluted with a gradient composition depending on the amino acid composition.

GP 4.4- Boc-Val-X(SEM)-PAB-Br

Boc-Val-X(SEM)-PAB-OH was dissolved in DCM (11 ml per mmol of reagent) and a 1 M solution of methanesulfonic anhydride in DCM (1.2 equiv.) followed by DIPEA (2.4 equiv.) were added at 0 °C under argon. Reaction mixture was stirred for 35 min and a

solution of lithium bromide (LiBr) in THF (5 equiv.) was added at 0 °C. After stirring at 0 °C for 10 min, the reaction mixture was allowed to reach the room temperature and being stirred for additional 3 h. The reaction was quenched by adding sodium citrate buffer (pH 6.40, 200 ml), and the mixture was diluted with MTBE (200 ml). The organic layer was washed with sodium citrate buffer (pH 4.76, 200 ml), saturated $NaHCO_3$ solution (200 ml) and NaCl solution (200 ml) in sequence. Organic layers were combined and dried over $MgSO_4$, concentrated under reduced pressure and purified by flash chromatography on silica column. Eluent composition varied according to the amino acid dipeptide composition.

GP 5. General procedure for conjugation to 6´-OH-Trp of α−amanitin

GP 5.1- General procedure for conjugation mediated by Cs_2CO_3

Vacuum dried α-amanitin is dissolved in dry dimethyl acetamide (DMA; 48.4 µl per mmol) under argon at room temperature. Bromide-functionalized linker (4.0 equiv.) and 0.2 M solution of cesium carbonate (Cs_2CO_3) (1.2 equiv.) are added. After 4 h at room temperature the reaction mixture is acidified to pH 5 with AcOH. The solvent is removed in vacuo and the residue is purified by preparative reversed phase high performance liquid chromatography (RP-HPLC).

GP 5.2- General procedure for conjugation mediated by LiOH

Vacuum dried α-amanitin is dissolved in dry dimethyl sulfoxide (DMSO; 26.7 µl per mmol) under argon at room temperature. Bromide-functionalized linker (8 equiv.) and 1 M solution of lithium hydroxide (LiOH; 1.2 equiv.) are added. After 3 h the reaction mixture is acidified to pH 5 with 1 M solution of AcOH in DMSO (1.2 equiv.). The solvent is removed in vacuo and the residue is purified by preparative RP-HPLC. Solvents are then evaporated.

GP 6. General procedure for boc- and SEM-deprotection of α−amanitin derivatives. α-Amanitin derivative is dissolved in TFA (53 µl per mmol) and stirred at room temperature for 2 min and then concentrated to dryness. The residue is dissolved in water (53 µl per mmol) and pH is adjusted to 10 with a 3.2% NH_3 aqueous solution added dropwise. The resulted suspension is freeze-dried and the resulting powder is purified by preparative RP-HPLC.

GP 7. General procedure for coupling of carboxylate-reactive linkers to NHS ester-activated compounds.

NHS-ester activated compound is dissolved in THF (11.85 µl per mmol of reagent). Carboxylate-reactive crosslinker (1.05 equiv.) and $NaHCO_3$ (1.1 equiv.) are dissolved in H_2O (0.18 µl per mmol of $NaHCO_3$) and added to the NHS-ester activated compound solution in THF. The reaction mixture is stirred at room temperature for 1 hour. Reaction is acidified with 0.2 M citric acid solution. EtOAc is added and the organic compound is extracted (x2). Combined aqueous phases are acidified to pH 3 with citric acid and extracted with EtOAc (x3). Organic phase is washed with H_2O, a saturated solution of NaCl, dried over $MgSO_4$ and then concentrated to dryness.

GP 8. General procedure for deprotection of disulfide-reactive DUPA-Pep sequences.

Disulfide-reactive DUPA-pep sequence is treated with a TFA/TIS/H_2O cocktail (95:2.5:2.5, v:v:v; 2 ml) and stirred at room temperature under argon for 1.5 h. Mixture is co-evaporated with toluene (2 ml, x 2). Addition of precooled MTBE (1 ml per mmol of starting material) causes precipitation of a solid. The mixture is centrifuged at 0 °C and the precipitate was collected. The precipitate was washed with additional precooled MTBE (1 ml per mmol of starting material), centrifuged at 0 °C, collected and then purified by preparative RP-HPLC.

GP 9. General procedure for the preparation of the DUPA-Pep sequences including the EG_n spacers (DUPA-Pep-EG_n).

GP 9.1- General procedure for the preparation of the Br-EG_n-Br spacers

Ph_3P (2.0 equiv.) was dissolved in dry DCM (0.82 ml per mmol of Ph_3P) and mixture was cooled down to 0 °C. Bromine (2.0 equiv.) was added dropwise. After 5 min, oligoethylene glycol (1.0 equiv.) dissolved in DCM (0.10 ml per mmol) was added dropwise, reaction mixture was thawed to room temperature and stirred for 74 hours. Afterwards, the reaction mixture was cooled down to 0 °C and diluted with a saturated $NaHCO_3$ solution to pH 7. A 10% $Na_2S_2O_3$ solution (20 ml) was added and phases were separated. Organic layer was washed with a saturated NaCl solution, dried over $MgSO_4$ and evaporated under reduced pressure. The residue was taken up with n-hexane and shaked for 0.5 h. Crystals were filtered off, taken up with n-hexane (x2), sonicated and filtered off. The filtrates were collected, evaporated and distilled (140 °C, 0.0062 mbar) to achieve the final product.

GP 9.2- General procedure for the preparation of the Br-EG_n-N_3 spacers

Br-EG_n-Br spacer (1.0 equiv.) was dissolved in dry DMF (2 ml per mmol). NaN_3 (1.0 equiv.) was added and the reaction mixture was stirred at room temperature under argon for 21 h and used directly in the following step.

GP 9.3- General procedure for the preparation of the (Trt)S-EG$_n$-N$_3$ spacers

Triphenylmethanethiol (1.0 equiv.) was dissolved in dry DMF (2 ml per mmol) and cooled down to 0 °C. NaOMe as 30% solution in MeOH (1.0 equiv.) was added. After 2 min, **Br-EG$_n$-N$_3$** compound was added and reaction was thawed to room temperature and stirred for 1.5 h. DMF was evaporated in vacuo and the residue was taken up with EtOAc and washed with a saturated NH_4Cl solution. a saturated $NaHCO_3$ solution, H_2O and a saturated NaCl solution in sequence. Organic layer was dried over $MgSO_4$ and the solvent was evaporated under reduced pressure. The crude product was purified on silica gel column with a gradient of 0 to 20% of MTBE in toluene (.λ= 285 nm). The product was collected and the solvents were evaporated to afford the final product.

GP 9.4- General procedure for the preparation of the (Trt)S-EG$_n$-NH$_2$ spacers

(Trt)S-EG$_n$-N$_3$ spacer (1.0 equiv.) was dissolved in THF (20 ml per mmol). PPh_3 (2.0 equiv.) and H_2O (2 ml per mmol) were added in sequence. The reaction mixture was stirred at room temperature for 42 h. After the solvents were evaporated, the crude product was purified on a silica gel column with a gradient of 0 to 100% of DCM:MTBE:MeOH (6:3:1, v:v:v) with 1% TEA in DCM (λ= 235 nm). The product was isolated and the solvents were evaporated in vacuo.

GP 9.5- General procedure for the preparation of the (O^{t}Bu)$_3$DUPA-Pep-EG$_n$-S(Trt) sequences

(O^{t}Bu)$_3$DUPA-Pep-OSu **75** (1.0 equiv.) was dissolved in THF (12 µl per mmol). **(Trt)S-EG$_n$-NH$_2$** spacer (1.05 equiv.) and $NaHCO_3$ (1.1 equiv.) were dissolved in H_2O (7.5 µl per mmol of amine) and added to the first solution. The reaction mixture was stirred at room temperature for 1 h, and then acidified with a citric acid solution (0.2 M). EtOAc was added and the organic compound was extracted (x2). Combined aqueous phases were acidified to pH 3 with citric acid and extracted with EtOAc (x3). The organic phase was washed with H_2O, saturated NaCl solution, dried over $MgSO_4$ and concentrated under reduced pressure

GP 9.6- General procedure for the preparation of the DUPA-Pep-EG$_n$-SH sequences

(O^{t}Bu)$_3$DUPA-Pep-EG$_n$-S(Trt) sequence (1.0 equiv.) was treated with a TFA:TIS:H_2O (95:2.5:2.5, v:v:v) cocktail (117 µl per mmol) and stirred at room temperature under argon for 1.5 h. The mixture was co-evaporated with toluene (x2). Addition of precooled MTBE and centrifugation at 0 °C caused the precipitation of a solid. The

precipitate was washed with additional cold MTBE. The pellet was collected and dried in vacuo.

GP 10. General procedure for the conjugation of the DUPA-Pep-EG$_n$-SH sequences to the mp-va-α-amanitin derivative 127

mp-va-α-Amanitin derivative **127** (1.0 equiv.) was dissolved in dry DMSO (133 µl per mmol). DUPA-Pep-EG$_n$-SH (1.0 equiv.), dissolved in DMSO (67 µl per mmol), and undilutedDIPEA (2.0 equiv.) were added sequentially. The reaction mixture was stirred at room temperature under argon for 24 h and the product was then purified by preparative RP-HPLC: λ= 305 nm; gradient: 0-1 min 5% B; 14 min 54% B; 18 min 69% B; 19-20 min 100%; 21-22 min 5% B; A= water with 0.05% TFA, B= acetonitrile. The product was collected and freeze-dried overnight.

3. Syntheses

Compound 41. (O^{t}Bu)$_3$-DUPA^{OBn}

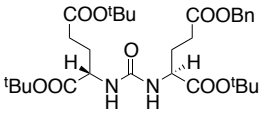

$C_{30}H_{46}N_2O_9$
MW: 578,69

DSC (1.73 g, 6.76 mmol) was dissolved in DMF (31.6 ml) at 0 °C, and α,γ-di-*tert*-butyl L-glutamate (2 g, 6.76 mmol) was added. Mixture was stirred for 50 min and then TEA (937 µl, 6.76 mmol) was added. Once formation of the NHS ester-activated intermediate **40** was completed, α-*tert*-butyl-γ-benzyl L-glutamate (2.23 g, 6.76 mmol) and TEA (1.87 ml, 13.52 mmol) were added. Reaction mixture was stirred overnight at room temperature, and afterwards DMF was removed in vacuo and the residue was taken up in MTBE (100 ml). The organic layer was washed with 15% (w/v) citric acid solution (100 ml, x2), water (100 ml, x2), saturated $NaHCO_3$ solution (100 ml, x2) and water (80 ml)
in sequence. The organic layer was dried over $MgSO_4$, filtered and solvent removed under reduced pressure. The resulting yellowish oil was purified by flash chromatography on silica gel column, eluting with a 0 to 33% gradient of EtOAc in n-hexane, to provide the urea **42** as colorless syrup

(O^{t}Bu)$_3$-DUPA^{OBn} (41): colorless syrup (3.02 g, yield= 77%). MS(ESI$^+$) *m*/z: calcd. for $C_{30}H_{47}N_2O_9$: 579.70, found: 579.17 $[M+H]^+$; calcd. for $C_{30}H_{46}N_2O_9Na$: 601.68, found: 601.35 $[M+Na]^+$; calcd. for $C_{60}H_{92}N_4O_{18}Na$: 1180.38, found: 1180.35 $[2M+Na]^+$.

Compound 42. $(O^tBu)_3$-DUPA

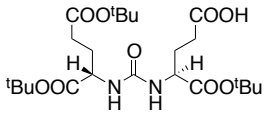

$C_{23}H_{40}N_2O_9$
MW: 488,57

Compound **41** (3.02 g, 5.21 mmol) was diluted in EtOAc (27.3 ml) and mixture was degassed in for 5 min with argon, Pd (10%) on activated charcoal was added and mixture was degassed for other 5 min. Mixture was hydrogenated with a hydrogen balloon overnight at room temperature and then filtered and washed with EtOAc through a filter. The filtrate was concentrated under reduced pressure to provide the DUPA precursor **42**.

$(O^tBu)_3$-DUPA (42): colorless syrup (2.45 g, yield= 96%). MS (ESI^+) *m/z:* calcd. for $C_{23}H_{41}N_2O_9$: 489.58, found: 489.20 $[M+H]^+$; calcd. for $C_{46}H_{81}N_4O_{18}$: 978.15 found: 978.22 $[2M+H]^+$.

Compound 44. DUPA-8-Aoc-Phe-Phe-Cys-OH

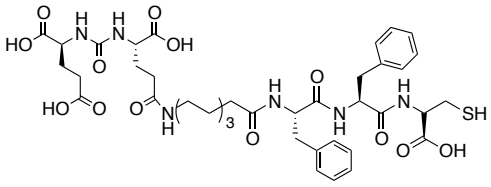

$C_{40}H_{54}N_6O_{13}S$
MW: 858,95

Compound **44** was prepared according to the general procedure **GP 1** described above for automated MW-assisted SPPS by using H-Cys(Trt)-CTC resin (0.25 mmol). The resin-bound peptide was cleaved from the resin, fully deprotected, as illustrated above in the general procedure (**GP 2**). Following isolation by ether precipitation (**GP 2**), the peptide was dissolved in ACN:H_2O (1:1, v:v; 2 ml) and purified by preparative RP-HPLC (λ= 210 nm; gradient: 0 min 5% B, 15-18 min 100% B, 18.5-22 min 5% B, A= H_2O with 0.05% TFA, B= ACN). The product as collected and the solvents were evaporated under reduced pressure. The residual peptide was lyophilized overnight in *tert*-butanol (^{t}BuOH):H_2O (4:1, v:v; 4 ml) affording the peptide reagent **44**.

DUPA-8-Aoc-Phe-Phe-Cys-OH (44): white powder (122.9 mg, yield= 85%). MS(ESI^+) *m/z:* calcd. for $C_{40}H_{55}N_6O_{13}S$: 859.96, found: 859.33 $[M+H]^+$; calcd. for: $C_{40}H_{54}N_6O_{13}SNa$: 881.94, found: 881.33 $[M+Na]^+$.

SMDC 37 (HDP 30.2284). DUPA-Pep-mc-va-α-amanitin

Compound 50a. Boc-Val-Ala-PAB-OH

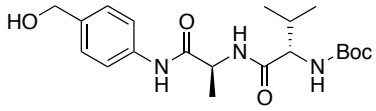

$C_{20}H_{31}N_3O_5$
MW: 393,48

Boc-Val-Ala-OH dipeptide (6.63 g, 22.73 mmol) and 4-amino-benzylalcohol (2.94 g, 23.87 mmol) were dissolved in THF (110 ml). EEDQ (5.90 g, 23.87 mmol) was added and reaction mixture was protected from light by wrapping the flask with aluminum foil. The reaction mixture was stirred at room temperature for 72 h. Solvent was then carefully evaporated under reduced pressure. The residue was purified by flash chromatography on a silica gel column and eluted with a gradient of 0 to 50% acetone in n-hexane. Solvents were concentrated under reduced pressure and residue dried overnight in vacuo.

Boc-Val-Ala-PAB-OH (50a): colorless residue (8.56 g, yield= 95%). MS (ESI+) *m/z:* calcd. for $C_{20}H_{31}N_3O_5Na$: 416.22, found 416.29 $[M+Na]^+$; calcd. for $C_{15}H_{23}N_3O_3Na$: 316.16, found: 316.44 $[M\text{-}Boc+Na]^+$. ^1H NMR (500 MHz, DMSO-d_6): δ(ppm)= 9.96 (s, 1H), 8.08 (d, J = 7.1 Hz, 1H), 7.57 – 7.50 (m, 2H), 7.27 – 7.21 (m, 2H), 6.77 (d, J = 8.9 Hz, 1H), 5.13 (t, J = 5.7 Hz, 1H), 4.43 (d, J = 5.6 Hz, 3H), 3.83 (dd, J = 8.9, 6.6 Hz, 1H), 3.37 (s, 1H), 1.96 (h, J = 6.7 Hz, 1H), 1.38 (s, 9H), 1.30 (d, J = 7.1 Hz, 3H), 0.87 (d, J = 6.8 Hz, 3H), 0.82 (d, J = 6.7 Hz, 3H). ^{13}C NMR (126 MHz, DMSO-d_6): δ(ppm) 170.94, 155.54, 137.56, 137.45, 126.94, 118.86, 78.08, 62.59, 59.51, 48.92, 30.48, 28.22, 26.87, 19.23, 18.28, 18.10.

Compound 51a. Boc-Val-Ala-PAB-OTBDMS

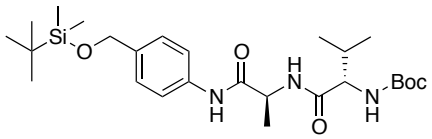

$C_{26}H_{45}N_3O_5Si$
MW: 507,74

Compound **51a** was synthesized according to the general procedure **GP 4.2** described above starting from 21.04 mmol of compound **50a.** Final compound was purified by flash chromatography and eluted with a gradient of 0 to 100% MTBE in n-hexane.

Boc-Val-Ala-PAB-OTBDMS (51a): white solid (9.12 g, yield= 85%). MS (ESI+) *m/z:* calcd. for $C_{26}H_{46}N_3O_5Si$: 508.32, found: 508.09 $[M+H]^+$; calcd. for $C_{26}H_{45}N_3O_5SiNa$: 530.30, found: 530.29 $[M+Na]^+$; calcd. for $C_{52}H_{91}N_6O_{10}Si_2$: 1015.63, found: ca. 1015 $[2M+H]^+$; calcd. for $C_{52}H_{90}N_6O_{10}Si_2Na$:1037.62, found: 1037.21 $[2M+Na]^+$. ^1H NMR (500 MHz, $CDCl_3$): δ(ppm)= 8.74 - 8.70 (m, 1H), 7.51 (d, J= 8.5 Hz, 2H), 7.24 (d, J= 8.4 Hz, 2H), 6.90 (d, J= 7.5 Hz, 1H), 5.12 (d, J= 7.8 Hz, 1H), 4.73 - 4.64 (m, 3H), 4.00 (s, 1H), 2.15 (dq, J= 13.4, 6.7 Hz, 1H), 1:45 (d, J= 7.0 Hz, 3H), 1.43 (s, 9H), 0.96 (d, J= 6.9 Hz, 3H), 0.94 - 0.90 (m, 12H), 0:07 (s, 6H). ^{13}C NMR (126 MHz, $CDCl_3$): δ(ppm)= 172.24, 170.17, 156.28, 137.53, 136.77, 126.81, 119.98, 80.60, 64.80, 60.31, 49.77, 30.84, 28.43, 26.08, 19:44, 18:55, 17.89, 17.78, -5.07.

Compound 52a. Boc-Val-Ala(SEM)-PAB-OTBDMS

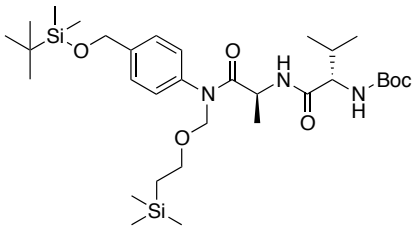

$C_{32}H_{59}N_3O_6Si_2$
MW: 638,00

Compound **52a** was prepared following the general procedure **GP 4.3** reported above starting from 17.93 mmol of intermediate **51a**. After 1 h, reaction was quenched by adding sodium citrate buffer (pH 6.40, 200 ml). The product was extracted with EtOAc (x2). The organic layers were combined, washed with sodium citrate buffer (pH 4.76, 200 ml), saturated $NaHCO_3$ solution (100 ml) and NaCl solution (100 ml), and dried over $MgSO_4$. Once solvents were removed under reduced pressure, the crude product was purified by flash chromatography on a silica gel column with a gradient of 0 to 50% of MTBE in n-hexane.

Boc-Val-Ala(SEM)-PAB-OTBDMS (52a): white foam (7.51 g, yield= 66%). MS (ESI+) *m/z:* calcd. for $C_{32}H_{60}N_3O_6Si_2$: 638.40, found: 638.03 $[M+H]^+$; calcd. for $C_{32}H_{59}N_3O_6Si_2Na$: 660.3, found: 660.47 $[M+Na]^+$. ^1H NMR (500 MHz, $CDCl_3$): δ(ppm)= 7.40 (d, J = 8.1 Hz, 2H), 7.25 (d, J = 8.0 Hz, 2H), 6:53 (d, J = 7.4 Hz, 1H), 5.14 (d, J = 10.0 Hz, 1H), 5.05 (d, J = 9.0 Hz, 1H), 4.97 (d, J = 10.0 Hz, 1H), 4.76 (s, 2H), 4.54 (p, J = 6.9 Hz, 1H), 3.93 (t, J = 7.6 Hz, 1H), 3.63 (dd, J = 9.6, 7.3 Hz, 2H), 2.10 (h, J = 6.7 Hz, 1H), 1.43 (s, 9H), 1.16 (d , J = 6.9 Hz, 3H), 0.98 - 0.92 (m, 14H), 0.90 (d, J = 6.8 Hz, 3H), 0:12 (d, J = 1.4 Hz, 6H), 0.00 (s, 9H).

Compound 53a. Boc-Val-Ala(SEM)-PAB-OH

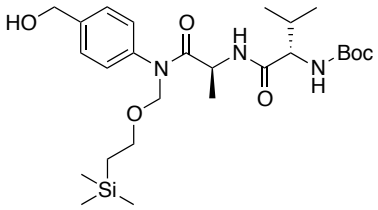

$C_{26}H_{45}N_3O_6Si$
MW: 523,74

Compound **53a** was obtained starting from 11.96 mmol of compound **52a** and applying the general procedure **GP 4.4** described above. The title compound was isolated by flash chromatography with a gradient of 0 to 50 % acetone in n-hexane, and concentrated to dryness.

Boc-Val-Ala(SEM)-PAB-OH (53a): white foam (6.16 g, yield= quantitative). MS (ESI+) *m/z:* calcd. for $C_{26}H_{46}N_3O_6Si$: 524.32, found: 524.09 $[M+H]^+$; calcd. for $C_{26}H_{45}N_3O_6SiNa$: 546.30, found: 546.46 $[M+Na]^+$; calcd. for $C_{26}H_{45}N_3O_6SiK$: 562.2, found: 562.41 $[M+K]^+$. ^1H NMR (500 MHz, $CDCl_3$): δ(ppm)= 7.40 (d, J = 8.1 Hz, 2H), 7.25 (d, J = 8.0 Hz, 2H), 6.53 (d, J = 7.4 Hz, 1H), 5.14 (d, J = 10.0 Hz, 1H), 5.05 (d, J = 9.0 Hz, 1H), 4.97 (d, J = 10.0 Hz, 1H), 4.76 (s, 2H), 4.54 (p, J = 6.9 Hz, 1H), 3.93 (t, J = 7.6 Hz, 1H), 3.63 (dd, J = 9.6, 7.3 Hz, 2H), 2.10 (h, J = 6.7 Hz, 1H), 1.43 (s, 9H), 1.16 (d, J = 6.9 Hz, 3H), 0.98 – 0.92 (m, 14H), 0.90 (d, J = 6.8 Hz, 3H), 0.12 (d, J = 1.4 Hz, 6H), 0.00 (s, 9H). ^{13}C NMR (126 MHz, $CDCl_3$): δ(ppm)= 173.82, 170.86, 155.88, 142.23, 138.97, 128.35, 127.32, 79.87, 77.58, 66.16, 64.39, 59.71, 46.53, 31.45, 28.44, 26.09, 19.39, 18.64, 18.56, 18.28, 17.78, -1.29, -5.16.

Compound 45a. Boc-Val-Ala(SEM)-PAB-Br

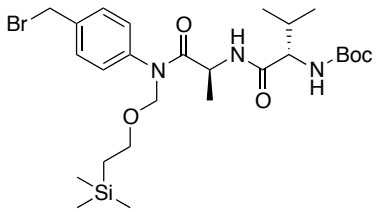

$C_{26}H_{44}BrN_3O_5Si$
MW: 586,63

Dipeptide **45a** was achieved according to the general procedure **GP 4.5** reported above by using 9.03 mmol of precursor **53a**. Compound **45a** was eluted from the column with a gradient of 0 to 100% MTBE in n-hexane, concentrated to dryness under reduce pressure and lyophilized overnight.

Boc-Val-Ala(SEM)-PAB-Br (45a): white powder (5.96 g, yield= 93%). MS (ESI+) *m/z:* calcd. for $C_{26}H_{45}BrN_3O_5Si$: 586.23/588.23, found: ca. 586/approx 588 $[M+H]^+$; calcd. for

$C_{26}H_{44}BrN_3O_5SiNa$: 608.21/610.21, found: ca. 608/610.28 $[M+Na]^+$. ^1H NMR (500 MHz, $CDCl_3$): δ(ppm)= 7.47 (d, J = 8.1 Hz, 2H), 7.29 (d, J = 8.2 Hz, 2H), 6.53 (d, J = 7.4 Hz, 1H), 5.14 (d, J = 10.1 Hz, 1H), 5.04 (d, J = 9.0 Hz, 1H), 4.96 (d, J = 10.2 Hz, 1H), 4.54 – 4.50 (m, 1H), 4.49 (s, 2H), 3.93 (t, J = 7.5 Hz, 1H), 3.68 – 3.54 (m, 2H), 2.10 (dq, J = 13.3, 6.4 Hz, 1H), 1.42 (s, 9H), 1.15 (d, J = 6.9 Hz, 3H), 0.96 (d, J = 6.8 Hz, 3H), 0.94 – 0.91 (m, 2H), 0.90 (d, J = 6.8 Hz, 3H), 0.00 (s, 9H). ^{13}C NMR (126 MHz, $CDCl_3$): δ(ppm) 173.45, 170.86, 155.70, 140.23, 138.20, 130.49, 128.75, 79.75, 77.24, 66.04, 59.49, 46.35, 32.20, 31.22, 28.26, 19.21, 18.33, 18.08, 17.62, -1.46.

Compound 46a. Boc-va-α-amanitin

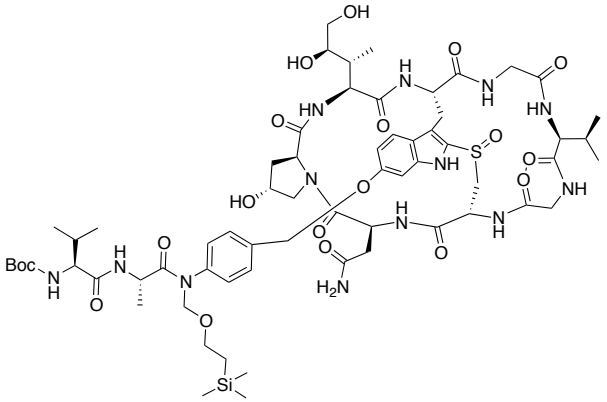

$C_{65}H_{97}N_{13}O_{19}SSi$
MW: 1424,69

Compound **45a** (145.5 mg, 0.248 mmol) was conjugated to natural α–amanitin (57 mg, 0.062 mmol) by following the general procedure **GP 5.1**. Compound was purified by preparative RP-HPLC using the following conditions: λ= 305 nm; gradient: 0-5 min 5% B; 20-25 min 100% B; 27-35 min 5% B; A= water; B= MeOH. Solvents were then evaporated to dryness.

Boc-va-α-amanitin (46a): colorless solid (54.46 mg; yield= 62%). MS (ESI+) *m/z*: calcd. for $C_{65}H_{98}N_{13}O_{19}SSi$: 1424,6, found: 1425,23 $[M+H]^+$.

Compound 47a. va-α-amanitin

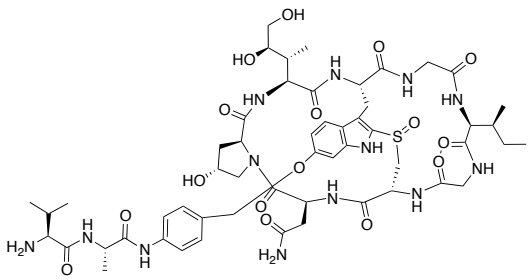

$C_{54}H_{75}N_{13}O_{16}S$
MW: 1194,32

Compound **46a** (134.29 mg, 0.0943 mmol) was deprotected according to the general procedure **GP 6** and purified by preparative RP-HPLC using the following conditions: λ= 305 nm; gradient: 0-2 min 5% B; 2-10 min 20% B; 10-10.5 min 25% B; 10.5-13 min 100% B; 13-14 min 5% B; A= water with 0.05% TFA; B= ACN. Upon elution, the title compound was directly freeze-dried overnight.

va-α-amanitin (47a): colorless powder (68.59 mg, yield= 55%). MS (ESI+) *m/z*: calcd. for $C_{60}H_{90}N_{13}O_{17}SSi$: 1194.53, found: 1194.8 $[M+H]^+$; calcd. for $C_{60}H_{89}N_{13}O_{17}SSiNa$: 1216.51 found: 1217.8 $[M+Na]^+$.

Compound 48a. mc-va-α-amantin

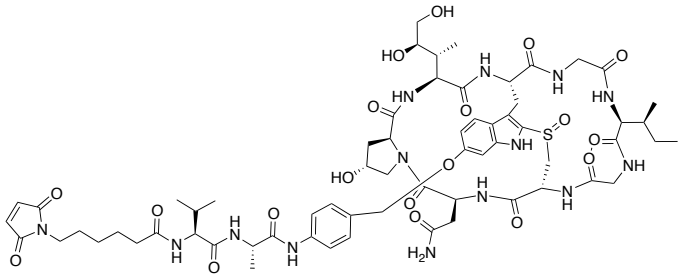

Compound **47a** (23.49 mg, 0.0179 mmol) was dissolved in dry DMF (400 μl). ECMS (11.07 mg, 0.036 mmol), dissolved in DMF (562 μl), and DIPEA (12.21 μl, 0.0716 mmol) were added. After 2 h at room temperature under argon, mixture was dripped into precooled MTBE (40 ml) and centrifuged at 0 °C. The precipitate was collected, washed with MTBE (40 ml) and centrifuged again. The crude product was dried in vacuo and purified by RP-HPLC [λ= 305 nm; gradient: 0-5 min 5% B; 20-25 min 100% B; 27-35 min 5% B; A= water with 0.05% TFA; B= methanol with 0.05% TFA]. The desired compound was collected and directly freeze-dried overnight.

mc-va-α-amantin (48a): colorless powder (21.03 mg, yield= 86%). MS (ESI+) *m/z*: calcd. for $C_{64}H_{86}N_{14}O_{19}SNa$: 1144.99, found: 1145.7 $[M+Na]^+$.

SMDC 37 (HDP 30.2284). DUPA-Pep-mc-va-α-amanitin

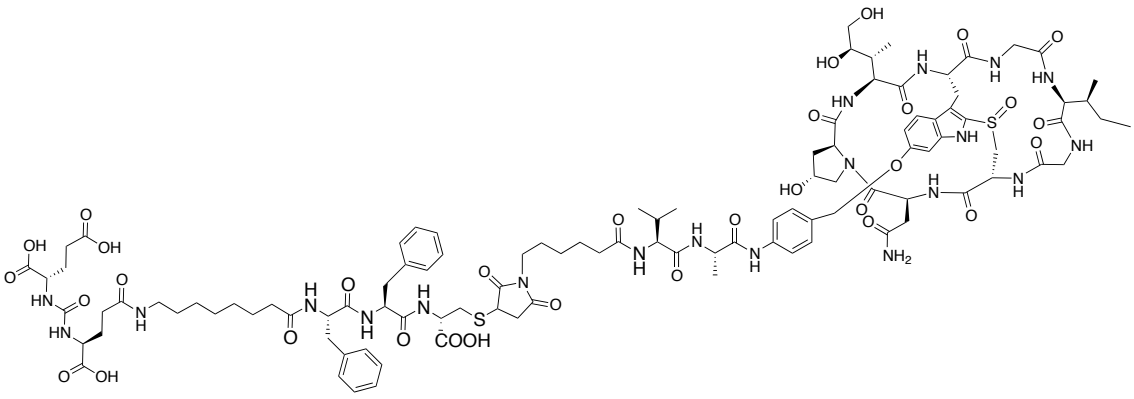

$C_{104}H_{140}N_{20}O_{32}S_2$
MW: 2246,47

Compound **44** (12.97 mg, 0.015 mmol) was dissolved in DMSO (1 ml) and a solution of **48a** (21.03 mg, 0.015 mmol) in DMSO (2 ml) was added at room temperature under argon. DIPEA (5.15 µl, 0.03 mmol) was added undiluted. The reaction mixture was stirred at room temperature for 20 h, and then purified by preparative RP-HPLC [λ= 305 nm; gradient: 0-5 min 5% B; 20-25 min 100% B; 27-35 min 5% B; A= water with 0.05% TFA; B= MeOH with 0.05% TFA]. Solvents were evaporated and SMDC **37** was freeze-dried overnight in ^{t}BuOH:H_2O (4:1, v:v; 4 ml)

DUPA-Pep-mc-va-α-amanitin (37): colorless powder (14.53 mg, yield= 43%). MS (ESI+) *m/z*: $[M+2Na]^{2+}$ calcd. for $C_{96}H_{124}N_{20}O_{32}S_2Na_2$: 1146.2, found: 1146.5.

SMDC 38 (HDP 30.2537). DUPA-Pep-mc-vc-α-amanitin

Compound 50b. Boc-Val-Cit-PAB-OH

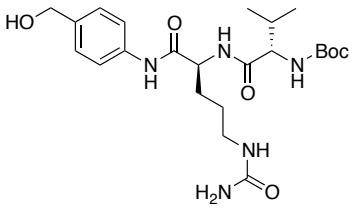

$C_{23}H_{37}N_5O_6$
MW: 479,57

Boc-Val-Cit-OH dipeptide (20.83 mmol, 7.8 g) and 4-amino-benzylalcohol (5.13 g, 41.66 mmol) were dissolved in DCM:MeOH (2:1, v:v; 500 ml). EEDQ (10.3 g, 41.66 mmol) was added and reaction mixture was protected from light by wrapping the flask with aluminum foil.

The reaction mixture was stirred at room temperature for 72 h. Solvent was then carefully evaporated under reduced pressure and residue dried in vacuo. The residue was taken up with MTBE (500 ml), sonicated and stirred until a fine precipitate was formed. The solid residue was filtered and then dried in vacuo. Compound **50b** was used for the next step without further purification.

Boc-Val-Cit-PAB-OH (50b): colorless residue (10.38 g, yield= quantitative).

Compound 51b. Boc-Val-Cit-PAB-OTBDMS

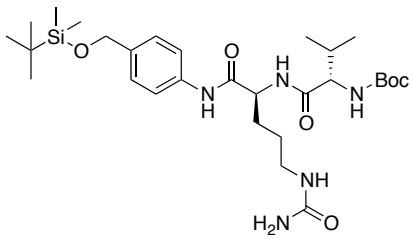

$C_{29}H_{51}N_5O_6Si$
MWt: 593,83

Synthesis of compound **51b** was accomplished according to the general procedure **GP 4.1** described above starting from 21.04 mmol of compound **50a**. Final compound was eluted from a silica gel column with a gradient of 0 to 10% of MeOH in DCM. Upon removal of solvents, the residue was lyophilized overnight in ^{t}BuOH (4 ml).

Boc-Val-Cit-PAB-OTBDMS (51a): white powder (3,0 g, yield= 43%). MS (ESI+) *m/z:* calcd. for $C_{29}H_{52}N_5O_6Si$: 594.37, found: 594.18 $[M+H]^+$; calcd. for $C_{29}H_{51}N_5O_6SiNa$: 616.35, found: 616.45 $[M+Na]^+$; calcd. for $C_{24}H_{44}N_5O4Si$: 494.32, found: 494.32 $[M\text{-}Boc+H]^+$; calcd. for $C_{16}H_{29}N_4O_5$: 357.21, found: 357.11 [Boc-Val-Cit-C□O]$^+$.

Compound 52b. Boc-Val-Cit(SEM)-PAB-OTBDMS

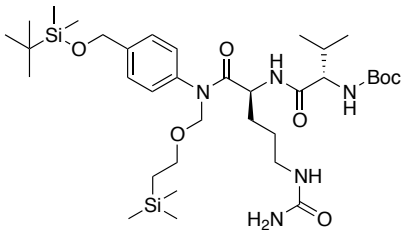

$C_{35}H_{65}N_5O_7Si_2$
MW: 724,09

Compound **52b** was prepared following the general procedure **GP 4.2** reported above starting from 1.52 mmol of intermediate **51a**. Reaction was quenched by adding a saturated solution of $NaHCO_3$. The mixture was diluted with EtOAc (200 ml), and the layers were separated. The aqueous layer was extracted with EtOAc (50 ml, x 2), while the organic layer was washed with saturated solutions of NH_4Cl (100 ml, x 2) and NaCl (100 ml) and then dried over $MgSO_4$. The solvent was evaporated. The residue was dissolved in DCM and adsorbed over diatomaceous earth for dry loading onto a silica gel column. Compound was eluted with a gradient of 0 to 10% of MeOH in DCM and concentrated to dryness.

Boc-Val-Cit(SEM)-PAB-OTBDMS (52b): white foam (468 mg, yield= 43%). MS (ESI+) *m/z:* calcd. for $C_{35}H_{66}N_5O_7Si_2$: 724.45, found: 724.28 $[M+H]^+$; calcd. for $C_{35}H_{65}N_5O_7Si_2Na$: 746.43, found: 746.53 $[M+Na]^+$; calcd for $C_{16}H_{29}N_4O_5$: 357.21, found: 357.20 $[Boc\text{-}Val\text{-}Cit\text{-}C{\equiv}O]^+$.

Compound 53b. Boc-Val-Cit(SEM)-PAB-OH

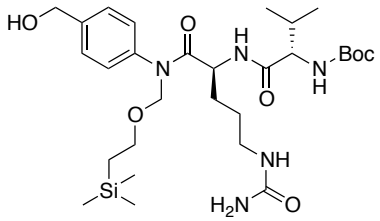

$C_{29}H_{51}N_5O_7Si$
MW: 609,83

Compound **53b** was obtained using 0.645 mmol of compound **52b** and applying the general procedure **GP 4.3** described above. Compound **53b** was eluted with a gradient of 0 to 10% of MeOH in DCM and concentrated to dryness.

Boc-Val-Ala(SEM)-PAB-OH (53b): white foam (332 mg, yield= 84%). MS (ESI+) *m/z:* calcd. for $C_{29}H_{52}N_5O_7Si$: 610.36, found: 610.13 $[M+H]^+$; calcd. for $C_{29}H_{51}N_5O_7SiNa$: 632.35, found: 632.34 $[M+Na]^+$; calcd. for $C_{16}H_{29}N_4O_5$: 357.21, found: 357.07 $[Boc\text{-}Val\text{-}Cit\text{-}C{\equiv}O]^+$.

Compound 45b. Boc-Val-Cit(SEM)-PAB-Br

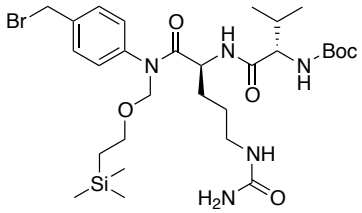

$C_{29}H_{50}BrN_5O_6Si$
MW: 672,73

General procedure **GP 4.4** reported above was applied for preparation of compound **45b** starting from 5.04 mmol of precursor **53b**. Compound **45b** was purified by flash column chromatography and eluted with a gradient of 0 to 100% DCM:MTBE:MeOH (6:3:1, v:v:v) in DCM.

Solvents were evaporated under reduced pressure and the residue was lyophilized from cyclohexane.

Boc-Val-Cit(SEM)-PAB-Br (45b): white powder (1.26 g, yield= 41%).

Compound 46b. Boc-vc-α-amanitin

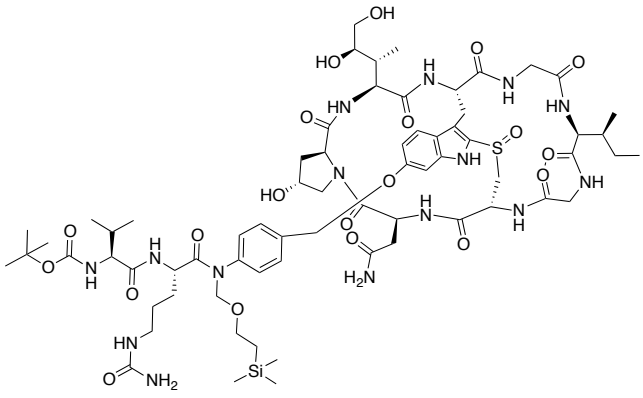

$C_{68}H_{103}N_{15}O_{20}SSi$
MW: 1510,78

Compound **45b** (160 mg, 0.238 mmol) was conjugated to natural α–amanitin (65 mg, 0.071 mmol) by following the general procedure **GP 5.1**. Compound was purified by preparative RP-HPLC using the following conditions: λ= 305 nm; gradient: 0-5 min 5% B; 20-25 min 100% B; 27-35 min 5% B; A= water; B= methanol. Solvents were then evaporated to dryness.

Boc-vc-α-amanitin (46b): colorless solid (88.38 mg; yield= 88%).

Compound 47b. H_2N-vc-α-amanitin

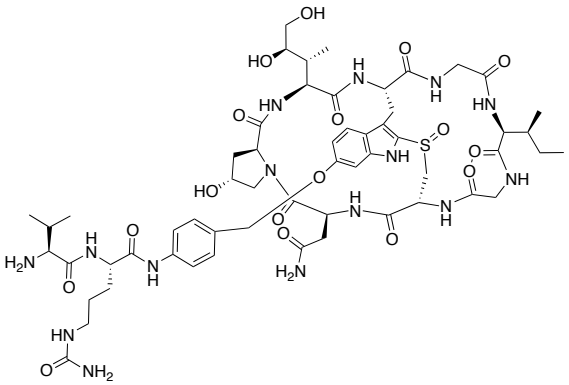

$C_{57}H_{81}N_{15}O_{17}S$
MW: 1280,41

Compound **46b** (88.38 mg, 0.0585 mmol) was deprotected according to the general procedure **GP 6** and purified by preparative RP-HPLC using the following conditions: λ= 305 nm; gradient: 0 min 5% B; 2 min 30% B; 13 min 54% B; 14-18 min 100% B; 19-23 min 5% B; A= water with 0.05% TFA; B= methanol with 0.05% TFA. Upon elution of the compound, solvents were evaporated and compound freeze-dried overnight in ^{t}BuOH:H_2O (4:1, v:v; 5 ml)

vc-α-amanitin (47b): colorless powder (45.92 mg, yield= 56%). MS (ESI+) *m/z*: calcd. for $C_{57}H_{82}N_{15}O_{17}S$: 1280.57, found: 1280.60 $[M+H]^+$.

Compound 48b. mc-vc-α-amanitin

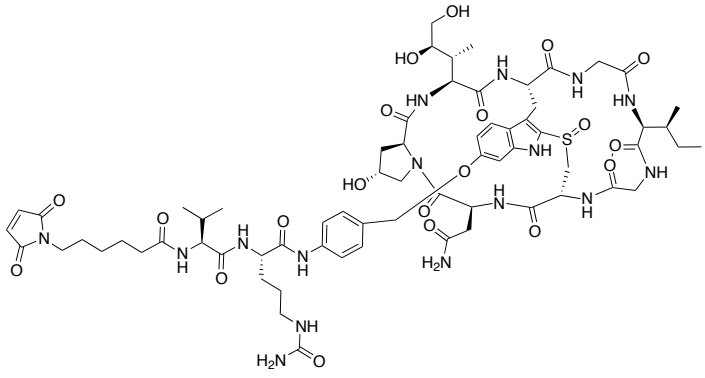

$C_{67}H_{92}N_{16}O_{20}S$
MW: 1473,61

Compound **47b** (13.94 mg, 0.010 mmol) was dissolved in dry DMF (400 μl). A 0.02 M solution of ECMS in DMF (0.020 mmol), and undiluted DIPEA (40 μl, 0.040 mmol) were added. After 2 h at room temperature the reaction mixture was directly purified by RP-HPLC [λ= 305 nm; gradient: 0 min 5% B; 2 min 30% B; 13 min 54% B; 14-18 min 100% B; 19-23 min 5% B; A= water with 0.05% TFA; B= MeOH with 0.05% TFA.]. The title compound was collected and

the solvents were evaporated under reduced pressure. Compound was freeze-dried overnight in ^{t}BuOH:H_2O (4:1, v:v; 2 ml).

mc-vc-α-amantin (48b): colorless powder (12.40 mg, yield= 84%). MS (ESI+) *m/z*: calcd. for $C_{67}H_{92}N_{16}O_{20}SNa$: 1495.63, found: 1496.43 $[M+Na]^+$.

SMDC 38 (HDP 30.2537). DUPA-Pep-mc-vc-α-amanitin

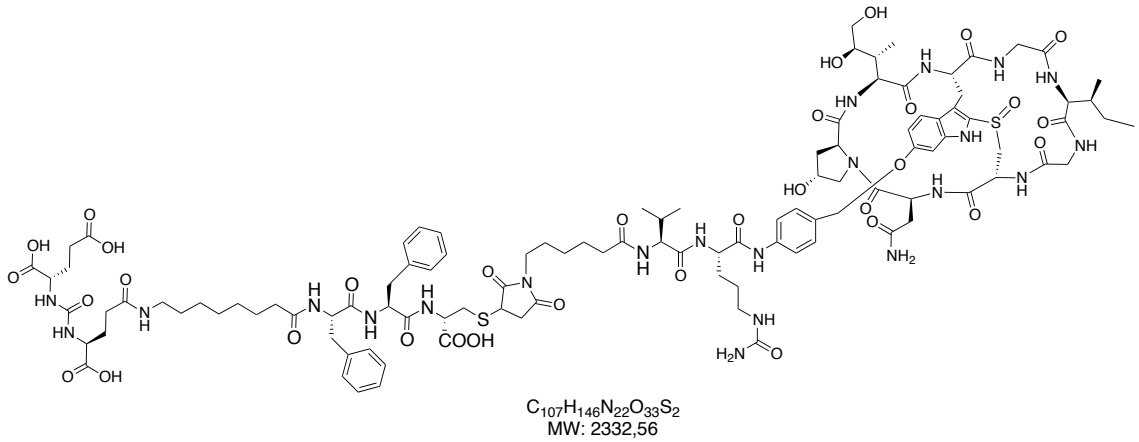

Compound **48b** (5.0 mg, 0.0034 mmol) was dissolved in dry DMSO (754 μl) and a solution of **44** (3.06 mg, 0.0036 mmol) in DMSO (250 μl) was added at room temperature under argon. DIPEA (1.16 µl, 0.0068 mmol) was added undiluted. The reaction mixture was stirred at room temperature for 2 h, and then purified by preparative RP-HPLC [λ= 305 nm; gradient: 0 min 5% B; 15-18 min 100% B; 18.50-22 min 5% B; A= water with 0.05% TFA; B= MeOH with 0.05% TFA]. Solvents were evaporated and SMDC **38** was freeze-dried overnight in ^{t}BuOH:H_2O (4:1, v:v; 4 ml).

DUPA-Pep-mc-vc-α-amanitin (38): colorless powder (6.42 mg, yield= 83%). MS(ESI-) m/z: calcd. for $C_{107}H_{145}N_{22}O_{33}S_2$: 2331.56, found: 2331.00 $[M-H]^-$; calcd. for $C_{107}H_{144}N_{22}O_{33}S_2$: 1164.77, found: 1164.92 $[M-2H]^{2-}$.

SMDC 39 (HDP 30.2301). DUPA-Pep-mc-α-amanitin

Compound 57. 1,7-dimethyl-10-oxa-4-azatricyclo[5.2.1.$0^{2,6}$]dec-8-en-3,5-dione (*exo* adduct)

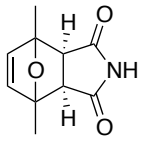

$C_{10}H_{11}NO_3$
MW: 193,20

2,5-dimethyl furan (4.00 g, 41.2 mmol) and maleimide (5.93 g, 61.7mmol) were dissolved in dry Et_2O (30 ml) and heated up to 90 °C in a Parr reactor for 12 h. The resulted precipitate was filtered off and re-crystallized from MeOH to yield crystals.

1,7-dimethyl-10-oxa-4-azatricyclo[5.2.1.$0^{2,6}$]dec-8-en-3,5-dione (*exo* adduct): colorless crystals (6.62 g, yield= 83%). M.p.: 137 °C. ^{1}H NMR (500 MHz, $CDCl_3$): δ(ppm)= 8.68 (broad singlet, 1H), 6.31 (singlet, 2H), 2.88 (singlet, 2H), 1.73 (singlet, 6H). ^{13}C NMR (100 MHz, $CDCl_3$): δ(ppm)= 175.04, 140.82, 87.68, 53.77, 15.76.

Compound 54. 4-(6-Bromohexyl)-1,7-dimethyl-10-oxa-4-azatricyclo[5.2.1.$0^{2,6}$]dec-8-en-3,5-dione (exo adduct)

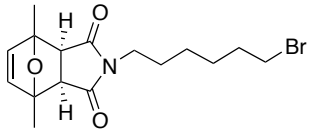

$C_{16}H_{22}BrNO_3$
MW: 356,25

Compound **57** (386 mg, 2 mmol) and 1,6-dibromohexane (1.95 g, 8 mmol) were dissolved in DMF (20 ml). K_2CO_3 (276 mg, 2 mmol) was added and the suspension was heated up to 50 °C for 3 h. Subsequently, DMF was evaporated, and the residue was taken up with DCM (100 ml). The inorganic salts were removed by filtration, diatomaceous earth (3 g) was added to the filtrate and the solvent removed under vacuum. The residue was purified by flash chromatography on a silica gel column eluting with a gradient of 0 to 50% of EtOAc in n-hexane to achieve linker **54**.

4-(6-Bromohexyl)-1,7-dimethyl-10-oxa-4-azatricyclo[5.2.1.$0^{2,6}$]dec-8-en-3,5-dione (*exo* adduct): waxy crystals (483 mg, yield= 68%). ^{1}H NMR (500 MHz, $CDCl_3$): δ(ppm)= 6.31 (s, 2H), 3.48 (t, *J*= 7.2 Hz, 2H), 3.39 (t, *J*= 6.8 Hz, 2H), 2.81 (s, 1H), 1.90 – 1.77 (m, 2H), 1.70 (s, 5H), 1.64 – 1.52 (m, 2H), 1.44 (dddd, *J*= 9.2, 7.4, 6.5, 5.4 Hz, 2H), 1.35 – 1.23 (m, 2H). ^{13}C NMR (126 MHz, $CDCl_3$): δ(ppm)= 174.81, 140.81, 87.52, 52.33, 38.42, 33.65, 32.50, 27.54, 27.33, 25.64, 15.87.

Compound 55. [*exo*-3,6-dimethyl-3,6-epoxy-1,2,3,6-tetrahydrophtalimide]-α-amanitin

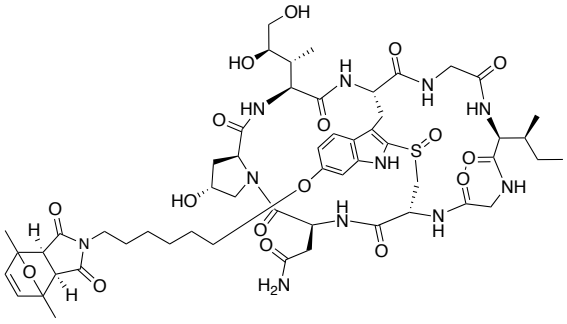

$C_{55}H_{75}N_{11}O_{17}S$
MW:1194,31

α-Amanitin (34.5 mg, 0.038 mmol) was conjugated to the linker **54** (106.8 mg, 0.304 mmol) according to the general procedure **GP 5.2**. After quenching the reaction, the product was purified by preparative RP-HPLC by using the following conditions: λ= 305 nm; gradient: 0-5 min 5% B; 20-25 min 100% B; 27-35 min 5% B; A= water; B= MeOH. The solvents were evaporated to dryness and the residue was freeze-dried in ^{t}BuOH (3 ml) overnight.

mc-α-amanitin (55): colorless powder (27.2 mg, yield= 59 %). MS (ESI+) *m/z*: calcd. for $C_{52}H_{70}N_{11}O_{17}S$: 1194.51, found: 1194.17 $[M+H]^+$; calcd. for $C_{52}H_{69}N_{11}O_{17}SNa$: 1216.50, found: 1216.10 $[M+Na]^+$.

Compound 56. mc-α-amanitin

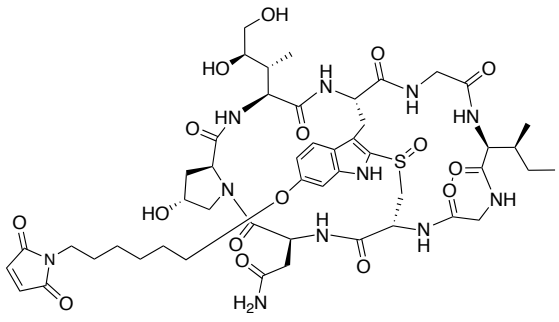

$C_{49}H_{67}N_{11}O_{16}S$
MW: 1098,19

55 (27.2 mg, 0.023 mmol) was dissolved in dry DMSO (3 ml). The reaction mixture was heated up to 100 °C and stirred for 1.5 h. After cooling down to 40 °C, DMSO was removed in vacuo and the residue purified by preparative RP-HPLC in the following conditions: λ= 305 nm; gradient: 0 min 5% B; 3 min 30% B; 12 min 45% B; 14-17 min 100% B; 19-22 min 5% B; A= water with 0.05% TFA; B= ACN. Compound was collected and freeze-dried overnight.

6´-(6-*N*-maleimido-hexyl)-α-amanitin (56): colorless powder (23.6 mg, yield= 94 %). MS (ESI+) *m/z*: calcd. for $C_{46}H_{62}N_{11}O_{16}S$: 1098.46, found: 1098.29 $[M+H]^+$; calcd. for $C_{46}H_{62}N_{11}O_{16}SNa$: 1120.44, found: 1120.36 $[M+Na]^+$.

SMDC 39 (HDP 30.2301). DUPA-Pep-mc-α-amanitin

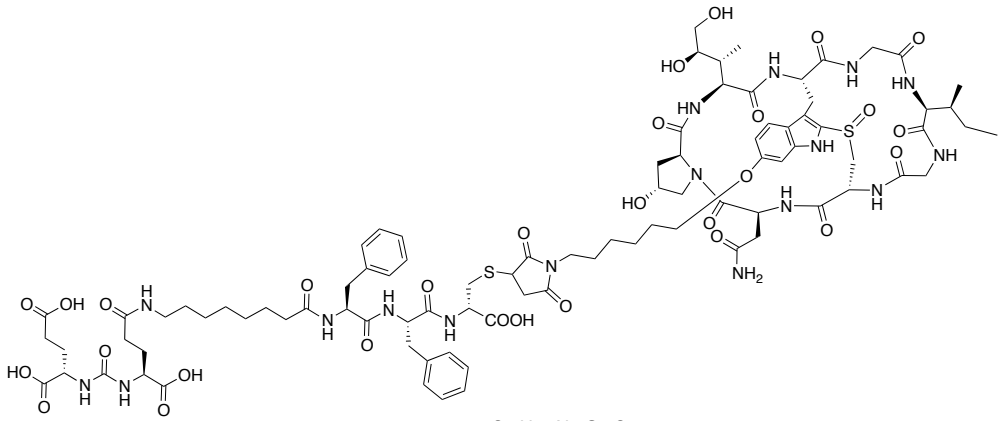

56 (20.48 mg, 0.019 mmol) was dissolved in DMF (0.5 ml) and a solution of **44** (16.0 mg, 0.019 mmol) in DMF (0.5 ml) was added at room temperature under argon. TEA (5.18 µl, 0.037 mmol) was added undiluted. The reaction mixture was stirred at room temperature for 4 days, and then injected into preparative RP-HPLC: λ= 268 nm; gradient: 0-1 min 5% B; 1-14 min 54% B; 14-26 min 100% B; 26-30 min 100% B; 30-35 min 5% B; A= water with 0.05% TFA; B= ACN. The product was collected, concentrated to dryness and lyophilized overnight in ^{t}BuOH:H_2O (4:1, v:v; 4 ml).

DUPA-Pep-mc-α-amanitin (39): colorless powder (6.03 mg, yield= 17%). MS (ESI+) *m/z*: calcd. for $C_{89}H_{123}N_{17}O_{29}S_2$: 979.58, found: 979.42 $[M+2H]^{2+}$.

Compound 66. (Trt)S-$(CH_2)_3$-α-amanitin

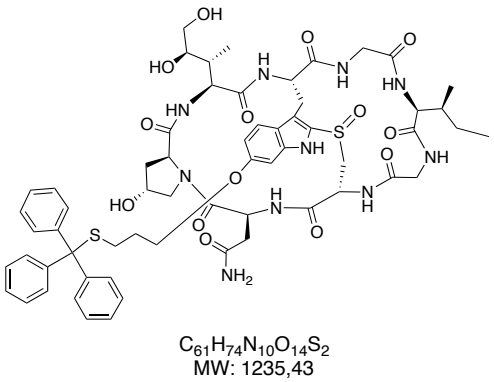

Following the general procedure **GP 5.2**, α–amanitin (36 mg, 0.039 mmol) was conjugated to the 3-(*S*-trityl)-mercaptopropyl-1-bromide linker **64** (62 mg, 0.157 mmol). Upon quenching and MTBE trituration, pellet was purified by preparative RP-HPLC under the following conditions: λ= 305 nm; gradient: 0 min 5 % B; 5 min 5 % B 20 min 100 % B; 25 min 100 % B; 27 min 5 % B, 35 min 5 % B, A= water with 0.05% TFA, B= MeOH with 0.05% TFA. The title compound was collected and the solvents were evaporated under reduced pressure.

(Trt)S-$(CH_2)_3$-α-amanitin (66): colorless solid (29 mg, yield= 60%). MS (ESI+) *m/z*: calcd. for $C_{61}H_{75}N_{10}O_{14}S_2$: 1235.49, found: 1235.08 $[M+H]^+$; calcd. for $C_{61}H_{74}N_{10}O_{14}S_2Na$: 1257.47, found: 1257.42 $[M+Na]^+$.

Compound 68. Npys-$(CH_2)_3$-α-amanitin

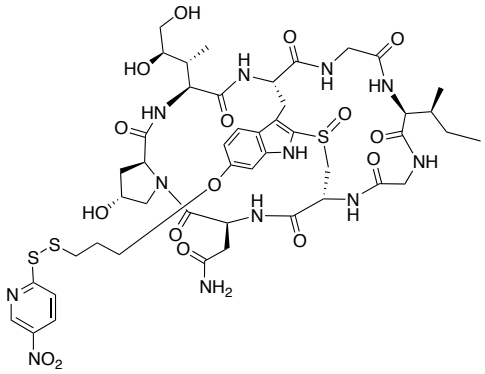

$C_{47}H_{62}N_{12}O_{16}S_3$
MW: 1147,26

DTNP (6.28 mg, 0.020 mmol) was dissolved in TFA (200 μl) and compound **66** (5.00 mg, 0.004 mmol) was added. After 4 min, the volatiles were distilled off and the residue was co-evaporated with MeOH (1 ml). The crude product was purified by RP-HPLC using the following conditions: λ= 305 nm; gradient: 0 min 5 % B; 5 min 5 % B 20 min 100 % B; 25 min 100 % B; 27 min 5 % B, 35 min 5 %, A= water with 0.05% TFA; B= MeOH with 0.05% TFA The compound was collected and the solvents were evaporated. The residue was freeze-dried in ^{t}BuOH (2 ml) overnight.

Npys-$(CH_2)_3$-α-amanitin (68): yellowish powder (99 mg, yield= 64 %). MS (ESI+) *m/z:* calcd. for $C_{47}H_{63}N_{12}O_{16}S_3$: 1148.29, found: 1146.97 $[M+H]^+$; calcd. for $C_{47}H_{62}N_{12}O_{16}S_3Na$: 1170.27, found: 1169.17 $[M+Na]^+$.

Compound 67. (Trt)S-CH(CH$_3$)-(CH$_2$)$_2$-α-amanitin

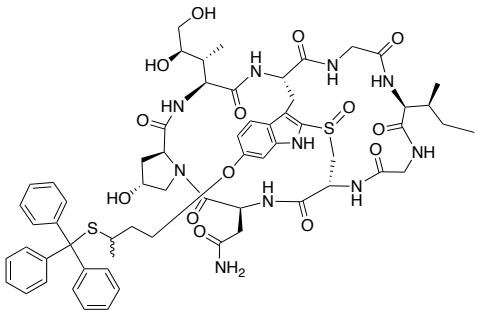

$C_{62}H_{76}N_{10}O_{14}S_2$
MW: 1249,46

General procedure **GP 5.2** was applied to conjugate α–amanitin (38 mg, 0.041 mmol) with the 3-(*S*-trityl)-mercaptobutyl-1-bromide linker **65** (68.1 mg, 0.164 mmol). Upon quenching and MTBE trituration, pellet was purified by preparative RP-HPLC under the following conditions: λ= 305 nm; gradient: 0 min 5 % B; 15-18 min 100% B; 18.5-22 min 5 % B; A= water with 0.05% TFA, B= MeOH with 0.05% TFA. The title compound was collected and the solvents were evaporated under reduced pressure.

(Trt)S-CH$_2$(CH$_3$)-(CH$_2$)$_2$-α-amanitin (67): colorless solid (31.3 mg, yield= 61%). MS (ESI+) *m/z:* calcd. for $C_{62}H_{76}N_{10}O_{14}S_2Na$: 1271.49, found: 1271.42 $[M+Na]^+$.

Compound 69. Npys-CH(CH$_3$)-(CH$_2$)$_2$-α-amanitin

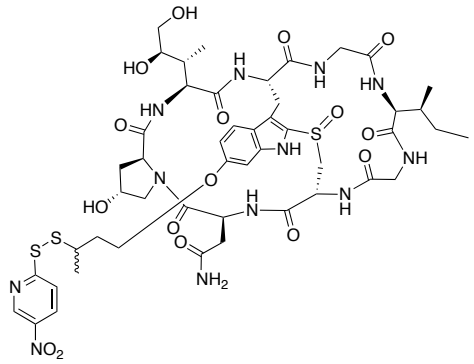

$C_{48}H_{64}N_{12}O_{16}S_3$
MW: 1161,29

A 0.5 M solution of DTNP in TFA (260 μl, 0.13 mmol) was added to the compound **67** (31.17 mg, 0.026 mmol). After 4 min, reaction mixture was dripped into precooled MTBE:n-hexane (1:1, v:v; 10 ml) mixture. The precipitate was cooled down to 0 °C for 10 min and isolated by centrifugation at 0 °C. The supernatants were discarded and the pellet was purified by RP-HPLC by using the following conditions: λ= 305 nm; gradient: 0 min 5 % B; 15-18 min 100% B; 18.5-22 min 5 % B; A= water with 0.05% TFA, B= MeOH with 0.05% TFA. Compound **69**

was isolated and the solvents were evaporated in vacuo. The residue was freeze-dried in ^{t}BuOH/H_2O (4:1, 10 ml) overnight.

Npys-CH(CH_3)-(CH_2)$_2$-α-amanitin (69): yellowish powder (17.92 mg, yield= 59%). MS (ESI+) *m/z:* calcd. for $C_{48}H_{64}N_{12}O_{16}S_3Na$: 1183.36, found: 1183.33 $[M+Na]^+$.

Compound 71. H_2N-(CH_2)$_2$C(CH_3)$_2$-SS-(CH_2)$_3$-α-amanitin

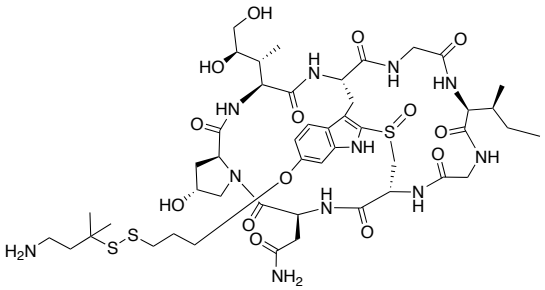

$C_{47}H_{71}N_{11}O_{14}S_3$
MW: 1110,33

Compound **68** (10.0 mg, 0.0081 mmol) was weighted into a 15 ml centrifuge tube and dissolved in a 0.5 M DTNP solution in TFA (80.94 μl, 0.041 mmol). Reaction mixture was stirred at room temperature for 4 minutes, and then diluted with MTBE:n-hexane (1:1, v:v; 10 ml). The precipitate was cooled down to 0 °C for 10 min, isolated by centrifugation at 0 °C and, subsequently, washed with MTBE (10 ml). The supernatants were discarded, the pellet was dissolved in MeOH (500 μl), and the 4-amino-2-methylbutane-2-thiol crosslinker **70** (17 mg, 0.073 mmol) was added. After 1 h at room temperature, the mixture was triturated with precooled MTBE containing 0.05% TFA (10 ml). The pellet was isolated by centrifugation at 0 °C and washed with fresh MTBE containing 0.05% TFA (10 ml). The precipitate was dissolved in MeOH (200 μl) and purified through preparative RP-HPLC: λ= 305 nm; gradient: 0-5 min 5% B; 20-25 min 100% B; 27-35 min 5% B; A= water with 0.05% TFA; B= MeOH with 0.05% TFA. Compound **71** was collected and the solvents were evaporated.

H_2N-(CH_2)$_2$C(CH_3)$_2$-SS-(CH_2)$_3$-α-amanitin (71): colorless residue (8.05 mg, yield= 81 %). MS (ESI+) *m/z*: calcd. for $C_{47}H_{72}N_{11}O_{14}S_3$: 1110.44, found: 1110.39 $[M+H]^+$.

Compound 72. H_2N-$(CH_2)_2C(CH_3)_2$-SS-$CH(CH_3)$-$(CH_2)_3$-α-amanitin

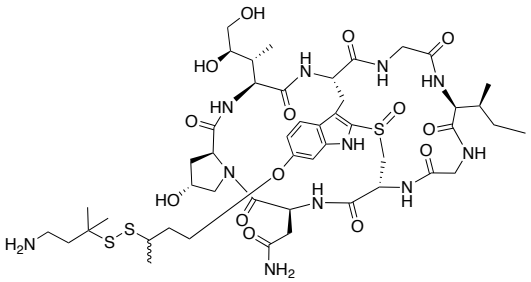

$C_{48}H_{73}N_{11}O_{14}S_3$
MW:: 1124,35

Compound **69** (20.3 mg, 0.016 mmol) was dissolved in a 0.5 M DTNP solution in TFA (162 μl, 0.081 mmol). The reaction mixture was stirred at room temperature for 4 minutes, and then diluted with MTBE:n-hexane (1:1, v:v; 10 ml). The precipitate was cooled down to 0 °C for 10 min, isolated by centrifugation at 0 °C and, subsequently, washed with MTBE (10 ml). The supernatants were discarded, the pellet was dissolved in MeOH (500 μl), and the 4-amino-2-methylbutane-2-thiol crosslinker **70** (19.4 mg, 0.162 mmol) was added. After 1 h at room temperature, the mixture was triturated with precooled MTBE containing 0.05% TFA (10 ml). The pellet was isolated by centrifugation at 0 °C and washed with fresh MTBE with 0.05% TFA (10 ml). The precipitate was dissolved in MeOH (200 μl) and purified by preparative RP-HPLC: λ= 305 nm; gradient: 0 min 5% B; 1 min 15% B; 15 min 70% B; 22 min 65% B; 25 min 50%; 26-27 min 100% B; 28-29 min 5% B; A= water with 0.05% TFA, B= ACN. Compound **72** was collected and freeze-dried overnight.

H_2N-$(CH_2)_2C(CH_3)_2$-SS-$CH(CH_3)$-$(CH_2)_2$-α-amanitin (72): colorless powder (3.18 mg, yield= 18%). MS (ESI+) *m/z*: $[M+H]^+$ calcd. for $C_{48}H_{74}N_{11}O_{14}S_3$: 1124.46, found: 1124.50.

Compound 74. $(O^tBu)_3$DUPA-Pep-OH

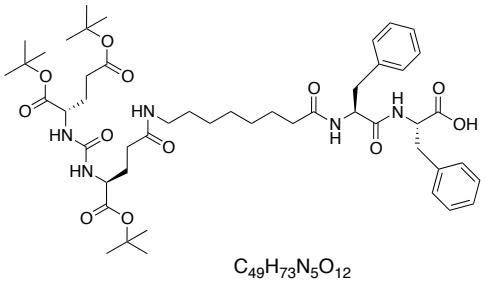

$C_{49}H_{73}N_5O_{12}$
MW: 924,13

Peptide sequence **74** was assembled onto H-Phe-2-CTC resin (417 mg, 0.25 mmol) by MW-assisted SPPS according to the general procedure **GP 1.** The resin-bound peptide was cleaved from the resin by using the general procedure **GP 2a**. Filtrates were collected and concentrated in vacuo.

(O^tBu)$_3$DUPA-Pep-OH (74): colorless solid (131.5 mg, yield= 57%). MS (ESI+) *m/z*: calcd. for $C_{49}H_{75}N_6O_{11}$: 924.18, found: 924.50 $[M+H]^+$; calcd. for $C_{49}H_{74}N_6O_{11}Na$: 946.58, found: 946.58 $[M+Na]^+$.

Compound 75. (O^tBu)$_3$DUPA-Pep-OSu

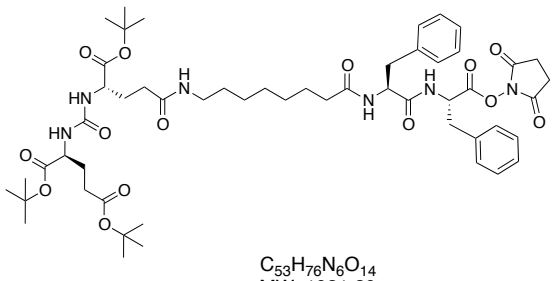

Compound **74** (131.01 mg, 0.15 mmol) was dissolved in THF (2.5 ml) at room temperature under argon. DCC (52.61 mg, 0.26 mmol) and HOSu (29.34 mg, 0.26 mmol) dissolved in THF (200 µl each) were added sequentially.

Reaction mixture was stirred at room temperature under argon for 18 hours. Dicyclohexylcarbodiurea (DCU) was filtered off and washed with a small amount of THF. The solvent was evaporated and the residue redissolved in ACN:MeOH containing 0.05% TFA (5:1, 6 ml), transferred into a 15 ml centrifuge tube, cooled down to 0°C and centrifuged at 10 °C (4500 rpm, 3 min). The solid residue was discarded and the supernatant was collected, evaporated under reduced pressure and freeze-dried in ^{t}BuOH with 0.05%TFA (5 ml) overnight.

(O^tBu)$_3$DUPA-Pep-OSu (75): colorless powder (147.77 mg, yield= 97%). MS(ESI+) *m/z*: calcd. for $C_{53}H_{77}N_6O_{14}$: 1021.55, found: 1021.80 $[M+H]^+$.

Compound 77. ($O^tBu)_3$DUPA-Pep-CO-NH-$(CH_2)_2$-$CH(CH_3)$-S(Trt)

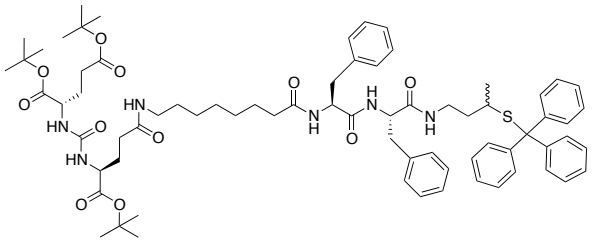

$C_{72}H_{96}N_6O_{11}S$
MW: 1253,63

Compound **75** (44 mg, 0.043 mmol) was coupled to 3-trytil-sulfanylbutylamine crosslinker **76** (15.72 mg, 0.045 mmol) according to the general procedure **GP 7**. The residue was purified by preparative RP-HPLC: λ= 210 nm; gradient: 0 min 5% B; 15-18 min 100% B; 18.5-22 min 5% B; A= water with 0.05% TFA, B= ACN. The compound **77** was collected and freeze-dried in $^tBuOH:H_2O$ (3:2, v:v; 5 ml).

DUPA-Pep-CO-NH-$(CH_2)_2$-$CH(CH_3)$-S(Trt) (77): colorless powder (30.29 mg, yield= 56%). MS(ESI+) *m/z*: $[M+H]^+$ calcd. for $C_{72}H_{97}N_6O_{11}S$: 1253.69, found: 1253.50.

Compound 73. DUPA-Pep-CO-NH-$(CH_2)_2$-$CH(CH_3)$-SH

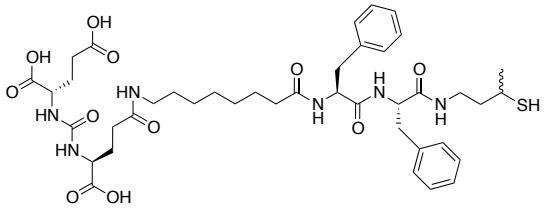

$C_{41}H_{58}N_6O_{11}S$
MW: 843,00

Compound **77** (30.29 mg, 0.0242 mmol) was fully deprotected under the conditions described in the general procedure **GP 8**. The pellet was purified by preparative RP-HPLC (λ= 210 nm; gradient: 0 min 5% B; 15-18 min 100% B; 18.5-22 min 5% B; A= water with 0.05% TFA, B= ACN), and the compound was collected and concentrated under reduced pressure. Residue was taken up in $^tBuOH:H_2O$ (4:1, v:v; 5 ml) and freeze-dried overnight.

DUPA-Pep-CO-NH-$(CH_2)_2$-$CH(CH_3)$-SH (73): colorless powder (6.10 mg, yield= 30%). MS(ESI-) *m/z*: $[M-H]^-$ calcd. for $C_{41}H_{57}N_6O_{11}S$: 841.38, found: 841.33; $[(M-2H)+Na]^-$ calcd. for $C_{41}H_{56}N_6O_{11}SNa$: 863.36, found: 863.33.

SMDC 58 (HDP 30.2246). DUPA-Pep-SS-α-amanitin

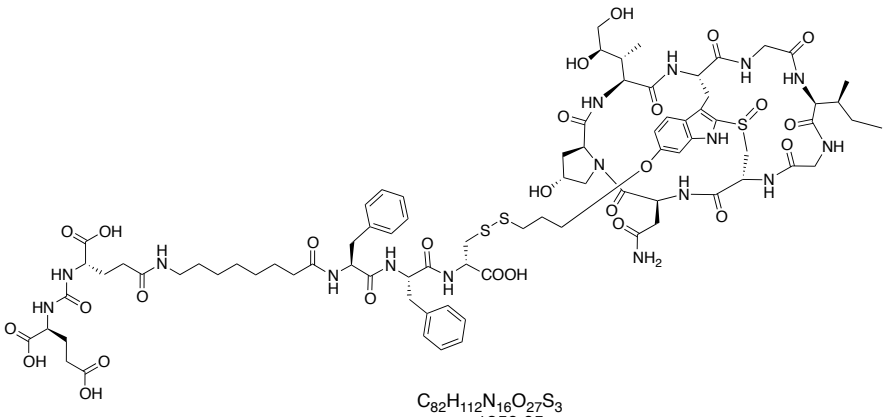

$C_{82}H_{112}N_{16}O_{27}S_3$
MWt: 1850,05

Compound **44** (13.4 mg, 0.016 mmol) was dissolved in dry DMSO (1.5 ml). α−Amanitin derivative **68** (17.9 mg, 0.016 mmol) dissolved in dry DMSO (1.6 ml) was added at room temperature under argon. DIPEA (5.15 µl, 0.030 mmol) was added undiluted. The reaction mixture was stirred at room temperature for 3 h. The orange crude product was purified by preparative RP-HPLC: λ= 305 nm; gradient: 0-1 min 5% B; 1-14 min 54% B; 14-16 min 60.6% B; 16-23 min 100% B; 23-26 min 5% B; A= water with 0.05% TFA; B= acetonitrile]. SMDC **58** was isolated and freeze-dried overnight.

DUPA-Pep-SS-α−amanitin SMDC (58): colorless powder (11.36 mg, yield= 40%). MS (ESI$^+$) *m/z*: $[M+Na]^+$ calcd. for $C_{82}H_{112}N_{16}O_{27}S_3Na$: 1871.69, found: 1872.4; $[M+2Na]^{2+}$ calcd. for $C_{82}H_{112}N_{16}O_{27}S_3Na_2$: 947.34, found: 947.5.

SMDC 59 (HDP 30.2589). DUPA-Pep-SS-Me-α-amanitin

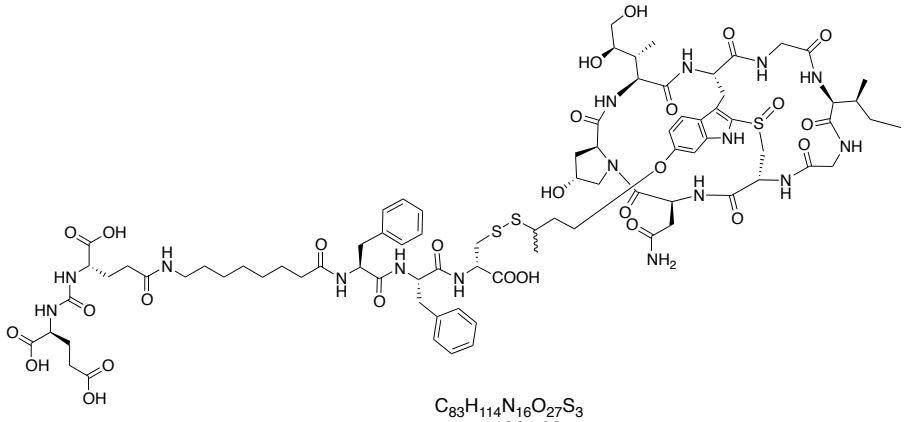

$C_{83}H_{114}N_{16}O_{27}S_3$
MW: 1864,08

Compound **44** (2.27 mg, 0.003 mmol) was dissolved in MeOH (135 μl) and a solution of the α−amanitin derivative **69** (3.07 mg, 0.003 mmol) in MeOH (280 μl) was added at room

temperature under argon. DIPEA (0.9 µl, 0.005 mmol) was added undiluted. The reaction mixture was stirred at room temperature for 24 h and the solvent was then evaporated. The residue was dissolved in MeOH (200 μl) and purified by preparative RP-HPLC: λ= 305 nm; gradient: 0 min 5% B; 15 min 100% B; 18 min 100% B; 18.50 min 100% B; 22 min 5% B; A= water with 0.05% TFA; B= ACN. SMDC **59** was collected and freeze-dried overnight.

DUPA-Pep-S-S-Me-α-amanitin (59): colorless powder (2.79 mg, yield= 58%). MS (ESI-) *m/z*: $[M-H]^-$ calcd. for $C_{83}H_{113}N_{16}O_{27}S_3$: 1861.71, found: 1862.58.

SMDC 60 (HDP 30.2618). DUPA-Pep-Me-SS-α-amanitin

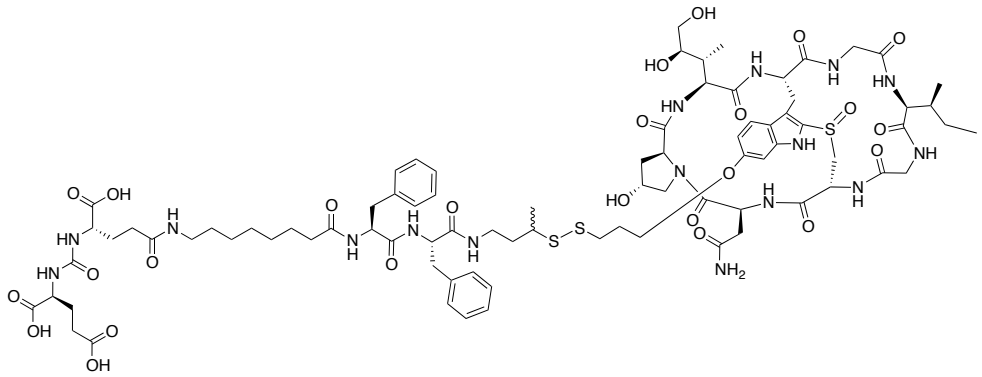

Compound **73** (4.64 mg, 0.006 mmol) was dissolved in MeOH (423 μl). A solution of the α–amanitin derivative **69** (6.31 mg, 0.006 mmol) was added at room temperature under argon. DIPEA (1.88 µl, 0.011 mmol) was added undiluted. The reaction mixture was stirred at room temperature for 0.5 h and solvent was then evaporated. The residue was dissolved in MeOH (200 μl) and purified by preparative RP-HPLC: λ= 305 nm; gradient: 0-1 min 5% B; 1-14 min 54% B; 14-16 min 61% B; 16-19 min 100% B; 19-22 min 100% B; 22-25 min 5% B A= water with 0.05% TFA; B= ACN. SMDC **60** was collected and freeze-dried overnight.

DUPA-Pep-Me-SS-α-amanitin (60): colorless powder (4.69 mg, yield= 47%). MS (ESI-) *m/z*: $[M-H]^-$ calcd. for $C_{83}H_{115}N_{16}O_{25}S_3$: 1831.74, found: 1832.58; $[M-2H]^{2-}$ calcd. for $C_{83}H_{114}N_{16}O_{25}S_3$: 915.37, found: 915.83.

SMDC 61 (HDP 30.2619). DUPA-Pep-Me-SS-Me-α-amanitin

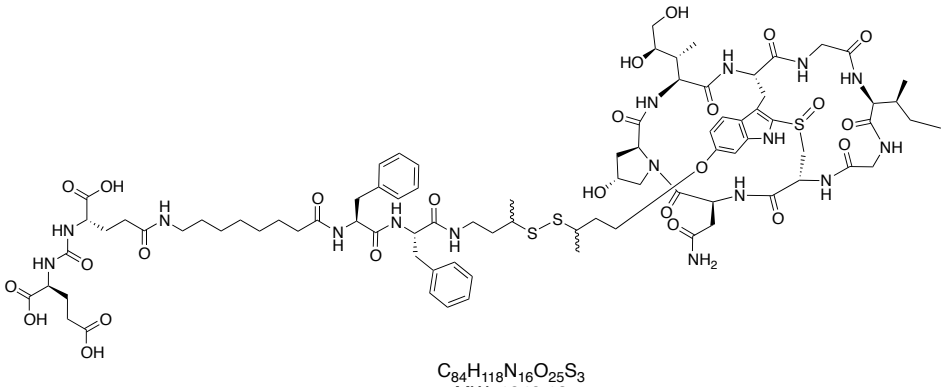

$C_{84}H_{118}N_{16}O_{25}S_3$
MW: 1848,12

α–Amanitin derivative **68** (3.0 mg, 0.003 mmol) was dissolved in MeOH (200 μl). Compound **73** (2.19 mg, 0.003 mmol) and DIPEA (0.89 μl, 0.0052 mmol) were added at room temperature under argon. The reaction mixture was stirred overnight and then purified by preparative RP-HPLC: λ= 305 nm; gradient: 0-1 min 5% B; 1-14 min 54% B; 14-16 min 61% B; 16-19 min 100% B; 19-22 min 100% B; 22-25 min 5% B A= water with 0.05% TFA; B= MeOH with 0.05% TFA. SMDC **61** was collected, the solvents were evaporated and the residue freeze-dried overnight in ^{t}BuOH:H_2O (4:1, v:v; 10 ml).

DUPA-Pep-Me-SS-Me-α-amanitin (61): colorless powder (2.9 mg, yield= 60%). MS(ESI-) *m/z*: calcd. for $C_{84}H_{117}N_{16}O_{25}S_3$: 1845.75, found: 1846.67 $[M-H]^-$; calcd. for $C_{84}H_{116}N_{16}O_{25}S_3$: 922.38, found: 922.92 $[M-2H]^{2-}$.

Compound 78. (O^tBu)$_3$DUPA-Pep-(Me)$_2$-SS-α-amanitin

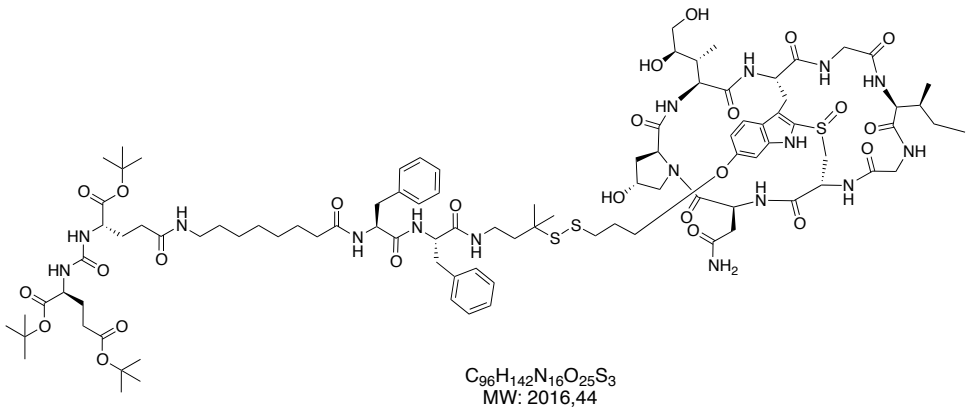

$C_{96}H_{142}N_{16}O_{25}S_3$
MW: 2016,44

α–Amanitin derivative **71** (5.07 mg, 0.0046 mmol) and the DUPA-Pep-OSu sequence **75** (5.13 mg, 0.005 mmol) were coupled according to the general procedure **GP 7**. The residue was dissolved in MeOH (200 μl) and purified by preparative RP-HPLC: λ= 305 nm; gradient: 0-5 min 5% B; 20-25 min 100% B; 27-35 min 5% B; A= water with 0.05% TFA; B= MeOH with

0.05% TFA. The solvents were evaporated and the residue was freeze-dried overnight from ^{t}BuOH:H_2O (4:1, v:v; 5 ml).

.

(O^{t}Bu)$_3$DUPA-Pep-Me$_2$-SS-α-amanitin (78): colorless powder (6.38 mg, yield= 75%). MS (ESI-) *m/z*: $[M+2Na]^{2+}$ calcd. for $C_{96}H_{142}N_{16}O_{25}S_3Na_2$: 1031.23, found: 1031.00.

SMDC 62. DUPA-Pep-(Me)$_2$-SS-α-amanitin

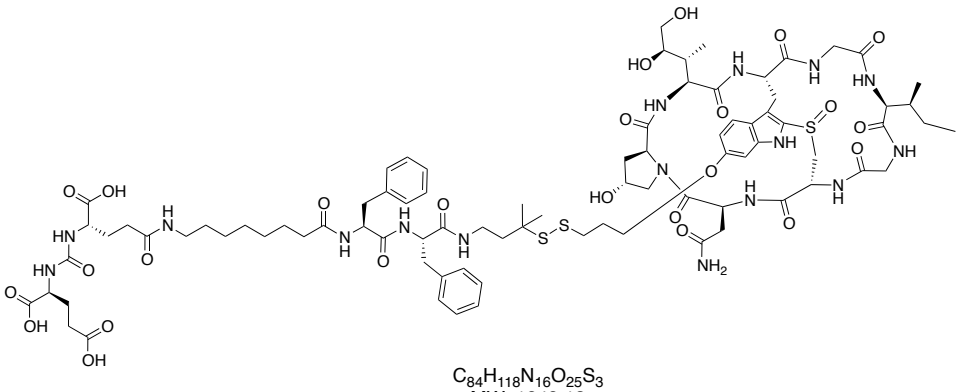

$C_{84}H_{118}N_{16}O_{25}S_3$
MW: 1848,12

Compound **78** (6.10 mg, 0.003 mmol) was dissolved in TFA (1 ml) and shaken at room temperature for 2 minutes. TFA was then evaporated and the residue was dissolved in TFA (1 ml) and shaken at room temperature for additional 5 minutes (x2). TFA was finally co-evaporated with toluene (1 ml; x 2).

Sample was dissolved in ACN:H_2O (8:2, 200 µl) and purified by preparative RP-HPLC: λ= 305 nm; gradient: 0 min 5% B; 15 min 100% B; 18 min 100% B; 18.50 min 100% B; 22 min 5% B; A= water with 0.05% TFA; B= ACN. SMDC **62** was collected and freeze-dried overnight.

DUPA-Pep-(Me)$_2$-SS-α-amanitin (62): colorless powder (1.1 mg, yield= 20%). MS(ESI-) *m/z*: $[M-H]^-$ calcd. for $C_{84}H_{117}N_{16}O_{25}S_3$: 1845.75, found: 1846.67; $[M-2H]^{2-}$ calcd. for $C_{84}H_{116}N_{16}O_{25}S_3$: 922.38, found: 922.44.

Compound 79. ($O^tBu)_3$DUPA-Pep-$(Me)_2$-SS-Me-α-amanitin

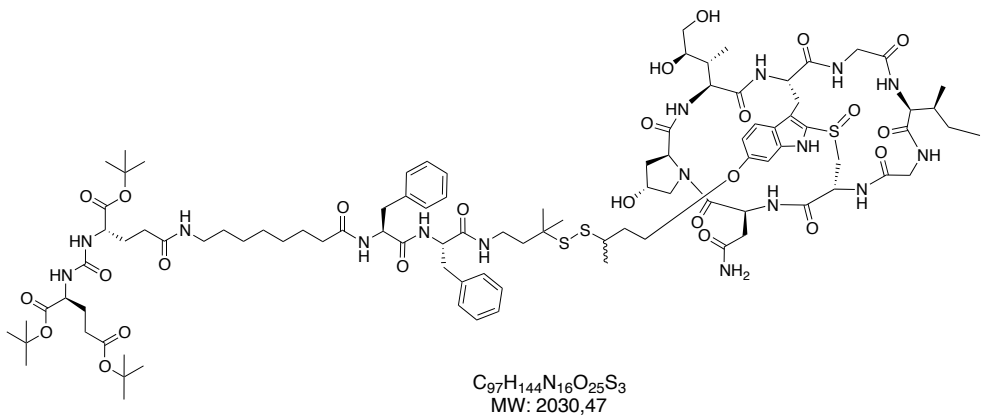

$C_{97}H_{144}N_{16}O_{25}S_3$
MW: 2030,47

α−Amanitin derivative **72** (2.88 mg, 0.0026 mmol) and the DUPA-Pep-OSu sequence **75** (5.23 mg, 0.0051 mmol) were coupled according to the general procedure **GP 7**. The residue was dissolved in MeOH (200 μl) and purified by preparative RP-HPLC: λ= 305 nm; gradient: 0-5 min 5% B; 20-25 min 100% B; 27-35 min 5% B; A= water with 0.05% TFA; B= MeOH with 0.05% TFA. The solvents were evaporated and the title compound was freeze-dried overnight from $^tBuOH:H_2O$ (4:1, v:v; 5 ml).

($O^tBu)_3$DUPA-Pep-$(Me)_2$-SS-Me-α-amanitin (79): colorless powder (3.22 mg, yield= 61%). MS (ESI+) *m/z*: calcd. for $C_{86}H_{124}N_{16}O_{25}S_3$: $[M-(3x^tBu)+2H]^{2+}$ 938.91, found: 936.62; $[M+ACN+2H]^{2+}$ calcd. for $C_{88}H_{127}N_{17}O_{25}S_3$: 959.42, found: 960.15.

SMDC 63 (HDP 30.2654). DUPA-Pep-$(Me)_2$-SS-Me-α-amanitin

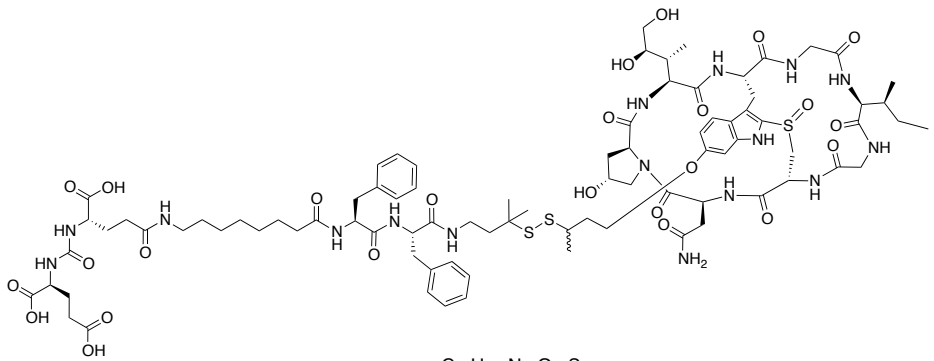

$C_{85}H_{120}N_{16}O_{25}S_3$
MW: 1862,15

Compound **79** (2.63 mg, 0.0013 mmol) was dissolved in TFA:phenol (95:5, v:w; 2 ml) and shaken at room temperature for 2 minutes. TFA was then evaporated and residue dissolved in TFA (2 ml) and shaken at room temperature for additional 5 minutes (x2). TFA was then co-

evaporated with toluene (2 ml; x2).

Sample was dissolved in ACN:H_2O (8:2, 200 µl) and purified by preparative RP-HPLC: λ= 305 nm; gradient: 0 min 5% B; 15 min 100% B; 18 min 100% B; 18.50 min 100% B; 22 min 5% B; A= water with 0.05% TFA; B= ACN. SMDC **63** was collected and freeze-dried overnight.

DUPA-Pep-Me_2-SS-Me-α-amanitin SMDC (63): colorless powder (traces).

SMDC 80 (HDP 30.2515). DUPA-Pep-ac-va-α-amanitin

Compound 82. bac-va-α-amanitin

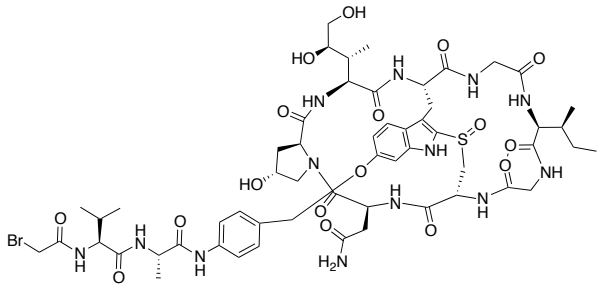

$C_{56}H_{76}BrN_{13}O_{17}S$
MW: 1315,25

va-α-Amanitin derivative **47a** (15 mg, 0.012 mmol) was dissolved in dry DMF (457.26 µl). A 0.1 M solution of bromoacetic acid *N*-hydroxysuccinimide ester (229.2 µl, 0.023 mmol) and a 0.1 M solution of DIPEA (458.4 µl, 0.046 mmol) were added. The reaction mixture was stirred at room temperature for 1 h. Subsequently, the reaction mixture was diluted with precooled MTBE (40 ml). The precipitate was cooled down to 0°C for 10 minutes with an ice bath, isolated by centrifugation at 0 °C (4500 rpm, 4 min) and washed with MTBE (40 ml). The pellet was collected, dried in vacuo, redissolved in MeOH (200 µl) and purified by preparative RP-HPLC: λ= 305 nm; gradient: 0-5 min 5% B; 20-25 min 100% B; 27-35 min 5% B; A= water with 0.05% TFA; B= MeOH with 0.05% TFA.

The product was collected and the solvents were evaporated. The resulting residue was freeze-dried overnight from ^tBuOH:H_2O (4:1, v:v; 5 ml).

bac-va-α-amanitin (82): colorless powder (6.26 mg, yield= 42%). MS(ESI+) *m/z:* calcd. for $C_{56}H_{76}BrN_{13}O_{17}SNa$: 1338.24, found: 1338.33 $[M+Na]^+$.

SMDC 80. DUPA-Pep-ac-va-α-amanitin

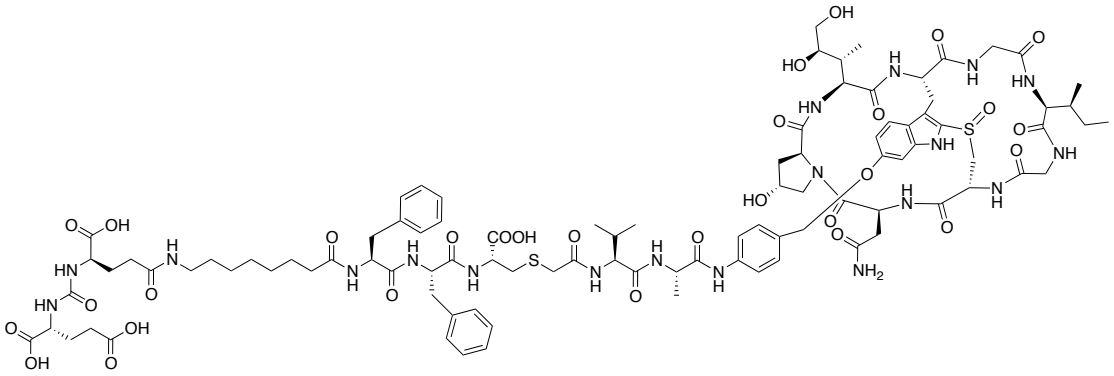

$C_{96}H_{129}N_{19}O_{30}S_2$
MW: 2093,29

A solution of **82** (4 mM, 2.60 mg, 0.002 mmol) in ACN:H_2O (1:1, v:v) and a solution of **44** (4 mM, 1.71 mg, 0.002 mmol,) in ACN:H_2O (1:1, v:v) were mixed and diluted with Na_2CO_3/$NaHCO_3$ buffer (100 mM, pH 9.3; 750 µl) to achieve a final concentration of **44** equal to 1.14 mM. The reaction mixture was stirred at room temperature for 1.5 h and the reaction mixture was purified by preparative RP-HPLC: λ= 305 nm; gradient: 0-5 min 5% B; 20-25 min 100% B; 27-35 min 5% B; A= water with 0.05% TFA; B= MeOH with 0.05% TFA. The product was isolated and the solvents were evaporated. The residue was freeze-dried overnight from ^{t}BuOH:H_2O (4:1, v:v; 5 ml).

DUPA-Pep-ac-va-α-amanitin SMDC (80): colorless powder (2.61 mg, yield= 62%).MS(ESI-) *m/z:* calcd. for $C_{96}H_{127}N_{19}O_{30}S_2$: 1045.64, found: 1045.42 $[M-2H]^{2-}$; $[M-3H]^{3-}$ calcd. for $C_{96}H_{126}N_{19}O_{30}S_2$: 696.76, found: 696.67.

SMDC 81 (HDP 30.2523). DUPA-Pep-ac-α—amanitin

Compound 83. Boc-NH-$(CH_3)_6$-α-amanitin

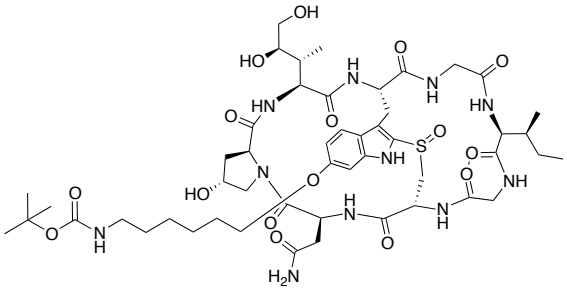

$C_{50}H_{75}N_{11}O_{16}S$
MW: 1118,26

A solution of α-amanitin (105 mg, 0.114 mmol) and 6-(Boc-amino)hexyl bromide (128 mg, 0.457 mmol) in DMSO (3.5 ml) was treated with a LiOH solution (2 M, 68.6 µl, 0.137 mmol)

under argon atmosphere. After stirring at room temperature for 40 min, the reaction mixture was acidified by addition of AcOH (7.84 µl) and the mixture was then added dropwise to a centrifuge tube containing precooled MTBE (40 ml). The precipitate was collected, dried in vacuo and purified by preparative RP-HPLC: λ= 305 nm; gradient: 0-5 min 5% B; 20-25 min 100% B; 27-35 min 5% B; A= water; B= MeOH. The product was isolated and the solvents were evaporated under reduced pressure. The residue was freeze-dried overnight from ^{t}BuOH:H_2O (4:1, v:v; 5 ml).

Boc-NH-$(CH_3)_6$-α-amanitin (83): colorless powder (84.37 mg, yield= 66%). MS (ESI+) *m/z*: $[M+H]^+$ calcd. for $C_{50}H_{76}N_{11}O_{16}S$: 1118.52, found: 1118.5.

Compound 84. NH_2-$(CH_3)_6$-α-amanitin

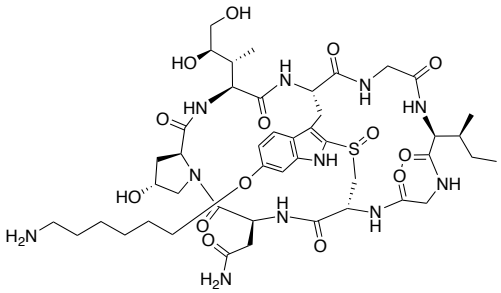

$C_{45}H_{67}N_{11}O_{14}S$
MW: 1018,14

Compound **83** (152 mg, 0.136 mmol) was dissolved in TFA (5 ml) and the reaction mixture was stirred for 2 min at room temperature. The reaction mixture was concentrated under reduced pressure, and the crude product was purified by preparative RP-HPLC: λ= 305 nm; gradient: 0 min 5% B; 0-1 min 30% B; 1-10 min 39% B; 10-13 min 100% B; 13-18 min 5% B; A= water with 0.05% TFA; B= MeOH with 0.05% TFA. The product was collected, and the solvents were evaporated under reduced pressure. The residue was freeze-dried overnight from ^{t}BuOH (5 ml).

NH_2-$(CH_3)_6$-α-amanitin (84): colorless powder (118.67 mg, yield= 86%). MS (ESI+) *m/z*: $[M+H]^+$ calcd. for $C_{45}H_{68}N_{11}O_{14}S$: 1018.47, found: 1018.5.

Compound 85. bac-$(CH_3)_6$-α-amanitin

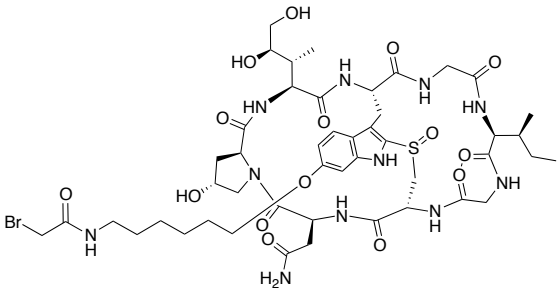

$C_{47}H_{68}BrN_{11}O_{15}S$
MW:1139,08

NH_2-$(CH_3)_6$-α-Amanitin derivative **84** (14.8 mg, 0.013 mmol) was dissolved in dry DMF (451.2 µl). A solution of bromoacetic acid *N*-hydroxysuccinimide ester (0.1 M, 250 µl, 0.025 mmol) and a solution of DIPEA (0.1 M, 497.9 µl, 0.050 mmol) were added. The reaction mixture was stirred at room temperature for 1 h. Subsequently, the reaction mixture was diluted with precooled MTBE (40 ml). The precipitate was cooled to 0°C for 10 minutes with an ice bath, isolated by centrifugation at 0 °C and washed with MTBE (40 ml). The pellet was collected, dried in vacuo, redissolved in MeOH (200 µl) and purified by preparative RP-HPLC: λ= 305 nm; gradient: 0-5 min 5% B; 20-25 min 100% B; 27-35 min 5% B; A= water with 0.05% TFA; B= MeOH with 0.05% TFA.

The product was collected and the solvents were evaporated under reduced pressure. The residue was freeze-dried overnight from ^{t}BuOH:H_2O (4:1, v:v; 5 ml).

Bac-$(CH_3)_6$-α-amanitin (85): colorless powder (12.34 mg, yield= 83%). MS(ESI+) *m/z*: $[M+Na]^+$ calcd. for $C_{47}H_{68}BrN_{11}O_{15}SNa$: 1162.07, found: 1162.42.

SMDC 81 (HDP 30.2523). DUPA-Pep-ac-α-amanitin

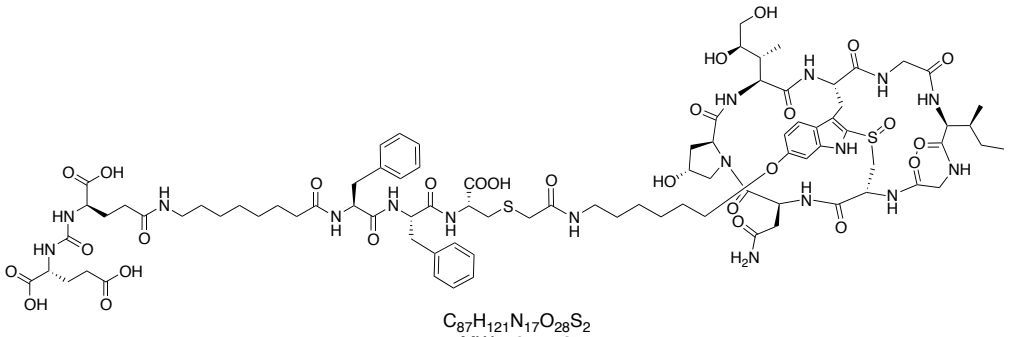

$C_{87}H_{121}N_{17}O_{28}S_2$
MW: 1917,12

A solution of **85** (4 mM, 5.01 mg, 0.0044 mmol) in ACN:H_2O (1:1, v:v) and a solution of **44** (4 mM, 3.78 mg, 0.0044 mmol) in ACN:H_2O (1:1, v:v) were mixed and diluted with Na_2CO_3/$NaHCO_3$ buffer (100 mM, pH 9.3; 1.8 ml) to achieve a final concentration of **44** equal

to 1.14 mM. The reaction mixture was stirred at room temperature for 1.5 h and then purified by preparative RP-HPLC: λ= 305 nm; gradient: 0-5 min 5% B; 20-25 min 100% B; 27-35 min 5% B; A= water with 0.05% TFA; B= MeOH with 0.05% TFA. The product was isolated and the solvents were evaporated. The residue was freeze-dried overnight in ^{t}BuOH:H_2O (4:1, v:v; 5 ml).

DUPA-Pep-ac-α-amanitin (81): colorless powder (5.68 mg, yield= 67%). MS(ESI-) *m/z*: $[M-H]^-$ calcd. for $C_{87}H_{120}N_{17}O_{28}S_2$: 1916.11, found: 1915.75; $[M-2H]^{2-}$ calcd. for $C_{87}H_{119}N_{17}O_{28}S_2$: 957.55, found: 957.42.

SMDC 88 (HDP 30.2594). DUPA-Pep-$(HE)_2$-va-α-amanitin

Compound 89. $(O^tBu)_3$DUPA-Pep-$(His^{Trt}$-$Glu^{OtBu})_2$-Cys^{Trt}-OH

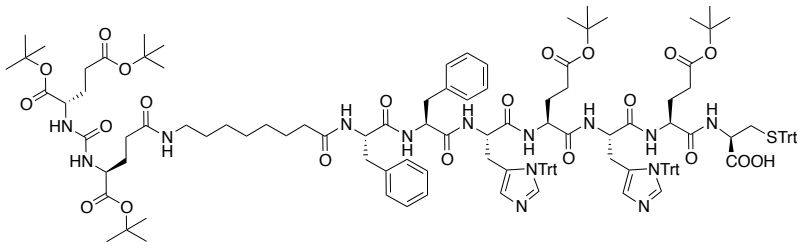

$C_{139}H_{164}N_{14}O_{21}S$
MW: 2398,94

Synthesis of compound **89** was performed by automated MW-assisted SPPS on preloaded H-Cys-CTC resin (391 mg, 0.25 mmol) according to the general procedure **GP 1**. The resin-bound peptide was then cleaved from the resin as described in **GP 2a**. The filtrates were collected and concentrated under reduced pressure. The residue was dried in vacuo.

$(O^tBu)_3$DUPA-Pep-$(His^{Trt}$-$Glu^{OtBu})$-Cys^{Trt}-OH (89): amorphous residue (284 mg, yield= 47%). MS (ESI-) *m/z*: $[M-H]^-$ calcd. for $C_{139}H_{163}N_{14}O_{21}S$: 2397.93, found: 2397.50.

Compound 90. DUPA-Pep-$(His\text{-}Glu)_2$-Cys-OH

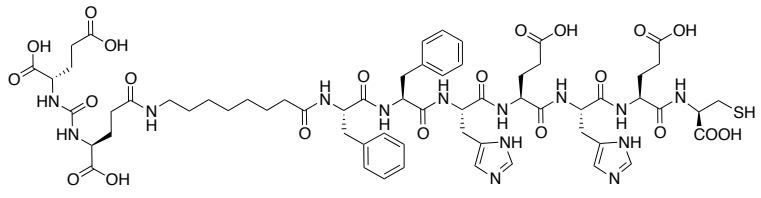

$C_{62}H_{82}N_{14}O_{21}S$
MW: 1391,46

Compound **89** (284 mg, 0.118 mmol) was fully deprotected by applying the procedure described in the general procedure **GP 2b** for total deprotection. The resulting peptide was first isolated as pellet by MTBE trituration (**GP 3**) and then purified by preparative RP-HPLC: λ= 246 nm; gradient: 0 min 5% B; 15-18 min 100% B; 18.50-22 min 5% B; A= water with 0.05% TFA, B= ACN. The product was collected and directly lyophilized overnight.

DUPA-Pep-(His-Glu)$_2$-Cys-OH (90): white solid (115.38 mg, yield= 70%). MS (ESI+) *m/z*: $[M+H]^+$ calcd. for $C_{62}H_{83}N_{14}O_{21}S$: 1391.56, found: 1391.50; $[M+2H]^{2+}$ calcd. for $C_{62}H_{84}N_{14}O_{21}S$: 696.29, found: 696.42.

SMDC 88. DUPA-Pep-(HE)$_2$-va-α-amanitin

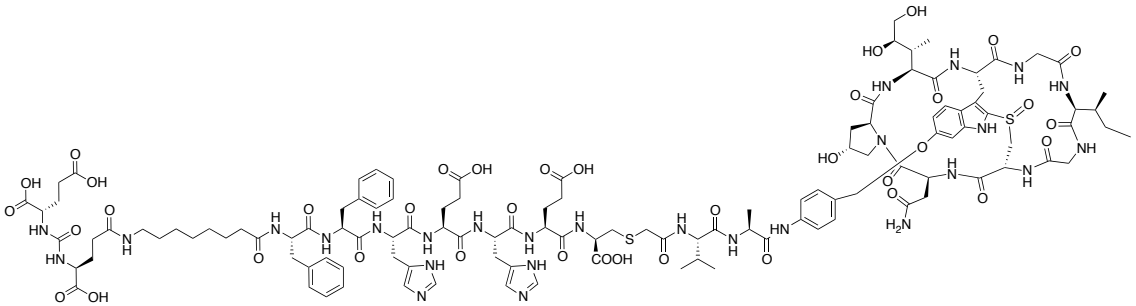

A solution of **82** (4 mM, 4.00 mg, 0.0030 mmol) in ACN:H_2O (1:1, v:v) and a solution of **90** (4 mM, 5.92 mg, 0.0043 mmol) in ACN:H_2O (1:1, v:v) were mixed and diluted with Na_2CO_3/$NaHCO_3$ buffer (100 mM, pH 9.3; 600 µl) to achieve a final concentration of **90** equal to 1.14 mM. The reaction mixture was stirred at room temperature for 1.5 h and subsequently purified by preparative RP-HPLC: λ= 305 nm; gradient: 0 min 5% B; 15-18 min 100% B; 18.50-22 min 5% B; A= water with 0.05% TFA; B= ACN. The product was isolated and the solvents were evaporated. The residue was freeze-dried overnight.

DUPA-Pep-(HE)$_2$-va-α-amanitin (88): colorless powder (6.13 mg, yield= 77%). MS(ESI-) *m/z*: $[M-H]^-$ calcd. for $C_{118}H_{156}N_{27}O_{38}S_2$: 2623.05, found: 2623.83; $[M-2H]^{2-}$ calcd. for $C_{118}H_{155}N_{27}O_{38}S_2$: 1311.03, found: 1311.50.

Compound 108. [3,4-*bis*(phenylthio)]-ma-va-α-amanitin

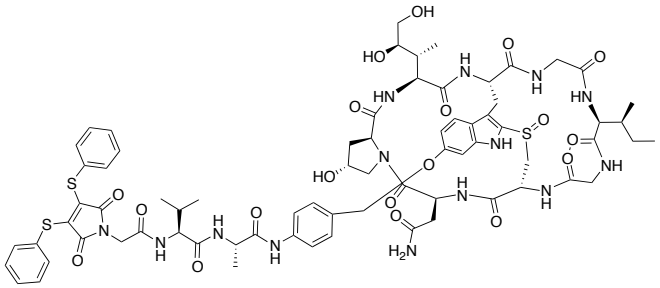

$C_{72}H_{86}N_{14}O_{19}S_3$
MW: 1547,73

va-α-Amanitin **47a** (15.00 mg, 0.0115 mmol) was dissolved in dry DMF (2 ml). A solution of NHS ester-activated [3,4-*bis*(phenylthio)] maleimide *N*-acetic acid in DMF (20 mM, 1.72 ml, 0.034 mmol) and undiluted DIPEA (5.85 μl, 0.034 mmol) were added. After 2 h of stirring at room temperature under argon, the reaction mixture was concentrated in vacuo. The residue was dissolved in MeOH (200 μl), precipitated in precooled MTBE (10 ml), and isolated by centrifugation (4500 rpm, 4 min) at 0°C. The precipitate was collected, and washed with additional MTBE (10 ml). The pellet was collected, dried in vacuo and then purified by preparative RP-HPLC: λ= 305 nm; gradient: 0 min 5% B; 0-1 min 30% B; 1-10 min 39% B; 10-13 min 100% B; 13-18 min 5% B; A= water; B= MeOH. The product was isolated and the solvents were evaporated in vacuo. The residue was lyophilized overnight from ^{t}BuOH:H_2O (4:1, v:v; 5 ml).

[3,4-*bis*(phenylthio)]-ma-va-α-amanitin (108): yellowish powder (9.27 mg, yield= 52%). MS (ESI+) *m/z*: $[M+2Na]^{2+}$ calcd. for $C_{72}H_{86}N_{14}O_{19}S_3Na_2$: 796.26, found: 796,63.

SMDC 101 (HDP 30.2300). (DUPA-Pep-Cys)$_2$-ma-va-α-amanitin

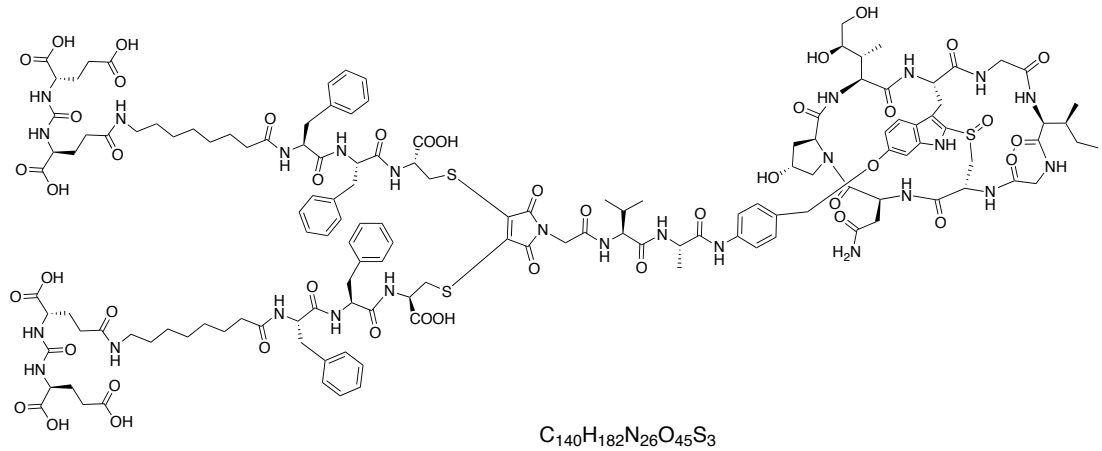

$C_{140}H_{182}N_{26}O_{45}S_3$
MW: 3045,29

α-Amanitin derivative **108** (21 mg, 0.014 mmol) was dissolved in DMSO (5.6 ml). A solution of **44** (23.2 mg, 0.027 mmol) and undiluted DIPEA (13.82 µl, 0.081 mmol) were added at room temperature under argon. The reaction mixture was stirred at room temperature for 49 h. The reaction mixture was then injected into preparative RP-HPLC: λ= 305 nm; gradient: 0-5 min 5% B; 20-25 min 100% B; 27-35 min 5% B; A= water with 0.05% TFA; B= MeOH with 0.05% TFA, The product were isolated, concentrated in vacuo and lyophilized overnight from ^{t}BuOH:H_2O (4:1, v:v; 5 ml).

(DUPA-Pep-Cys)$_2$-ma-va-α-amanitin (101): colorless powder (4.0 mg, yield= 10%). MS(ESI$^+$) *m/z*: $[M+2H]^{2+}$ calcd. for $C_{140}H_{184}N_{26}O_{45}S_3$: 1522.6, found: 1522.60; $[M+3H]^{3+}$ calcd. for $C_{140}H_{185}N_{26}O_{45}S_3$: 1015,40, found: 1015.40.

SMDC 102 (HDP 30.2448). (DUPA-Pep-EG$_4$-Cys)$_2$-mc-va-α-amanitin

Compound 112. Br-EG$_4$-Br

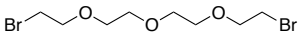

$C_8H_{16}Br_2O_3$
MW: 320,02

Commercially available tetraethylene glycol (20 ml, 115.4 mmol) was converted to the corresponding dibromine by applying the general procedure **GP 9.1.**

Br-EG$_4$-Br (112): colorless oil (34.70 g, yield= 94%).

Compound 115. Br-EG$_4$-N$_3$

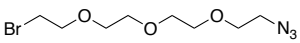

$C_8H_{16}BrN_3O_3$
MW: 282,13

Compound **112** (4.8 g, 15 mmol) was converted to the corresponding monoazide according to general procedure **GP 9.2**.

Compound 118. (Trt)S-EG$_4$-N$_3$

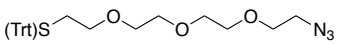

$C_{27}H_{31}N_3O_3S$
MW: 477,62

Compound **118** was obtained from the precursor **115** (4.23 g, 15 mmol theoretical) following the general procedure **GP 9.3**.

(Trt)S-EG$_4$-N$_3$ (118): colorless oil (3.12 g, yield= 74%).

Compound 121. (Trt)S-EG$_4$-NH$_2$

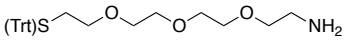

$C_{27}H_{33}NO_3S$
MW: 451,62

The general procedure **GP 9.4** was applied to convert compound **118** (478 mg, 1.0 mmol) into the corresponding primary amine.

(Trt)S-EG$_4$-NH$_2$ (121): yellowish oil (354 mg, yield= 77%). ^{1}H NMR (500 MHz, $CDCl_3$): δ=7.46-7.37 (m, 6H), 7.32-7.16 (m, 9H), 3.65-3.53 (m, 6H), 3.51-3.40 (m, 4H), 3.31 (t, J= 6.9 Hz, 2H), 2.84 (t, J= 5.2 Hz, 2H), 2.43 (t, J= 6.9 Hz, 2H), 1.47 (bs, 2H). ^{13}C NMR (126 MHz, $CDCl_3$): δ= 144.78, 129.57, 127.81, 126.58, 73.38, 70.55, 70.43, 70.24, 69.57, 66.55, 41.75, 31.63.

Compound 124. (O^{t}Bu)$_3$DUPA-Pep-EG$_4$-SH

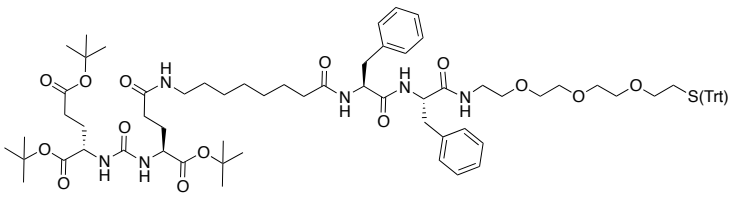

$C_{76}H_{104}N_6O_{14}S$
MW: 1357,74

(O^{t}Bu)$_3$DUPA-Pep-OSu **75** (20 mg, 0.020 mmol) was coupled to the carboxylate-reactive spacer **121** (9.29 mg, 0.021 mmol) as described in the general procedure **GP 9.5**. The residue was freeze-dried overnight from ^{t}BuOH:H_2O (3:2, v:v) to yield the final compound.

(O^{t}Bu)$_3$DUPA-Pep-EG$_4$-SH (124): colorless powder (15.8 mg, yield 59%). MS(ESI+) *m/z*: $[M+Na]^+$ calcd. for: 1379.72, found: 1379.75.

Compound 98. DUPA-Pep-EG$_4$-SH

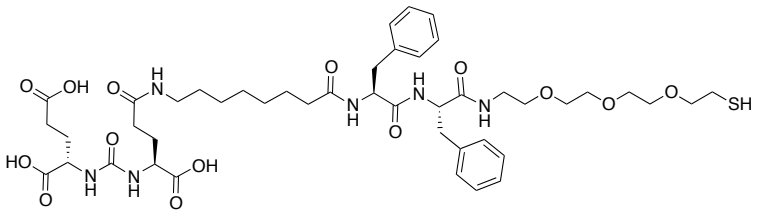

$C_{45}H_{66}N_6O_{14}S$
MW: 947,10

Following the general procedure **GP 9.6**, the compound **124** (15.8 mg, 0.012 mmol) was fully deprotected. The pellet was lyophilized overnight from ^{t}BuOH:H_2O (3:2, v:v, 5 ml) to afford the desired product.

DUPA-Pep-EG$_4$-SH (98): colorless powder (6.7 mg, yield= 61%). MS(ESI+) *m/z*: $[M+H]^+$ calcd. for $C_{45}H_{66}N_6O_{14}S$: 947.44, found: 947.50; $[M+Na]^+$ calcd. for $C_{45}H_{66}N_6O_{14}SNa$: 969.43, found: 969.50.

SMDC 102. (DUPA-Pep-EG$_4$)$_2$-ma-va-α-amanitin

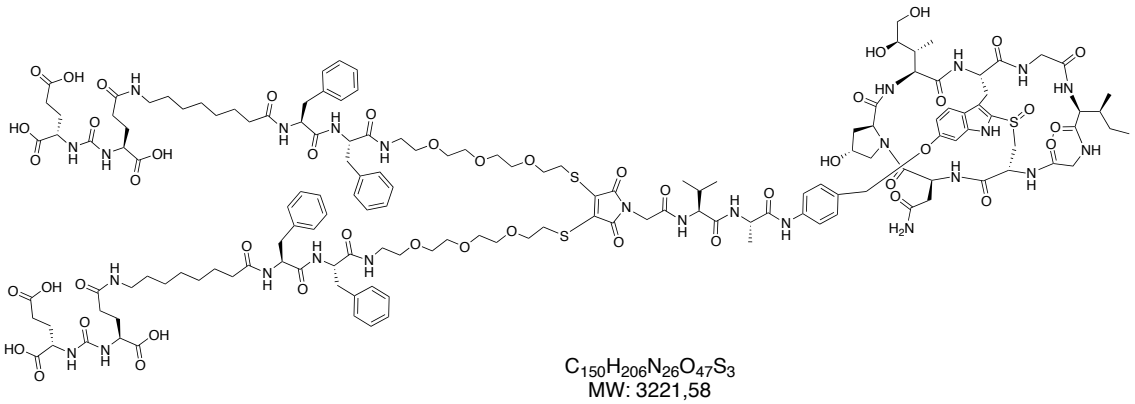

$C_{150}H_{206}N_{26}O_{47}S_3$
MW: 3221,58

α-Amanitin derivative **108** (5.17 mg, 0.0034 mmol) was dissolved in dry DMF (340 μl). The heterobifunctional linker **98** (6.26 mg, 0.0067 mmol) was dissolved in dry DMF (340 μl) and added to the solution of **108**. Subsequently, TEA (1.90 μl, 0.014 mmol) was added undiluted and the reaction mixture was stirred at room temperature under argon atmosphere for 28 h. DMF was then removed in vacuo and the residue was dissolved in ACN:H_2O (1:1, v:v) and purified by preparative RP-HPLC: λ= 305 nm; ; gradient: 0-1 min 5% B; 1-14 min 54% B; 26 min 100% B; 26-30 min 100% B; 30-35 min 5% B; A= water with 0.05% TFA; B= ACN.
The product was isolated and freeze-dried overnight from ^{t}BuOH:H_2O (3:2, v:v, 3 ml).

(DUPA-Pep-EG$_4$)$_2$-ma-va-α−amanitin (102): yellowish powder (1.26 mg; yield= 17%). MS(ESI+) *m/z*: $[M+3Na]^{3+}$ calcd. for $C_{150}H_{206}N_{26}O_{47}S_3Na_3$: 1096.85, found: 1095.25;

$[M+2Na]^{2+}$ calcd. for $C_{150}H_{206}N_{26}O_{47}S_3Na_2$: 1633.79, found: 1633.67.

SMDC 103 (HDP 30.2490). (DUPA-Pep-EG_8-Cys)$_2$-mp-va-α-amanitin

Compound 113. Br-EG_8-Br

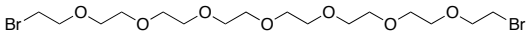

$C_{16}H_{32}Br_2O_7$
MW: 496,23

Commercially available octaethylene glycol (5.0 g, 13.5 mmol) was converted to the corresponding dibromine by applying the general procedure **GP 9.1.**

Br-EG_8-Br (113): orange oil (5.78 g, yield= 86%).

Compound 116. Br-EG_8-N_3

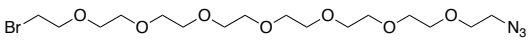

$C_{16}H_{32}BrN_3O_7$
MW: 458,35

Compound **113** (5.78 g, 12 mmol) was converted to the corresponding monoazide according to general procedure **GP 9.2**.

Compound 119. (Trt)S-EG_8-N_3

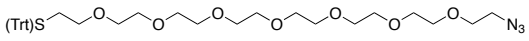

$C_{35}H_{47}N_3O_7S$
MW: 653,83

Compound **119** was obtained from the precursor **113** (5.5 g, 12 mmol theoretical) following the general procedure **GP 9.3**.
S(Trt)-EG_8-N_3 (119): orange oil (1.93 g, yield= 51%). MS(ESI$^+$) *m/z*: $[M+H]^+$ calcd. for $C_{35}H_{47}N_3O_7SNa$: 676.30, found: 676.42.

Compound 122. (Trt)S-EG_8-NH_2

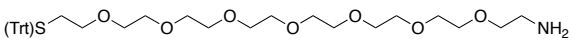

$C_{35}H_{49}NO_7S$
MW: 627,83

The general procedure **GP 9.4** was applied to convert compound **119** (654 mg, 1.0 mmol) into the corresponding primary amine.

S(Trt)-EG$_8$-NH$_2$ (122): yellowish oil (622.7 mg, yield= 99%). MS(ESI+) *m/z*: $[M+H]^+$ calcd. for $C_{35}H_{50}NO_7S$: 628.33, found: 628.42.

Compound 125. (O^{t}Bu)$_3$DUPA-Pep-EG$_8$-S(Trt)

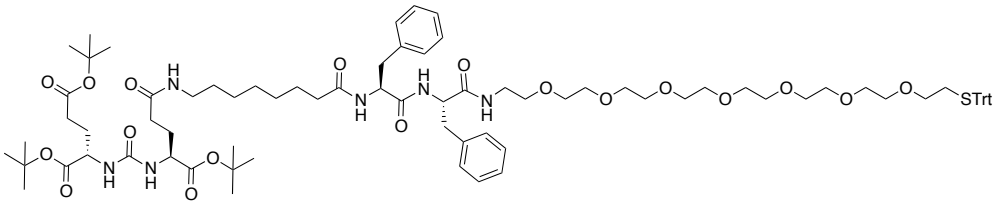

$C_{84}H_{120}N_6O_{18}S$
MW: 1533,95

(O^{t}Bu)$_3$DUPA-Pep-OSu **75** (78 mg, 0.077 mmol) was coupled to the carboxylate-reactive spacer **122** (50.8 mg, 0.081 mmol) as described in the general procedure **GP 9.5**.
The residue was dissolved in ACN:H_2O (9:1, v:v, 500 µl) and purified by preparative RP-HPLC: λ= 210 nm; gradient: 0-1 min 5% B; 1-14 min 54% B; 14-26 min 100% B; 26-30 min 100% B; 30-35 min 5% B; A= water with 0.05% TFA; B= ACN. The product was collected and directly lyophilized overnight.

(O^{t}Bu)$_3$DUPA-Pep-EG$_8$-S(Trt) (125): colorless powder (46.38 mg, yield= 40%). MS (ESI+) *m/z*: $[M+Na]^+$ calcd. for $C_{84}H_{120}N_6O_{18}SNa$: 1555.83, found: 1555.75; $[M+H+K]^{2+}$ calcd. for $C_{84}H_{121}N_6O_{18}SK$: 786.41, found: 786.92.

Compound 99. DUPA-Pep-EG$_8$-SH

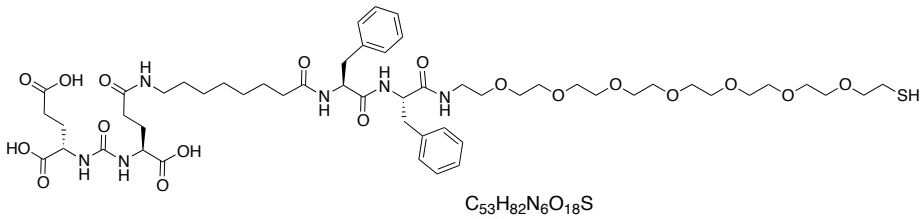

$C_{53}H_{82}N_6O_{18}S$
MW: 1123,31

As described in the general procedure **GP 9.6**, the compound **125** (46 mg, 0.030 mmol) was fully deprotected. The pellet was dissolved in ACN:H_2O (5:5, v:v, 200 µl) and purified by preparative RP-HPLC: λ= 210 nm; gradient: 0-1 min 5% B; 1-14 min 54% B; 14-26 min 100% B; 26-30 min 100% B; 30-35 min 5% B; A= water with 0.05% TFA; B= ACN. The product

was collected and lyophilized overnight.

DUPA-Pep-EG$_8$-SH (99): colorless powder (18.1 mg, yield= 54%). MS (ESI+) *m/z*: $[M+Na]^+$ calcd. for $C_{53}H_{82}N_6O_{18}SNa$: 1145.53, found: 1145.50; $[M+H+Na]^{2+}$ calcd. for $C_{53}H_{83}N_6O_{18}SNa$: 573.23 found: 573.33.

SMDC 103. (DUPA-Pep-EG$_8$)$_2$-ma-va-α-amanitin

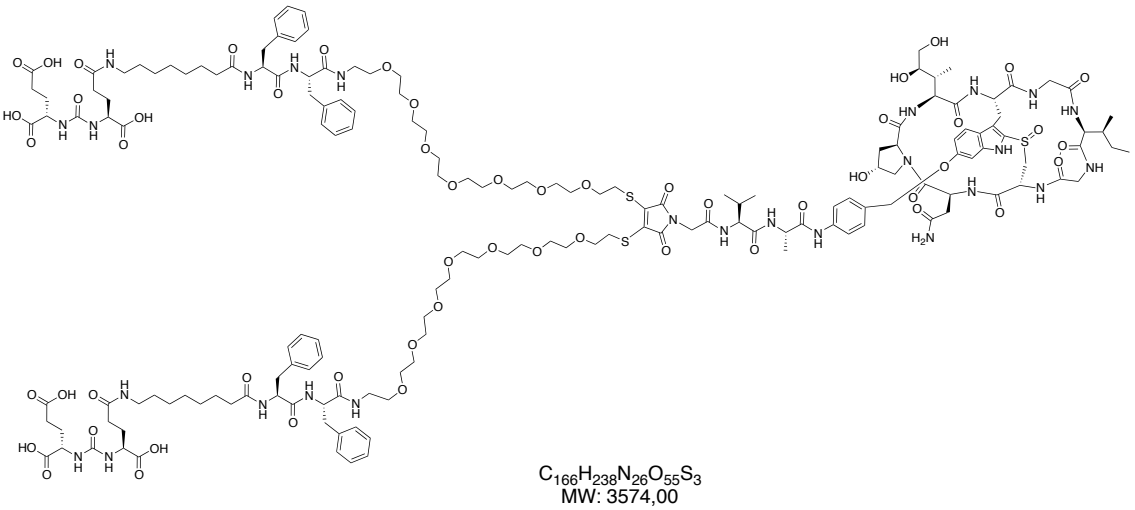

[3,4-*bis*(phenylthio)]-ma-α-Amanitin **108** (1.80 mg, 0.0012 mmol) was dissolved in MeOH (259 µl). A solution of **99** in MeOH (0.03 M, 174 µl, 0.0052 mmol) and a solution of NaOAc in MeOH (0.1 M, 90.5 µl, 0.009 mmol) were added sequentially. The reaction mixture was stirred at room temperature under argon for 20 h. The reaction mixture was then evaporated under reduced pressure. The residue was dissolved in ACN:H_2O (1:1, v:v, 200 µl) and purified by preparative RP-HPLC: λ= 210 nm; gradient: 0-1 min 5%-30% B; 1-18 min 50% B; 18-20 min 100% B; 20-22 min 100% B; 22-23 min 5% B; 23-25 min 5% B; A= water with 0.05% TFA, B= ACN. The product was collected and the solvents were evaporated. The residue was lyophilized overnight from ^{t}BuOH:H_2O, (4:1, 3 ml).

(DUPA-Pep-EG$_8$)$_2$-ma-va-α−amanitin (103): yellowish powder (3.12 mg, yield= 49%). MS(ESI-) *m/z*: $[M-2H]^{2-}$ calcd. for $C_{166}H_{236}N_{26}O_{55}S_3$: 1785.99, found: 1785.75; $[M-3H]^{3-}$ calcd. for $C_{166}H_{235}N_{26}O_{55}S_3$: 1190.33, found: 1190.17; $[M-4H]^{4-}$ calcd. for $C_{166}H_{234}N_{26}O_{55}S_3$: 892.49, found: 892.42.

SMDC 104 (HDP 30.2595). (DUPA-Pep-EG$_{12}$)$_2$-ma-va-α-amanitin

Compound 114. Br-EG$_{12}$-Br

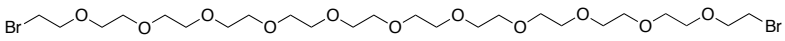

$C_{24}H_{48}Br_2O_{11}$
MW: 672,44

Commercially available dodecathylene glycol (2.48 g, 0.0045 mmol) was converted to the corresponding dibromine by applying the general procedure **GP 9.1.**

Br-EG$_{12}$-Br (114): yellowish oil (1.74 g, yield= 57%). MS(ESI+) *m/z*: $[M+H]^+$ calcd. for $C_{24}H_{49}Br_2O_{11}$: 673.45, found: 673.17; $[M+NH_4]^+$ calcd. for $C_{24}H_{52}Br_2O_{11}N$: 690.48, found: 690.25.

Compound 117. Br-EG$_{12}$-N$_3$

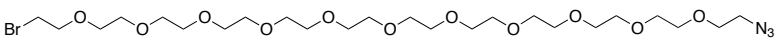

$C_{24}H_{48}BrN_3O_{11}$
MW:: 634,56

Compound **114** (1.74 g, 0.0026 mmol) was converted to the corresponding monoazide according to general procedure **GP 9.2**.

Compound 120. (Trt)S-EG$_{12}$-N$_3$

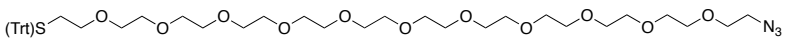

$C_{43}H_{63}N_3O_{11}S$
MW: 830,04

Compound **120** was obtained from the precursor **114** (1.64 g, 0.0026 mmol theoretical) following the general procedure **GP 9.3**.

S(Trt)-EG$_8$-N$_3$ (119): orange oil (1.94 g, yield= quant.).

Compound 123. (Trt)S-EG$_{12}$-NH$_2$

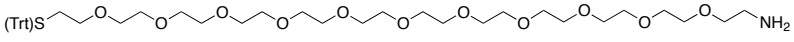

$C_{43}H_{65}NO_{11}S$
MW: 804,04

The general procedure **GP 9.4** was applied to convert compound **120** (2.91 g, 0.0035 mmol) into the corresponding primary amine.

S(Trt)-EG$_{12}$-NH$_2$ (123): yellowish oil (627 mg, yield= 22%). MS(ESI+) *m/z*: $[M+H]^+$ calcd.

for $C_{43}H_{66}NO_{11}S$: 804.44, found: 804.50; $[M+Na]^+$ calcd. for $C_{43}H_{65}NO_{11}SNa$: 826.42, found: 826.42.

Compound 126. $(O^tBu)_3$DUPA-Pep-EG_{12}-S(Trt)

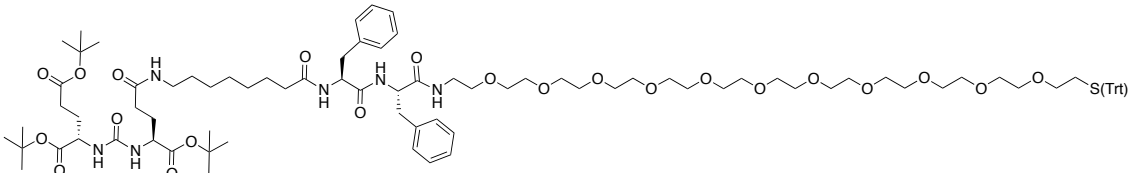

$C_{92}H_{136}N_6O_{22}S$
MW: 1710,16

$(O^tBu)_3$DUPA-Pep-OSu **75** (50.0 mg, 0.045 mmol) was dissolved in THF (545 µl). Compound **123** (41.3 mg, 0.051 mmol) and $NaHCO_3$ (4.16 mg, 0.050 mmol) were dissolved in H_2O (362 µl) and added to the first solution. The reaction mixture was stirred at room temperature for 2 h. The solvents were evaporated under reduced pressure and the residue dissolved in ACN:H_2O (1:1, v:v, 400 µl) for purification by preparative RP-HPLC: λ= 210 nm; gradient: 0 5% B; 15 min 100% B; 18 min 100% B; 18.5 min 5% B; 22 min 5% B; A= water with 0.05% TFA; B= ACN. The product was isolated and lyophilized overnight.

$(O^tBu)_3$DUPA-Pep-EG_{12}-S(Trt) (126): colorless powder (43.75 mg, yield= 57%). MS(ESI+) *m/z*: $[M-H]^-$ calcd. for $C_{92}H_{135}N_6O_{22}S$: 1707.94, found: 1707.67; $[M+HCOOH-H]^-$ calcd. for $C_{93}H_{137}N_6O_{24}S$: 1753.94, found: 1754.50; $[M+CF_3COOH-H]^-$ calcd. for $C_{94}H_{136}N_6O_{24}SF_3$: 1821.93; found: 1822.58.

Compound 100. DUPA-Pep-EG_{12}-SH

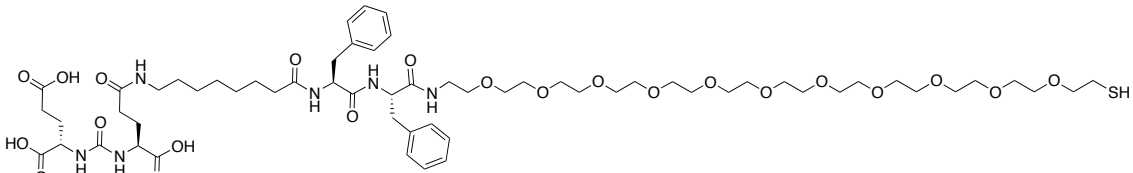

$C_{61}H_{98}N_6O_{22}S$
MW: 1299,52

$(O^tBu)_3$DUPA-Pep-EG_{12}-S(Trt) **126** (43.18 mg, 0.033 mmol) was deprotected according to the general procedure **GP 9.6**. The pellet was dissolved in ACN:H_2O (8:2, v:v, 200 µl) and purified by preparative RP-HPLC: λ= 210 nm; gradient: 0-1 min 5% B; 1-14 min 54% B; 14-26 min 100% B; 26-30 min 100% B; 30-35 min 5% B; A= water with 0.05% TFA; B= acetonitrile. The product was collected and lyophilized overnight.

DUPA-Pep-EG$_{12}$-SH (126): colorless powder (18.2 mg, yield= 55%). MS(ESI+) *m/z*: $[M+H]^+$ calcd. for $C_{61}H_{99}N_6O_{22}S$: 1299.65, found: 1299.58; $[M+NH_4]^+$ calcd. for $C_{61}H_{102}N_7O_{22}S$: 1316.68, found: 1316.42; $[M+Na]^+$ calcd. for $C_{61}H_{98}N_6O_{22}SNa$: 1321.64, found: 1321.58; $[M+K]^+$ calcd. for $C_{61}H_{98}N_6O_{22}SK$: 1337.61, found 1337.50; $[M+H+NH_4]^{2+}$ calcd. for $C_{61}H_{103}N_7O_{22}S$: 658.85, found: 658.92.

SMDC 104. (DUPA-Pep-EG$_{12}$)$_2$-mp-va-α-amanitin

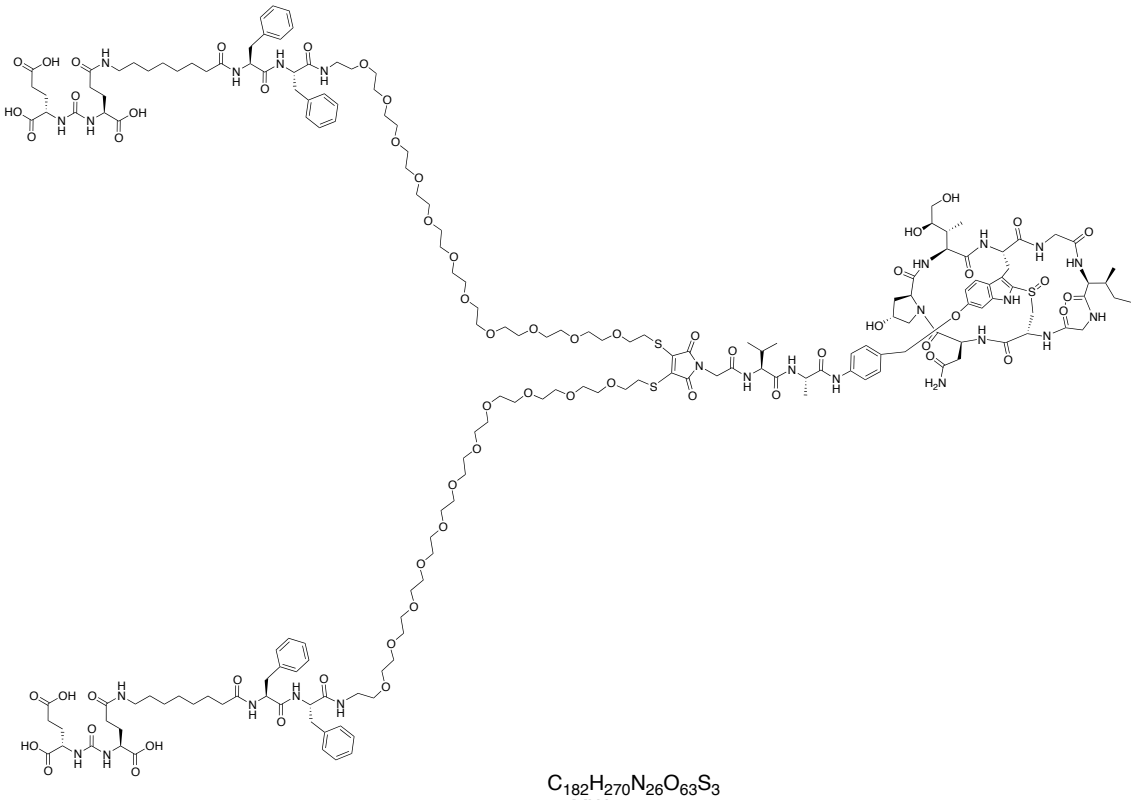

[3,4-*bis*(phenylthio)]-ma-α-Amanitin **108** (2.41 mg, 0.0016 mmol) was dissolved in MeOH (347 µl). A solution of **100** in MeOH (0.03 M, 230 µl, 0.0073 mmol) and a solution of NaOAc in MeOH (0.1 M, 140 µl, 0.013 mmol) were added sequentially and the mixture was stirred at room temperature under argon for 20 h. The reaction mixture was then evaporated under reduced pressure to dryness. The residue was dissolved in ACN:H_2O (1:1, v:v, 200 µl) and purified by preparative RP-HPLC: λ= 210 nm; gradient: 0-1 min 5%-30% B; 1-18 min 50% B; 18-20 min 100% B; 20-22 min 100% B; 22-23 min 5% B; 23-25 min 5% B; A= water with 0.05% TFA, B= ACN. The product was collected and the solvents were evaporated. The residue was lyophilized overnight in ^{t}BuOH:H_2O, (4:1, 3 ml).

(DUPA-Pep-EG$_{12}$)$_2$-mp-va-α-amanitin (104): yellowish powder (3.12 mg, yield= 49%).

MS(ESI-) *m/z*: $[M-2H]^{2-}$ calcd. for $C_{182}H_{268}N_{26}O_{63}S_3$: 1962.21, found: 1961.83; $[M-3H]^{3-}$ calcd. for $C_{182}H_{267}N_{26}O_{63}S_3$: 1307.8, found: 1307.58; $[M-4H]^{4-}$ calcd. for $C_{182}H_{267}N_{26}O_{63}S_3$: 980.60, found: 980.42.

Compound 127. mp-va-α-amanitin

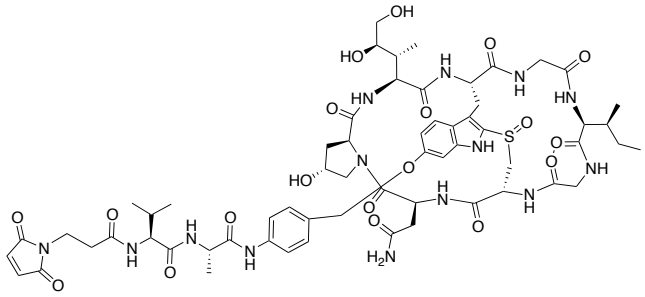

$C_{61}H_{80}N_{14}O_{19}S$
MW: 1345,44

va-α-Amanitin derivative **47a** (17.09 mg, 0.014 mmol) was dissolved in dry DMF (350 μl). BMPS (7.62 mg, 0.029 mmol) dissolved in DMF (350 µl), and undiluted DIPEA (9.79 µl, 0.057 mmol) were then added. After 1.5 h of stirring at room temperature under argon, the reaction mixture was dripped into precooled MTBE (40 ml) and centrifuged at 0 °C. The precipitate was collected and washed with MTBE (40 ml). The crude product was dried in vacuo and purified by RP-HPLC: λ= 305 nm; gradient: 0-5 min 5% B; 20-25 min 100% B; 27-35 min 5% B; A= water with 0.05% TFA; B= MeOH with 0.05% TFA. The product was isolated and lyophilized overnight.

mp-va-α-amanitin (127): colorless powder (12.51 mg, yield= 65%). MS(ESI+) *m/z*: $[M+Na]^+$ calcd. for $C_{61}H_{80}N_{14}O_{19}SNa$: 1367.53, found: 1367.50.

SMDC 105. DUPA-Pep-EG$_4$-mp-va-α-amanitin

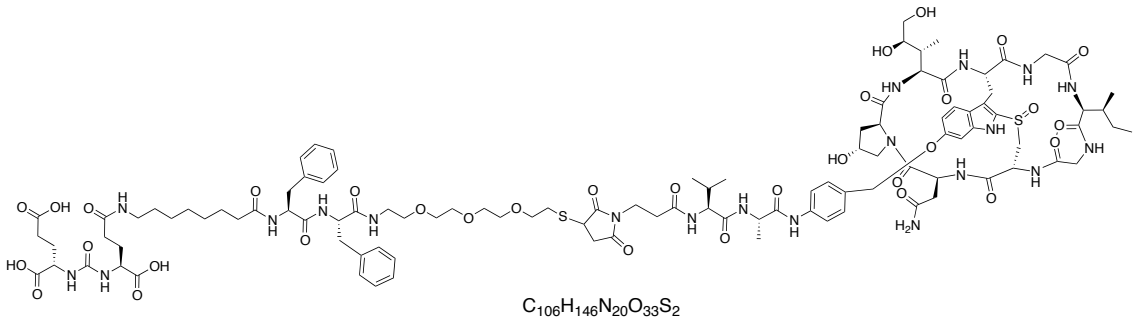

$C_{106}H_{146}N_{20}O_{33}S_2$
MW: 2292,54

mp-va-α-Amanitin derivative **127** (5.24 mg, 0.00439 mmol) was coupled to the sequence DUPA-Pep-EG$_4$-SH **98** (5.7 mg, 0.0039 mmol) as reported in the general procedure **GP 10.**

DUPA-Pep-EG$_4$-mp-va-α-amanitin (105): colorless powder (3.54 mg, yield= 43%). MS(ESI-) *m/z*: [M-H]$^-$ calcd. for $C_{106}H_{145}N_{20}O_{33}S_2$: 2289.97, found: 2290.92; [M-2H]$^{2-}$ calcd. for $C_{106}H_{144}N_{20}O_{33}S_2$: 1144.48, $^-$ found: 1144.92.

SMDC 106. DUPA-Pep-EG$_8$-mp-va-α-amanitin

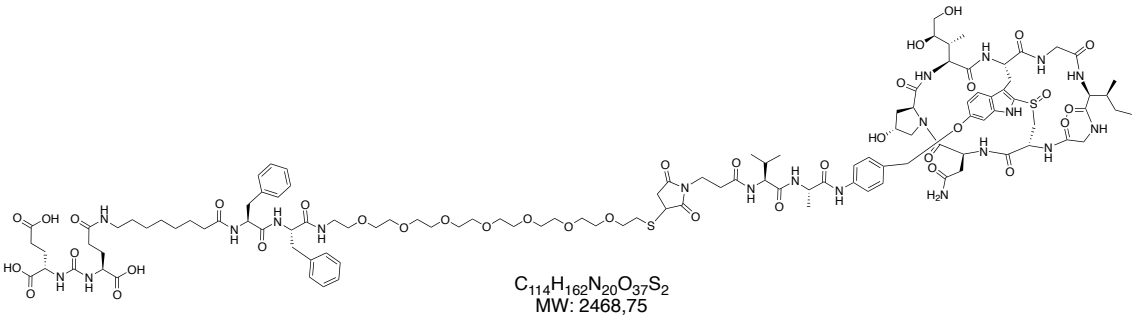

According to the general procedure **GP 10**, mp-va-α-amanitin derivative **127** (7.20 mg, 0.0046 mmol) was coupled to the sequence DUPA-Pep-EG$_8$-SH **99** (5.22 mg, 0.0046 mmol).

DUPA-Pep-EG$_8$-mp-va-α-amanitin (106): colorless powder (2.95 mg, yield= 41%). MS(ESI+) *m/z*: [M+H+K]$^{2+}$ calcd. for $C_{114}H_{163}N_{20}O_{37}S_2K$: 1254.43, found: 1254.80.

SMDC 107. DUPA-Pep-EG$_{12}$-mp-va-α−amanitin

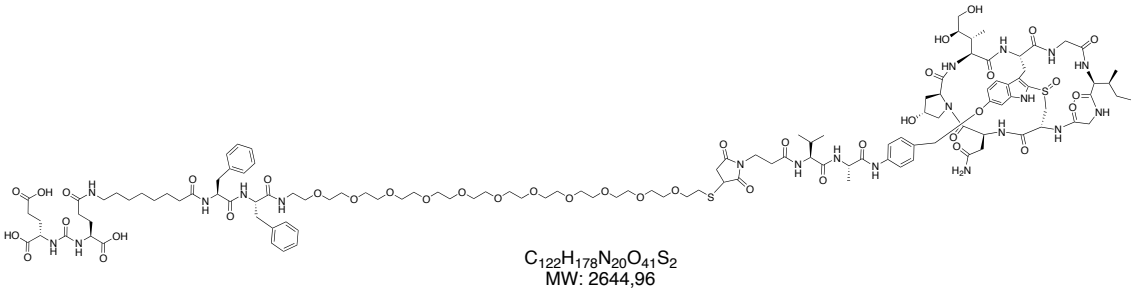

The geneeral procedure **GP 10** was used to couple the mp-va-α-amanitin derivative **127** (3.28 mg, 0.0021 mmol) to the sequence DUPA-Pep-EG$_{12}$-SH **100** (2.75 mg, 0.0021 mmol).

DUPA-Pep-EG$_{12}$-mp-va-α−amanitin (107): colorless powder (1.08 mg, yield= 20%). MS(ESI-) *m/z*: [M-H]$^-$ calcd. for $C_{122}H_{177}N_{20}O_{41}S_2$: 2643.95, found: 2643.33; [M+AcOH-H]$^-$ calcd. for $C_{124}H_{181}N_{20}O_{43}S_2$: 2704.00, found: 2703.42; [M-2H]$^{2-}$ calcd. for $C_{122}H_{176}N_{20}O_{41}S_2$: 1321.47, found: 1321.25; [M+TFA-2H]$^{2-}$ calcd. for $C_{124}H_{177}N_{20}O_{43}S_2F_3$: 1378.49, found:

1377.85 ca.; $[M+2TFA-2H]^{2-}$ calcd. for $C_{126}H_{178}N_{20}O_{45}S_2F_6$: 1435.50, found: 1434.42.

Fc-SMDC (128). DUPA-Pep-Fc-α-amanitin

Compound 130. DUPA-Pep-$(EG_3)_2$-Orn(N_3)-Lys(Gly-Gly-Gly)-NH_2

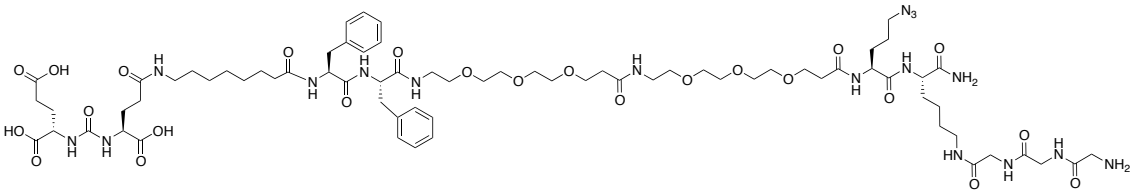

$C_{72}H_{113}N_{17}O_{24}$
MW: 1600,77

AmphiSpheres® 40 RAM resin (703 mg, 0.267 mmol) was swollen for 1 h in DCM, and then washed with and resuspended in DMF for 0.5 h. The resin was deprotected with 20% piperidine in DMF (rt, 30 s, [x1]; 30 W, 50 °C, [x1]) and then shaken with Fmoc-Lys(Mtt)-OH (4.0 equiv), TBTU (3.99 equiv), DIPEA (8.0 equiv) in DMF (8 ml) for 1 h at rt and then under MW irradiation (30 W, 50 °C, 3 min). Coupling was repeated twice with several DMF washing in between. The Fmoc protecting group was removed by suspending the resin in 20% piperidine in DMF (3 ml) under the conditions described above. Each coupling was then performed by shaking the resin with the Fmoc-protected amino acid (4.0 equiv), TBTU (3.99 equiv), DIPEA (8.0 equiv) in DMF (8 ml) under MW irradiation (30 W, 50 °C, 3 min, x3), followed by Fmoc-removal in the conditions mentioned herein. Protected DUPA precursor **44** (3.0 equiv) was coupled by using TBTU (2.99 equiv), DIPEA (6.0 equiv) under MW irradiation (30 W, 50 °C, 3 min, x3). Prior to cleavage, Mtt protecting group was removed by suspending the resin-bound peptide in DCM:TIS:TFA (97:2:1, v:v:v, 4 ml) and shaking at rt for 10 min (approx. 20 cycles). The Fmoc-Gly-Gly-Gly-OH was then coupled to the Lys-N(ε) primary amine and the Fmoc group was removed by using the same conditions here described for coupling and Fmoc-deprotection, respectively. The resin was then extensively washed with DCM and dry in vacuo. The peptide was cleaved from the resin and totally deprotected by suspending the resin-bound peptide in the TFA:anisole:TIS:H_2O (94:2:2:2, v:v:v:v, 20 ml) mixture for 2 h at rt. The mixture was precipitated in four portions in precooled MTBE (40 ml each) and pellet collected by centrifugation at 0 °C (4500 rpm, 10 min). The pellets were collected, dried in vacuo and dissolved in ACN:H_2O (1:1, v:v) for purification by RP-HPLC: λ= 210 nm; gradient: 0 min 5% B; 14 min 40% B; 19 min 45% B; 20-21 min 100% B; 22 min 5% B; A= water with 0.05% TFA, B= ACN. The title compound was collected and directly lyophilized overnight.

DUPA-Pep-$(EG_3)_2$-Orn(N_3)-Lys(Gly-Gly-Gly)-NH_2 (130): colorless powder (119.46 mg, yield= 28%). t_R= 14.51 min. MS(ESI-) *m/z*: $[M-H]^-$ calcd. for $C_{72}H_{112}N_{17}O_{24}$: 1598.81, found: 1598.83; $[M-2H]^{2-}$ calcd. for $C_{72}H_{111}N_{17}O_{24}^-$: 798.9, found 799.00.

Compound 132. DBCO-va-α-amanitin

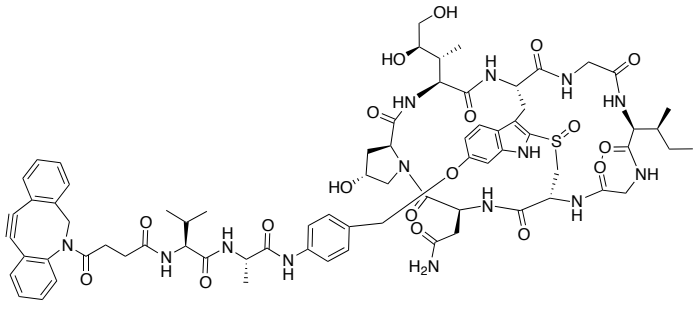

$C_{73}H_{88}N_{14}O_{18}S$
MW: 1481,63

Precursor **47a** (80.32 mg, 0.067 mmol) was dissolved in dry DMF (1.6 ml). DBCO-SE (29.8 mg, 0,074 mmol) dissolved in DMF (1,6 ml) and undiluted DIPEA (22,9 µl, 0,13 mmol) were added to the solution. The reaction mixture was stirred at room temperature for 2.5 h. The reaction was quenched by adding H_2O (100 µl) and DMF was evaporated in vacuo. The residue was dissolved in MeOH (2 ml) and dripped into precooled MTBE (40 ml) and centrifuged at 0 °C (4500 rpm, 4 min). The pellet was washed with MTBE (40 ml), collected and dried in vacuo. The compound was purified by RP-HPLC: λ= 305 nm; gradient: 0-15 min 5% B; 18 min 100% B; 1,5-22 min 5% B; A= water with 0.05% TFA, B= ACN. The product was isolated and directly lyophilized overnight.

DBCO-va-α-amanitin (132): colorless powder (77.88 mg, yield= 78%). MS(ESI+) *m/z*: $[M+H]^+$ calcd. for $C_{73}H_{89}N_{14}O_{18}S$: 1481.62, found 1481.42; $[M+2H]^{2+}$ calcd. for $C_{73}H_{90}N_{14}O_{18}S$: 741.32, found 741.42.

Cloning of plasmid for protein expression

pEXPR-TEV-G5-H20C-Fc-LPETGG vector was kindly provided us by Prof. H. Kolmar (TU Darmstadt, Germany). The plasmid encoded for the following sequence:

Fc-LPETGG:

AENLYFQGGGGGEPKSCDKTHTCPPCPAPELLGGPSVFLFPPKPKDTLMIS RTPEVTCVVVDVSHEDPEVKFNWYVDGVEVHNAKTKPREEQYASTYRVVS VLTVLHQDWLNGKEYKCKVSNKALPAPIEKTISKAKGQPREPQVYTLPPSR DELTKNQVSLTCLVKGFYPSDIAVEWESNGQPENNYKTTPPVLDSDGSFFL YSKLTVDKSRWQQGNVFSCSVMHEALHNHYTQKSLSLSPGGSLPETGG

TEV cleavage site

H20 region
Fc domain (CH2-CH3)
SrtA tag

Expression and purification of the protein Fc-LPETGG (129)

Expi293F™ cells were transiently transfected with the Fc-LPETGG construct using the polyethylenimine (PEI) reagent in accordance to the manufacturer's instructions. Expi293F™ cells were cultivated in 2 l flasks with a final volume of 500 ml of Expi293 culture medium per flask. Transfection complex was prepared by mixing 1.5 ml of PEI reagent (1 mg/ml in H_2O) with 500 µg of DNA in 50 ml of Opti-MEM medium. After 15 min incubation at room temperature, the transfection mixture was added to a suspension of Expi293F™ cells in 425 ml volume. At 16 h after transfection, cells were centrifuged at 460 *x g* at room temperature for 20 min, supernatant was discarded and 500 ml of fresh Expi293F™ expression medium was added. At day 6 after transfection, cells were centrifuged at 3488 *x g* and 4 °C for 40 min, while the supernatant was centrifuged at 10947 *x g* at 4 °C for 20 min. The culture medium was diluted with 500 ml of PBS buffer and centrifuged through 1.2, 0.65, 0.45, 0.22 µm sterile filters. The final solution was applied to a Protein A column. The column was washed with binding buffer (PBS pH 7.4) and bound fraction eluted with elution buffer (glycine 0.1 M pH 3.0) and neutralized with neutralization buffer (Tris-HCl 1 M pH 9.0). Collected protein sample was dyalized against SrtA buffer (Tris-HCl 50 mM pH 7.4, NaCl 150 mM) at 4 °C overnight. Protein concentration was determined by $Abs_{280\ nm}$ to be 4.8 mg/ml (122.5 mg/l of culture).

Production of eSrtA enzyme

eSrtA was kindly provided us by Prof. Kolmar (TU Darmstadt, Germany).

Programmed protein conjugate 131. DUPA-Pep-Fc

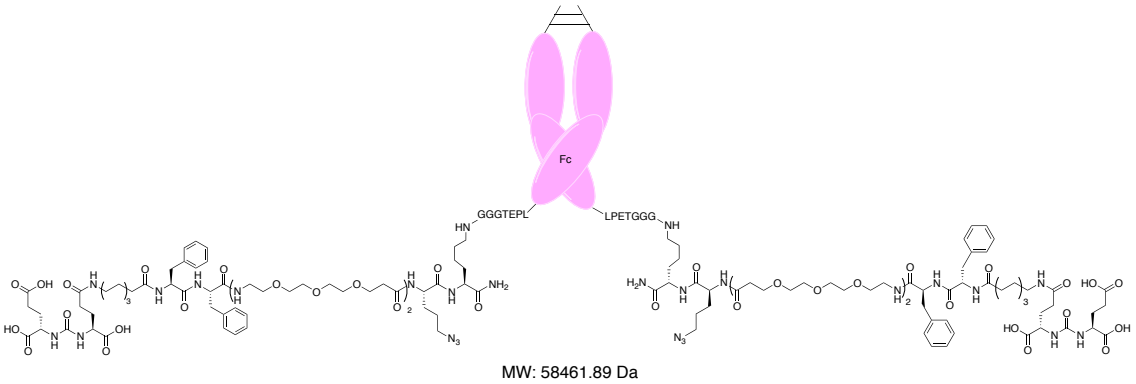

Protein A purified Fc-LPETGG **129** (40 mg, 20.65 µM) was mixed with the linker **130** (50 equiv., 1 mM) in the SrtA reaction-buffer (Tris-HCl 50 mM pH 7.5, NaCl 150 mM, $CaCl_2$ 5

mM) in presence of the eSrtA enzyme (0.125 eq, 2.6 µM). The reaction was allowed to proceed for 18 h at 25°C and then purified using SEC-FPLC over a HiLoad™ 26/600 Superdex™ 200 pg column to remove eSrtA and excess of peptide **130**. The column was first equilibrated with PBS buffer (pH 7.4) and then DUPA-Fc **131** eluted by using the same buffer as used for column equilibration. The flow through from the column was concentrated using an Amicon® Ultra-15 Centrifugal Filter (MWCO 50000) and filtered through a 0.22 µm sterile filter (Sterile Millex® Filter). Concentration of DUPA-Fc conjugate **131** was determined to be 3.6 mg/ml (27.87 mg) by $Abs_{280\ nm}$ (MW= 58461.89 Da, ε_{280}= 74675.1 $cm^{-1}M^{-11}$).

Protein and armed protein conjugate 128 (HDP 30.2972). DUPA-Pep-Fc-α-amanitin DC

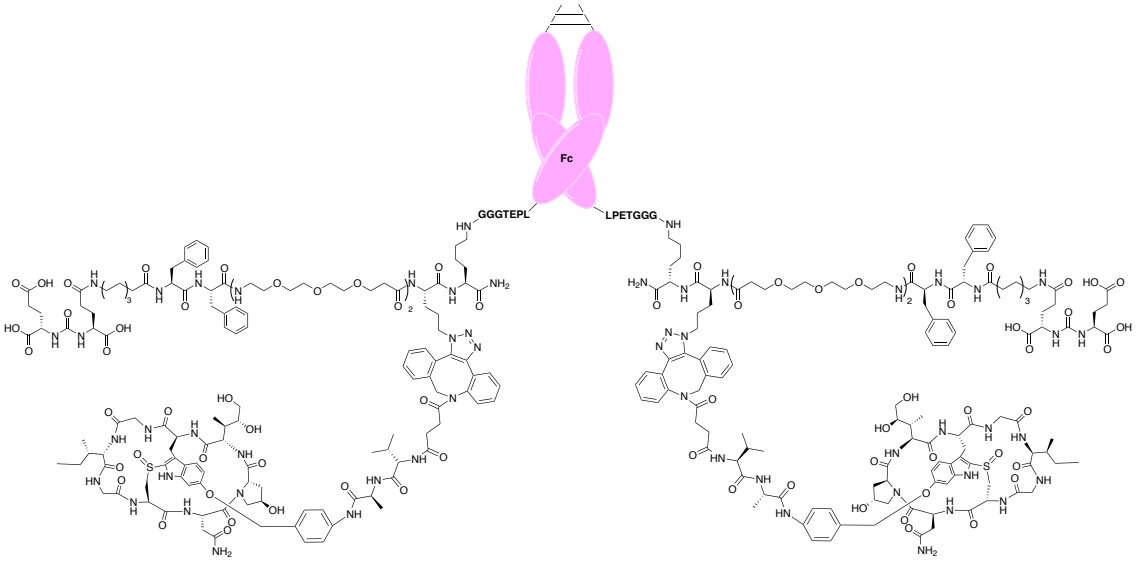

DBCO-va-α-amanitin derivative **132** (12.18 mg, 20 equiv.) was dissolved in ACN:H_2O (3:1, v:v, 1.28 ml) and added to DUPA-Pep-Fc **131** (24 mg, 48.6 µM) in PBS buffer (pH 7.4, 8.46 ml). DMSO (2.24 ml; ca. 20%) was added. The mixture was incubated at 37 °C for 24 h. Purification was performed by SEC-FPLC over a HiLoad™ 16/600 Superdex™ 200 pg column. The conjugate was concentrated to a final volume of 7.5 ml and then filtered through a 0.22 µm sterile filter prior to its use in biological assays. Concentration of DUPA-Pep-Fc-α-amanitin conjugate **128** was determined to be 3.16 mg/ml (23.7 mg) by $Abs_{280\ nm}$ (MW= 61425.21 Da, ε_{280}= 85500 $cm^{-1}M^{-11}$).

In vitro and *in vivo* studies

In vitro studies were performed at Heidelberg Pharma Research GmbH, Dept. of Biochemistry. *In vivo* studies were carried out at the animal facility of Heidelberg Pharma Research GmbH,

Dept. of Pharmacology.

Detailed procedures are described in the thesis of the PhD candidate Barbara Korsak.

Appendix

Figure A1. Analytical HPLC trace of SMDC **37**. Gradient: 0-1 min 5% B, 14 min 54% B, 26-30 min 100% B, 31-35 min 5%B (A= H_2O with 0.05% TFA, B= ACN); l= 305 nm; flow rate= 1.4 ml min^{-1}.

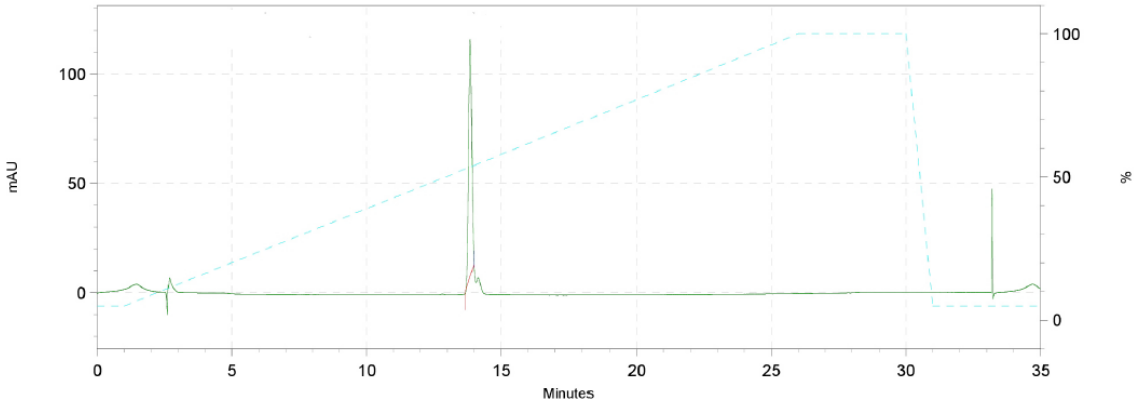

Figure A2. Analytical HPLC trace of SMDC **38**. Gradient: 0-1 min 5% B, 14 min 54% B, 26-30 min 100% B, 31-35 min 5%B (A= H_2O with 0.05% TFA, B= ACN); l= 305 nm; flow rate= 1.4 ml min^{-1}.

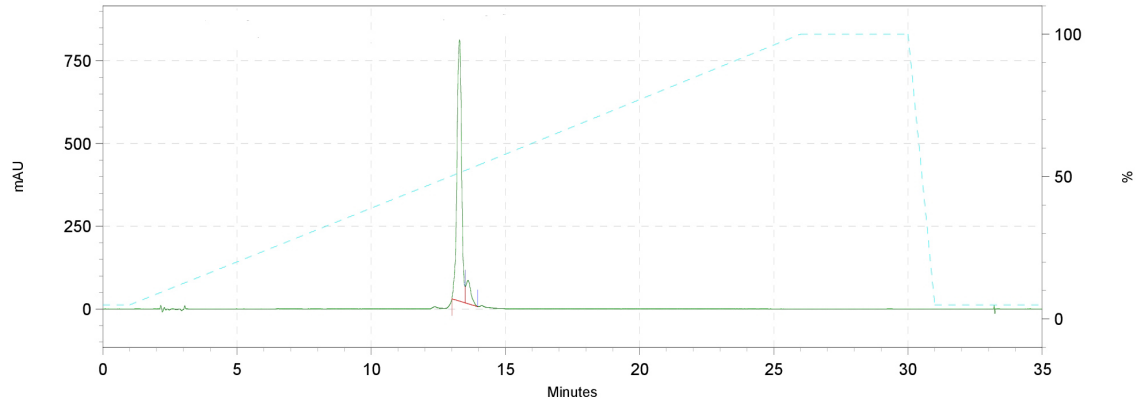

Figure A3. Analytical HPLC trace of SMDC **39**. Gradient: 0-1 min 5% B, 21 min 54% B, 26-30 min 100% B, 31-35 min 5%B (A= H_2O with 0.05% TFA, B= ACN); l= 305 nm; flow rate= 1.4 ml min^{-1}.

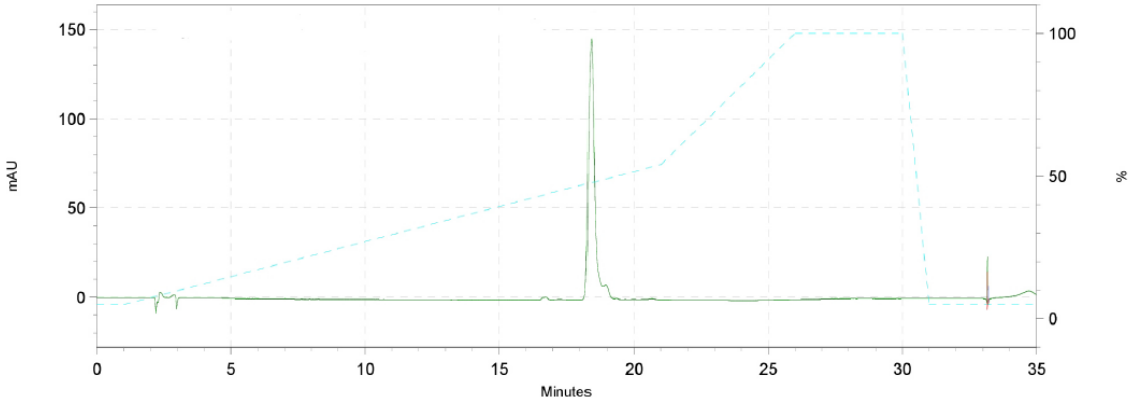

Figure A4. Analytical HPLC trace of SMDC **58**. Gradient: 0 min 5% B, 14 min 54% B, 16 min 61% B, 19-22 min 100%B, 23-26 min 5% B (A= H_2O with 0.05% TFA, B= ACN); l= 305 nm; flow rate= 1.4 ml min^{-1}.

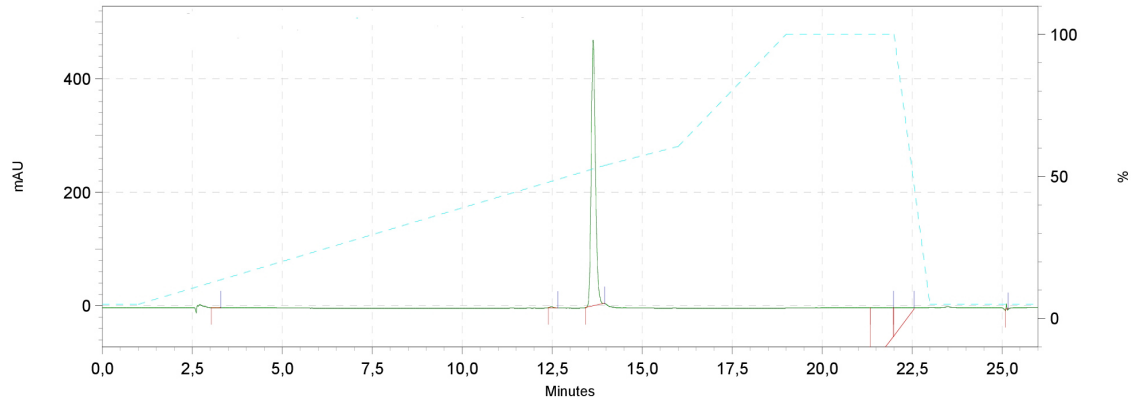

Figure A5. Analytical HPLC trace of SMDC **59**. Gradient: 0 min 5% B, 15-18 min 100% B, 18.5-22 min 5% B (A= H_2O with 0.05% TFA, B= ACN); l= 305 nm; flow rate= 1.4 ml min^{-1}.

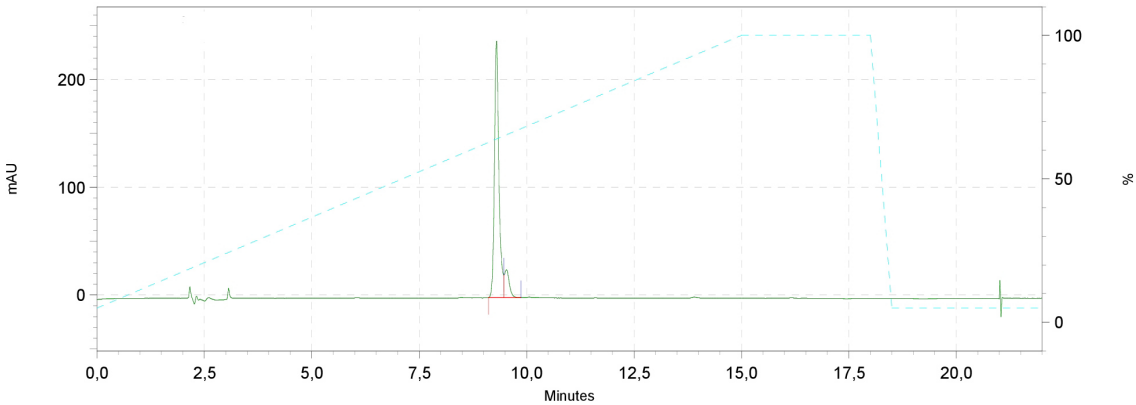

Figure A6. Analytical HPLC trace of SMDC **60**. Gradient: 0 min 5% B, 14 min 54% B, 16 min 61% B, 19-22 min 100%B, 23-26 min 5% B (A= H_2O with 0.05% TFA, B= ACN); l= 305 nm; flow rate= 1.4 ml min^{-1}.

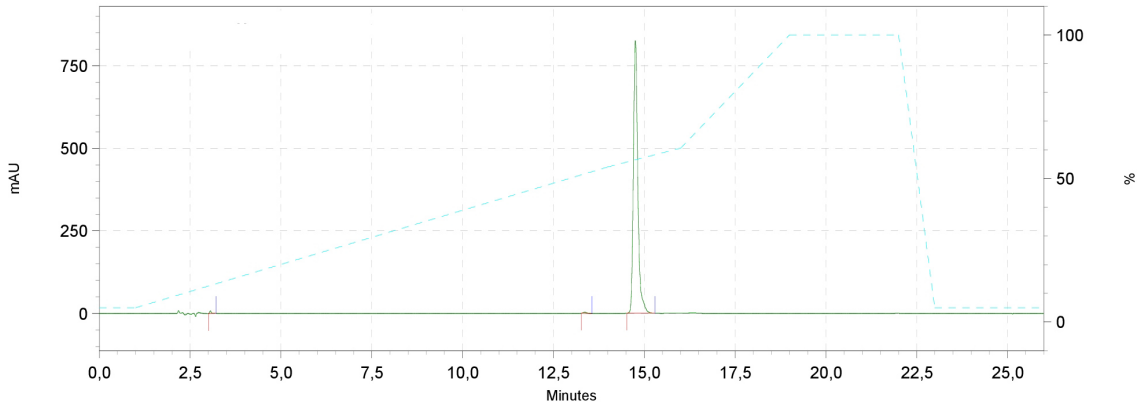

Figure A7. Analytical HPLC trace of SMDC **61**. Gradient: 0 min 5% B, 15-18 min 100% B, 18.5-22 min 5% B (A= H_2O with 0.05% TFA, B= ACN); l= 305 nm; flow rate= 1.4 ml min^{-1}.

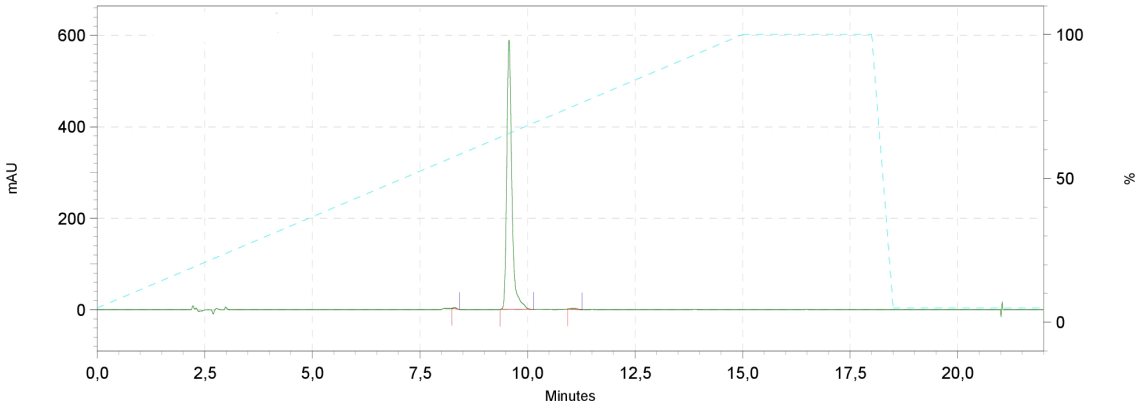

Figure A8. Analytical HPLC trace of SMDC **62**. Gradient: 0 min 5% B, 15-18 min 100% B, 18.5-22 min 5% B (A= H_2O with 0.05% TFA, B= ACN); l= 305 nm; flow rate= 1.4 ml min^{-1}.

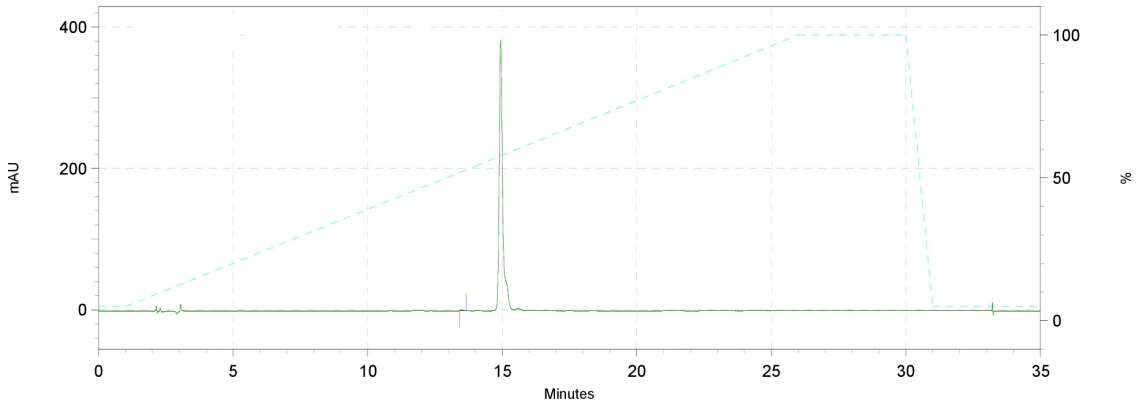

Figure A9. Analytical HPLC trace of SMDC **80**. Gradient: : 0-5 min 5% B; 20-25 min 100% B; 27-35 min 5% B (A= water; B= MeOH); l= 305 nm; flow rate= 1.4 ml min^{-1}.

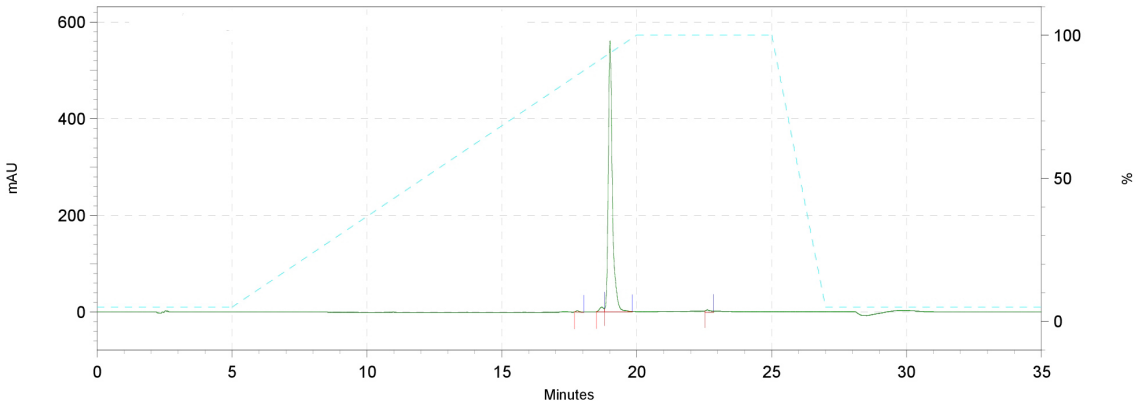

Figure A10. Analytical HPLC trace of SMDC **81**. Gradient: 0-1 min 5% B, 14 min 54% B, 26-30 min 100% B, 31-35 min 5%B (A= H_2O with 0.05% TFA, B= ACN); l= 305 nm; flow rate= 1.4 ml min^{-1}.

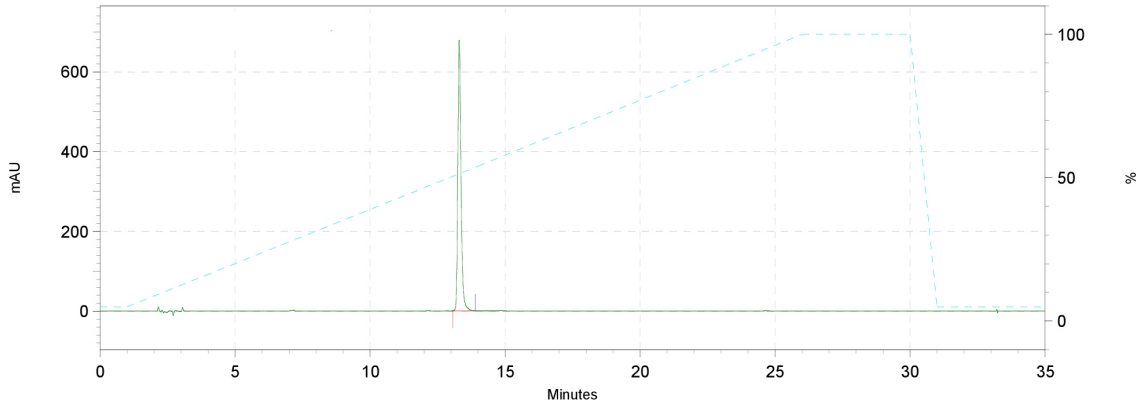

Figure A11. Analytical HPLC trace of SMDC **88**. Gradient: 0-1 min 5% B, 14 min 54% B, 26-30 min 100% B, 31-35 min 5%B (A= H_2O with 0.05% TFA, B= ACN); l= 305 nm; flow rate= 1.4 ml min^{-1}.

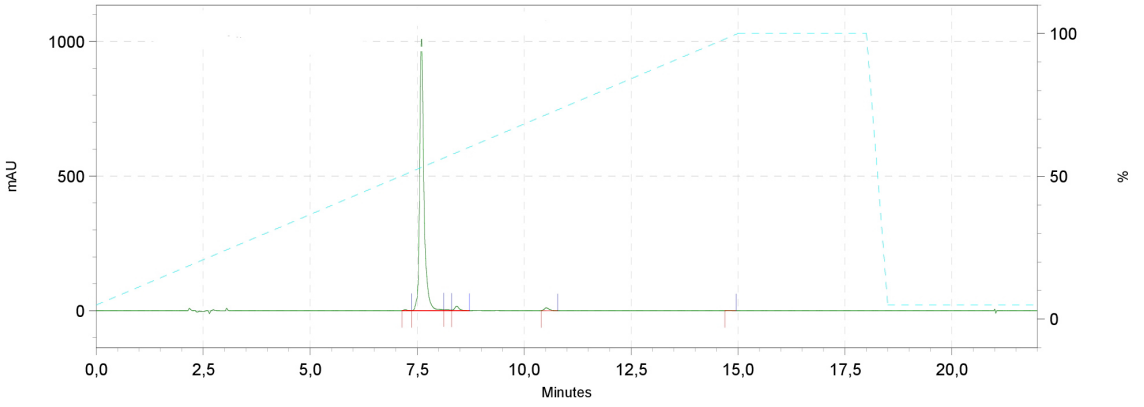

Figure A12. Analytical HPLC trace of SMDC **101**. Gradient: 0-1 min 5% B, 14 min 54% B, 26-30 min 100% B, 31-35 min 5%B (A= H_2O with 0.05% TFA, B= MeOH); l= 246 nm; flow rate= 1.4 ml min^{-1}.

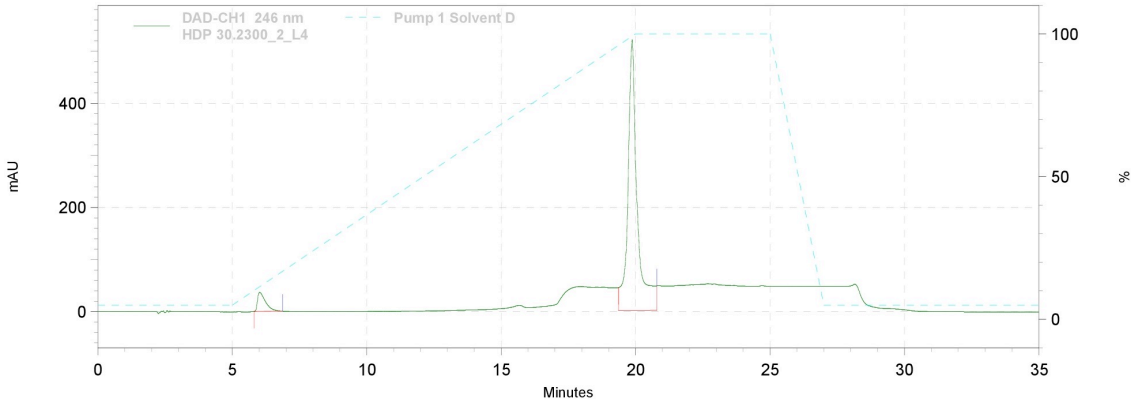

Figure A13. Analytical HPLC trace of SMDC **102**. Gradient: 0-1 min 5% B, 14 min 54% B, 26-30 min 100% B, 31-35 min 5%B (A= H_2O with 0.05% TFA, B= ACN); l= 305 nm; flow rate= 1.4 ml min^{-1}.

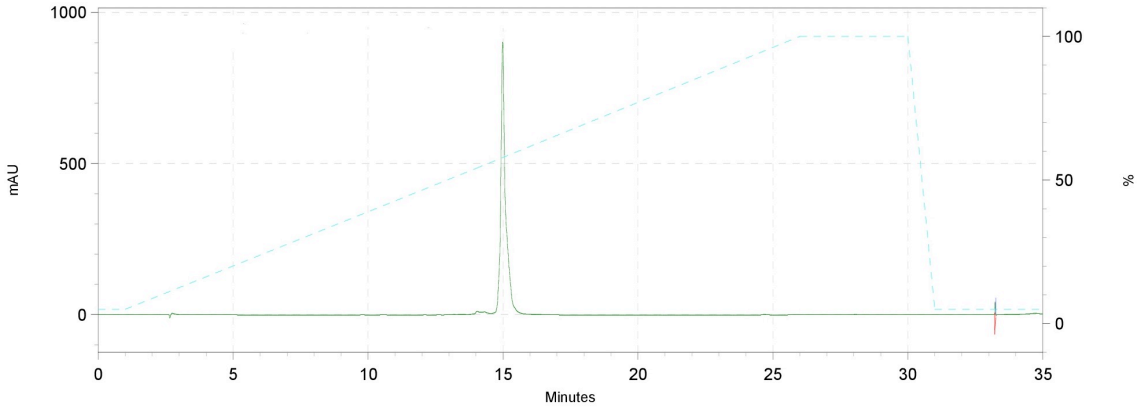

Figure A14. Analytical HPLC trace of SMDC **103**. Gradient: 0-1 min 5%-30% B; 1-18 min 50% B; 18-20 min 100% B; 20-22 min 100% B; 22-23 min 5% B; 23-25 min 5% B; A= water with 0.05% TFA, B= ACN); l= 305 nm; flow rate= 1.4 ml min^{-1}.

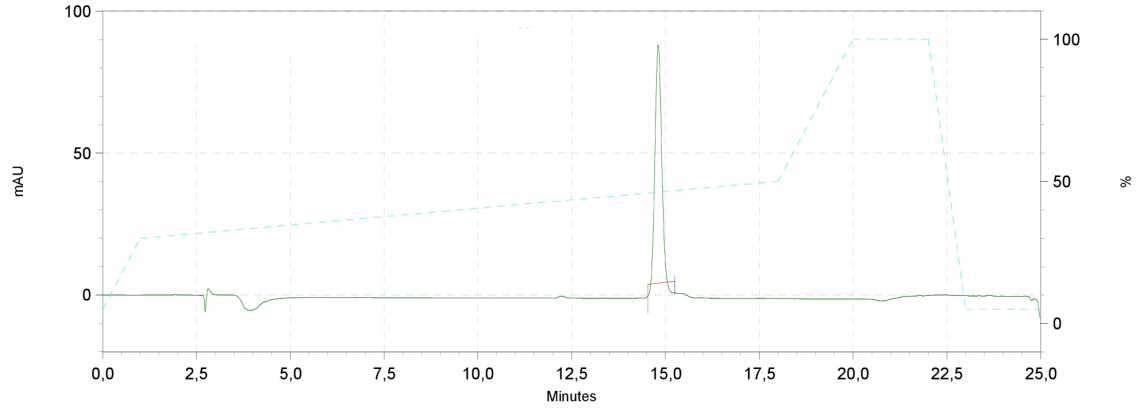

Figure A15. Analytical HPLC trace of SMDC **104**. Gradient: 0 min 5% B, 15-18 min 100% B, 18.5-22 min 5% B; 23-25 min 5% B (A= water with 0.05% TFA, B= ACN); l= 305 nm; flow rate= 1.4 ml min^{-1}.

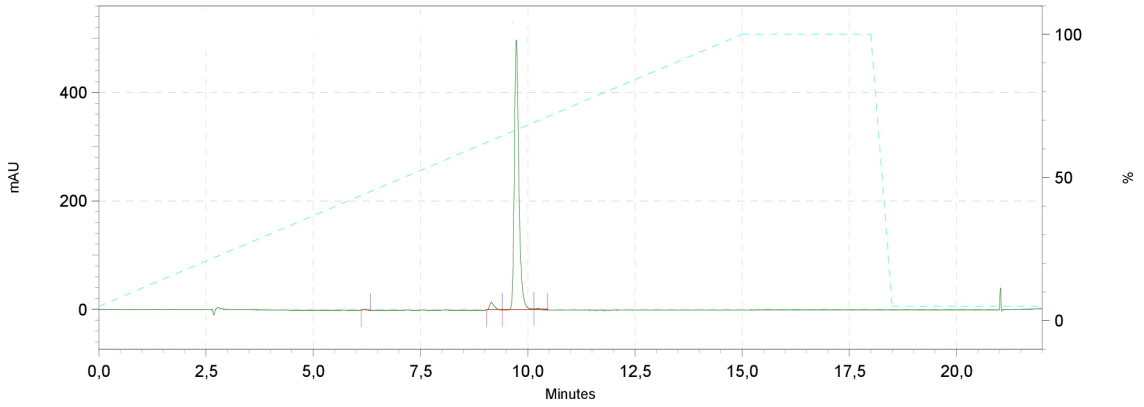

Figure A16. Analytical HPLC trace of SMDC **105**. Gradient: 0-1 min 5%-30% B; 14-18 min 54% B; 18 min 69% B; 19-20 min 100% B; 21-22 min 5% B (A= water with 20.05% TFA, B= ACN); l= 305 nm; flow rate= 1.4 ml min^{-1}.

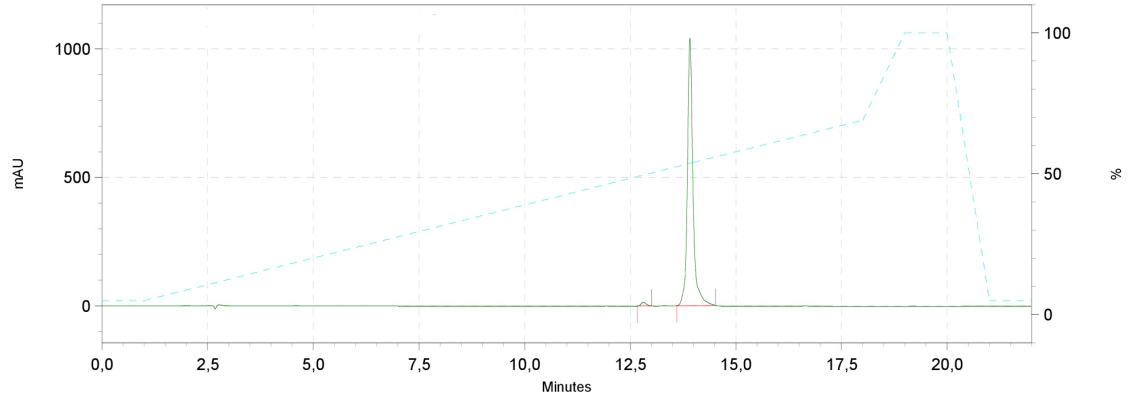

Figure A17. Analytical HPLC trace of SMDC **106**. Gradient: 0-1 min 5% B, 14 min 54% B, 26-30 min 100% B, 31-35 min 5%B (A= H_2O with 0.05% TFA, B= ACN); l= 305 nm; flow rate= 1.4 ml min^{-1}.

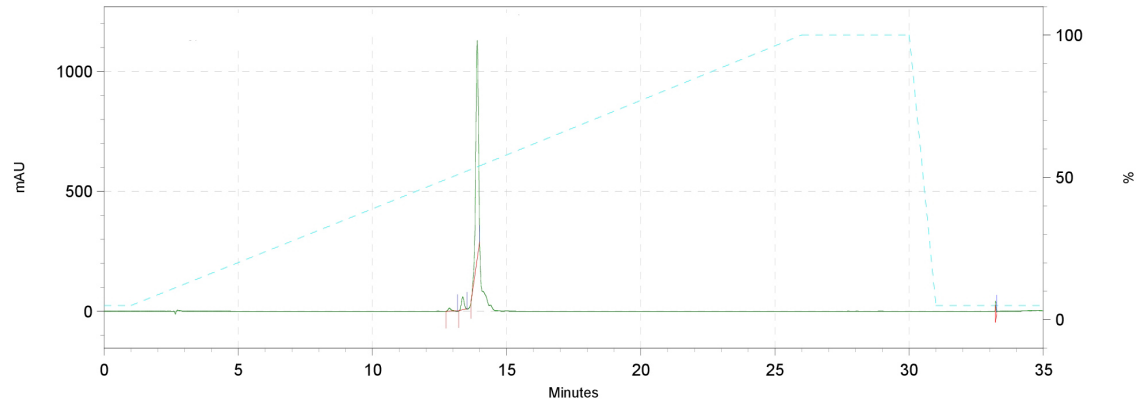

Figure A18. Analytical HPLC trace of SMDC **107**. Gradient: 0-1 min 5% B, 14 min 54% B, 26-30 min 100% B, 31-35 min 5%B (A= H_2O with 0.05% TFA, B= ACN; A= water with 0.05% TFA, B= ACN); l= 305 nm; flow rate= 1.4 ml min^{-1}.

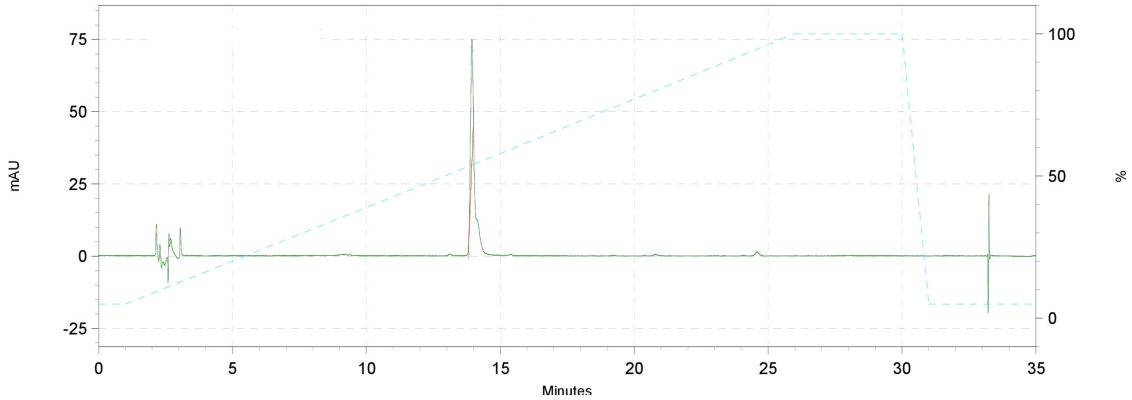

Figure A19. SEC-HPLC trace of purified Fc-LPETGG (**129**) under native non-reducing conditions (λ= 280 nm; buffer: 0.05% NaN_3 + 0.1mol/l Na_2SO_4 in 0.1 mol/l $NaPO_4$ pH 6.7; flow rate: 0.35 ml/min).

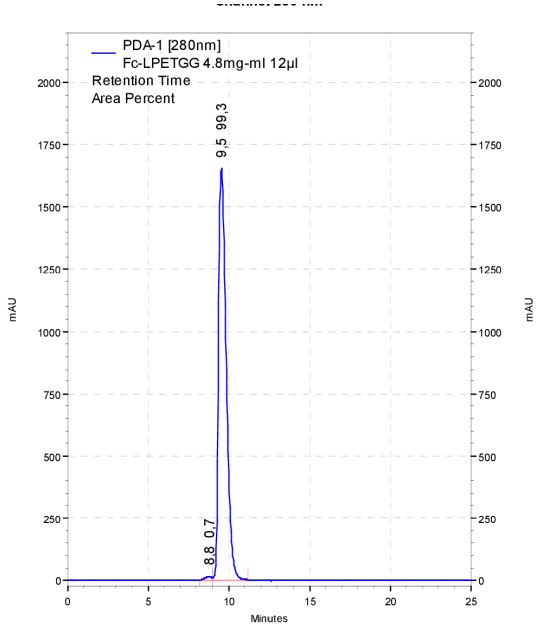

Figure A20. SEC-HPLC of purified DUPA-Pep-Fc (**131**) under native non-reducing conditions (λ= 280 nm; buffer: 0.05%NaN_3 + 0.1mol/l Na_2SO_4 in 0.1 mol/l $NaPO_4$ pH 6.7; flow rate: 0.35 ml/min).

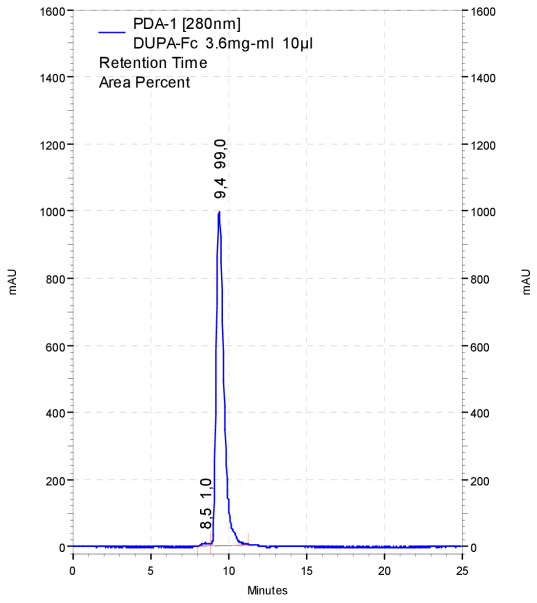

Figure A21. SEC-HPLC of purified DUPA-Pep-Fc-α-amanitin Fc-SMDC (**128**) under native non-reducing conditions at λ= 280 nm (left panel) and λ= 310 nm (right panel) (buffer: 0.05%NaN_3 + 0.1mol/l Na_2SO_4 in 0.1 mol/l $NaPO_4$ pH 6.7; flow rate: 0.35 ml/min).

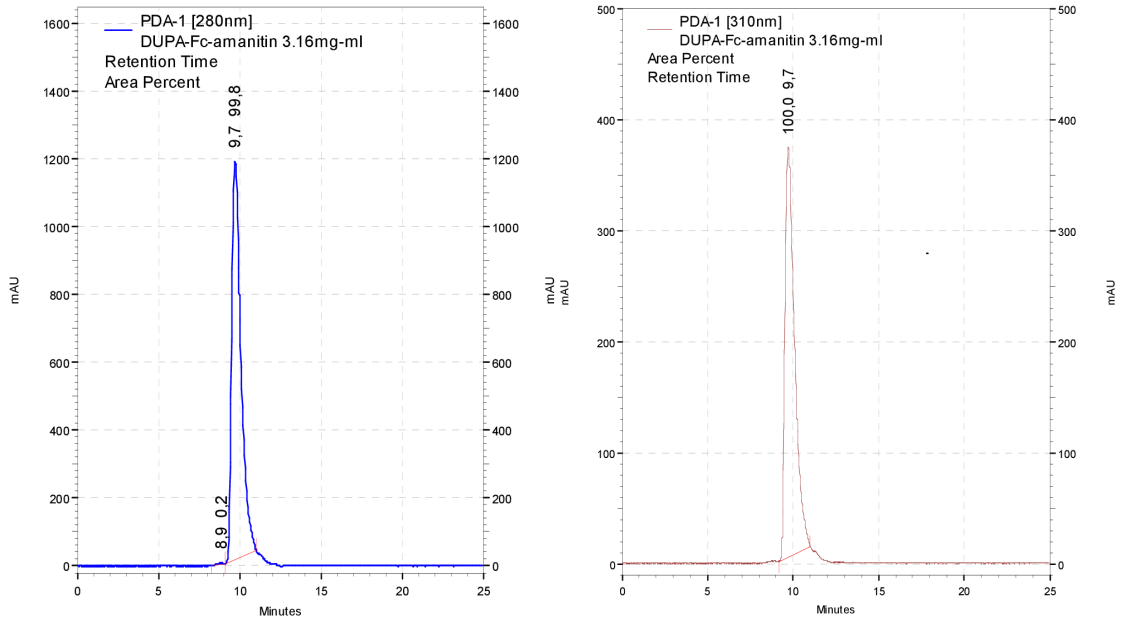

Bibliography

(1) Xu, J. and Mao, W. *J. Cancer. Ther.* **2016**, *7*, 762-772.

(2) Bray, F.; Ferlay, J.; Soerjomataram, I.; Siegel, R. L.; Torre, L. A. and Jemal, A. *CA Cancer J. Clin.* **2018**, *68*, 394-424.

(3) "Focusing on the cell biology of cancer". *Nat. Cell Biol.* **2013**, *15*(1). Editorial.

(4) Hanahan, D. and Weinberg, R. A. *Cell* **2000**, *100*, 57-70.

(5) Hanahan, D. and Weinberg, R. A. *Cell* **2011**, *144*, 646-674.

(6) Gilman, A. *Science* **1946**, *103*, 409-436.

(7) Cheung-Ong K.; Glaever, G. and Nislow, C. *Chem. Biol.* **2013**, *20*, 648-659.

(8) Avedaño C., Menéndez J. C. (**2008**). Antimetabolites. *Medicinal Chemistry of Anticancer Drugs* (pp. 9-52). doi: 10.1016/B978-0-444-52824-7.00002-0

(9) Rosenberg, B.; Vancamp, L. and Krigas, T. *Nature* **1965**, *205*, 698-699.

(10) Dasari, S. and Tchounwou, P. B. *Eur. J. Pharmacol.* **2014**, *740*, 364-378.

(11) Montecucco, A.; Zanetta, F. and Biamonti, G. *EXCLI J.* **2015**, *14*, 95-108.

(12) Minotti, G.; Menna, P.; Salvatorelli, E.; Cairo, G. and Gianni L. *Pharmacol. Rev.* **2004**, *56*(2), 185-229.

(13) Weiss, R. B. *Semin. Oncol.* **1992**, *19*(6), 670-686.

(14) Pasquier, E. and Kavallaris, M. *IUBMB Life* **2008**, *60*(3), 165-170.

(15) Jordan, M. A. and Wilson, L. *Nat. Rev. Cancer* **2004**, *4*, 253-265.

(16) Mukhtar, E.; Adhami, Y. M. and Mukhtar, H. *Mol. Cancer Ther.* **2014**, *13*(2), 275-284.

(17) Baudino, T. *Curr. Drug. Disc. Tech.* **2015**, *12*(1), 3-20.

(18) Waller, D. G. and Sampson, A. P. (**2018**). *Medical Pharmacology and Therapeutics*. Retrieved from: https://www.elsevier.com/books/medical-pharmacology-and-therapeutics/waller/978-0-7020-7190-4.

(19) Yao, X.; Panichpisal, K.; Kurtzman, N. and Nugent, K. *Am. J. Med. Sci.* **2007**, *334*, 115-124.

(20) Lameire, N.: Kruse, V. and Rottey, S. *Acta Clin. Belg.* **2011**, *66*(5), 337-345.

(21) Maor, Y. and Malnick, S. *Int. J. Hepatol.* **2013**, 1-8.

(22) Muller, P. Y. and Milton, M. N. *Nat. Rev. Drug Disc.* **2012**, *11*, 751-761.

(23) Remesh, A. *Int. J. Basic Clin. Pharmacol.* **2012**, *1*(1), 2-12.

(24) Coley, H. M. *Eur. J. Cancer Suppl.* **2009**, *7*(1), 3-7.

(25) Gottesmann, M.M. *Ann. Med. Rev.* **2002**, *56*, 615-627.

(26) Dickens E. and Ahmed S. *Surgery* , *36*(3), 134-138.

(27) Chorawala, M. R.; Oza, P. M. and Shah, G. B. *Int. J. Pharm. Sci. Drug Res.* **2012**, *4*(1), 1-9.

(28) Chari, R. V. R; Miller, M. L. and Widdison, W. C. *Angew. Chem. Int. Ed.* **2014**, *53*, 3796-38.

(29) Kupchan, S. M.; Komoda, Y.; Branfman, A. R.; Sneden, A. T.; Court, W. A.; Thomas, G. J.; Hintz, H. P. J.; Smith, R. M.; Karim, A.; Howie, G. A.; Verma, A.K.; Nagao, Y.; Dailey, R. G., Jr.; Zimmerly, V. A. and Summer, W. C., Jr. *J Org Chem* **1977**, *42*, 2349-2357.

(30) Kupchan, S. M.; Komoda, Y.; Court, W. A.; Thomas, J. C.; Smith, R. M.; Karim, A.; Gilmore, C. J.; Haltiwanger, R. C. and Byan, R. F. *J. Am Chem Soc* **1972**, 94, 1354–1356.

(31) Remillard, S.; Rebhun, L. I.; Howie, G. A. and Kupchan, S. M. *Science* **1975**, *189*(4207), 1002-1005.

(32) Issell, B. F. and Crooke, S. T. *Cancer Treat. Rev.* **1978**, *5*, 199-207.

(33) Pettit, G. R.; Kamano, Y.; Herald, C. L.; Tuinman, A. A.; Boettner, F. E.; Kizu, H.; Schmidt, J. M.; Baczynskyj, L.; Tomer, K. B.; Bontems, R. J. *J. Am. Chem. Soc.* **1987**, *109*, 6883 – 6885.

(34) Pettit, G. R.; Kamano, Y.; Dufresne, C.; Cerny, R. L.; Herald, C. L.; Schmidt, J. M. *J. Org. Chem.* **1989**, *54*, 6005 – 6006.

(35) Pitot, H. C.; McElroy, E. A., Jr.; Reid, J. M.; Windebank, A. J.; Sloan, J. A.; Erlichman, C.; Bagniewski, P. G.; Walker, D. L.; Rubin, J.; Goldberg, R. M.; Adjei, A. A. and Ames, M. M. *Clin. Cancer Res.* **1999**, *5*, 525 – 531.

(36) Vaishampayan, U.; Glode, M.; Du, W.; Kraft, A.; Hudes, G.; Wright, J.; Hussain, M. *Clin. Cancer Res.* **2000**, *6*, 4205 – 4208.

(37) Eggen, M. and Georv, G. I. *Med Res Rev* **2002**, *22*(2), 85-101.

(38) Edelmans, M. J.; Gandara, D. R.; Hausner, P.; Israel, V.; Thorntn, D.; DeSanto, J. and Doyle, L. A. *Lung Cancer* **2003**, *39*(2), 197-199.

(39) Dobbelstein, M. and Moll, U. *Nat. Rev. Drug Disc.* **2014**, *13*, 179-196.

(40) Torti, D. and Trusolino, L. *EMBO Mol. Med.* **2011**, *3*, 623-636.

(41) Zhang, J.; Yang, P. L. and Nathanael, S. G. *Nat. Rev. Cancer* **2009**, *9*, 28-39.

(42) Roskoski, R., Jr. *Pharmacol. Res.* **2019**, *152*, 104609.

(43) Köhler, J. C. and Milstein, C. *Nature* **1975**, *256*, 495-497.

(44) Majidi, J.; Barar, J.; Baradaran, B.; Abdolalizadeh, J. and Omidi, Y. *Hum. Antib.* **2009**, *18*, 81-100.

(45) Zhang, Q.; Chen, G.; Liu, X. and Qian, Q. *Cell Res.* **2007**, *17*, 89.99.

(46) Chames, P.; Van Regenmortel, M.; Weiss, E. and Baty, D. *Brit. J. Pharmacol.* **2009**, *157*, 220-233.

(47) Kaplon, H.; Muralidharan, M.; Schneider; Z. and Reichert, J. M. *mAbs* **2020**, *12*(1), e1703531.

(48) Petersen, B. H.; DeHerdt, S. V.; Schneck, D. W. and Bumol, T. F. *Cancer Res.* **1991**, *51*, 2286-2290.

(49) Tolcer, A. W.; Sugarman, S.; Gelmon, K.A.; Cohen, R.; Saleh, M.; Isaacs, C.; Young, L.; Healey, D.; Onetto, N. and Slichenmyer, W. *J. Clin. Oncol.* **1999**, *17*, 478-484.

(50) Hoffmann, R. M.; G. T. Coumbe, B.; H. Josephs, D.; Mele, S.; M. Ilieva, K.; Cheung, A.; N. Tutt, A.; F. Spicer, J.; E. Thurston, D.; Crescioli, S. and N. Karagiannis, S. *Oncoimmunol.* **2018**, *7*(3)

(51) Godwin, C. D.; Gale, R. P. and Walter, R. B. *Leukemia* **2017**, *31*, 1855-1868.

(52) Younes, A.; Yasothan, U. and Kirkpatrik, P. *Nat. Rev. Drug Discov.* **2012**, *11*, 19-20.

(53) a- Lambert, J. and Chari, R. V. *J. Med. Chem.* **2014**, *57*, 6949-6964. b- Mysliwy, J. *Future Drug Discov.* **2020**, *2*(2), FDD35.

(54) Srinivasarao, M. and Low, P. S. *Chem. Rev.* **2017**, *117*, 12133-12164.

(55) Wittrup, K. D.; Thurber, G. M.; Schmidt, M. M. and Rhoden, J. J. *Methods Enzymol.* **2012**, *503*, 255-268.

(56) Casi, G. and Neri, D. *J. Med. Chem.* **2015**, *58*(22), 8751-8761.

(57) Rudnick, S. I.; Lou, J.; Shaller, C. C.; Tang, Y.; Klein-Szanto, A. J. P.; Weiner, L. M.; Marks, J. D. and Adams, G. P. *Cancer Res.* **2011**, *71*, 2250-2259.

(58) Mack, F.; Ritchie, M. and Sapra, P. *Semin. Oncol.* **2014**, *41*(5), 637-652.

(59) Sedlacek, H. H. (**1992**). *Antibodies as Carries of Cytotoxicity*. pp. 1-145.

(60) Deonarain, M. P.; Yahioglu, G.; Stamati, I.; Pomowski, A.; Clarke, J.; Edwards, B. M.; Diez-Posada, S. and Stewart, A. C. *Antibodies* **2018**, *7*, 16.

(61) Hermeling, S.; Crommelin, D. J. A.; Schellekens, H. and Jiskoot, W. Pharm. Res. 2004, 21(6), 897-903.

(62) K. Fiorotti, C. *Bioanal.* **2018**, *10*(2), 65-70.; Wan, H. *ADMET & DMPK* **2016**, *4*(1), 1-22.

(63) Srinivasarao, M.; Galliford, C. V. and Low, P. S. *Nat. Rev. Drug Disc.* **2015**, *14*, 203-219.

(64) McCombs, J. R. and Owen, S. C. *AAPS J.* **2015**, *17*(2), 339-351.

(65) Lu, J.; Jiang, F.; Lu, A. and Zhang, G. *Int. J. Mol. Sci.* **2016**, *17*(4), 561.

(66) A. Teicher, B. and V.J. Chari, R. *Clin. Cancer Res.* **2011**, *17*(20), 6389-6397.

(67) Chari, R. V. J.; Miller, M. L. and Widdison, W. C. *Angew. Chem. Int. Ed.* **2014**, *53*, 3796-3827.

(68) Diamantis, N. and Banerji, U. *Brit. J. Cancer* **2016**, *114*, 362-367.

(69) Chen, K-S; Koh, G-C. and Li, H.-Y. *Cell Death Disease* **2012**, *3*, e411.

(70) Beck, A.; Goetsch, L.; Dumontet, C. and Corvaïa, N. *Nat. Rev. Drug Discov.* **2017**, *16*(5), 315-337.

(71) Wieland, H. and Hallermayer, R. *Justus Liebigs Ann. Chem.* **1941**, *458*, 1-18.

(72) Gong, X. Q.; Nedialkov, Y. A. and Burton, Z. F. *J. Biol. Chem.* **2004**, *279*(26), 27422-27427.

(73) Moldenhauer, G.; Salnikov, A. V.; Lüttgau, S.; Herr, I.; Anderl, J. and Faulstich, H. *JNCI* **2012**, *104*(8), 622-634.

(74) Lindell, T. J.; Weinberg, F.; Morris, P. W.; Roeder, R. G. and Rutter W. J. *Sci.* **1970**, *170,* 447-449.

(75) Cochet-Meilhac, M. and Chambon, P. *Biochim. Biophys. Acta* **1974**, *353*, 160-184.

(76) Bushnell, D. A.; Cramer, P. and Kornberg, R. D. *PNAS* **2002**, *99*(3), 1218-1222.

(77) Magdalan, J.; Ostrowska, A.; Piotrowska, A.; Izykowska, I.; Nowak, M.; Gomulkiewicz, A.; Podhorska-Oklów, M.; Szelag, A. and Dziegiel, P. *Folia Histochem. Cytobiol.* **2010**, *48*(1), 58-62.

(78) Nguyen, Van T.; giannoni, F.; Dubois, M.-F-; Seo S.-J.; Vigneron, M.; Kédinger, C. and Bensaude, O. *Nucleic Acids Res.* **1996**, *24*(159), 2924-2929.

(79) Anderl, J.; Faulstich, H.; Hechler, T. and Kulke, M. (2013). Antibody-Drug Conjugate Payloads. *Antibody-Drug Conjugates* (pp. 51-70). Doi: 10.1007/978-1-62703-541-5

(80) Letschert, K.; Faulstich, H.; Keller, D. and Keppler, D. *Toxicol. Sci.* **2006**, *91*(1), 140-149.

(81) Garcia, J.; Costa, V. M.; Carvalho, A. T.; Baptista, P.; Duarte, J. A.; Dourado, D. F.; Arbo, M. D.; Baltazar, T.; Dinis-Oliveire, R. J.; Baptista, P.; de Lourdes, B. M. and Carvalho, F. *Arch. Toxicol.* **2015**, *89*(12), 2305-2323.

(82) Fiume, L.; Marinozzi, V. and Nardi, F. *Br. J. ex. Path.* **1969**, 50, 270-276.

(83) Roche, B.; Arcangioli, B. and Martienessen, R. *RNA Biol.* **2017**, *14*(7), 843-853.

(84) Liu, Y.; Zhang, X.; Han, C.; Wan, G.; Huang, X.; Ivan, C.; Jiang, D.; Rodriguez-aguayo, C.; Lopez-Berestein, G.; Rao, P. H. Maru, D. M.; Pahl, A.; He, X.; Sood, A. K.; Ellis, L. M.; Anderl, J. and Liu, X. *Nature* **2015**, *520*, 697-701.

(85) Pushner, B. (**2018).** Mushroom toxins. *Veterinary Toxicology* (pp. 955-966) doi: 10.1016/B978-0-12-811410-0.00067-2

(86) Retrieved from https://heidelberg-pharma.com/en/press-and-investors/strategy-and-facts/strategy.

(87) Bodero, L.; López Rivas, P.; Korsak, B.; Hechler, T.; Pahl, A.; Müller, C.; Arosio, D.; Pignataro, L.; Gennari, C. and Piarulli, U. *Beilstein J. Org. Chem.* **2018**, *14*, 407-415..

(88) Zhao, L.; May, J. P.; Blanc, A.; Dietrich, D. J.; Loonchanta, A.; Matinkhoo, K.; Pryyma, A. and Perrin, D. M. *ChemBioChem.* **2015**, *16*, 420-425.

(89) Wang, X.; Dangshe, M.; C. Olson, W. and D.W. Heston, W. *Mol. Cancer Ther.* **2011**, *10*(9), 1728-1739.

(90) Staudacher, A. H. and Brown, M. P. *Brit. J. Cancer* **2017**, *117*, 1736-1742.

(91) Perez, H. L.; Cardarelli, M. P.; Deshpande, S.; Gangwar, S.; Schroeder, G. M.; D. Vite, G. and Borzilleri, M. R. *Drug Discov. Today* **2013**.

(92) Beck, A.; Goetsch, L.; Dumontet, C. and Corvaïa, N. *Nat. Rev. Drug Discov.* **2017**, *16*(5), 315-337.

(93) Szot, C.; Saha, S.; M. Zhang, X.; Zhu, Z.; Hilton, M. B.; Morris, K.; Seaman, S.; Dunleavey, M. J.; Hsu, K.-S.; Yu, G.-J.; Morris, H.; Swing, A. D.; Haines, C. D.; Wang, Y.; Hwang, J.; Feng, Y.; Welsch, D.; DeCrescenzo, G.; Chaudhary, A.; Zudaire, E.; Dimitrov, S. D. and St. Croix, B. *J. Clin. Invest.* **2018**, *128*(7), 2927-2943.

(94) Gerber, H.-P.; Senter, D. P. and Grewal, S. I. *MAbs* **2009**, *1*(3), 247-253.

(95) Bray, F.; Ferlay, J.; Soerjomataram, I.; Siegel, R. L.; Torre, L. A. and Jemal, A. *Ca Cancer J. Clin.* **2018**, *68*, 394-424.

(96) Olson, W. C. and Israel, R. J. *Front. Biosci.* **2014**, *19*, 12-33.

(97) Mesters, J. R.; Barinka, C.; Li, W.; Tsukamoto, T.; Majer, P.; Slusher, S. B.; Konvalinka, J. and Hilgenfeld, R. *EMBO J.* **2006**, *25*, 1375-1384.

(98) Barinka, C.; Byun, Y.; Dusich, C. L.; Banerjee, S. R.; Chen, Y.; Castanares, M.; Kozikowski, A. P.; Mease, R. C.; Pomper, M. G. and Lubkowski, J. *J. Med. Chem.* **2008**, *51*, 7737-7743.

(99) Zhang, A. X.; Murelli, R. P.; Barinka, C.; Michel, J.; Cocleaza, A.; Jorgensen, W. L.; Lubkowski, J. and Spiegel, D. A. *J. Am. Chem. Soc.* **2010**, *132*, 12711-12716.

(100) Bostwick, D. G.; Pacelli, A.; Blute, M.; Roche, P. and Murphy, G. P. *Cancer* **1998**, *82*(11), 2256-2261.

(101) Silver, D. A.; pellicer, I.; Fair, W. R.; Heston; W. D. W. and Cordon-Cardo, C. *Clin. Cancer Res.* **1997**, *3*, 81-85.

(102) Gosh, A. and Heston, W. D. W. *Prostate* **2003**, *57*, 140-151.

(103) Ristau, B. T.; O´Keefe, D. and Babich, D. J. *Urol. Oncol.* **2014**, *32*(3), 272-279.

(104) Liu, H.; Rajasekaran, A. K.; Moy, P.; Xia, Y.; Kim, S.; Navarro, V.; Rahmati, R. and Bander, N. H. *Cancer Res.* **1998**, *58*, 4055-4060.

(105) Liu, J.; Kopeckova, P.; Buhler, P.; Wolf, P.; Pan, H.; Bauer, H; Elsasser-Beile, U. and Kopecek, J. *Mol. Pharm.* **2009**, *6*(3), 959-970.

(106) Sokoloff, R. L.; Norton, K. C.; Gasior, C. L.; Marker, K. M. and Grauer, L. S. *Prostate* **2000**, *43*(2), 150–157.

(107) Yao, V. and Babich, D. J. *Prostate* **2006**, *66*, 867-875.

(108) Kaittanis, C.; Andreou, C.; Hieronymus, H.; Mao, N.; Foss, C. A.; Eiber, M.; Weirich, G.; Panchal, P.; Gopalan, A.; Zurita, J.; Achilefu, S.; Chiosis, G.; Ponomarev, V.;

Schwaiger, M.; Carver, B. S.; Pomper, M. G. and Grimm, G. *JEM* **2018**, *215*(1), 159.

(109) Wright, G. L., Jr.; Haley, C.; Beckett, M. L. and Schellhammer, P. F. *Urol. Oncol.* **1995**, *1*, 18-28.

(110) Tsourlakis, M. C.; Klein, F.; Kluth, M.; Quaas, A.; Graefen, M.; Haese, A.; Simon, R.; Sauter, G.; Sclomm, T. and Minner, S. *Appl. Immunohistochem. Mol. Morphol.* **2015**, *23*86), 449-455.

(111) Evans, M. J.; Smith-Jones, P. M.; Wongvipat, J.; Navarro, V.; Bander, N. H.; Larson, S. M. and Sawyers, C. L. *PNAS* **2011**, *108*(23), 9578-9582.

(112) Bander, N. H. Androgen suppresssion, prostate-specific membrane antigen and the concept of conditionally enhanced vulnerability. US patent 2018/0208676 A1. July 26, 2018.

(113) Liu, H.; Moy, P. and Kim, S. *Clin. Cancer Res.* **1997**, *57*, 3629-3634.; Chang, S. S.; Reuter, V. E.; Heston, W. D. W.; Bander, N. H.; Grauer, L. S. and Gaudin, B. *Cancer Res.* **1999**, *59*, 3192-3198.; Chang, S. S.; Reuter, V. E.; Heston, W. D. W. and Gaudin, P. *Urol.* **2001**, *57*(4), 801-805.; Haffner, M. C.; Kronberger, I. E.; Ross, J. E.; Sheehan, C. E.; Zitt, M.; Muhlmann, G.; Ofner, D.; Zelger, B.; Ensinger, C.; Yang, X. J.; Geley, S.; Margreiter, S. and Bander, N. H. *Hum. Pathol.* **2009**, *40,* 1754-1761.

(114) Conway, R. E.; Petrovic, N.; Li, Z.; Heston, W.; Wu, D. and Shapiro, L. H. *Mol. Cell. Biol.* **2006**, *26*(14), 5310-5324.

(115) Henry, M.D.; Wen, S.; Silva, M.D.; Chandra, S.; Milton, M. and Worland, P.J. *Cancer Res.* **2004**, *64*(21), 7995-8001.) (Galsky, M.D.; Eisenberger, M.; Moore-Cooper, S.; Kelly, W.K.; Slovin, S.F.; DeLaCruz, A.; Lee, Y.; Webb, I.J. and Scher, H.I. *J. Clin. Oncol.* **2008**, *26(*13), 2147-2154.

(116) Ma, D.; Hopf, C.E.; Malewicz, A.D.; Donovan, G.P.; Senter, P.D.; Goeckeler, W.F.; Maddon, P.J. and Olson, W.C. *Clin. Cancer Res.* **2008**, *12*(8), 2591-2596.

(117) Cho, S.; Zammarchi, F.; Williams, D. G.; Havenith, C. E. G.; Monks, N. R.; Tyrer, P.; D´Hooge, F.; Fleming, R.; Vashisht, K.; Dimasi, N.; Bertelli, F.; Corbett, S.; Adams, L.; Reinert, H. W.; Dissanayke, S.; Britten, C. E.; King, W.; Dacosta, K.; Tammali, R.; Schifferli, K.; Strout, P.; Korade III, M.; Masson Hinrichs, M. J.; Chivers, S.; Corey, E.; Liu, H.; Kim, S.; Bander, N. H.; Howard, P. W.; Hartley, J. A.; Coats, S.; Tice, D. A.; Herbst, R. and van Berkerl P. H. *Mol. Cancer Ther.* First online publication. July 31, **2018**. Doi: 10.1158/1535-7163.MCT-17-0982.

(118) Breunig, C.; Pálfi, A.; Hechler, T.; Müller, C.; Lutz, C.; Pahl, A. and Kulke, M. AACR Annual Meeting 2018. Abstract#740.

(119) Ferraris, D. V.; Shukla, K. and Tsukamoto, T. *Curr. Med. Chem.* **2012**, *19*, 1282-1294.

(120) Kozikowski, A. P.; Nan, F.; Conti, P.; Zhang, J.; Ramadan, E.; Bzdega, T.; Wroblewska, B.; Neale, J. H.; Pshenichkin, S. and Wrobleski, J. T. *J. Med. Chem.* **2001**, *44*, 298-301.

(121) Kozikowski, A. P.; Zhang, J.; Nan, F.; Petukhov, P. A.; Grajkowska, E.; Wrobleski, J. T.; Yamamoto, T.; Bzdega; T.; Wroblewska, B. and Neale, J. H. *J. Med. Chem.* **2004**, *47*, 1729-17-38.

(122) Kularatne, S. A.; Zhou, Z.; Yang, J.; Post, C. B. and Low, P. S. *Mol. Pharm.* **2009**, *6*(3), 790-800.

(123) Kularatne, S. A.; Wang, K.; Santhapuram, H.-K. R. and Low, P. S. *Mol. Pharm.* **2009**, 6(3), 780-789.

(124) Vallabhajosula, S.; Nikolopoulou; Babich, J. W.; Osborne, J. R.; Tagawa, S. T.; Lipai, I.; Solnes, L.; Maresca, K. P.; Armor, T.; Joyal, J. L.; crummet, R:; Stubbs, J. B. and Goldsmith, S. J. *J. Nucl. Med.* **2014**, *55*(11), 1791-1798.

(125) Benešová, M.; Schäfer, M.; Bauder-Wüst, U.; Afshar-Oromieh A.; Kratochwil, C.; Mier, W.; Haberkorn, U.; Kopka, K. and Eder, M. *J. Nucl. Med.* **2015**, *56*, 914-920.

(126) Hoffman, M. S.; Violet, J.; Hicks, R: J.; Ferdinandus, J.; Thang, S. P. and Akhurst, T. *Lancet Oncol.* **2018**, *19*(6), 825-833.

(127) Roy, J.; Nguyen, T. X.; Kanduluru, A. K.; Venkatesh, C.; Lv W.; Reddy, P. V. N.; Low, P. S. and Cushman, M. *J. Med. Chem.* **2015**, *58*. 3094-3103.

(128) a. Vlahov, I. R.; Reddy, J. A.; Bloomfield, A.; Dorton, R.; Nelson, M.; Vetzel, M.; Leamon, C. P. Drug delivery conjugates, and methods for treating diseases caused by PSMA expressing cells.WO patent 2014/078484. May 10, 2014. b. Morris, M.; Vogelzang, N.J.; Sartor, O.; Armour, A. and Groaning, M. *Ann. Oncol.* **2017**, *28* (Suppl. 5), 370.

(129) Lv, Q.; Yang, J.; Zhang, R.; Yang, Z.; Yang, Z.; Wang, Y.; Xu, Y. and He, Z. *Mol. Pharm.* **2018**, *15*(5), 1842-1852.

(130) Stark, M. and Assaraf, Y. G. *Oncotarget* **2017**, *8*(30), 49973-49987.

(131) Oldham, Ro. K. and Dillman, R. O. Principles of cancer biotherapy (**1987**).

(132) Hechler, T.; Kulke, M.; Müller, C.; Pahl, A. and Anderl, J. AACR Annual Meeting **2014**. Abstract#664.

(133) Caculitan, N. G.; dela Cruz Chuh, J.; Ma, Y.; Zhang, D.; Kozak, K. R.; Liu, Y.; Pillow, T. H.; Sadowsky, J.; Cheung, T. K.; Phung, Q.; Haley, B.; Lee, B.-C.; Akita, R. W.; Sliwkowski, M. X. and Polson, A. G. *Cancer Res.* **2017**, *77*(24), 7027-7037.

(134) Gondi, C. S. and Rao, J. S. *Expert Opin. Ther. Targets* **2013**, *17*(3), 281-291.

(135) Otto, H.-H. and Schirmeister, T. *Chem. Rev.* **1997**, *97*, 133-172.

(136) Löser, R. and Pietzsch, J. *Front. Chem.* **2015**, *3*(37).

(137) Stein, E. M.; Walter, R. B.; Erba, H. P.; Fathi, A. T.; Advani, A. S.; Lancet, J. E.;

Ravandi, F.; Kovacsovics, T.; DeAngelo, D. J.; Bixby, D.; Faderl, S.; Jillella, A. P.; Ho,
P. A.; O´Meara, M. M.; Zhao, B.; Biddle-Snead, C. and Stein, A. S. *Blood* **2018**, *131*(4),
387-396.

(138) Crisp, J. L.; Savariar, E. N.; Glasgow, H. L.; Ellies, L. G.; Whitney, M. A. and Tsien, R. Y.
Bioconjugate Chem. **2014**, *13*, 1514-1525.; Dal Pozzo A.; Esposito, E.; Ni, M.; Pisano, C.; Bucci,
F.; Vesci, L.; Castorina, M. and Penso, S. *Bioconjugate Chem*. **2010**, *21*, 1956-1967.

(139) Hochdörfffer, K.; Abu Ajaj, K.; Schäfer-Obodozie, C. and Kratz, F. *J. Med. Chem*. **2012**, *55*,
7502-7515.; Dal Corso, A.; Caruso, M.; Belvisi, L.; Arosio, D.; Piarulli, U.; Albanese, C.;
Gasparri, F.; Marsiglio, A.; Sola, F.; Troiani, S.; Valsasina, B. *et al*. *Chem. Eur. J*. **2015**, *21*, 6921-6929.

(140) Cazzamalli, S.; Dal Corso, A. and Neri, D. *J. Control Release* **2017**, *246*, 39-45.; Dubwchik, G. M.; Firestone, R. A.; Padilla, L.; Willner, D.; Hofstead, S. J.; Mosure, K.; Knipe, J. O.; Lasch, S. J. and Trail, P. A. *Bioconjugate Chem*. **2002**, *13*, 855-869.

(141) Anderl J., Mueller C., Simon W. Amatoxin-conjugates with improved linkers. WO Patent
WO2012041504, April 5, 2012; Anderl J., Hechler T., Mueller C., Pahl A. Amatoxin-antibody conjugates. WO Patent WO2016142049, September 15, 2016.

(142) Jeffrey, S. C.; Torgov, M. Y.; Andreyka, J. B.; Boddington, L.; Cerveny, C. G.; Denny, W. A.; Gordon, K. A.; Gustin, D.; Haugen, J.; Kline, T.; Nguyen, M. T. and Senter, P. D. *J. Med. Chem*. **2005**, *48*, 1344-1358.

(143) Gorges, T. M.; Riethdorf, S.; von Ahsen, O.; Nastały, P.; Röck, K.; Boede, M.; Peine, S.; Kuske, A.; Schmid, E.; Kneip, C.; König, F.; Rudolph, M.; Pantel, K. *Oncotarget* **2016**, *7*(23).

(144) Weineisen, M.; Simecek, J.; Schottelius, M.; Schwaiger, M. and Wester, H.-J. *EJNMMI Res*. **2014**, *4*(63).

(145) Alley, S. C.; Benjamin, D. R.; Jeffrey, S. C.; Okeley, N. M.; Meyer, D. L.; Sanderson, R. J.; Senter, P. D. *Bioconjugate Chem*. **2008**, *19*, 759-765.

(146) Colclough, N.; Ruston, L.; Wood, J. M. and MacFaul, P. A. *Med. Chem. Comm*. **2014**.

(147) Danial, M. and Postma, A. *Ther. Deliv*. **2017**, *8*(6), 359-362.

(148) Pillow, T. H.; Sadowsky, J. D.; Zhang, D.; Yu, S.-F.; Del Rosario, J.; Xu, K.; He, J.; Bhakta, S.; Ohri, R.; Kozak, K. R.; Ha, E.; Junutula, J. R. and Flygare, J. A. *Chem. Sci*. **2017**, *8*, 366-370.

(149) Anderl, J.; Faulstich, H.; Hechler, T. and Kulke, M. (2013). Linker technologies for Antibody-Drug Conjugates. *Antibody-Drug Conjugates* (pp. 71-100). Doi: 10.1007/978-1-62703-541-5.

(150) Thorpe, P. E.; Wallace, P. M.; Knowles, P. P.; Relf, M. G.; Brown, A. N. F.; Watson, G. J.; Knyba, R. E.; Wawrzynczak, E. J.; Blakey, D. C. *Cancer Res*. **1987**, *47*(22), 5924-5932.; Thorpe, P. E.; Wallace, P. M.; Knowles, P. P.; Relf, M. G.; Brown, A. N. F.; Watson, G. J.; Blakey, D. C. and Newell, D. R. *Cancer Res*. **1988**, *48*(22), 6396-6403.

(151) Leamon, C. P.; Reddy, J. A.; Vlahov, I. R.; Westrick, E.; Dawson, A.; Dorton, R.; Vetzel, M.; Santhapuram, H. K. and Wang, Y. *Mol. Pharm*. **2007**, *4*(5), 659-667.; Gokhale, M.; Thakur, A. and Rinaldi, F. *Drug Dev. Ind. Pharm*. **2013**, *39*, 1315-1327.; Dhawan, D.; Ramos-Vara, J. A.; Naughton, J. F.; Cheng, L.; Low, P. S.; Rothenbuhler, R.; Leamon, C. P.; Parker, N.; Klein, P. J.; Vlahov, I. R.; Reddy, J. A.; Koch, M.; Murphy, L.; Fourez, L. M.; Stewart, J. C. and Knapp, D. W. *Cancer Res*. **2013**, *73*(2); 875-884.

(152) Perrino, E.; Steiner, M.; Krall, N.; Bernandes, G. J. L.; Pretto, F.; Casi, G. and Neri, D. *Cancer Res*. **2014**, *74*(9), 2569-2578.)

(153) Smith, D. A.; Beaumont, K.; Maurer, T. S. and Di, L. *J. Med. Chem*. **2018**, *61*, 4273-4282.

(154) Dorywalska, M.; Dushin, R.; Moine, L.; Farias, S. E.; Zhou, D.; Navaratnam, T.; Lui, T.; Hasa-Moreno, A.; Casa, M. G.; Tran, T.-T.; Delaria, K.; Liu, S.-H.; Foletti, D.; O´Donnell, C. J.; Pons, J.; Shelton, D. L.; Rajpal, A. and Strop, P. *Mol. Cancer Ther*. **2016**, *15*(5), 958, 970.

(155) Unger, C.; Haring, B.; Medinger, M. Drevs, J.; Steinbild, S.; Kratz, F. and Mross, K. *Clin. Cancer Res*. **2007**, *13*(16), 4858-4866.

(156) Faulstich, H.; Kirchner, K. and Derenzini, M. *Toxicon* **1988**, *26*(5), 491-499.

(157) Lu, H.; Choudhuri, S.; Ogura, K.; Csanaky, I. L.; Lei, X.; Cheng, X.; Song, P. and Klaassen, C. D. *Toxicol. Sci*. **2008**, *103*(1), 35-45.

(158) Anderl, J.; Müller, C.; Heckl-Östreicher, B. and Wehr, R. AACR 102nd Annual Meeting 2011. #Abstract 3616.

(159) Fontaine, S. D.; reid, R.; Robinson, L.; Ashley, G. W. And Santi, D. V. *Bioconjugate Chem*. **2015**, *26*, 145-152.

(160) Melis, M.; Krenning, E. P.; Bernard, B. F.; de Visser, M.; Rolleman, E. and de Jong, M. *Nucl. Med. Biol*. **2007**, *34*, 633-641.

(161) a-Haraldsson, B.; Nyström, J. and Denn, W. M. *Physiol. Rev.* **2008**, *88*, 451-487.; b-Briggs, J. P.; Kriz, W. and Schnermann, J. B. *Overview of kidney function and structure*. In: National Kidney Foundation Primer on Kidney Disease. 6th Edition; Gilbert, S. J. and Weiner, D. E.; Elsevier, **2014**; 2-28.

(162) Vegt, E.; de Jong, M.; Wetzels, J. F. M.; Masereeuw, R.; Meli, M.; Oyen, W. J.G.; Gotthardt, M. and Boerman, O. C. *J. Nucl. Med.* **2010**, *51*(7), 1049-1058.

(163) De Jong, M.; Barone, R:, Krenning, E. P.; Bernard, B. F.; Melis, M.; Visser, T.; Gekle, M.; Willnow, T. E.; Walrand, S.; Jamar, F. and Pauwels, S. *J. Nucl. Med.* **2005**, *46*(10), 1696-1700.

(164) a- Melis, M.; Krenning, E. P.; Bernard, B. F.; Barone, R.; Visser, T. J. and de Jong, M. *Eur. J. Nucl. Med. Mol. Imaging* **2005**, *32*, 1136-1143.; b- Behr, T. M.; Sharkey, R. M.; Juweld, M. E.; Blumenthal, R. D.; Dunn, R. M.; Griffiths, G. L.; Bair, H. J.; Wolf, F. G.; Becker, W. S. and Goldenberg, D. M. *Cancer Res.* **1995**, *55*(17), 3825-3834.; c-Behé, M.; Kluge, G.; Becker, W.; Gotthardt, M. and Behr, T. M. *J. Nucl. Med.* **2005**, *46*(6), 1012-1015.

(165) Gianesello, L.; Ceol, M.; Priante, G.; Anglani, F. and Del Prete, D. *J. Clin. Nephrol. Kid. Dis.* **2016**, *1*(1), article 1002.

(166) Liu, S. *Mol. Pharmaceutics* **2006**, *3*(5), 472-487.

(167) Eder, M.; Löhr, T.; Bauder-Wüst, U.; Reber, M.; Mier, W.; Schäfer, M.; Heberkorn, U. and Eisenhut, M. *J. Nucl. Med.* **2013**, *54*(8).

(168) Liolios, C.; Schäfer, M.; Haberkorn, U.; Eder, M. and Kopka, K. *Bioconjugate Chem.* **2016**, *27*, 737-751.

(169) Chittasupho, C. *Ther. Deliv.* **2012**, *3*(10), 1171-1187.

(170) Fasting, C.; Schalley, C. A.; Weber, M.; Seitz, O.; Hecht, S.; Koksch, B.; Dernedde, J.; Graf, C.; Knapp, E.-W. and Haag, R. *Angew. Chem.* **2012**, *124*, 10622-10650.

(171) Yan, Y. and Chen, X. *Amino Acids* **2011**, *41*(5), 1081-1092.

(172) Ordanini, S.; Verga, N.; Porkolab, V.; Thépaut, M.; Belvisi, L.; Bertaglia, A.; Palmioli, A.; Berzi, A.; Trabattoni, D.; Clerici, M.; Fieschi, F. and Bernardi, A. *Chem. Comm.* **2015**, *51*, 3816-3819..

(173) Banerjee, S. R.; Pullambhatla, M.; Shallal, H.; Lisok, A.; Mease, R. C. and Pomper, M G. *Oncotarget* **2011**, *2*(12), 1244-1253.

(174) Schäfer, M.; Bauder-Wüst, U.; Leotta, K.; Zoller, F.; Mier, W.; Haberkorn, U.; Eisenhut, M. and Eder, M. *EJNMMI Res.* **2012**, *2*(23).

(175) Aggarwal, S.; Singh, P.; Topaloglu, O.; Isaacs, J. T. and Denmeade, S. R. *Cancer Res.* **2006**, *66*(18), 9171-9177.

(176) Kubas, H.; Schäfer, M.; Bauder-Wüst, U.; Eder, M.; Oltmanns, D.; Haberkorn, U.; Mier, W. and Eisenhut, M. *Nucl. Med. Biol.* **2010**, *37*, 885-891.

(177) Handl, H. L.; Vagner, J.; Han, H.; Mash, E.; Hruby, V. J. and Gillies, R. J. *Expert Opin. Ther. Targets* **2004**, *8*(6), 565-586.

(178) Pyzik, M.; Rath, T.; Lencer, W. I.; Baker, K. and Blumberg, R. S. *J. Immunol.* **2015**, *194*(10), 4595-4603.

(179) Sockolosky, J. T. and Szoka, F. C. *Adv. Drug Deliv. Rev.* **2015**, *91*, 109-124.

(180) Rath, T.; Baker, K.; Dumont, J. A.; Peters, R. T.; Jiang, H.; Qiao, S.-W.; Lencer, W. I.; Pierce, G. F. and Blumberg, R. S. *Crit. Rev. Biotechnol.* **2015**, *35*(2), 235-254.

(181) Wu, B. and Sun, Y.N. *J. Pharm. Sci.* **2014**, *103*, 53-64.

(182) Pechtner, V.; Karanikas, C. A.; García-Pérez, L. E. and Glaesner, W. *Prim. Health Care* **2017**, *7*(1).

(183) Rader, C. *Trends in Biotechnol.* **2014**, *32*(4), 186-197.

(184) a-Thomas, J. D.; Cui, H.; North, P. J.; Hofer, T.; Rader, C. and Burke, Jr, T. R. *Bioconjugate Chem.* **2012**, *23*, 2007-2013.; b- Thomas, J. D.; Hofer, T.; Rader, C. and Burke, Jr, T. R. *Bioorg. Med. Chem. Lett.* **2008**, *18*, 5785-5788.

(185) a- Swee L. K., Guimares C. P., Sehrawat S., Spooner E., Barrasa M. I., Ploegh H. L. *Proc. Natl. Acad. Sci. USA* **2013**, *110*, 1428-1433; b- Kornberger P., Skerra A. *mAbs* **2014**, *6*, 354-366; c- Wagner K., Kwakkenbos M. J., Claassen Y. B., Maijoor K., Bohne M., van der Sluijs K. F., Witte M. D., van Zoelen D., J., Cornelissen L. A., Beaumont T., Bakker A. Q., Ploegh H. L., Spits H. *Proc. Natl. Acad. Sci. USA* **2014**, *111*, 16820-16825; d- Dickgiesser S., Rasche N., Nasu D., Middel S., Hörner S., Avrutina O., Diederichsen U., Kolmar H. *ACS Chem. Biol.* **2015**, *10*(9), 2158-2165.

(186) Chen L.; Cohen, J.; Song, X.; Zhao, A.; Ye, Z.; Feulner, C. j.; Doonan, P.; Somers, W.; Lin, L. and Chen, P.R. *Sci. Rep.* **2016**, *6*, 31899.

(187) a- Rath, T.; Baker, K.; Dumont, J. A.; Peters, R. T.; Jiang, H.; Qiao, S.-W-: Lencer, W. I.; Pierce, G. F. and Blumberg, R. S. *Crit. Rev. Biotechnol.* **2015**, *35*(2), 235-254. b- Saunders, K. O. *Front. Immunol.* **2019**, *10*, 1-20.

(188) Dmitrij Hristodorov, Rainer Fischer, Lars Linden *Mol. Biotechnol.* **2013**, *54*, 1056-1068.

(189) Chen I., Dorr B., Liu D. R. *Proc. Natl. Acd. Sci. USA* **2011**, *108*, 1139-11404.

(190) Currier, N. V.; Ackerman, S. E.; Knitzing, J. R.; Chen, R.; Filsinger Interrante, M.; Steiner, A.; Sato, A. K. and Cochran, J. R. *Mol. Cancer. Ther.* **2016**, *15*(6), 1291-300.

(191) Wang, Y. M.; Sloey, B.; Wong, T.; Khandelwal, P.; Melara, R. and Sun, Y. N. *Pharm. Res.* **2011**, *28*(8), 1931-1938.

(192) Wu, B.; Johnson, J.; Soto, M.; Ponce, M.; Calamba, D. and Sun, Y. N. *Pharm. Res.* **2012**, *29*(4), 1057-1065.

(193) Ober, R.J.; Radu, C.G.; Ghetie, V. and Ward, E.S. *Int. Immunol.* **2001**, *13*(12), 1551-1591.

(194) Tsumura, R.; Manabe, S.; Takashima, H.; Koga, Y.; Yasunaga, M. and Matsumura, Y. *J. Control. Release* **2018**, 284, 49-56.